2019

Fly ash-based geopolymer as innovative material for environmental applications

Guyu Shi
Iowa State University

Fly ash-based geopolymer as innovative material for environmental applications

by

Guyu Shi

A dissertation submitted to the graduate faculty

in partial fulfillment of the requirements for the degree of

DOCTOR OF PHILOSOPHY

Major: Civil Engineering (Environmental Engineering)

Program of Study Committee:
Say Kee Ong, Co-major Professor
Kejin Wang, Co-major Professor
Roy Gu, Co-major Professor
Michael Thompson
James Alleman

The student author, whose presentation of the scholarship herein was approved by the program of study committee, is solely responsible for the content of this dissertation. The Graduate College will ensure this dissertation is globally accessible and will not permit alterations after a degree is conferred.

Iowa State University

Ames, Iowa

2019

TABLE OF CONTENTS

Page

LIST OF TABLES

Page

LIST OF FIGURES

Page

NOMENCLATURE

FAG	Fly ash-based geopolymer
MFAG	Magnetic fly ash-based geopolymer
MCFAG	Magnetic coating fly ash-based geopolymer
AMD	Acid mine drainage
BET	Brunauer–Emmett–Teller
ICP	Inductively coupled plasma
SEM	Scanning electron microscope
EDX	Energy dispersive X-ray

ACKNOWLEDGEMENTS

Firstly, I would like to express my sincere gratitude to my advisor Prof. Say Kee Ong for the continuous support of my Ph.D study and related research, for his patience, motivation, and immense knowledge. I would like to thank him for encouraging my research and for allowing me to grow as a research scientist. I could not have imagined having a better advisor and a tremendous mentor for me. His advice on both research as well as on my career have been priceless.

Besides my advisor, I would like to thank my co-major professors, Prof. Kejin Wang and Prof. Roy Gu, for their guidance and financial support throughout the course of this research. I would also like to thank the rest of my committees, Prof. Michael Thompson and Prof. James Alleman, for letting my defense be an enjoyable moment, for their insightful comments and suggestions, but also for the rigorous questions which incented me to widen my research from various perspectives.

In addition, my sincere appreciation also goes to my colleagues, department faculties, and staffs for making my time at Iowa State University a wonderful experience. I would especially like to thank an ISU Scientist Dr. Baozhi Cui from Ames Laboratory for his precious support and technical suggestions.

Last but not the least, a special thanks to my family. Words cannot express how grateful I am to my mother Haiyuan Yu and my father Renqiang Shi for all the sacrifices that they have made on my behalf. Their encouragement for me was what sustained me thus far. I would also like to thank all my friends who incented me to strive towards my goal. At the end I would like express appreciation to my beloved Xiaomeng who spent sleepless nights with and was always my support in the moments when there was no one to answer my queries.

ABSTRACT

Fly ash-based geopolymer were synthesized from Class-F fly ash and slag with an alkaline activating solution and characterized for their physical-chemical properties. The geopolymer samples were tested to investigate their environmental impacts when used for environmental applications. Batch adsorption studies were conducted using fly ash-based geopolymer as a reactive material or an adsorbent for heavy metals (Cu^{2+}, Cd^{2+} and Pb^{2+}). The removal capacities for Cu^{2+}, Cd^{2+} and Pb^{2+} ranged from 20.66 – 35.21, 28.74 – 42.02, and 116.28 – 121.95 mg/g for initial pHs ranged from 2.5 to 4.0, respectively, at room temperatures of 21 – 23 ^{o}C. Fixed bed column studies were carried out using fly ash-based geopolymer as a filtration medium for removal of metal (Cu^{2+}, Cd^{2+}, and Pb^{2+}) in low pH solutions. Breakthrough curves showed that the adsorption affinity of the geopolymer for metals was in the order of $Pb^{2+} > Cd^{2+} > Cu^{2+}$ for a single metal solution and in the order of $Pb^{2+} > Cu^{2+} > Cd^{2+}$ for a multi-metal solution which shows that there was a competition for adsorption sites on the geopolymer. The geopolymer can be used to neutralize the pH of acidic waste streams and at the same time adsorb or precipitate metal pollutants. In addition, magnetic geopolymers were synthesized by incorporating magnetic Fe_3O_4 particles to modify the fly ash-based geopolymer. Magnetic fly ash geopolymer showed similar adsorption properties as fly ash-based geopolymer with a maximum adsorption capacity of 111.1 mg/g. The magnetic fly ash geopolymer has a saturation magnetization of 18 emu/g and was found to separate out from an aqueous solution within 2 minutes by using a magnetic field of 0.48 Tesla. Applications of the magnetic fly ash geopolymer include using it as a powdered adsorbent to maximize heavy metals removal and recovery in wastewater treatment.

CHAPTER 1. GENERAL INTRODUCTION

1.1. Background

Proper waste management and maintaining good water quality are essential to a sustainable environment. Accumulation of waste from urbanization and industrialization have resulted in release of pollutants such as organic compounds and heavy metals in the environment. Heavy metals such as copper (Cu^{2+}), cadmium (Cd^{2+}), and lead (Pb^{2+}) pose serious health threats to humans and animals and must be removed from the environment. Besides industrial discharges, heavy metals in water can be derived naturally though soil erosion or from contact with subsurface minerals. Removal of heavy metals from water and wastewater include but not limited to chemical precipitation, ion exchange, adsorption, membrane filtration, and electrochemical process. Although many of treatment processes are adequate, some of them are unable to meet the stringent disposal concentration limits. One widely used treatment process is adsorption. Common adsorbents used include activated carbon, zeolite, and specially prepared proprietary materials. With the recent emphasis on sustainability, researchers have taken an approach in using abundant waste materials from industrial, agricultural and food production to produce suitable adsorbent. This helps to reduce the waste products produced and at the same time produce a material that can remove pollutants.

Coal-fine power plants produce a large quantity of waste fly ash, bottom ash and slag which must be disposed of safely (Wang and Wu, 2006). Fly ash and slag are rich in silicon (Si) and aluminum (Al) which can be activated using alkaline solution to obtain cementitious properties. Depending on the preparation steps, the geopolymer may have a porous structure and large surface area which are similar to clay materials and zeolite. In addition, these fly ash-based geopolymers exhibit mechanical properties (compressive strength, flexural strength, and tensile strength), fire

resistance that are similar to that of concrete and can be used for solidification of hazardous waste (Davidovits, 2002). Some researchers have classified geopolymer as a kind of novel green cementitious materials similar to concrete (Duxson et al., 2007). Several researchers have investigated geopolymer as a potential material for removal of pollutants such as Cd^{2+}, Ni^{2+}, Pb^{2+}, Cu^{2+}, ammonium, and dyes (Ahmaruzzaman, 2010; Al-Harahsheh et al., 2015; Zhang and Liu, 2013; Ariffin et al., 2017; Zhang et al., 2011). Results of these research showed that geopolymers can be used for environmental applications such as removal of heavy metals and other pollutants in contaminated waters. The properties of geopolymer can be modified by using different amounts and types of materials to optimize their surface characteristics for environmental applications. Due to the alkaline nature of the geopolymers, one particular application is to treat acid mine drainage, where the acidic drainage can be neutralized along with removal of heavy metals. The potential of geopolymer as a material for environmental applications needs further investigation.

By adding different specialized materials such as nanoparticles or magnetic iron materials, the properties of the geopolymer can be modified. For example, adding magnetic iron oxide (Fe_3O_4) to fly ash-based geopolymer can make the geopolymer magnetic which will allow for rapid separation from wastewaters. Consequently, the material can be collected, regenerated and reused (Zhang et al., 2011). The ability to separate treatment materials from the treated wastewater is essential as it will improve the operational efficiency and reduce the cost of the materials for water/wastewater treatment (Lin et al., 2012).

1.2. Problem Statement

Metals such as lead, cadmium, copper, arsenic, nickel, chromium, zinc and mercury have been recognized as hazardous heavy metals. Unlike organic wastes, heavy metals are non-biodegradable and can accumulate in living tissues and organs, causing various diseases and

disorders. Precipitation and adsorption are some of the most effective processes for removal of heavy metals from aqueous solutions. For example, activated carbon is a widely used adsorbent with good metal ions removal and adsorption capabilities. However, the high cost of adsorption materials and the need for pretreatment of the waste streams limit the widespread utilization of adsorption materials in wastewater treatment. Thus, low-cost treatment materials or adsorbents with high efficiencies for removal of heavy metals are desired.

Treatment materials or adsorbents can be made from various waste materials. One of the waste materials is fly ash produced by coal-fired power plants. Due to the large amounts of fly ash produced, power plants are continuously finding innovative ways to safely dispose and/or reuse the fly ash. Fly ash has been used as a source material to make geopolymer, a binder or cement-like material roughly comparable to hydrated cement in appearance, reactivity and properties. Some researchers have indicated that fly ash-based geopolymer may be considered as a kind of novel green cement for infrastructure and environmental applications. Finding new applications for fly ash-based geopolymer will help to reduce the existing large piles of fly ash at power plants and will minimize future land disposal of fly ash.

1.3. Objectives

The overall goal of this research is to develop and investigate fly ash-based geopolymer for environmental applications such as for treatment of industrial wastewaters. The specific objectives of this study are:

1) Synthesize and characterize fly ash-based geopolymer and investigate its environmental impact and applications.

2) Investigate fly ash-based geopolymer for removal of heavy metals from acidic solutions.

3) Investigate the feasibility and application of fly ash-based geopolymer as filtration media in fixed-bed column for removal of heavy metals.

4) Synthesize magnetic fly ash-based geopolymer and investigate its environmental applications.

1.4. Organization

This thesis consists of seven chapters and several appendices. Chapter 1 provides the research background, problem statement, and the research objectives. Chapter 2 presents a review of current literature on synthesis and characterizations of geopolymer, magnetic modification of geopolymer and its applications for heavy metals in wastewaters. Chapter 3 describes the synthesis method of geopolymers and the physical-chemical characterization and environmental impact results of Objective 1. Batch experimental studies on metal removal for Objective 2 are presented in Chapter 4. Chapter 5 describes the fixed-bed column studies using geopolymer as a filtration media for Objective 3. Chapter 6 investigates the synthesis of magnetic iron oxide geopolymer materials and its environmental applications (Objective 4). Chapter 7 summarizes the conclusions of the entire study, discusses the applicability of novel synthesized adsorbent materials, and provides recommendations for future work.

Appendix A presents the procedures and results of the physical-chemical characterization of the geopolymer.

Appendix B presents experimental data conducted with fly ash-based geopolymer for removal of metals in Chapter 3.

Appendix C presents experimental data of batch studies by fly ash-based geopolymer for removal of metals in Chapter 4.

Appendix D presents experimental data of fixed-bed column studies by fly ash-based geopolymer for removal of metals in Chapter 5.

Appendix E presents experimental data of magnetic fly ash-based geopolymer for removal of metals in Chapter 6.

1.5. References

Ahmaruzzaman, M. (2010). A review on the utilization of fly ash. *Progress in Energy and Combustion Science*, *36*(3), 327-363.

Al-Harahsheh, M. S., Al Zboon, K., Al-Makhadmeh, L., Hararah, M., & Mahasneh, M. (2015). Fly ash based geopolymer for heavy metal removal: a case study on copper removal. *Journal of Environmental Chemical Engineering*, *3*(3), 1669-1677.

Ariffin, N., Abdullah, M. M. A. B., Zainol, M. R. R. M. A., Murshed, M. F., Faris, M. A., & Bayuaji, R. (2017). Review on Adsorption of Heavy Metal in Wastewater by Using Geopolymer. In *MATEC Web of Conferences* (Vol. 97). EDP Sciences.

Davidovits, J. (2002). 30 years of successes and failures in geopolymer applications. Market trends and potential breakthroughs. In *Geopolymer 2002 Conference*, (Vol. 28, p. 29). Saint-Quentin, France; Melbourne, Australia: Geopolymer Institute.

Duxson, P., Provis, J. L., Lukey, G. C., & Van Deventer, J. S. (2007). The role of inorganic polymer technology in the development of 'green concrete'. *Cement and Concrete Research*, 37(12), 1590-1597.

Lin, P. C., Yu, C. C., Wu, H. T., Lu, Y. W., Han, C. L., Su, A. K., Chen, Y. J., & Lin, C. C. (2012). A chemically functionalized magnetic nanoplatform for rapid and specific biomolecular recognition and separation. *Biomacromolecules*, *14*(1), 160-168.

Zhang, H., Zhao, Z., Xu, X., & Li, L. (2011). Study on industrial wastewater treatment using superconducting magnetic separation. *Cryogenics*, *51*(6), 225-228.

Zhang, M., Zhang, H., Xu, D., Han, L., Niu, D., Tian, B., Zhang, J., Zhang, L., & Wu, W. (2011). Removal of ammonium from aqueous solutions using zeolite synthesized from fly ash by a fusion method. *Desalination*, *271*(1-3), 111-121.

Zhang, Y., & Liu, L. (2013). Fly ash-based geopolymer as a novel photocatalyst for degradation of dye from wastewater. *Particuology*, *11*(3), 353-358.

CHAPTER 2. LITERATURE REVIEW

2.1. Introduction

With rapid industrialization and lack of environmental enforcement in many countries, industrial wastes and wastewaters containing toxic organic compounds and heavy metals are increasingly released into the environment. To protect human health and the environment, desirable treatment systems are needed to remove pollutants from the contaminated water and wastewater effectively and reliably before they are discharged. Different technologies are available for different conditions with varying degree of effectiveness and cost. Adsorption technology is one of the effective methods for removal of pollutants in particular heavy metals. Researchers have developed different adsorbents to increase their effectiveness and reduce costs of treatment. This work studies an innovative material, fly ash-based geopolymer, and evaluates its environmental impacts. This material can be also modified to incorporate various properties, such as magnetic properties, to enhance pollutant removal and separation from wastewater after use. The overall goal of this dissertation is to develop a successful environmental-friendly product and understand the import operational parameters for effective heavy metals removal by geopolymer. The aim of this chapter is to review the current knowledge of environmental issue in water/wastewater treatment and effects of fly ash-based geopolymer, i.e. its synthesis methods, physical-chemical properties, potential for pollutant removal and magnetic modifications.

2.2. Environmental Issue and Methods

2.2.1. Heavy Metals Pollution

Drainage from mines and discharges from industrial activities may contain high concentrations of heavy metals. Some of these wastewaters may be discharged without proper treatment, which can directly impact the receiving waters such as river waters and groundwater

(EPA, 2002). Surface waters and groundwaters are also impacted by nonpoint sources pollutants contributed by human activities, where the chemicals leach into runoffs and groundwaters. Metals such as lead, cadmium, copper, arsenic, nickel, chromium, zinc and mercury have been recognized as hazardous heavy metals. Unlike organic wastes, heavy metals are non-biodegradable and they can be accumulated in living organisms, causing various diseases and disorders.

Removal of metal ions from wastewaters in an effective manner are desired globally. There are various treatment processes available for metal contaminated waste waters, such as, chemical precipitation, coagulation, extraction, ultra-filtration, biological uptake systems, electrolytic processes, reverse osmosis, oxidation or reduction followed by precipitation, membrane filtration, ion exchange, and adsorption. Many of these conventional methods for treating wastewater have not been widely applied on large scale due to their high cost of operation and secondary disadvantages such as production of large amounts of sludge. Adsorption has been found to have certain specific advantages as compared to other techniques in terms of initial cost, flexibility and simplicity of design, ease of operation and insensitivity to toxic pollutants. Adsorption can be used to concentrate a particular pollutant and recycle the pollutant, if needed.

2.2.2. Heavy Metals in Acid Mine Drainage

Acid mine drainage (AMD) is an unavoidable by-product of the mining and mineral industry, which is mainly caused by oxidation of sulfide minerals in the presence of water and oxygen (Langmuir, 1997). Acid mine drainage typically contains high concentrations of dissolved heavy metals and sulfate with a pH in the range of 2.5 to 6 (Kleinmann, 1990). For example, iron pyrite, FeS_2, is the most widespread of all sulfide minerals and can be found in many ore bodies. In the process of mining operations, particularly coal mining, iron pyrite in the ore is exposed to

air and water, causing it to oxidize to sulfuric acid and ferrous iron. These dissolved ferrous iron can be oxidized by dissolved oxygen to ferric iron which is dependent on acidity of water. When below the pH 4 and in presence of iron oxidizing bacteria, the rate of oxidation is greatly accelerated. On the other hand, the reaction sequence is rate limited-step when pH above 4 and without iron-oxidizing bacteria (Weiner, 2012). The generated ferric iron can further oxidize pyrite, where ferric iron is reduced back to ferrous iron and more acidity is released. The ferric iron precipitates out as insoluble ferric hydroxide causing more protons to be released into solution. The ferric hydroxide coats the streambeds with the yellow-orange deposits known as *yellowboy*. The overall reactions scheme for generation of acid mine drainage by pyrite oxidation is shown in Figure 2-1.

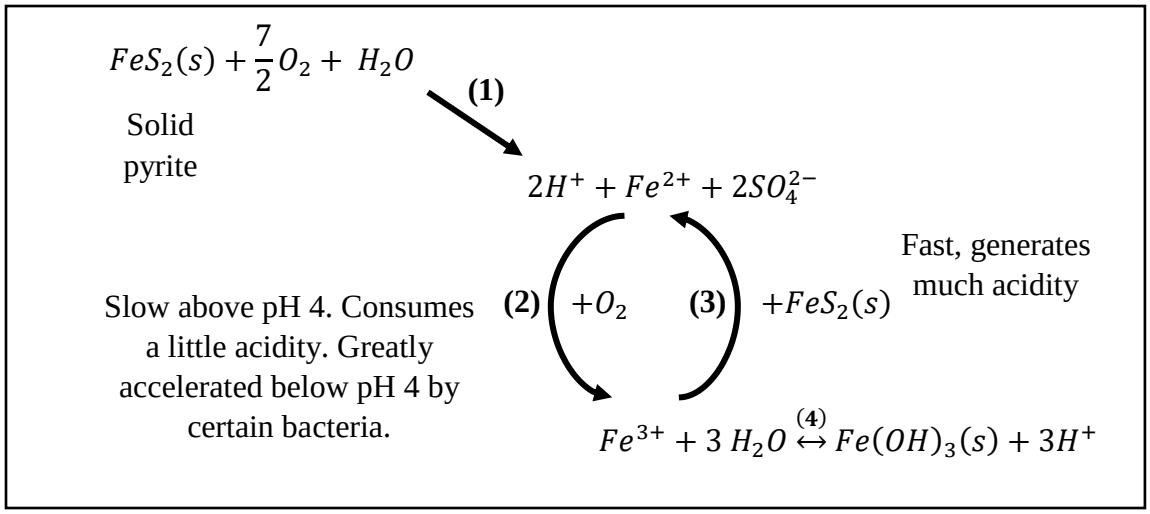

Figure 2-1. Reaction scheme of generation of acid mine drainage by pyrite oxidation (Weiner, 2012)

Similar to pyrite oxidation, other metal sulfides, such as *CuS* (covellite), *ZnS* (sphalerite), *PbS* (galena), and $CuFeS_2$ (chalcopyrite), can be oxidized to dissolved cations, but does not generate significant amounts of acidity. For example,

$$CuS(s) + 2O_2 \leftrightarrow Cu^{2+}(aq) + SO_4^{2-}(aq)$$

$$ZnS(s) + 2O_2 \leftrightarrow Zn^{2+}(aq) + SO_4^{2-}(aq)$$

$$PbS(s) + 2O_2 \leftrightarrow Pb^{2+}(aq) + SO_4^{2-}(aq)$$

$$CuFeS_2(s) + 4O_2 \leftrightarrow Cu^{2+}(aq) + Fe^{2+}(aq) + 2SO_4^{2-}(aq)$$

Also, the ferric iron can oxidize these minerals, which is similar to its oxidation of FeS_2, releasing metal cations into water without generating acidity. Apparently, the constituents of AMD are highly variable depending on many factors, such as location, mineral types, weather, that influence its formation (Force, 1989).

As a result, acid mine drainage contains high concentrations of acid and dissolved metals. Those toxic mixtures can flow and pollute groundwater, streams and rivers. The concentration of heavy metals and pH of several AMDs from different locations are given in Table 2-1.

Table 2-1. Metal concentration (mg/L) and pH for different locations in the world

Constituent	Tinto river [a]	Odiel River [a]	South African gold mine [b]	Silver Peak mine [c]	Afon Goch [d]	Lake Hope [e]	Avoca Mine [f]	Elizabeth Copper Mine [g]
pH	2.89	3.76	1.65	3.7	2.4	5.8	2.67	3.26
Fe	123	4.9	942	140	193.24	40.4	996	123
Cu	15.7	5.4	1.8	35.9	19.23	11.6	185	4.6
Mn	6.8	8.1	113	7.35	10.8	832	N/A	2.6
Zn	24.1	11.5	10.1	362	30.03	9.8	229	1.47
As	147	4	N/A	30.6	N/A	N/A	0.223	N/A
Ba	15	21	0.075	N/A	N/A	N/A	N/A	0.01
Cd	107	52	0.26	11	N/A	< 0.001	0.916	0.011
Co	476	269	1.94	N/A	N/A	0.7	N/A	0.147
Cr	11	5	4.85	N/A	N/A	5.9	N/A	N/A
Li	113	58	N/A	N/A	N/A	N/A	N/A	0.031
Ni	135	145	5.75	0.37	N/A	3.7	N/A	0.038
Pb	121	45	0.349	0.87	N/A	0.6	N/A	0.0006
Sr	257	114	1.77	N/A	N/A	N/A	N/A	0.46
SO_4	1221	643	6305	N/A	N/A	45	10203	1200

([a]: Nieto et al., 2007; [b]: Feng et al., 2000; [c]: Archer et al., 2004; [d]: Boult et al., 1994; [e]: López, et al., 2010; f: Gray, 1998; g: Balistrieri et al., 2007)

Table 2-1 clearly shows the wide variation of mineral content and dissolved metal ions in AMD as a result of the different geological properties of mining areas. The released heavy metals

from the mines in acid mine drainage can persist in natural ecosystems for an extended period and accumulate in successive levels of the biological chain, which can cause acute and chronic diseases. Cadmium, copper, and lead are metals of particular concern because of their severe toxicity to plants, animals and human (Dudka and Adriano, 1997).

In addition, high acidity in mine drainage can have direct and indirect and devastatingly effect on the physiological functions of aquatic organisms. Most of freshwater lakes, streams, and ponds are maintained at pHs between 6 – 8, which is safe for fish and for maximum productivity (Simate & Ndlovu, 2014). Therefore, desired long-term environmental sustainability will require effective and efficient technology that can minimize the negative impacts of AMD.

2.2.3. Treatment of Heavy Metals in AMD

A lot of research has been dedicated to the development of remediation techniques consisting of source control and migration control of AMD (Johnson, & Hallberg, 2005). Source control directly prevent the formation of AMD by removal of oxygen and/or water from the system, to eliminate or minimize metal sulfides oxidation. For example, removing water by pumping before it contacts pyrite minerals could minimize the formation of acidic products. However, this method has proven to be practically difficult. Instead migration controls are considered as a major approach for minimizing the transport of AMD. Migration treatment technologies are divided into two categories: active and passive treatment. For active treatment, it is more appropriately used in mines under operation, since fast remediation of enormous amounts of water is needed. Passive treatment is a more realistic treatment for abandoned mine sites in the absence of any accountable entity and the remote area requires the use of a long lasting, low cost and environmentally sustainable treatment option.

Active treatment is a widespread method such as the addition of a chemical – neutralizing agent to AMD, i.e. alkaline materials, which can raise the pH, accelerate the rate of chemical oxidation of ferrous iron and cause the majority of dissolved metals to precipitate out as hydroxides or carbonates (Coulton et al., 2003). Some alkaline materials used in the treatment of AMD are presented in Table 2-2.

Table 2-2. Chemical – neutralizing agent for AMD active treatment (Coulton et al., 2003)

Agent	Chemical	Advantages	Disadvantages
Limestone	$CaCO_3$	Simple operation, low cost, and formation of a dense, easily handled sludge	Slow reaction, loss in efficiency due to limestone chips are easily coated rendering them useless; Periodic replacement is necessary
Hydrated lime	$Ca(OH)_2$	Economically favorable alkaline reagent	Require mixing operation, difficult to handle as a slurry
Pebble Quick Lime	CaO	Very reactive	Require hopper and feeder
Soda Ash Briquette	Na_2CO_3	Reactive, effective for treating small AMD flows in remote areas	Expensive, poor settling properties of the sludge
Caustic soda	NaOH	Very highly soluble, relatively easy to handle, effective for treating low flows in remote locations	High cost, the dangers involved with handling the chemical, poor sludge properties, and freezing problems in cold weather
Ammonia	NH_3 or NH_4OH	Very reactive and soluble	Difficult and dangerous to use and can affect biological conditions downstream from the mining operation; require permission and monitoring
Fly ash	CaO, SiO_2, Al_2O_3	Low cost	Efficiency varies with different product

In addition to precipitation, other techniques of active treatment include adsorption (Fu and Wang, 2011; Motsi et al., 2011) and ion exchange (Gaikwad et al., 2010; Feng et al., 2000). Even though active treatment is the most common method used to treat AMD due to its simple operation

and effective removal of heavy metals and acidity, it has several drawbacks such as high initial capital costs, expensive chemicals used in process, and the disposal of metal laden sludge.

Compared to active treatment, passive treatment option as an economic alternative does not require continuous chemical inputs but are subjected to high cost of sludge disposal (Johnson and Hallberg, 2005). Some common passive systems include constructed wetlands, limestone drains, vertical flow system, and permeable reactive barrier (PRB) (Jamal, 2015). Passive treatment has lower environmental impacts since environmentally relevant materials are used during the process, such as alkaline industrial by-products, neutrally available resources, plant and animal-based wastes (Kefeni et al., 2017). However, there are several drawbacks, such as requiring longer process time for effective remediation of AMD, investment and maintenance costs, and initial construction costs (Kefeni et al., 2017; Jamal, 2015).

The metals seldom precipitate directly in solution if the concentrations are low and are far below the solubility limit. In this case, metals tend to co-precipitate, e.g. metal ion precipitate in the presence of other metal precipitates or coalesce into solid phase of substances and are removed from solution. Also, the behavior of different metal ions are depended on their solubility, valence state, tendency to form complexes with other substances, and affinity for the solid phases formed from the precipitation of the major metal ions (Freeze & Cherry, 1979). Even when the major metals such as iron is precipitated out, other toxic metal ions may remain in solution that may continue to impact the water quality (Smith et al., 2001).

In order to meet all treatment goals, it is necessary to develop a treatment material or an AMD remediation structure that can not only reduce the acidity and improve the pH of the water, but also provide adequate removal of metals on the site.

2.3. Adsorption Technology

Adsorption is a phase transfer process that is widely used to remove substances from fluid phases (gases or liquids). In water treatment, adsorption is a proven technology for efficient removal of organic and inorganic pollutants.

2.3.1. Adsorption Processes in Water/wastewater Treatment

Adsorption processes are widely used in water/wastewater treatment, and they are either a batch or fixed bed process.

In the batch process, the adsorbent is mixed with a solution of adsorbate (pollutants). The mixture is mixed for a predetermined time and the adsorbent separated from the solution by sedimentation and/or filtration for disposal or reuse (Crittenden and Thomas, 1998). Sufficient time is required to reach the steady state conditions. Either powdered or granular adsorbents are used to form slurry to allow adequate dispersion of the adsorbent. After separation of the fluid from the adsorbent, the fluid can be treated further with another fresh batch of adsorbent.

Fixed-bed systems are carried out with the solution moving through a stationary bed of adsorbent particles. Advantages of a fixed bed system is that the adsorbent can be easily be separated, if needed, form the fluid, the column can be simple and minimal attrition of adsorbent occurs. However, despite the apparent simplicity of fixed beds, the fixed bed processes are difficult to design accurately because of the progress of the mass transfer zone (MTZ) which increases the complexity of the design. Several short-cut design techniques have been proposed such as Rapid Small Scale Column Test (RSSCT).

2.3.2. Adsorbents and Characterization

Currently, activated carbon is the most popular engineered adsorbent which is widely used to remove heavy metal and organic substances from different types of water such as drinking water,

wastewater, groundwater, and landfill leachate. Other adsorbents (such as zeolite, silica gel, and activated alumina) are less often applied, because their application are restricted to special adsorbates or types of water or wastewaters. Typical requirements for commercial adsorbents include high porosity and high internal surface, hydrophobic chemical structure, thermal stability unaffected by a cyclic regeneration, mechanical stability during handling, and low cost for acquisition and eventually disposal of adsorbents (Worch, 2012). As an example, activated carbon can be applied as powdered activated carbon (PAC) in slurry reactors or as granular activated carbon (GAC) in fixed-bed column. The particle sizes of powdered activated carbons are in the medium micrometer range (< 200 μm), whereas the GAC particles have diameters in the lower millimeter range (0.4 – 5 mm) (Baker et al., 2000).

Since adsorption is a surface process, the surface area of the adsorbent is of great importance for the extent of adsorption and therefore a key quality parameter. Also, the porosity of the materials allows for internal pore surfaces which will further contribute to the overall surfaces area. In contrast, the external surface is typically less than 1 m^2/g and therefore of minor relevance. As an example, the external surface of powdered activated carbon with a particle density of 0.6 g/cm^3 and a particle radius of 0.02 mm has only 0.25 m^2/g (Worch, 2012).

Adsorbents used for water treatment are either of natural origin or the result of an industrial production and/or activation process. Typical natural adsorbents are clay minerals, natural zeolites, and oxides. Engineered adsorbents can be classified into carbonaceous adsorbents, polymeric adsorbents, silica or alumina oxidic adsorbents, and zeolite molecular sieves. In general, natural adsorbents have much smaller surface areas than highly porous engineered adsorbents.

The properties of several engineered adsorbents are shown in the Table 2-3.

Table 2-3. Properties of engineered adsorbents (Buekens and Zyaykina, 2001)

Adsorbent	Nature	Average pore diameter, nm	Particle porosity, %	Surface area, m^2/g	Sorption capacity, g/g
Activated carbon	Hydrophobic, amorphous	1-4	40-85	200-1200	0.3-0.7
Molecular sieve zeolites	Hydrophilic, crystalline	0.3-1	20-50	600-700	0.12-0.42
Polymeric adsorbents	Hydrophobic, amorphous	4-25	40-60	80-700	0.45-0.55
Silica gel	Hydrophilic, amorphous	2-5	47-71	300-850	0.35-0.5
Activated alumina	Hydrophilic, amorphous	4-14	50	320	0.1-0.33
Molecular sieve carbon	Hydrophobic, structured	0.3-0.6	35-50	400	0.2-0.5

Activated carbon produced from carbonaceous material are the most widely applied adsorbents in water treatment due to high surface area (200 – 1200 m^2/g). Polymeric adsorbents made by copolymerization of nonpolar or weakly polar monomers show adsorption affinities due to large pore size (4 – 25 nm), but the high material costs and costly regeneration have prevented a broader application to date. Molecular sieve zeolites and silica or alumina oxides are adsorbents with stronger hydrophilic surface properties, which can contribute to removal of polar, in particular ionic, compounds. However, engineered adsorbents are relatively expensive. In recent decades, an increase interest in using wastes and by-products as alternative low-cost adsorbents (LCAs) can be observed.

Currently, there is a huge amount of solid waste materials and by-products generated from industrial activities. Some of these materials have not been utilized and are dumped in landfills when it can be available for almost free of cost. These solid waste materials can be made into low-cost adsorbents with some advantages such as partial reduction of the volume of waste materials disposed and reduce pollution of wastewater at a reasonable cost (Ahmaruzzaman, 2010). Thus, a

number of industrial waste materials have been investigated with or without treatment as adsorbents for the removal of pollutants from water and wastewaters.

Many investigations have been reported in the literature on the utilization of fly ash for adsorption of different pollutants in an aqueous solution. The results of removal of heavy metals and organics from wastewater are presented in Table 2-4. Also, other industrial wastes, such as blast furnace slag, activated slag, and modified basic oxygen furnace slag, are listed in Table 2-4.

Panday et al. (1985) used fly ash without any pretreatment for the removal of Cu^{2+} and found that adsorption followed the Langmuir model. Sen and Arnab (1987) investigated the potential of fly ash for Hg(II) removal and found that adsorption capacity was 2.82 mg/g. The removal of lead and copper from aqueous solution by fly ash under various experimental conditions, such as contact time, pH and temperature, were investigated by Alinnor, 2007. The adsorption capacities of Pb^{2+} and Cu^{2+} on fly ash were found to increase at higher pH and lower temperature. The main mechanisms involved in the removal of heavy metal ions form solution were adsorption at the surface of the fly ash and precipitation. Li et al. (2009) used iron-abundant fly ash as a novel adsorbent for arsenic (V) removal from wastewater. The inherent iron in the fly ash was rearranged and loaded on the surface of the fly ash by using a dissolution and precipitation process. The results showed that the adsorption capacity for arsenic removal was 19.46 mg/g.

Wang et al. (2005a) investigated low calcium fly ash for methylene blue adsorption in wastewater. Results showed that low calcium fly ash exhibits adsorption capacity (2.5×10^{-4} mol/g) that is higher than raw fly ash (5×10^{-5} mol/g). Wang et al. (2005b) studied the heat treatment and chemical treatment of fly ash (1.4×10^{-5} mol/g) and found that heat treatment reduces the adsorption capacity of fly ash (2.5×10^{-6} mol/g) and nitric acid treatment resulted in an increase in adsorption capacity of fly ash (2.5×10^{-5} mol/g). Wang and Zhu (2005) studied fly ash samples modified by

NaOH solution and sonochemical treatment on (methylene blue) adsorption in aqueous solution. They found that sonochemical treatment of fly ash can significantly increase the adsorption capacity depending on the concentration of NaOH and treatment time. The untreated fly ash and the sonochemically treated sample exhibited adsorption capacities of 6×10^{-6} mol/g and 1.2×10^{-5} mol/g at 30 ◦C. Viraraghavan and Ramakrishna (1999) investigated the use of coal fly ash from the Shand power plant in Canada for removal of dyes from wastewater. The negative values of free energies indicate the feasibility and spontaneous nature of the process, and the positive heats of enthalpy suggested the endothermic nature of the process. Other studies using fly ash for dyes removal include Rao & Rao (2006), Vasanth (2003), Dizge et al. (2008), Ramakrishna and Viraraghavan (1997), and Hsu (2008).

Table 2-4. Application of industrial wastes as adsorbent in pollutants adsorption

Adsorbent	Adsorbate	Adsorption capacity, mg/g	Reference
Fly ash	Cu^{2+}	1.39	Panday et al., 1985
Fly ash	Hg^{2+}	2.82	Sen and Arnab, 1987
Fly ash	Pb^{2+}	5.5 - 22	Alinnor, 2007
	Cu^{2+}	4.5 - 21.5	
Fly ash	As^{5+}	19.46	Li et al., 2009
Unburned carbon	Methylene blue	0.08	Wang et al., 2005a
Fly ash		0.016	
FA treated with HNO_3	Methylene blue	7.996	Wang et al., 2005b
FA heated at 800 ºC		4.478	
FA after sonochemical treatment with NaOH	Methylene blue	5.12 – 12.79	Wang and Zhu, 2005
Fly ash	Methylene blue	4.61	Viraraghavan and Ramakrishna, 1999
Fly ash	Methylene blue	3.07	Rao, V. B., & Rao, S. R. M.,2006
Fly ash	Methylene blue	2.85	Vasanth, 2003
Coal fly ash	Reactive Yellow 84	37.26	Dizge et al., 2008
	Reactive Blue 19	133.69	
Fly ash	Acid red 91	1.46	Ramakrishna and Viraraghavan, 1997
	Acid Blue 9	4.31	
Coal fly ash	Acid red 1	92.59	Hsu, 2008
Coal fly ash - NaOH		12.66	

2.3.3. Adsorption Isotherms

Generally, solid-liquid adsorption system is dependent on equilibrium isotherm models. The mechanistic models are based on the mechanism of metal ion adsorption and are able to explain and predict the observed experimental behavior.

For the single solute adsorption systems, Langmuir and Freundlich models are found to be the most widely used isotherm models reported in the literature. The Brunauer–Emmett–Teller (BET) model describes multi-layer adsorption at the adsorbent surface while it assumes that the Langmuir isotherm applies to each layer.

All of these models can provide information on the adsorption capacity of metals from their aqueous solution, which were described as follows:

- Langmuir model (Langmuir, 1917):

$$q_e = \frac{q_m K_L C_e}{1 + K_L C_e}$$

where q_e is the equilibrium metal sorption capacity (mg/g); C_e is the equilibrium solute concentration in solution (mg/L); q_{max} and K_L are the Langmuir constants (L/mg) related to maximum sorption capacity (monolayer capacity) and bonding energy of adsorption (or "affinity"), respectively.

The Langmuir isotherm assumes that adsorption happens at specific homogeneous sites within the adsorbent, and there is no interaction between the adsorbate molecules.

- Freundlich model (Freundlich, 1906):

$$q_e = K_F C_e^{1/n}$$

where K_F is the adsorption equilibrium constant, representative of the sorption capacity; and n is a constant indicative of adsorption intensity. K_F and n are indicative of the extent of the adsorption and the degree of non-linearity between solution concentration and adsorption, respectively.

The Freundlich isotherm is an empirical equation used to describe heterogeneous systems.

- BET model:

$$q_e = \frac{q_s C_{BET} C_e}{(C_s - C_e)[1 + (C_{BET} - 1)(C_e/C_s)]}$$

where C_{BET}, C_s, q_s and q_e are the BET adsorption isotherm (L/mg), adsorbate monolayer saturation concentration (mg/L), theoretical isotherm saturation capacity (mg/g) and equilibrium adsorption capacity (mg/g), respectively (Brunauer et al., 1938; McMillan & Teller, 1951).

2.3.4. Fixed-bed Column

The dynamic column adsorption method allows the solute solution to flow continuously through a fixed bed packed with the adsorbent. The bed height, the rate of flow and the concentration of the solute can be varied, and column adsorption can be monitored by continuously measuring the concentrations of the solute in the eluent with time or volume flowing out of the column.

The experiment normally aims at determination of the breakthrough point at which the concentration of the solute in the eluent becomes equal to the initial concentration and the adsorbent bed becomes saturated with the solute.

Typical breakthrough curves are shown in Figure 2-2 (Tchobanoglous et al., 2003, Ahamad and Jawed, 2011).

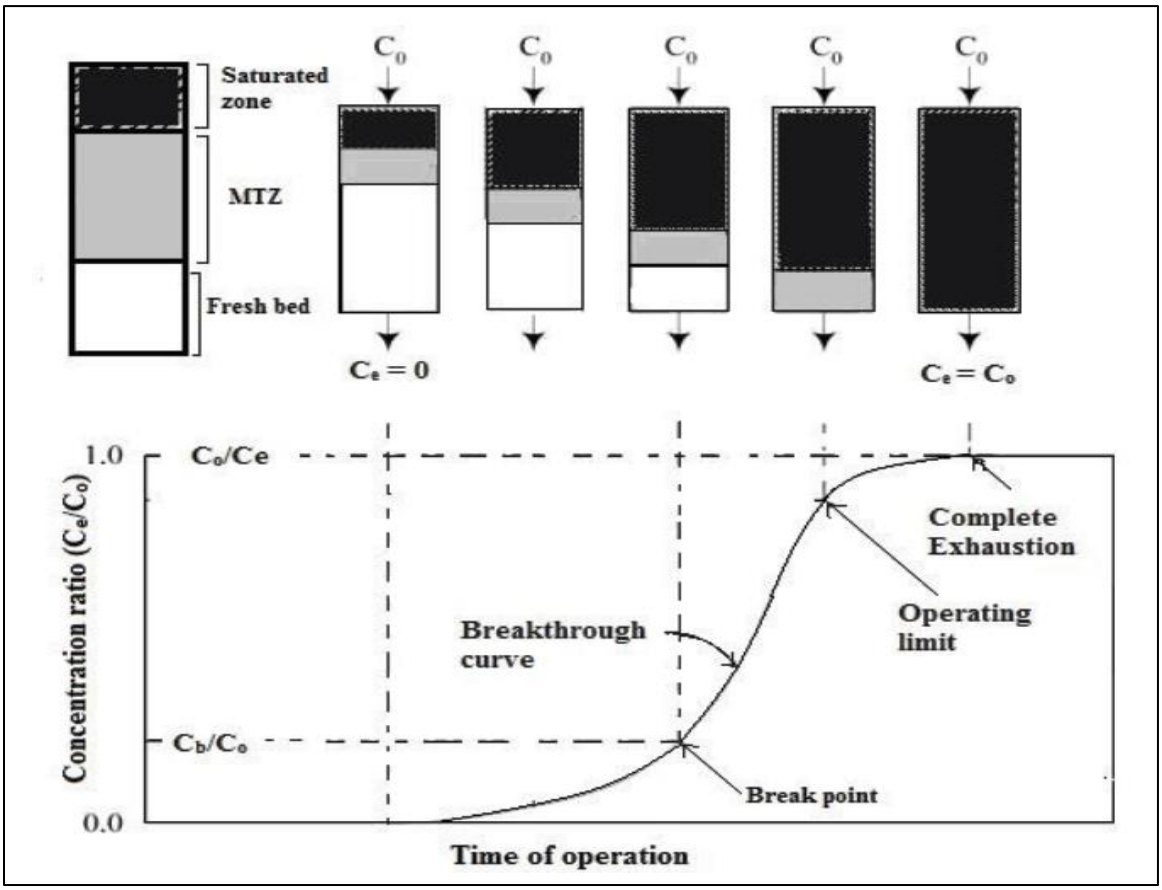

Figure 2-2. Typical breakthrough curve for column study (Tchobanoglous et al., 2003)

At first, the adsorbent in the column is fresh with all its adsorption sites. As time passes, some of the adsorption sites are used up and concentration in the effluent rises with time. The efficiency of the column can be explained by means of the breakthrough curves. A breakthrough curve is obtained by plotting column effluent concentration versus volume treated or time of treatment (Moreno-Piraján et al., 2006). The shape of the graph may vary considerably for different situations. However, in general an S-shaped breakthrough curve is obtained. Breakthrough is deemed to have occurred at some time t_b, breakthrough time, when the concentration of the adsorbate leaving the bed increases to an arbitrarily defined value, *Ce*, breakthrough concentration, which is often the minimum detectable or maximum allowable concentration of the component to

be removed. In other words, the breakthrough point can be defined as the point at which the effluent concentration increases rapidly (Nidheesh et al., 2012).

Breakthrough capacity, exhaustion capacity, degree of column utilization and mass transfer zone (MTZ) are the important features of the breakthrough curves. The breakthrough capacity is defined as the mass of sorbate removed by the sorbent bed at breakthrough concentration or breakthrough time. The exhaustion capacity is defined as the mass of the sorbate removed by unit weight of the sorbent at saturation point and the degree of column utilization is defined as the mass sorbed at breakthrough point divided by the mass sorbed at complete saturation. The mass transfer zone (MTZ) in a packed bed system is defined as the zone of the packed column where the active adsorption happens (Patel, 2019).

In packed-bed column, since the feed solution is introduced through the inlet of the column, the solute is sorbed most rapidly and effectively by the upper few layers of the fresh sorbent during the initial stages of the operations. The mass transfer zone is concentrated near the top or influent end of the column. As the polluted feed water continues to flow into the column, the top layers of the sorbent become practically saturated or in other words becomes exhausted with the incoming solute and then the mass transfer zone starts moving downward to a region of fresher sorbent in the column. When the MTZ moves across the adsorbent bed, it leaves behind a section of adsorbent bed, which is completely exhausted, and in front of MTZ, there exists only fresh adsorbent. The MTZ will continue to move through the packed bed until it hits its breakthrough point, when a preset concentration of the adsorbate in the effluent is reached. When breakthrough occurs, the adsorbent will need to be replaced to keep excessive concentrations of impurities out of the effluent.

Several models have been proposed to describe the breakthrough curves of fixed bed adsorption process. These models can be complex, requiring extensive computation and needing thorough verification. For this purpose, the essential requirements are: (a) accurate and available fundamental data; and (b) the number and importance of the assumptions and approximations that have been made to arrive at the data. For the simplest case, in which many simplified assumptions and approximations are made, the solution may be analytical. The events occurring in the MTZ during adsorption are,

- Transfer of adsorbate molecules from the bulk fluid to the solid surface by convection or diffusion across the fluid film which is external to the solid surface.
- The adsorbate penetrates the fluid film through surface diffusion mechanisms, and adsorb onto the internal surface with release of the heat of adsorption.

An additional complexity during sorption is that the flow through a packed bed may not be uniform across its entire cross-sectional area. This may be due to channeling of the fluid at the wall or because of temperature gradients created when the heat of adsorption is released.

Empty bed contact time (EBCT) method is generally used by the water industry for designing large-scale columns. In this method, numbers of pilot scale columns in series are used to obtain breakthrough curves with desired flow rates. Three or more columns are usually used to represent different bed depths and different contact times. The empty bed contact time (EBCT) is defined as,

$$EBCT = \frac{bed\ volume}{flow\ rate}$$

The range of EBCT in fixed-bed adsorption process was normally ranged from 5 to 60 min, in particular for granular activated carbon (Crittenden et al., 2012).

Generally, the smaller, scaled-down fixed bed can be used to predict the performance of full-scale column. It is called rapid small-small column test (RSSCT), which own several advantages including:

- RSSCT can be conducted in a fraction of the time required to conduct pilot studies.
- It does not require extensive isotherm or kinetic studies.
- RSSCT requires a small volume of water for evaluation.
- Instead of pilot studies, RSSCT significantly reduces the time and cost of a full-scale design.

Thus, the RSSCT test can be used to evaluate important design variables such as EBCT. The relationship between the empty bed contact time of the full-scale column ($EBCT_{LC}$) and the empty bed contact time of rapid small-scale column ($EBCT_{SC}$) is obtained by the following equation (Crittenden et al., 2012):

$$\frac{EBCT_{SC}}{EBCT_{LC}} = \frac{d_{SC}^2}{d_{LC}^2} = \frac{t_{SC}}{t_{LC}}$$

where d_{SC} and d_{LC} are the diameters of the columns, and t_{SC} and t_{LC} are the operating times. And it is assumed the intra-particle pore and surface diffusivities of adsorbent particles are identical.

2.3.5. Column Analysis and Models

The information obtained from column analysis is important for estimating the probable column applications. The breakthrough curves were obtained from the experimental data and prepared by plotting the values of C/C_0 ratio as a function of the pore volume, effluent volume (V_{eff}, L) or time (t, min) for a given bed height. These parameters could determine the feasibility of the fixed-bed column. Thus, it is necessary to calculate the column parameters by mathematical analysis (Hasan et al., 2009).

The total mass of adsorbed metal (m_{ads}, mg) in column for a given influent metal concentration and flow rate was calculated the area (A) under the mass transfer curve (or above the breakthrough curve) which is obtained by integrating the adsorbed metal concentration (C_{ads}, mg/L) by functioned with time as following equation:

$$m_{ads} = \frac{QA}{1000} = \frac{Q}{1000} \int_{t=0}^{t=t_{total}} C_{ads} dt$$

The uptake capacity (q_0, mg/g) was calculated by the known amount of the geopolymer particles (m_s, g) packed in column using equation:

$$q_0 = \frac{m_{ads}}{m_s}$$

In order to determine the maximum adsorption capacity of column process, various models have been developed to predict the dynamic behavior of the fixed-bed column. In this study, breakthrough curves were analyzed using three models to characterize the adsorption of heavy metals in a fixed bed column, which include the Bohat-Admas's model (Bohart & Adams, 1920), Thomas model (Thomas, 1944), and Yan model (Yan et al., 2001).

- Bohat-Admas model

The Bohart-Admas model was proposed by Bohart and Adams in 1920 for design of the adsorption column. The Bohart–Adams model has a great significance in terms of its simplicity. The basic assumptions of this model is that intra-particle diffusion and external mass resistance are negligible, and that adsorption kinetics is controlled by the surface chemical reaction between the solute and the adsorbent. Although these assumptions are usually not validate in real systems, it is easy to make some simplifications from this model that lead to the equations showed as below. This simple equation can describe the breakthrough curves with accuracy in most of the cases, and

also can provide important system parameters such as rate constant, uptake capacity, etc... Moreover, it can be used to predict the service time of the column for the scale up of the experiments. (Lodeiro, et al., 2006)

$$\ln\left(\frac{C_0}{C_t}\right) = k_{BA}C_0 t - k_{BA}C_{BA}\frac{H}{v}$$

where C_0 is initial solute concentration (mg/L), C_t is effluent solute concentration (mg/L), k_{BA} is rate constant (mL/mg min), C_{BA} is removal capacity (mg/L), H is bed depth (cm), v is linear flow velocity (cm/min) and t is service time (min).

The removal capacity q_{BA} in mg/g is calculated as following equation:

$$q_{BA} = \frac{C_{BA}BV_s}{m} = \frac{C_{BA}}{\rho}$$

where q_{BA} is removal capacity (mg/g), BVs is fixed bed volume (L), m is mass of the bed (g) and p is apparent density of the adsorbent in the fixed bed (g/L).

The values describing the characteristic operational parameters of the column (k_{BA} and q_{BA}) can be determined from the plot of $In\ (C_0/C_t)$ versus t at a given bed depth, initial concentration and flow rate through the column.

- Thomas model

Thomas model is one of the most general methods among these models, and is applied to the experimental data of the column studies for the evaluation of the breakthrough results. This model assumes that the adsorption isotherm and kinetics obey from Langmuir model and second order kinetics, respectively. In addition, it suggests that the sorption is not limited by the chemical reaction and is controlled by the mass transfer at the interface (Ghasemi et al., 2011). The linearized form of the Thomas model is expressed as (Biswas & Mishra, 2015):

$$\ln\left(\frac{C_0}{C_t}-1\right)=\frac{k_{Th}q_{Th}m}{Q}-k_{Th}C_0t$$

where k_{Th} is the Thomas kinetic coefficient (mL/min mg), t is the total flow time (min), and Q is the volumetric flow rate (mL/min). Adsorption capacity and mass of the adsorbent are denoted as q_{Th} (mg/g) and m (g). Plot of $ln\ [(C_0/C_t)-1]$ versus t gives the value of k_{Th} and q_{Th}.

- Yan's model

Yan model is an empirical model which is frequently used to describe the adsorption process in a fixed-bed system. The mathematical description of this model is given as:

$$\log\left(\frac{C_e}{C_0-C_e}\right)=a\log(V)-a\log\left(\frac{q_Y m_s}{C_0}\right)$$

The model parameters a, and adsorption capacity, q_Y can be estimated by non-linear fitting to the experimental data of breakthrough curves as presented as:

$$\frac{C_e}{C_0}=1-\frac{1}{1+\left(\frac{V_{eff}C_0}{m_s q_Y}\right)^a}$$

Even if Yan model can generally describe the complete breakthrough curves with great accuracy, the model has an empirical parameter a, which is specific to the experimental conditions (Lodeiro, et al., 2006). Thus, it cannot be used to scale up the system, but an indicator to estimate the properties of the column and to compare the parameters with other models.

2.4. Fly Ash-based Geopolymer

Davidovits (1988; 1994) proposed that an alkaline liquid could be used to react with the silicon (Si) and the aluminum (Al) in a source material of geological origin or in by-product materials such as fly ash and rice husk ash to produce binders. Because the chemical reaction that

takes place is a polymerization process, he coined the term 'Geopolymer' to represent these binders.

Geopolymers are members of the family of inorganic polymers. The chemical composition of the geopolymer material is similar to natural zeolitic materials, but the microstructure is amorphous. The polymerization process involves a substantially fast chemical reaction under alkaline condition on Si-Al minerals, that results in a three-dimensional polymeric chain and ring structure consisting of Si-O-Al-O bonds (Davidovits, 1994). A schematic diagram of typical geochemical reactions associated with mineral polymer (polysialate) and geopolymer formation is provided in Figure 2-3.

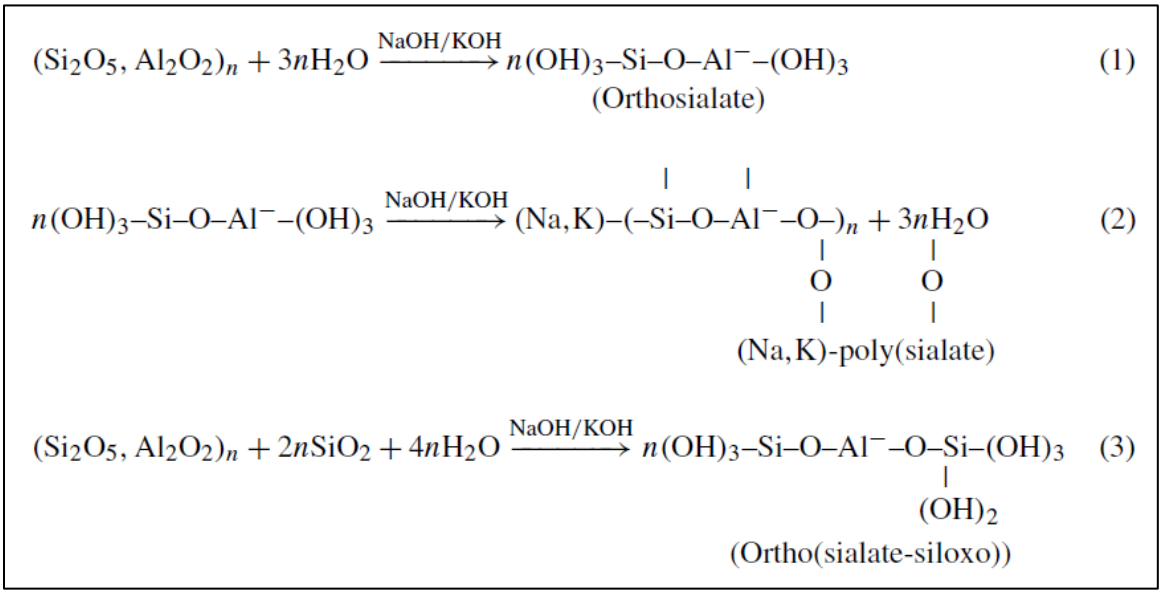

Figure 2-3. Schematic diagram of geopolymerization reactions (Davidovits, 1991).

There are two main constituents of geopolymers, namely the source materials and the alkaline liquids. The source materials for geopolymers based on alumina-silicate should be rich in silicon (Si) and aluminum (Al). These could be natural minerals such as kaolinite and clays. Alternatively, by-product materials such as fly ash, silica fume, slag, rice-husk ash, and red mud,

could be used as source materials. The choice of the source materials for making geopolymers depends on factors such as availability, cost, type of application, and specific demand of the end users.

Among the by-product materials, fly ash and slag are commonly used to be potential source materials for making geopolymers. Because of its high reactivity that comes from its finer particle size, fly ash is a more favorable source material than slag. Moreover, low-calcium fly ash is more desirable than slag for geopolymer feedstock material. Some low-calcium fly ash with chemical composition are listed in Table 2-5.

Table 2-5. Examples of chemical composition of precursor and its synthesized geopolymer

Oxide Composition (%)	Raw Ash	Geopolymer	Raw Ash	Geopolymer
Si	50.73	39.90	42.03	51.15
Al	28.87	19.70	27.51	28.23
Fe	11.93	7.50	4.37	4.78
Ca	1.73	2.43	3.42	3.37
Mg	1.39	1.13	0.48	0.53
K	0.74	1.08	1.66	1.67
Na	0.30	11.72	0.26	4.70
Ti	1.41	0.50	1.09	0.94
S	0.35	0.25	--	--
L.O.I	2.53	14.69	19.19	4.63
Reference	Al-Zboon et al., 2011; Al-Harahsheh et al., 2015		Zhang and Liu, 2013	

The alkaline liquids are from soluble alkali metals that are usually sodium or potassium based. The most common alkaline liquid used in geopolymerization is a combination of sodium hydroxide (NaOH) or potassium hydroxide (KOH) and sodium silicate or potassium silicate.

More recently, fly ash has been used as a component in geopolymers, where the reactivity of the fly ash glass is used to generate a binder comparable to a hydrated Portland cement in appearance and properties but with dramatically reduced CO_2 emissions (Duxson et al., 2007).

In future, the binders activated by alkalis may offer the possibility to process inorganic wastes because the properties of the bodies on the basis of binders activated by alkalis are often better than those of the materials prepared on the basis of current Portland cements. For instance, the resistance to acids or the ability to immobilize heavy metals is improved.

2.4.1. Synthesis Method

The process of converting fly ash into geopolymers has been studied in many researches recently (Table 2-6). Distinct from group of ceramic materials, geopolymers are formed by a geopolymerization of aluminosilicate minerals in the presence of an alkali solution (sodium hydroxide and/or sodium silicate) at low temperatures (<100 °C) (Davidovits, 1991 and Xu and VanDeventer, 2000).

Palomo et al. (1999) used different types of alkaline liquid to form geopolymer. They found that use of sodium or potassium silicate solution can cause high reaction rate of geopolymerization, compared to the use of only sodium or potassium hydroxide solution. Xu and Van Deventer (2000) made alkaline activator by adding sodium silicate solution to the sodium hydroxide solution, and they found this mixed solution can improve the geopolymerization and sodium hydroxide solution has a higher extent of dissolution of aluminosilicate minerals than the potassium hydroxide solution.

The reaction of alkaline solution (NaOH and Na_2SiO_3) and aluminosilicate minerals (e.g. fly ash) results in the disintegration of bonds of the Si-O-Si type and in the subsequent formation of hydrates of alkaline calcium aluminosilicates similar to zeolites. The molar ratio (Ms) of SiO_2 to Na_2O, named “Modulus”, is an important factor in geopolymerization. It represents alkaline activator that can be adjusted by NaOH addition to the soluble Na_2SiO_3 (“water glass”) with value of Ms in a range 1.0 to 1.6 (Škvára et al., 2005).

In general, Class-C fly ash-based geopolymer was found to have a short setting time within 1-2 hours at room temperature (Rattanasak et al., 2011). High content of calcium in Class-C fly ash can hydrate rapidly and form calcium aluminum silicate hydrate (C-A-S-H) gel and calcium silicate hydrate (C-S-H) gel, and rapid formation of gel results in a short setting time and decreases the porosity (Geetha and Ramamurthy, 2013).

In addition, the high concentration of NaOH from activator can prolong the setting time by limiting the leaching of calcium and allows normal geopolymerization process to control the setting of geopolymer paste (Hanjitsuwan et al., 2014). Most of the studies focused on the effect of sodium (Na^+) and potassium (K^+) hydroxide solution used in geopolymerization reaction (Van Jaarsveld et al., 2002). The difference of NaOH and KOH used in activation process is that the extent of dissolution was higher when NaOH was used. The reason is that smaller size of Na^+ which can better stabilize the silicate monomers and dimmers present in the solution and enhance the minerals dissolution rate, compared to K^+ (Bakharev, 2006).

However, the dissolution of fly ash cannot be completed at a room temperature. Hardjito and Rangan (2005) found that the curing temperature increases from 30 to 50 ^oC, the reactivity of fly ash increases significantly, and the geopolymerization is almost complete when the curing temperature ranged from 60 to 90 ^oC.

In addition, Van Jaarsveld et al. (2003) found that fly ash with higher amount of CaO produced higher compressive strength, due to the formation of calcium-aluminate-hydrate and other calcium related crystals, especially in the early ages. Thus, small amount of slag, chitosan, fiber, and rice husk-bark ash can be added into mixture of geopolymer to improve the mechanical properties of fly ash-based geopolymer.

Table 2-6. Examples of synthesis methods and physical properties of fly ash-based geopolymer

Type of fly ash	Alkaline solution	Liquid to Fly ash ratio	Curing time	Temperature (°C)	28-day Compressive strength (MPa)	Particle size, μm	Pore size, nm	Reference
Class C	Na_2SiO_3 + NaOH (10 M)	--	48 hr	65	26.9-32.2	--	--	Rattanasak et al., 2011
Class C	9.5–14.0 M NaOH	0.3		25-28	20-23	--	--	Somna et al., 2011
Seeded FA	Na_2SiO_3 + NaOH (4, 8, and 12 M)	--	36 hr – 28 day	25-90	14.8-55.6	--	--	Bohlooli et al., 2012
Class F	Na_2SiO_3 + NaOH (5-12 M)	--	2 – 7 day	25-90	12.6-35.1	--	--	Riahi and Nazari, 2012
Class F	$Na_2SiO_3 \cdot 9H_2O$	0.11	1-27 day	25-60	20	120-425	3−10,000	Zhang and Liu, 2013
Class F	NaOH (14M)	0.75	--	105	--	<200		Al-Harahsheh et al., 2015
Class F	NaOH (14M)	0.8	1-3 day	25 - 105	--	<200		Al-Zboon et al., 2011
Class F	Na_2SiO_3 + NaOH (16M)	0.4	1-3 day	25-85	--	71-90	--	Muzˇek et al., 2014

2.4.2. Characterization

The compressive strength of fly ash-based geopolymer is mostly depending on alkali solution, Si/Al ratios, calcium content, curing conditions and the various additives. During the geopolymerization, the release of Si^{4+} and Al^{3+} from fly ash were affected by the type and concentration of the alkaline solution. High concentration of sodium hydroxide solution (greater than 10 M) can achieve the high compressive strength in an optimal range (De Vargas et al., 2011). In addition, Na_2SiO_3 solution is used with NaOH to increase the compressive strength (Criado et al., 2005). The Na_2SiO_3 helps with the formation of geopolymer gels and achieves a compact final fly ash-based geopolymer micro-structure.

The Si/Al ratios area determined by the source materials and alkali solution. High Si/Al ratios increase the amount of –Si–O–Si– bonds to get a higher compressive strength of fully condensed structural matrix of geopolymer, since the –Si-O-Si- bonds area stronger than –Si–O–Al– and –Al–O–Al– bonds. Calcium content can interfere with the gelation of silica and alumina in geopolymerization process and alter the microstructures of fly ash-based geopolymer and the compressive strength (Schmucker and Mackenzie, 2005). Also, longer curing time (6 hour to 28 days) can generate high compressive strengths of fly ash-based geopolymer. The higher temperature curing increases the compressive strength by removing water from the fresh geopolymer, which can cause the collapse of the capillary pores with a denser structure (Leung and Pheerapha, 1995). Usually, fly ash-based geopolymer can be cured at room temperature, and the compressive strength develops slowly and need prolonged curing time (Somna et al., 2011). However, Palomo et al. (1999) prolonged curing at higher temperatures (85 ^{o}C) to break down the granular structure of geopolymer. This resulted in the dehydration of the geopolymer and excessive shrinkage, which decreased the compressive strength.

Davidovits (2002) point that the use of Na_2SiO_3 or K_2SiO_3 with NaOH for the activation of fly ash can increase the Si/Al ratios of the geopolymer system, thereby leading to a more compact structure with higher compressive strength. Moreover, the presence of calcium in fly ash is beneficial for forming the amorphous C-S-H gel and C-A-S-H gel and decrease the porosity and obtains geopolymer with a higher compressive strength. Similar results were found by Oltulu & Şahin (2013).

In addition to increase in compressive strength, the fly ash-to-NaOH ratio has influence on adsorption capacity efficiency. The lower fly ash-to-NaOH ratio results in lower adsorption capacity. Li et al. (2006) found that the adsorption capacity on dye removal would be stable for NaOH-to-Fly ash ratio greater than 1.2. Lower fly ash-to-NaOH ratio will result in lower conversion of fly ash to geopolymer, resulting in low adsorption capacity.

Adsorption capacity is also dependent on the porous structure and their surface properties. Higher surface area will generally result in higher adsorption capacity. Li et al. (2006) investigated the surface area and pore volume of different fly ash-based geopolymers (31.8 – 56 m^2/g), natural zeolite (16 m^2/g), and fly ash (8.4 m^2/g), and their results of adsorption followed the same order of surface area, i.e., geopolymer > natural zeolite > fly ash.

In addition to physical properties, Lee et al. (2017) found that cation exchange capacity of geopolymer was 202.04 cmol/kg, which is similar to the zeolites. However, they found that the disadvantage of geopolymer was that it was unstable in acidic environment at pH 2. Also, point of zero charge (pH_{pzc}) as an important factor can determines the linear range of pH sensitivity and indicates type of charges on the surface (Poghossian, 1997). The values of pH_{pzc} were found to be 8.7, 10.2 and 9.7 for three geopolymers GP-1, GP-2 and GP-3, respectively (Maingi et al., 2017). At higher solution pH ($pH \geq pH_{pzc}$), the geopolymers were possibly negatively charged and this

may enhance adsorption of the positively charged dye cations through electrostatic forces of attraction (Ebrahimian et al., 2014). Li et al. (2006) reported that the synthesized geopolymer exhibited strong basicity (pH = 11.48), and they suggested that the negative charge on the solid surface and the surface hydroxyl groups of the adsorbent have the main effect on the adsorption of cationic pollutants.

The geopolymer strength characteristics especially fly ash is dependent on the nature of surface charges over the reactive component generally amorphous/glassy content. During the alkali activation, surface layer of the fly ash particles gets deprotonated forming soluble form of SiO^- species.

Normally surface layer fly ash particles contain a significant amount of readily leachable elements mostly anionic groups of silicates [-O-SiO^{2-}] and aluminates [-O-AlO^-]. Zeta potential value of fly ashes is in the negative range of -20 to -25 mv (López et al., 2014; Revathi, et al., 2017; Ghosh & Ghosh, 2018). The negative zeta potential indicates that activator solution (sodium hydroxide and sodium silicate) help prevent agglomeration of fly ash particles to facilitate geopolymerization reaction. Increased concentration of NaOH could decrease the zeta potential and impact the compressive strength.

During the geopolymerization reaction, the OH^- from activator solution can react with the aluminate species on the surface of fly ash to form $[Al(OH)_4]^-$ and react with silicate species to form either $[SiO(OH)_3]^-$or $[SiO_2(OH)_2]^{2-}$, so that negatively charged double layer was established. Also, Na^+ from alkaline activator was involved into reaction to form a sodium-alumino-silicate-gel layer $[Na_z(AlO_2)_x(SiO_2)_y \cdot nNaOH \cdot mH_2O]$ (Schmücker & MacKenzie, 2005). This reaction step is very important to achieve desirable mechanical strength. While

forming Na-Al-Si-H gel the accumulation of more Na+ ions in the double layer decrease the zeta potential.

2.4.3. Adsorption Properties of Fly Ash-based Geopolymer

As summarized above, the chemical structure of geopolymer is composed of a negatively charged aluminosilicate framework balanced by alkali metals (i.e., Na^+ and K^+). These ions could be exchanged with heavy metals cations in aqueous solution. Therefore, the geopolymer could be used for the removal of heavy metals cations from water chemically.

Geopolymers have newly come into use as an effective alternative for the adsorption of heavy metals from wastewater. Geopolymer defines amorphous alkali alumina-silicates derived from alkali activation of amorphous aluminosilicates, such as metakaolin and fly ash, by alkali silicate solutions (Rangan, 2010). Amorphous aluminosilicates dissolve in alkali silicate solution and form 3D network of alumina and silica building blocks by polymerization (Cheng et al., 2012; Comrie and Davidovits, 1988 and Davidovits et al., 1990).

- Heavy metals

Currently, there is limited number of studies dealing with the use of geopolymers for heavy metal removal from aqueous solutions. Some of the studies are summarized in Table 2-7. For example, adsorption capacities (Q_m) of different metals reported were 48.78 mg/g, 98.4 mg/g, 79.11 mg/g of Cu^{2+} (Cheng et. al., 2012; Wang et al., 2007; Mužek et al., 2014; Al-Harahsheh et al., 2015), 147.06 mg/g and 166.55 mg/g of Pb^{2+} (Cheng et. al., 2012; Al-Zboon et al., 2011), and 67.57 mg/g of Cd^{2+} (Cheng et al., 2012). It can be assumed that the adsorption behavior of geopolymer are partially depended on the source of the fly ash or metakaolin, preparation conditions and adsorption conditions. As reported, the adsorption process can sometimes be slow (30 hours equilibrium time) (Wang et al., 2007) or fast (15 – 30 min) (Al-Zboon et al., 2011).

Wang et al. (2007) studied Cu^{2+} ions removal by using a fly ash based geopolymer and reported an adsorption capacity of 92 mg/g much higher than natural zeolites and fly ash (0.1 mg/g). In addition after geopolymerization, the surface area increased from 8.4 m^2/g in fly ash to 56 m^2/g in the geopolymer. These evidences indicate that geopolymerization contributed towards creating new surface for adsorption. Mužek et al. (2014) reported an adsorption capacity of 79.11 mg/g for Cu^{2+} for fly ash based geopolymer. They also found that Na^+, K^+, Ca^{2+}, Mg^{2+}, Al^{3+}, and Si^{2+} ion were leached out from the fly ash-based geopolymer as a result of adsorption of Cu^{2+} ions. The reason provided by the researchers was that Na^+ ion was not the only cation contributing towards the ion exchange of Cu^{2+} ion. They also found that the amounts of leached Al and Si were small (less than 3%) because of the stability of the geopolymer (Mužek et al., 2016).

Besides using fly ash source, other aluminosilicate source such as metakaolin or zeolite were considered to prepare geopolymer. Cheng et al. (2012) demonstrated the effectiveness of metakaolin-based geopolymer as adsorbent for the removal of heavy metal ions Cu^{2+}, Pb^{2+}, Cr^{3+}, and Cd^{2+} ions. López et al. (2014) also reported that the metakaolin-based geopolymer with composition of Si/Al = 2 is optimum for the heavy metal ions adsorption. They found that adsorption capacities increased in the following order: $Cs^+ > Pb^{2+} > Cu^{2+} > Cd^{2+} > Ni^{2+} > Zn^{2+}$ for a mixture of the multicomponent (metal) system, while the individual experiment showed higher adsorption for Pb^{2+} relative to Cs^+. Ge et al. (2015; 2017) used different alkali activator to functionalize metakaolin geopolymer for copper removal. Their results suggested that the geopolymer spheres as an adsorbent was not only environmentally friendly, cost-effective but also could be applied for the continuous treatment of heavy metals containing water.

El-Eswed et al. (2012) added various amounts of zeolitic tuffs to kaolin-based geopolymers and investigated the adsorption properties of Cu^{2+}, Ni^{2+}, Zn^{2+}, Cd^{2+} and Pb^{2+} ions. Both isothermal

and kinetic studies revealed that increasing the zeolitic tuff: kaolin ratio improved the adsorption capacity of geopolymer toward metal ions. The adsorption process of metal ions onto geopolymers was observed to be reversible.

Liu et al. (2016) found that fly ash-based geopolymer has the similar adsorption properties to faujasite zeolite. They prepared geopolymer and then modified it to zeolite by in situ hydrothermal method, i.e. soaking in 1 M NaOH solution at 70 ^{o}C. The results showed that the synthesized zeolite had higher surface area of 174.35 m^2/g and adsorption capacity 143.3 mg/g for removal of Pb than that of geopolymer (surface area of 20.48 m^2/g and adsorption capacity 118.6 mg/g), and much higher than that of fly ash (surface area of 16.45 m^2/g and adsorption capacity 49.8 mg/g).

- Other pollutants

In addition to heavy metals, geopolymer can be used as the adsorbent for dyes, as summarized in Table 2-8. Only a few researches have been reported on adsorption of organic pollutants using geopolymer. Li et al. (2006) studied adsorption of methylene blue and crystal violet on fly ash-based geopolymer using sodium hydroxide as an activator. The adsorption capacity was 32.0 and 40.8 mg/g, respectively. The adsorption capacities on geopolymer were much higher than that on unreacted fly ash, (Li et al., 2006). Zhang and Liu (2013) reported about 93% degradation of methylene blue (MB) dye from wastewater when using fly ash-based geopolymer used as a novel photo-catalyst. Wang et al. (2006) reported synthesis of fly ash with NaOH solution that would significantly enhance the adsorption capacity depending on the treatment temperature and time, and the base concentration. The adsorption capacity of methylene blue would increase with the pH of the dye solution and the sorption capacity of geopolymer could reach $5x10^{-5}$ mol/g.

Table 2-7. Application of geopolymer as adsorbent for heavy metals

Geopolymer materials	Precursors	Alkali activator	Particle size, mm	Surface area, m^2/g	CEC, cmol/kg	Metal	pH	Dosage, g/L	Contact time, hr	Adsorption capacity, mg/g	Reference
Fly ash-based	Class F fly ash	14 M NaOH	0.2	--	--	Cu^{2+}	6	2	2	152.31	Al-Harahsheh et al., 2015
Fly ash-based	Class F fly ash	NaOH	0.045	56	--	Cu^{2+}	6.2	1.5	72	98.4	Wang et al., 2007
Fly ash-based	Class F fly ash	16 M NaOH, Na_2SiO_3	0.071-0.09	--	--	Cu^{2+}	--	5	2	79.11	Mužek et al., 2014
Fly ash-based	coal fly ash	14M NaOH	0.2	--	--	Pb^{2+}	5	1.4	2	174.34	Al-Zboon et al., 2011
Fly ash and iron ore tailing-based	Class F fly ash /iron ore tailing	10 M NaOH and Na_2SiO_3	0.03	--	--	Cu^{2+}	6	3	1.5	69.11	Duan et al., 2016
Zeolite-based (600°C)	Class F fly ash	Solid NaOH	0.075	8.22	--	Cd^{2+}	5	0.08	7	26.246	Javadian et al., 2015
Porous geopolymeric sphere	Metakaolin	Na_2SiO_3, H_2O_2, K12	2-4	53.95	--	Cu^{2+}	5	1.5	72	52.63	Ge et al., 2015
Geopolymer/alginate hybrid spheres	Metakaolin	NaOH, Na_2SiO_3, Alginate	hybrid spheres	16.2	--	Cu^{2+}	5	1.5	42	62.5	Ge et al., 2017
Metakaolin-based	Metakaolin	10 M NaOH and Na_2SiO_3	1.19-1.41	50.9 – 65.7	129.5	Pb^{2+}	4	20	24	147.06	Cheng et. al., 2012
						Cu^{2+}				48.78	
						Cr^{3+}				19.94	
						Cd^{2+}				67.57	
Metakaolin-based	Metakaolin	NaOH and Na_2SiO_3	0.15	39.24	--	Zn^{2+}	4	2	1.5	74.53	Kara et al., 2017
						Ni^{2+}		3.2		42.61	
Metakaolin-based	Metakaolin	8 M NaOH	0.125	3.3	--	Cs^{+}	5	0.00125	--	43	López et al., 2014
						Pb^{2+}				35	
						Cu^{2+}				15	
						Cd^{2+}				3	
						Ni^{2+}				1	
						Zn^{2+}				2	

Table 2-8. Application of geopolymer as adsorbent for dye and ammonium in aqueous solution

Geopolymer materials	Precursors	Alkali activator	Particle size, mm	Surface area, m^2/g	CEC, cmol/kg	Target pollutant	pH	Dosage, g/L	Contact time, hr	Adsorption capacity, mg/g	Removal %	Reference
Fly ash-based	Class F fly ash	sodium hydroxide	--	56	--	methylene blue	6.3	0.2	--	38.38	85	Li et al., 2006
						Crystal violet			--	97.92	90	
Fly ash-based	Class F fly ash	500 g/L NaOH	0.045	25.7	--	methylene blue	> 9	1	--	17	--	Wang et al. 2006
						rhodamine B	> 6		--	1.9	--	
Fly ash-based	Class C fly ash	3 M NaOH	0.09	28.5	--	Thionine (TH)	5-10	10	24	0.008	--	Atun et al., 2011
						safranine T (ST)				0.006		
Fly ash-based	Class F fly ash	12 M NaOH	< 0.2	--	--	methylene blue	5	1	2	37.04	--	Alouani et al., 2018
Fly ash-based without UV	Class F fly ash	$Na_2SiO_3 \cdot 9H_2O$	0.12-0.45	--	--	methylene blue	11.1	2	--	0.669	89.15	Zhang and Liu, 2013
Fly ash-based with UV									--	0.696	92.79	
Zeolite-based	Class F fly ash (600°C)	NaOH powder	< 0.15	27.015	279	ammonium	8	4	1.25	37.45	--	Zhang et al., 2011

2.4.4. Factors Affecting Adsorption of Heavy Metals

- Contact time and initial concentration

The initial concentrations of heavy metals have a strong effect on the adsorption capacities of various adsorbents. Generally, adsorption capacity increased with increased concentrations of the heavy metals. However, several investigations have shown that the removal efficiency of heavy metals is concentration dependent and there is a decreasing trend with an increase of initial concentration. Al-Harahshah et al. (2015) reported the effect of contact time and initial concentration of heavy metals on the adsorption of Cu^{2+} on fly ash-based geopolymer. They showed that increasing the contact time from 5 min to 15 min enhanced significantly the percent removal of Cu^{2+}, and only a slight change in removal efficiency occurred from 15min to 180min. Cu^{2+} removal efficiency remained higher than 80% when the initial concentration were less than 140 mg/L. Similar results were found by Wang et al. (2007), indicating that Cu^{2+} adsorption efficiency on geopolymer were found to be dependent on concentration, i.e., the higher the initial concentration, the lower was the removal efficiency. Al-Zboon et al. (2011) found that adsorption of Pb^{2+} ions on geopolymer increased with an increase in contact time and then reached a maximum value after 120 min and remained constant. The removal efficiency remained at high level (>80%) with initial concentration less than 140 mg/L. With low initial concentration, the available pores in the adsorbent surface were sufficient to adsorb most of heavy metals, which had filled the possible available sites so that the adsorption efficiency increases to a certain level. When the initial concentration increases, the accessible sites become inadequate to adsorb them, therefore, a major part of heavy metals remain in the solution without being adsorbed by the adsorbent. Lee et al. (2017) found that the adsorption process for granular solids was slow where 24 hours is required to reach equilibrium time, however for pulverized samples, the equilibrium

time was 30 min. They suggested that considerable time is required for diffusion of metal ion through the bulk of mesoporous geopolymer and the adsorption mechanism was considered to be ion exchange and electrostatic adsorption of metal ion on the negatively charged Al tetrahedral of the geopolymer matrix.

- pH of solution

The pH of solution has a pronounced influence on the adsorption of heavy metals on various adsorbents. In the certain pH range, heavy metals adsorption increases with increasing pH up to a certain value and then decrease with further increase in pH. The effect of pH may also be accounted in terms of the pH at point of zero charge, at which the surface charge of adsorbent is at zero charge. The surface charge of the adsorbent is positive when the media pH is below the pH_{zpc} value, while it is negative at a pH over the pH_{zpc}. On the other hand at pH below the pH_{zpc}, the predominant metal species (i.e. M^{2+} and $M(OH)^{+}$) are positively charged and therefore, the uptake of metals in the pH range below pH_{zpc} is H^{+}—M^{2+} (or $M(OH)^{+}$) exchange process. With an increase in pH above pH_{zpc}, the surface of the adsorbent is negatively charged with an increase in adsorption as long as the metal species are still positively charged or neutral. When both the surface charge of the adsorbent and metal species charge become negative, adsorption will decrease significantly. According to the mechanism and the discussion of pH effect, the adsorption will lead to a decrease in pH as equivalent H^{+} will be released along with adsorption. However, other interactions may be stronger than purely electrostatic forces, making the effect of surface charge not so important. Additionally, a cation is often complexed with ligands such as, some of them are being possibly negatively charged. Therefore, in such a case, the cation is in fact a negative complex, which may adsorb very well on a positively charged surface.

Table 2-9 shows that the selected heavy metals (Cu^{2+}, Cd^{2+}, and Pb^{2+}) were dominating species at various pH ranges (acidic, neutral, and basic) in typical natural water from Yousef et al. (1985).

Table 2-9. Dominating inorganic speciation of selected heavy metals at various pH ranges in typical natural surface (Yousef et al., 1985)

Heavy Metal	pH < 6.5	6.5 < pH < 7.5	pH > 7.5
Copper, Cu	Cu^{2+}	Cu^{2+} $CuCO_3$ $Cu(OH)_2$	$Cu(OH)_2$
Cadmium, Cd	Cd^{2+}	Cd^{2+}	Cd^{2+} $CdCO_3$ $Cd(OH)_2$
Lead, Pb	Pb^{2+}	Pb^{2+} $PbCO_3$	$PbCO_3$ $Pb(CO_3)_2^{2-}$ $Pb(OH)_3^-$ $Pb(OH)_4^{2-}$

Ibrahim (2011) evaluated synthetic zeolite for permeable reactive barrier application. He found that the change of solution pH can influence the sorption of Zn^+ and Cd^{2+} ions from aqueous solution using synthetized zeolite, which is due to its influence in metal speciation and integrity of the zeolite. Free metal ions were predominant up to pH = 7 for Zn^{2+} ions and pH=8 for Cd^{2+} ions. Zinc is present mainly as Zn^{2+} and $Zn(OH)_2$ and in lesser quantity as $Zn(OH)^+$ at pH between 7-10 and cadmium is present as Cd^{2+} and $Cd(OH)_2$, and in lesser quantity as $Cd(OH)^+$ and $CdCl^+$ at pH between 8-11. At low pH values, excess H^+ present in solution competes with Zn^{2+} and Cd^{2+} ions for active sites leading to less metal ion removal. At near neutral or neutral pH values, the surface has a low net negative charge due to increase in positively charged surfaces. As the solution pH increases, the number of negatively charged sites increases which would favor the sorption of metal cations and their hydroxides, forming surface metal complexes. Al-Harahsheh et al. (2015) reported that geopolymer sorption effectiveness increased from 5.6% to 88.21% when the pH of

the solution increased from 1 to 6. The expected trend for the effect of pH on metal sorption were sorption increase with increasing pH values up to a certain value, and then decreased with further increase in pH (>12) (lBrahim, 2011). Similar results showed increasing pH to values higher than 6 will favor the precipitation of Cu^{2+} as $Cu(OH)_2$ (Goyal et al.,2001). Also, Al-Zboon (2011) suggested that for pH value is greater than 5.0, lead hydroxide such as $Pb(OH)_3^{1-}$ begins to form resulting in the decrease of Pb(II) adsorption on geopolymer. Li et al. (2006) reported that the pH of fly ash, natural zeolite and fly ash-based geopolymeric adsorbents. The results showed that fly ash slurry exhibits acidity (pH=5.35) while natural zeolite showed weak basic property (pH=8.5). The fly ash-synthesized geopolymers exhibited strong basicity (pH=10-11), suggesting the presence of negative charges on the solid surface. Therefore, the produced hydroxyl function groups on the surface adsorbent have the main effect on the adsorption of cationic dyes.

- Particle size

Particle size is one of the important physical properties in determining the effectiveness as a material for treatment medium. In general, fine particles (0.177 – 0.024 mm) is used more often due to the low initial cost and to the flexibility of dosage which allows the fine particle dose to be adjusted to deal with changing contaminant levels (Crittenden et al., 2012). However, fine particle has a high operating cost if used continuously, as it cannot be regenerated, and produces large quantities of sludge. In addition, the dust resulting from the small particles make handling difficult, as does the flammability of the particles. Granular particles (0.42 – 2.36 mm) is a more economical choice in larger systems or where pollutants must be controlled continuously. Disadvantages of granular particles include a high initial cost to buy the filter or contactor, and the tendency of granular particles filters to grow bacteria. Also, the particle size influences the head loss on a bed of column. If smaller particles are used, the head loss will be higher and media in the bed may be

crushed. Intra-particle diffusion study shows that particle size of the adsorbents greatly influences the adsorption rate. Decrease in particle size would lead to increase in surface area and therefore increase in the adsorption opportunity at the outer surface of the adsorbents. There is also a possibility of intra-particle diffusion from the outer surface into the pores of the material. The diffusional resistance to mass transfer is higher for large particles. Due to various factors, such as diffusional path length or mass transfer resistance, contact time, and blockage of some diffusional path, most of the internal surface of the particle may not be utilized for adsorption. Consequently, the adsorption efficiency may become low. The adsorption capacity of waste materials is dependent on the specific surface area available for solute surface interaction. It is expected that adsorption capacity will increase with a larger surface area. In other words, smaller particle size increases the adsorption capacity.

Al-Zboon et al. (2011) crushed the fly ash-based geopolymer paste and reduced the size down to 0.2 mm as adsorbent. López et al. (2014) crushed the metakaolin-based geopolymer sample and sieved by the 120 mesh (0.125mm) to control the particle size range. Kara et al. (2017) ground metakaolin-based geopolymer samples and sieved to obtain 150 μm particle size for adsorption of Zn(II) and Ni(II) ions. Mužek et al. (2014) used the fly ash-based geopolymer particles with size ranging from 0.071 to 0.09 mm as an adsorbent for copper ion. Zhang and Liu (2013) obtain a fly ash-based geopolymer sample with particle size in the range of 120−425 μm.

2.4.5. Parameters of Isotherm Model

Three isotherm models were listed in Section 3.3, which have been applied and reported in some research work related to geopolymer. The parameters of the isotherm models used are presented in Table 2-10. For example, Al-Harahsheh et al. (2015) showed both Langmuir and Freundlich models could explain the adsorption of Cu^{2+} on synthesized geopolymer. They found

that the Langmuir model is slightly better than Freundlich model. Similar results were obtained by Wang et al. (2007), Duan et al. (2016), and Ge et al. (2015; 2017). Also, Al-Zbooon et al. (2011) found that Langmuir model was more applicable than the Freundlich model to describe the adsorption of Pb^{2+} on geopolymer. Similar results of Zn^{2+} and Ni^{2+} were reported by Kara et al. (2017).

In addition to metals, Li et al. (2006) found that for the adsorption isotherm of dye by geopolymers Freundlich model was better than single-site Langmuir model while the two-site Langmuir model was the better model of the three. This suggests that some heterogeneity on the surface or pores of the adsorbents played a role in dye adsorption. Geopolymer adsorbent may contain minor unconverted fly ash that contain mineral oxides and unburned carbon which provide heterogeneous active sites for dye sorption. As such, the two-site Langmuir isotherm model fit the experimental data.

2.4.6. Application of Fixed-bed Column

Table 2-11 summarizes some studies that are focused on fixed-bed column packed with different adsorbents for heavy metals removal. And also, Table 2-11 presents the parameters of Thomas model from these studies. Hasfalina et al. (2012) used Kenaf fibres as adsorbent in a fixed-bed column for copper removal from aqueous solution. They found that either a deeper bed (15 – 30 cm) or a slower flow rate (4 – 9 mL/min) would increase the copper adsorption. The Thomas model was successful into evaluating the column performance. Similarly, Yahaya et al. (2011) found that copper adsorption increased for lower inlet concentration (5 – 15 mg/L), slower flow rate (10 – 30 mL/min), and deeper bed depth (3 – 8 cm). They found that the Thomas and Yoon-Neson models fitted well with the data compared to Adam-Bohart model. Similar results were also found by Futalan et al. (2010). Trgo et al. (2011) reported Thomas model was the most suitable

model as compared to Bohart-Adams and Yoon-Nelson models to model the breakthrough curve of lead adsorption of natural zeolite for EBCT ranging from 1 – 13 mins. Similar model analysis was investigated by Biswas & Mishra (2015), and the Thomas was found to be a good predictor for the entire breakthrough curve. They also reported that the breakthrough curve and adsorption capacity was influenced by pH, and pH 5.2 gave the highest adsorption capacity (35.36 mg/g) as compared to adsorption capacities of 12.95 and 31.034 mg/g at pH 3.1 and 6.4, respectively. Han et al. (2009) synthesized Iron oxide-coated zeolite for copper removal and reported that the Thomas model could describe all the breakthrough curve for different bed depths, flow rates, and initial concentrations. Han et al. (2006) also synthesized manganese oxide coated zeolite for copper and lead removal. They found removal by columns followed the following order of $Pb^{2+} > Cu^{2+}$. Similar competitive adsorption was reported by Shahbazi et al. (2011) where they modified mesoporous silica (SBA-15) with melamine-based dendrimer amines (MDA) and investigated metals adsorption by fixed-bed column. The breakthrough curves show that decreasing flow rate, increasing bed height, and decreasing initial metal concentration would increase the adsorption capacity. In addition, they found the adsorption capacity was in order of $Pb^{2+} > Cu^{2+} > Cd^{2+}$.

There are not many reported literatures on fixed-bed column studies packed with geopolymer as adsorbent. Ge et al. (2015) investigated the column test for geopolymeric spheres to evaluate copper removal by three different bed heights, i.e. 0.5, 2.2, and 3 cm. Ge et al. (2017) reported that all three models (Thomas, Adams-Bohart, and Yoon-Nelson) have moderate fitness for the breakthrough curves.

Table 2-10. Parameters of Isotherm models for metal ions adsorption on geopolymer

Metal	Temperature, °C	pH	Langmuir isotherm			Freundlich isotherm			Reference
			K_L, L/mg	Q_m, mg/g	R^2	K_F	1/n	R^2	
Cu^{2+}	30	6.2	0.13	99	0.75	41	0.17	0.67	Wang et al., 2007
Cu^{2+}	25	4	0.062	50.81	0.9844	6.09	0.48	0.9815	Al-Harahsheh et al., 2015
		5	0.032	83.13	0.9903	4.73	0.63	0.9787	
		6	0.061	96.84	0.9941	8.47	0.61	0.9855	
Cu^{2+}	20	4	0.058	63.36	0.9882	5.51	0.52	0.9890	Duan et al., 2016
		5	0.049	69.11	0.9859	6.12	0.53	0.9802	
		6	0.060	81.55	0.9936	9.35	0.55	0.9639	
Pb^{2+}	25	3	0.0298	40.76	0.9700	3.19	0.51	0.9791	Al-Zboon et al., 2011
		4	0.0163	166.55	0.9773	4.47	0.73	0.9715	
		5	0.0607	134.95	0.9719	11.73	0.61	0.9350	
Cu^{2+}	25	5	0.1359	52.63	0.9971	8.08	0.45	0.8289	Ge et al., 2015
Cu^{2+}	25	5	0.11	62.5	0.997	27.5	0.24	0.843	Ge et al., 2017
Zn^{2+}	25	4	0.0346	74.75	0.999	1.59	0.059	0.807	Kara et al., 2017
Ni^{2+}			0.196	150	0.996	3.35	0.287	0.991	

Table 2-11. Parameters of different fixed-bed columns on heavy metal removal

Adsorbent	Size, mm	Height, cm	Inter diameter, cm	Flow rate, mL/min	EBCT, min	Metal	pH	Initial Con., mg/L	Uptake capacity, mg/g	Thomas model			Reference
										k_{Th}, mL/min mg	q_{Th}, mg/g	R^2	
MDA-SBA-15	powder	8	0.6	0.6	3.77	Cu^{2+}	4	50	--	2.9	37.6	0.993	Shahbazi et al., 2011
						Cd^{2+}			--	3.1	27.6	0.975	
						Pb^{2+}			--	2.8	39.6	0.988	
Kenaf Fibres	1	20	10	4	392.5	Cu^{2+}	5	100	--	24.7	45.86	0.91	Hasfalina et al., 2012
Rice husk activated carbon	1-2	6	1.2	10	0.68	Cu^{2+}	--	10	--	0.44	29.42	0.98	Yahaya et al., 2011
Chitosan immobilized on bentonite	0.21-0.5	4.3	1.2	0.2	24.3	Cu^{2+}	4	500	--	0.0008	32.93	0.9758	Futalan et al. 2011
Zeolite	0.1-0.5	11.5	1.2	1	13	Pb^{2+}	--	84	--	0.232	43	0.938	Trgo et al., 2011
Carbonized rubber wood sawdust	0.5-1	5	2.54	15	1.69	Pb^{2+}	5.2	20	--	0.73	35.36	0.92	Biswas & Mishra, 2015
Manganese oxide coated zeolite	0.42-0.84	15	1	7.69	1.53	Cu^{2+}	5	62.45	--	0.115	7.296	0.943	Han et al. 2006
						Pb^{2+}		260.82	--	0.026	71.62	0.98	
Iron oxide-coated zeolite	0.42-0.84	11	0.95	11	0.71	Cu^{2+}	6.5	60	--	0.37	11.1	0.917	Han et al. 2009
Metakaolin-based geopolymer	Spheres 2 – 4	1	1	1	0.785	Cu^{2+}	5	50	--	0.02	26.1	0.943	Ge et al., 2017
Metakaolin-based geopolymer	0.15	--	1.1	0.5	--	Co^{2+}	--	100	24.33	--	--	--	Kara et al., 2018
						Mn^{2+}			32.32				

2.5. Magnetic Assistance on Water/wastewater Treatment

As mentioned earlier, adsorption plays an important role in water and wastewater treatments. Water is commonly contaminated with pollutants from industrial activities, runoff from polluted sites, and from various other sources. These pollutants, which can range from heavy metals and various organic molecules, must be removed to render the water safe and to comply with environmental regulations. This is often accomplished by contacting the polluted water with an adsorbent. The treated water and adsorbent are then separated, and the adsorbent is treated to dispose of the pollutants. The water is often contacted with the adsorbent by passing the water through fixed beds of the carbon. However, some operational efficiencies may be derived by mixing the water and adsorbent in, for example, a stirred tank. However, this requires separation by mechanical screening, or a separation process to separate the adsorbent particles from the treated water.

Even though fine particle adsorbents have proven to be effective in the removal of pollutants from wastewater, they suffer one inherent disadvantage, which is difficult to separate from wastewater in a continuous flow system. Separation of adsorbent from the slurry phase by screening has significant problems. The screens may be plugged or clogged, requiring considerable horsepower to operate, and need frequent maintenance and screen replacement. In general, a method to separate adsorbent particles from a liquid solution that avoids the problems of mechanical screening would be desirable. Since screening depends upon the particles having a relatively large size, abrasion or other unintended comminution, produces small particles which defeats the screening. Hence, an alternative to screening would be magnetic separation, using a magnetic media or adsorbent. Magnetic technology is a physical treatment technique that has been reported to affect the coagulation of various particles in suspension, such as iron or other particles

in electrolyte solutions (Okada et al., 1991; Wang et al., 1994). Some studies have been conducted to explore the use of magnetism as an effective means of separating the suspended adsorbents from water (Ambashta & Sillanpää, 2010). Use of magnetic adsorbents offers a significant advantage over other adsorbents which has the ability to separate them from an aqueous solution on application of a magnetic field.

Recently, utilization of iron oxide nanomaterials with novel characteristics and functionality has been widely studied due to their small size, high surface area, and magnetic property (Oh and Park, 2011; Laurent et al., 2008). Iron oxide nanoparticles can be synthesized using includes physical, chemical, and biological methods. Chemical methods are well known and widely accepted, such as chemical so-precipitation, thermal decomposition, and electrochemical. The main advantage of thermal decomposition method is that, it improves control over the size and shape of iron oxides nanoparticles. The size and shape of iron oxides nanoparticles depend on the precursor and temperature (Belaïd, et al., 2013).

Synthesis of iron oxides can result in magnetic phase-magnetite (Fe_3O_4) and maghemite (γ-Fe_2O_3) and non-magnetic, hematite (α-Fe_2O_3). This section only reviews the magnetite (Fe_3O_4) nanoparticles, with different synthesis methods, surface modifications, and forming composites with other material.

2.5.1. Synthesis Methods of Magnetic Iron Oxides (Fe_3O_4)

Currently, magnetic Fe_3O_4 nanoparticles are generated by various chemical-based synthesis methods, including co-precipitation, reverse micelle method, microwave synthesis, sol–gel techniques, freeze drying, ultrasound irradiation, hydrothermal methods, laser pyrolysis, and thermal decomposition (Blaney, 2007; Carlos et al., 2013, Wieczorek-Ciurowa & Kozak, 1999). The different synthesis method determines the properties of the iron oxide, such as particle size,

morphology, magnetization, and surface functionality. Many methods have been studied and developed. In this section, a few methods will be reviewed including co-precipitation, hydrothermal or solvothermal synthesis, and thermal decomposition.

Co-precipitation is the simplest and most efficient synthesis method to generate magnetic particles. In this synthesis method, a stoichiometric mixture of ferrous and ferric precursors in solution phase are used as an iron source (Massart, 1981). The mixture is reacted under alkaline conditions to generate superparamagnetic nanoparticles (Matei et al., 2011). Two ways are used for this reaction procedure, one is that the alkaline solution, i.e. ammonia hydroxide (NH_4OH) or sodium hydroxide (NaOH), is introduced into the mixed Fe^{2+} and Fe^{3+} iron solution. Another way is titration hydrolysis, which consists of gradually adding mixed Fe^{2+} and Fe^{3+} iron solution into the alkaline solution. Precipitation is desirable to control at pH ranging from 8 to 14. The particle size, shape, and composition of the magnetic iron oxides are dependent on the type of salts used (e.g. chlorides, sulfate, nitrates), the mass ratio of Fe^{2+}/ Fe^{3+}, reaction temperature, types of stabilizing agent, pH value of solution, and ionic strength of the reaction media (Laurent et al., 2008; Gupta & Gupta, 2005). Generally, the particles size of Fe_3O_4 made by this method ranged from 5 to 100 nm.

Hydrothermal is another popular synthesis method which has been widely used to prepare magnetic iron oxides. Due to the successful and better formation of crystalline under this process, the properties of magnetic iron oxides can be improved with narrow size distribution and shape control. This method is used 100 – 300 ^oC calcination temperature for a mixture of ferrous salts (e.g., chloride, sulfate, and nitrates) and sodium hydroxide solution. In addition, in some particular cases, organic solvent can be used as a medium instead of water, such as diamine hydrate (Wang et al., 2003), 2-methoxyethanol (Chen & Xu, 1998), sodium thiosulfate (Fan et al., 2001),

polyethylene glycol (Yan et al., 2008). The process called solvothermal synthesis and the solvent could expand the range of hydrothermal method. The selection of solvent, type of ferrous salts, reaction temperature, and reaction time are important factors to control the particle size and shape. Another advantage of the solvothermal method is that it can avoid surface contamination compared to hydrothermal and co-precipitation methods (Li et al., 2011). However, this method requires long time for the reaction and more energy is consumed as compared to the fast co-precipitation method with low-cost precursors.

Recently, thermal decomposition is considered as the synthesis method due to the avoidance of harmful sodium hydroxide or external organic solvents. Some mesoporous method oxides with high surface and well controlled pore structure, i.e. α-Fe_2O_3, has already been successfully synthesized (Yu et al., 2008). However, it is still insufficient compared to the well-developed co-precipitation and hydrothermal methods. The existing deficiencies of this method need to be further overcome by improving the time consumed and making it favorable for large scale production. Cui et al. (2015) used the thermal decomposition of $Fe(NO_3)_3 \cdot 9H_2O$ to form the α-Fe_2O_3 particles, and the results indicated that the surface area of prepared α-Fe_2O_3 would dramatically decreased when the crystallinity is continuously improved by increasing the crystallizing temperature. As similar results were found by Gao et al. (2010). The properties of prepared iron oxides were highly depending on the heating rate, calcination time, and calcination temperature (Guo et al., 2013). Also, the thermal decomposition method usually forms γ-Fe_2O_3 from the Fe_3O_4 as a precursor which is prepared by co-precipitation, due to the limited successful pure crystalline formation (Aliahmad & Moghaddam, 2013). Thus, the calcination temperature ranged from 300 to 600 ^oC were used to provide homogeneous and pure phase specimens with a narrow size particle. However, this thermal decomposition was commonly used to prepare α-Fe_2O_3

and γ-Fe_2O_3, which is rarely used in Fe_3O_4 preparation compared to faster and simpler co-precipitation method.

For the environmental application, iron oxides have limitations including poor recovery (i.e., α-Fe_2O_3) and the size of the particle can be a factor on its overall performance. For the magnetic iron oxides, if the size is too small (<12 nm) magnetic separations would require large external magnetic fields to overcome opposing forces, which can lead to high cost separator. There are no investigations mentioned on the possibilities of scaling up the synthesis for the iron oxides nanomaterials in order to demonstrate their real-world application to remove heavy metals from wastewater effluent. Most of researches were studying adsorption capacity of pollutants. Also, research done applied simple magnet separation, which lack a comprehensive magnetic separation system, such as magnetic field, size, shape, and placement of designed magnet. For example, Zhao et al. (2014) investigated prepared S-doped Fe_3O_4 by hydrothermal for copper adsorption and found that the adsorption capacity of 54.7 mg/g and the magnetic Fe_3O_4 particles could be magnetically separated and regenerated.

However, iron oxide is abundant, relatively non-toxic and low-cost product. Iron oxides can be an effective and specific adsorption of heavy metals as reviewed in the literature. Nevertheless, they often lead to problems such as activity loss due to agglomeration, difficult separation, and excessive pressure drops when applied in flow-through systems, since they are usually present as fine or ultrafine particles (Cumbal & SenGupta, 2005).

Synthesis methods and adsorption properties of iron oxides are summarized and presented in Table 2-12.

Table 2-12. Comparison of Fe3O4 on synthesis method, properties and adsorption on heavy metals

Materials	Precursors	Method of synthesis	Size, nm	Surface area, m^2/g	Magnetization, emu/g	Pollutant	dose, g/L	pH	Time, hr	Adsorption	Reference
Fe_3O_4	$FeCl_2$, $FeCl_3$, and 1M NaOH	Chemical co-precipitation	17	--	--	As^{3+}	2	6	24	5.68 mg/g	Luther et al. 2012
Fe_3O_4	$FeCl_2$, $FeCl_3$, and 1M NaOH	Chemical co-precipitation	8	190	--	Cu^{2+}	25	4	24	99.8%	Shen et al., 2009
						Cr^{2+}				97.6%	
						Cd^{2+}				84.7%	
						Ni^{2+}				88.5%	
Fe_3O_4	$FeCl_2$, $FeCl_3$, and 2M NaOH	Chemical co-precipitation	20	--	32.9	Cu^{2+}	1.07	5.5	1	97.8%	Kanthimathi et al., 2013
						Co^{2+}	2.7	5.4	0.17	99.2%	
Fe_3O_4	$FeCl_2$, $FeCl_3$, and 5M NaOH	Chemical co-precipitation	19.3	60	--	As^{3+}	0.1	8	1	1.13 mg/g	Shipley et al. 2010
n-Fe3O4	$FeCl_2$, $FeCl_3$, and 5M NaOH	Chemical co-precipitation	12	100.52	--	As^{5+}	10	5	24	66.53 mg/g	Iconaru et al. 2016
						Cu^{2+}				10.67 mg/g	
c-Fe_3O_4	Sigma Aldrich (CAS no. 637106)		80	6.81	--	As^{5+}	10	5	24	39.26 mg/g	
						Cu^{2+}				9.06 mg/g	
S-doped Fe_3O_4	$FeCl_2$, $FeCl_3$, NaOH (433 K, 6 h)	Hydrothermal	5-20	Fail	14.8	Cu^{2+}	0.625	5	24	54.7 mg/g	Zhao et al. 2014
Fe_3O_4	$FeCl_3$, Citric acid (200 °C, 24 h)	Hydrothermal	120	123	82.5	Cr^{5+}	0.6	5	5.5	4.16	Han et al., 2011
						Hg^{2+}				10	
α-Fe_2O_3	$FeSO_4 \cdot 7H_2O$ (200 °C)	Thermal decomposition	9.8	111	--	Congo Red	1.5	--	2	53 mg/g	Yu et al., 2008
urchin-like α-Fe_2O_3	$Fe(NO_3)_3 \cdot 9H_2O$ (200 °C, 20 min)	Thermal decomposition	10-130	38	0.72	--	--	--	--	--	Cui et al, 2015
$NiFe_2O_4$	$FeSO_4 \cdot 7H_2O$, $NiCl_2 \cdot 6H_2O$, AOT (300 °C, 60 min)	Thermal decomposition	2.5	301.6	4	AO7	1.5	--	2	61.3 mg/g	Gao et al., 2010

2.5.2. Surface Modified Iron Oxide Adsorption of Heavy Metals from Aqueous Solution

Currently, there is a challenge to separate and recover sorbent materials from contaminated water. The magnetic iron oxide nanomaterials provide a viable solution to collect and remove toxic species. This advantage is that materials can be easily removed from the system by simply applying an external magnetic field. There have been many studies reported using these materials for cleanup of heavy metals including arsenic, chromium, cobalt, copper, lead, and nickel from the aqueous synthetic solutions and natural water systems. Table 2-13 summarized heavy metal ions adsorption by modified magnetic Fe_3O_4.

For copper ion (Cu^{2+}), Lin et al., (2011) modified the surface of magnetic Fe_3O_4 with SiO_2 and N-[3-(trimethoxysilyl)propyl]-ethylenediamine (TPED) to generated a new adsorbent, which has a higher surface area then Fe_3O_4. They found that the maximum adsorption capacity was 10.41 mg/g at pH 5.5. The adsorption process was rapid initially but gradually became slower due to the decreasing active sites. Also, they found 0.1 M of HNO_3 would be a great desorbing agent and there was a 13.6% loss in adsorption capacity from the regeneration test. Hao et al. (2011) modified the surface Fe_3O_4 with 1,6-hexadiamine to synthesize MNP-NH_2 nanoparticles. They found that the maximum adsorption capacity was 25.77 mg/g and no difference was observed in desorption capacity of the adsorbent during 15 sorption–desorption cycles indicating that the nano-adsorbent had good reusability. Peng et al. (2010) modified the surface of magnetic chitosan particles which was an effective adsorbent to remove copper from aqueous solution. They found that the maximum adsorption capacity was 144.9 mg/g which was due to the hydroxyl and amino groups on the adsorbent surface. Badruddoza et al. (2011) used the carbodiimide method to graft the carboxymethyl-β-cyclodextrin (CM-β-CD) onto the magnetite surface. They found that the maximum adsorption capacity is 47.2 mg/g which is due to the oxygen atoms on the adsorbent

surface as the main binding sites for copper removal. Liu et al. (2013) investigated EDTA functionalized magnetic nanoparticles for removal of copper with adsorption capacity of 46.27 mg/g. Lan et al. (2013) synthesized magnetic hyaluronic acid (Fe_3O_4@SiO_2-HA) microspheres and they found that adsorption capacity increased from 6 to 12.2 mg/g as pH increased from 2 to 6.8 and slowly decreased to 11.6 at pH 8.

For cadmium ion (Cd^{2+}), Yang et al. (2014) used synthesized chitosan combined with Fe_3O_4 nanoparticles to remove Cd^{2+} ion. The maximum removal efficiency of 93% occurred at pH 6 with initial Cd^{2+} concentration of 100 mg/L. They also found that Cd^{2+} removal capacity increased with initial concentration and the maximum adsorption capacity reached 201.2 mg/g for an initial concentration of 1000 mg/L. They suggested that this adsorption behavior was impacted by surface charge and proton competitive adsorption. Tu et al. (2012) used magnetic CuFe2O4, manufactured from industrial sludge, as green low-cost adsorbent to remove Cd^{2+} ion. From their results, Cd^{2+} adsorption capacity was 13.9 mg/g at an initial concentration of 100 mg/L and pH of 6.0. Gong et al. (2012) synthesized the shellac coated iron oxide particles to adsorb Cd^{2+} ion chemically. They found that the maximum adsorption capacity was 18.8 mg/g and was due to the surface charge and carboxyl groups on the adsorbent surface interacting with Cd^{2+} ion.

For lead ion (Pb^{2+}), Han and Wei (2012) fabricated Fe_3O_4 microroses and explored the possibility of (Pb^{2+}) removal during water treatment. The Fe_3O_4microroses with surface area of 43 m^2/g and maximum adsorption capacity was 46.5 mg/g occurred at pH of 5.5 and initial (Pb^{2+}) concentration of 80 mg/L. Peng et al. (2014) synthesized magnetic Fe_3O_4 with silica xanthan gum to remove Pb^{2+} ion from aqueous solution. They found the maximum adsorption capacity was 21.32 mg/g and the order of adsorption was in the order of: $Pb^{2+} > Cu^{2+} > Cd^{2+}$.

Table 2-13. Modified magnetic Fe_3O_4 for heavy metal ions adsorption

Surface modification	Size, nm	Surface area, m2/g	Magnetization, emu/g	Metal	Dosage, g/L	pH	Equilibrium time, hr	Adsorption, mg/g	Reference
SiO_2 and TPED	--	72.89	61.8	Cu^{2+}	10	5.5	24	10.41	Lin et al., 2011
1,6-hexadiamine	78.7	--	90.6	Cu^{2+}	0.1	6	0.08	25.77	Hao et al., 2010
chitosan	98	--	--	Cu^{2+}	1.5	4.5	1	144.9	Peng et al. 2010
CM-β-CD	--	110.9	--	Cu^{2+}	12	6	0.5	47.2	Badruddoza et al. 2011)
EDTA	312.3	--	81.42	Cu^{2+}	0.1	6	0.08	46.27	Liu et al. 2013
SiO_2-HA	32	--	44.59	Cu^{2+}	0.6	6.8	2.5	29.42	Lan et al. 2013
chitosan	--	--	26.42	Cd^{2+}	1.3	6	0.5	201.2	Yang et al. 2014
$CuFe_2O_4$	20-90	69.06	62.52	Cd^{2+}	5	6	0.5	13.87	Tu et al. 2012
shellac	25	56.95	39.1	Cd^{2+}	41.6	8	1	18.8	Gong et al. 2012
microroses	500	43	--	Pb^{2+}	1.67	5.5	1.3	46.5	Han and Wei, 2012
silica–XG	20-50	137.48	32.84	Pb^{2+}	2.5	6	2	21.32	Peng et al. 2014

2.5.3. Magnetic Iron Oxides Composites with Porous Support

An effective approach to overcome these technical drawbacks is to fabricate hybrid adsorbents by impregnating or coating iron oxides particles into/onto porous supports of larger size (Hua et al., 2012). Some widely used supports include natural materials such as bentonite (Oliveira et al., 2003), sand (Hansen et al., 2001), zeolite (Oliveira et al., 2004; Faghihian et al., 2013), and synthetic polymer materials (Pan et al., 2010). Some host-supported iron oxides for heavy metal removal are summarized in Table 2-14.

Trakal et al. (2016) reported impregnating biochar with magnetite to improve the adsorption of Cd^{2+} and Pb^{2+} ions. Oliveira et al. (2003) investigated metals adsorption behavior of a composite of clay (bentonite) combined with magnetic iron oxides in a mass ratio of clay/iron oxide of 0:1, 1:1, 1.5:1, and 2:1. The results showed that magnetization decreased as follows: 62, 27, 18, and 8 emu/g with the iron oxide content decreased as follows: 95%, 55%, 40%, and 33% *wt*. Oliveira et al. (2004) investigated the adsorption of a composite made of NaY-zeolite and magnetic iron oxides in a mass ratio of 3:1. They found magnetization is 18 emu/g with an iron oxide content 8% *wt*, as compared to 62 emu/g of pure iron oxide. Both studies showed that adsorption capability of magnetic composites were not reduced but the magnetization could improve the magnetic separation of the adsorbent from its medium. Also, Faghihian et al. (2013) used different zeolites as support materials to impregnate iron oxide by direct liquid precipitation and thermal method (Pan et al., 2010), and obtained magnetization of 19.5 emu/g. Jang et al. (2008) used similar synthesis method to prepare iron oxide-coated granular activated carbon. Maleki et al. (2019) investigated that use of geopolymer combined with magnetic iron oxide of different mass ratios for heavy metals removal. Their results showed that the adsorbent has high removal efficiency for heavy metals.

Table 2-14. Comparison of magnetic composites' properties and adsorption on heavy metals.

Host material	Method of synthesis	Size	BET surface area, m^2/g	CEC, cmol/kg	Ms, emu/g	Pollutants	dose, g/L	pH	Time, hr	Adsorption capacity	Reference
Nut shield biochar	Chemical co-precipitation	25-100 nm	356	366	--	Pb^{2+}	2	5	24	179 mg/g	Trakal et al., 2016
						Cd^{2+}				50.6 mg/g	
bentonite	Chemical co-precipitation	--	58	--	8	Ni^{2+}	2	3	24	40 mg/g	Oliveira et al., 2003
						Cu^{2+}				50 mg/g	
						Cd^{2+}				74 mg/g	
						Zn^{2+}				75 mg/g	
NaY-Zeolite	Chemical co-precipitation	16 nm	381	--	18	Cr^{3+}	1.67	5	24	49 mg/g	Oliveira et al., 2004
						Cu^{2+}				87 mg/g	
						Zn^{2+}				114 mg/g	
Zeolite A	Chemical co-precipitation	65.8 nm	--	81.4 – 95.2	19.5	Cs^{+}	10	8	2	229.3 mg/g	Faghihian et al., 2013
						Sr^{2+}				89.05 mg/g	
Porous cation-exchange resin D-001	Direct liquid precipitation and thermal treatment	0.4 – 0.6 μm	28200	430	--	Pb^{2+}	0.5	4.5-6	2	332 mg/g	Pan et al., 2010
						Cu^{2+}				89 mg/g	
						Cd^{2+}				157 mg/g	
granular activated carbon	Direct liquid precipitation and thermal treatment	126 μm	300 – 600	--	--	As^{5+}	0.1	7.5	8	60 mg/g	Jang et al., 2008
Geopolymer	Chemical co-precipitation	--	2.32	--	--	Cu^{2+}	5	7	2	99%	Maleki et al., 2019
						Ni^{2+}				99%	
						Pb^{2+}				92-94%	
						Cd^{2+}				96-97%	
						Hg^{2+}				92%	

2.5.4. Application of Magnetic Field in Water/wastewater Treatment

As in above sections, the magnetic iron oxides or its composites can be used as adsorbent for the removal of heavy metals in aqueous solution. However, there is still a drawback in its application for water/wastewater treatment, if it is in fine particle or powdered form. The additional separation step to remove such materials from solution is inevitable.

A problem with these materials is that the magnetic material is widely dispersed in the host material particle or upon its surface. This is inherent in their compositions, since powdered magnetic material (magnetite) is used and in only a minor amount to impart the magnetic property. Thus, depending on the particular composition, the magnetic material is dispersed throughout a matrix as small particles of the host material, or concentrated on the surface.

When these magnetic materials are comminuted, host fines are usually formed that free the magnetic material cannot be magnetically separated. Thus, magnetic separation requires the particles to be relatively large to maintain their magnetic properties. Accordingly, the non-magnetic fines formed cannot be recovered. Thus, the recovery requires relatively large host particles.

Another problem with some magnetic compositions, is that their magnetic properties are not sufficiently “soft” compared to the Fe_3O_4. It is desired that the host become magnetic only during exposure to the magnetic field used to separate the carbon particles from the solution. Any residual or “hard” magnetism that remains only complicates the separation process since the host particles stick together and foul the process machinery.

Table 2-15 presents the several researches studying the effects of magnetic field on the wastewater treatment.

For instance, magnetic field were applied for removal of heavy metals (Kamariah, 2006; Bée et al., 2011; Girginova et al., 2010, Xu et al., 2009) and organic dyes (Hao et al., 2009; Fang et al., 2010; Hu et al., 2010).

Turbidity and suspended solids have also been significantly removed by the application of magnetic field (Kamariah, 2006, Chin et al., 2006, Zularisam et al., 2007).

Chin et al. (2006) used magnetic nanoparticles as an adsorbent to reduce the turbidity of wastewater. In treating chemical polishing wastewater, turbidity was reduced from 9500 to 1.07 NTU under an 80 mT magnetic separator with further decreased to 1.04 NTU under 130 mT at 30 min (Chin et al., 2006). This reduction differs greatly from that achieved by the process without magnetic treatment, in which a smaller reduction in turbidity, 9500 to 6.3 NTU, was obtained even within a longer period (60 min) (Chin et al., 2006).

In this particular modified magnetic treatment of a coagulation system, magnetite seeding was employed, and a magnetic separator of the specified intensity was used in the later stage. This was achieved by electrostatic attraction arising from the fact that they are highly oppositely charged. Collisions between magnetite seeds and silica nanoparticles eventually enhanced the coagulation process, thus improving turbidity reduction.

In general, significant enhancements were observed when wastewater treatment systems are coupled with magnetic application. This technique shortens the start-up time and removal performance of the systems. In addition, physical treatment systems are remarkably improved with the implementation of a magnetic field.

Table 2-15. Applications of magnetic field on the wastewater treatment

Treatment	Magnetic material	Magnet type	Magnetic intensity, mT	Removal	Reference
Pb^{2+}	magnetic beads	*NdFeB* magnet	80 or 4.5×10^{-5} N	50%	Bée et al., 2011
Fe^{2+}	--	Permanent magnet	550	98.7%	Kamariah, 2006
Mn^{2+}				92.5%	
Turbidity				94.3%	
Hg^{2+}	silica coated magnetite	*NdFeB* magnet	1480	74%	Girginova et al., 2010
Cr^{5+}	Magnetic powder	Magnetic pieces	6	84.73	Xu et al., 2009
Turbidity	--	Electromagnetic system	67	49%	Zularisam et al., 2007
Turbidity	Magnetite nanoparticles	Permanent magnets	80	110 NTU to 7 NTU	Chin et al., 2006
organic dyes	ferromagnetic particles	Permanent magnet	200	80%	Fang et al., 2010
Methylene blue	magnetite nanoparticles	*NdFeB* magnet	300	95.3%	Hu et al., 2010
Methylene blue	magnetic piece	Permanent magnet	80 – 320	> 10% with increased intensity	Hao et al., 2009

2.5.5. Advantages and Limitations of Magnetic Adsorbent in Water/wastewater Treatment

Many studies have been conducted on the potential application of magnetic field in various environmental engineering systems, specifically, in water and wastewater treatment systems. As mentioned earlier, the application of a magnetic field as an aid would facilitate the system significantly due to its ability to overcome the constraints of conventional treatment processes. The advantages of magnetic field implementation in water and wastewater systems can be summarized as follows:

- Use of permanent magnets as an aid in the system is its low initial cost. The strength of the magnet can last for many years (Higashitani & Oshitani, 1997).
- The operation time is potentially shortened with magnetic field exposure towards a treatment system, since the effect of magnetic field can speed up the treatment processes (Chin et al., 2006).
- The operation is simple as it is applied directly to the influent or sludge requiring treatment. When a magnetite or magnetic adsorbent is used as the mode of magnetization, the adsorbent can be recycled and regenerated for further use, while maintaining higher adsorption efficiency (Girginova et al., 2010).

Nevertheless, there are also limitations that need to be considered in the implementation of magnetic field in water and wastewater treatment systems. In terms of practical use, exposure to magnetic intensity is the most critical aspect that has to be considered. Also, the adsorption capacity of the adsorbent maybe limited by the magnetite as compared the adsorbents with magnetite. To prolong the efficiency of magnetite, proper synthesis method is required to form the large surface area so that the life of magnetite can be extended. In addition, using an effective

adsorbent as support or host material (i.e. geopolymer materials) with magnetic aid could be developed to be used as the magnetic separator.

Based on the advantages and limitations of the magnetic field applications, it can be inferred that this technology can be reliable and beneficial for the enhancement of water and wastewater treatment systems. The limitations are challenges that can be overcome through further research and improvement.

2.6. Knowns and Unknowns

The role of fly ash-based geopolymer in removal of heavy metals from wastewater has been investigated. Adsorption can be affected by a number of factors, such as adsorbent dosage, particle size, contact time, initial concentration, pH, temperature of the aqueous solution. Generally, percent adsorption increased with increased adsorbent dose, contact time, and agitation speed. However, favorable conditions may be different for different materials and adsorptions. For each type of material, there is a neutral pH beyond at which the material will be either positively or negatively charged. For every heavy metal, there is a favorable pH range in which maximum adsorption was observed.

Adsorption of heavy metal ions from aqueous solutions using fly ash-based geopolymer as an adsorbent has been studied. However, there are several issues and drawbacks that need to be addressed. These can be summarized as shown below:

- In most studies, little attempts were made to relate the characterization results with the performance of the adsorbents for the removal of heavy metals.
- Metal ion adsorption is known to be pH dependent. In most of the cases, the pH effect was invariably investigated in terms of the initial pH of the solution. However, there were no mention in these studies the change in the solution pH during the course of exposure.

- Competitive metal adsorption on various adsorbents was reported in a few cases. However, there is scarce of data on the adsorption of heavy metals in presence of organic and other contaminants.
- Selection and identification of an appropriate low-cost adsorbent is one of the key issues in the development of adsorption technologies.
- Leaching of fly ash-based geopolymer in water is very important in order to see the dissolution of the various substances present in the wastes. This interference will lead to erroneous results in the adsorption experiments. However, very few authors studied the leaching of geopolymer when used as an environmental material such as an adsorbent.
- Adsorption mechanisms of heavy metals from wastewater need to be studied in detail such as the binding mechanism of heavy metals with fly ash-based geopolymer. This can be done by blocking the functional group responsible for the adsorption of heavy metals. However, in very few cases the binding mechanism is reported.
- To promote the adsorption capacities, composite materials with a mixture of geopolymer and other materials can be developed.
- The cost of the fly ash-based geopolymer compared to other adsorbents is seldom reported in any of the publications. However, the expense of individual adsorbents varies, depending on the processing conditions and local availability. In spite of the scarcity of consistent cost information, the widespread uses of low-cost adsorbents for wastewater treatment applications today strongly shows the research efforts in this area. If low-cost adsorbents such as fly ash-based geopolymer can perform well in removing heavy metals at a low cost, they can be adopted and widely used in industries. Therefore, a cost–benefit analysis of

using low-cost adsorbents for heavy metal removal needs to be conducted to judge the economic feasibility of its practical use in wastewater treatment applications today.

Some future work is proposed below.

- To control the production and improve the performances of fly ash-based geopolymer, reaction mechanisms of the silica-aluminate polymer need to be explored in detail.
- Changes in preparation and curing conditions to create improved fly ash-based geopolymer with high stability and of high porosity is still needed.
- Stabilizing the fly ash-based geopolymer by changing the recipes so that toxic metals adsorption or just exposure to aqueous conditions will minimize release of secondary cations.
- Instead of using fly ash-based geopolymer as alternative cement, it is also possible to create fly ash-based geopolymer with more functionalities or unique properties. Consequently, new applications of fly ash-based geopolymer are worth exploring and can be found.
- Fly ash-based geopolymer with addition of magnetic iron oxides is an improvement in terms of adding more functionalities to the geopolymer. However, it is possible that further refinements can be made to the magnetization properties such as tunable properties to optimize separation, recycle and regeneration of the magnetized particles.

2.7. References

Ahamad, K. U., & Jawed, M. (2012). Breakthrough studies with mono-and binary-metal ion systems comprising of Fe (II) and As (III) using community prepared wooden charcoal packed columns. *Desalination*, *285*, 345-351.

Ahmaruzzaman, M. (2010). A review on the utilization of fly ash. *Progress in Energy and Combustion Science*, *36*(3), 327-363.

Al-Harahsheh, M. S., Al Zboon, K., Al-Makhadmeh, L., Hararah, M., & Mahasneh, M. (2015). Fly ash based geopolymer for heavy metal removal: a case study on copper removal. *Journal of Environmental Chemical Engineering*, *3*(3), 1669-1677.

Aliahmad, M., & Moghaddam, N. N. (2013). Synthesis of maghemite (γ-Fe_2O_3) nanoparticles by thermal-decomposition of magnetite (Fe_3O_4) nanoparticles. *Materials Science-Poland*, *31*(2), 264-268.

Alinnor, I. J. (2007). Adsorption of heavy metal ions from aqueous solution by fly ash. *Fuel*, *86*(5), 853-857.

Allen, S. J., Mckay, G., & Khader, K. Y. H. (1989). Intraparticle diffusion of a basic dye during adsorption onto sphagnum peat. *Environmental Pollution*, *56*(1), 39-50.

Alouani, M. E. L., Alehyen, S., Achouri, M. E. L., & Taibi, M. (2018). Removal of cationic dye-methylene blue-from aqueous solution by adsorption on fly ash-based geopolymer. *J. Mater. Environ. Sci.*, *9*(1), 32-46.

Al-Zboon, K., Al-Harahsheh, M. S., & Hani, F. B. (2011). Fly ash-based geopolymer for Pb removal from aqueous solution. *Journal of Hazardous Materials*, *188*(1), 414-421.

Ambashta, R. D., & Sillanpää, M. (2010). Water purification using magnetic assistance: a review. *Journal of Hazardous Materials*, *180*(1-3), 38-49.

Archer, M. J. G., & Caldwell, R. A. (2004). Response of six Australian plant species to heavy metal contamination at an abandoned mine site. *Water, Air, and Soil Pollution*, *157*(1-4), 257-267.

Atun, G., Hisarlı, G., Kurtoğlu, A. E., & Ayar, N. (2011). A comparison of basic dye adsorption onto zeolitic materials synthesized from fly ash. *Journal of Hazardous Materials*, *187*(1-3), 562-573.

Azizian, S. (2004). Kinetic models of sorption: a theoretical analysis. *Journal of Colloid and Interface Science*, *276*(1), 47-52.

Badruddoza, A. Z. M., Tay, A. S. H., Tan, P. Y., Hidajat, K., & Uddin, M. S. (2011). Carboxymethyl-β-cyclodextrin conjugated magnetic nanoparticles as nano-adsorbents for removal of copper ions: synthesis and adsorption studies. *Journal of Hazardous Materials*, *185*(2-3), 1177-1186.

Baker, F. S., Miller, C. E., Repik, A. J., & Tolles, E. D. (2000). Activated carbon. *Kirk-Othmer Encyclopedia of Chemical Technology*. Vol. 2, pp. 881–899

Bakharev, T. (2006). Thermal behaviour of geopolymers prepared using class F fly ash and elevated temperature curing. *Cement and Concrete Research*, *36*(6), 1134-1147.

Balistrieri, L. S., Seal II, R. R., Piatak, N. M., & Paul, B. (2007). Assessing the concentration, speciation, and toxicity of dissolved metals during mixing of acid-mine drainage and ambient river water downstream of the Elizabeth Copper Mine, Vermont, USA. *Applied Geochemistry*, *22*(5), 930-952.

Bée, *A., Talbot, D., Abramson, S., and Dupuis, V. (2011). Magnetic alginate beads for Pb(II) ions removal from wastewater. J. Coll. Inter. Sci.,* 362 (2): 486–492.

Belaïd, S., Laurent, S., Vermeersch, M., Vander Elst, L., Perez-Morga, D., & Muller, R. N. (2013). A new approach to follow the formation of iron oxide nanoparticles synthesized by thermal decomposition. *Nanotechnology*, *24*(5), 055705.

Biswas, S., & Mishra, U. (2015). Continuous fixed-bed column study and adsorption modeling: removal of lead ion from aqueous solution by charcoal originated from chemical carbonization of rubber wood sawdust. *Journal of Chemistry*, Vol. 2015, Article ID 907379, 9 pages, https://doi.org/10.1155/2015/907379.

Blaney, L. (2007). Magnetite (Fe_3O_4): Properties, synthesis, and applications. *Lehigh University, Volume 15 - 2007. Paper 5.* http://preserve.lehigh.edu/cas-lehighreview-vol-15/5.

Bohart, G. S., & Adams, E. Q. (1920). Some aspects of the behavior of charcoal with respect to chlorine. *Journal of the American Chemical Society*, 42(3), 523-544.

Bohlooli, H., Nazari, A., Khalaj, G., Kaykha, M. M., & Riahi, S. (2012). Experimental investigations and fuzzy logic modeling of compressive strength of geopolymers with seeded fly ash and rice husk bark ash. *Composites Part B: Engineering*, *43*(3), 1293-1301.

Boult, S., Collins, D. N., White, K. N., & Curtis, C. D. (1994). Metal transport in a stream polluted by acid mine drainage—the Afon Goch, Anglesey, UK. *Environmental Pollution*, *84*(3), 279-284.

Brunauer, S., Emmett, P. H., & Teller, E. (1938). Adsorption of gases in multimolecular layers. *J. Am. Chem. Soc.*, *60*(2), 309-319.

Buekens, A., & Zyaykina, N. N. (2001). Adsorbents and Adsorption Processes for Pollution Control. *Pollution Control Technologies*, *2*.

Carlos, L., Einschlag, F. G., González, M. C., & Mártire, D. O. (2013). Applications of magnetite nanoparticles for heavy metal removal from wastewater. *Waste Water-treatment Technologies and Recent Analytical Developments*, 2013, 63-77.

Chen, D., & Xu, R. (1998). Hydrothermal synthesis and characterization of nanocrystalline Fe3O4 powders. *Materials Research Bulletin*, *33*(7), 1015-1021.

Cheng, T. W., Lee, M. L., Ko, M. S., Ueng, T. H., & Yang, S. F. (2012). The heavy metal adsorption characteristics on metakaolin-based geopolymer. *Applied Clay Science*, *56*, 90-96.

Chin, C.-J.M., Chen, P.-W., and Wang, L.-J. (2006). Removal of nanoparticles from CMP wastewater by magnetic seeding aggregation. *Chemosphere*, 63 (10): 1809–1813.

Coulton, R., Bullen, C., & Hallett, C. (2003). The design and optimisation of active mine water treatment plants. *Land Contamination and Reclamation*, *11*(2), 273-280.

Criado, M., Palomo, A., & Fernández-Jiménez, A. (2005). Alkali activation of fly ashes. Part 1: Effect of curing conditions on the carbonation of the reaction products. *Fuel*, *84*(16), 2048-2054.

Crittenden, B., & Thomas, W. J. (1998). *Adsorption technology and design*. Elsevier.

Crittenden, J. C., Trussell, R. R., Hand, D. W., Howe, K. J., & Tchobanoglous, G. (2012). *MWH's water treatment: principles and design*. John Wiley & Sons, Hoboken, NJ.

Cui, B., Li, T., Liu, J., & Marinescu-Jasinski, M. (2015). Mesoporous urchin-like α-Fe2O3 superstructures with high coercivity and excellent gas sensing properties. *Materials Research Express*, *2*(4), 045011.

Cumbal, L., & SenGupta, A. K. (2005). Arsenic removal using polymer-supported hydrated iron (III) oxide nanoparticles: role of Donnan membrane effect. *Environmental Science & Technology*, *39*(17), 6508-6515.

Davidovits, J. (1991). Geopolymers: inorganic polymeric new materials. *Journal of Thermal Analysis and Calorimetry*, *37*(8), 1633-1656.

Davidovits, J. (1994). High-Alkali Cements for 21st Century Concretes in Concrete Technology, Past, Present and Future, *Proceedings of V. Mohan Malhotra Symposium*, Editor: P. Kumar Metha, ACI SP- 144, 383-397

Davidovits, J. (2002). 30 years of successes and failures in geopolymer applications. Market trends and potential breakthroughs. In *Geopolymer 2002 Conference*, (Vol. 28, p. 29). Saint-Quentin, France; Melbourne, Australia: Geopolymer Institute.

Davidovits, J., Comrie, D. C., Paterson, J. H., & Ritcey, D. J. (1990). Geopolymeric concretes for environmental protection. *Concrete International*, *12*(7), 30-40.

De Vargas, A. S., Dal Molin, D. C., Vilela, A. C., Da Silva, F. J., Pavão, B., & Veit, H. (2011). The effects of Na 2 O/SiO 2 molar ratio, curing temperature and age on compressive strength, morphology and microstructure of alkali-activated fly ash-based geopolymers. *Cement and Concrete Composites*, *33*(6), 653-660.

Dizge, N., Aydiner, C., Demirbas, E., Kobya, M., & Kara, S. (2008). Adsorption of reactive dyes from aqueous solutions by fly ash: Kinetic and equilibrium studies. *Journal of Hazardous Materials*, *150*(3), 737-746.

Duan, P., Yan, C., Zhou, W., & Ren, D. (2016). Development of fly ash and iron ore tailing based porous geopolymer for removal of Cu (II) from wastewater. *Ceramics International*, *42*(12), 13507-13518.

Dudka, S., & Adriano, D. C. (1997). Environmental impacts of metal ore mining and processing: a review. *Journal of Environmental Quality*, *26*(3), 590-602.

Duxson, P., Provis, J. L., Lukey, G. C., & Van Deventer, J. S. (2007). The role of inorganic polymer technology in the development of 'green concrete'. *Cement and Concrete Research*, 37(12), 1590-1597.

Ebrahimian P., A., Saberikhah, E., Badrouh, M., and Emami, M. S. (2014). Alkali treated Foumanat tea waste as an efficient adsorbent for methylene blue adsorption from aqueous solution. *Water Resources and Industry*, 6, 64–80.

El-Eswed, B. I. (2018). Solidification versus adsorption for immobilization of pollutants in geopolymeric materials: a review. *Solidification*, 77.

El-Eswed, B., Yousef, R. I., Alshaaer, M., Hamadneh, I., & Khalili, F. (2013). Adsorption of Cu (II), Ni (II), Zn (II), Cd (II) and Pb (II) onto kaolin/zeolite based-geopolymers. *Advances in Materials Physics and Chemistry*, *2*(04), 119.

Environmental, Protection Agency EPA. (2002). National primary drinking water regulations: Long Term 1 Enhanced Surface Water Treatment Rule. Final rule. *Federal register*, *67*(9), 1811.

Faghihian, H., Moayed, M., Firooz, A., & Iravani, M. (2013). Synthesis of a novel magnetic zeolite nanocomposite for removal of Cs+ and Sr2+ from aqueous solution: Kinetic, equilibrium, and thermodynamic studies. *Journal of Colloid and Interface science*, *393*, 445-451.

Fan, R., Chen, X. H., Gui, Z., Liu, L., & Chen, Z. Y. (2001). A new simple hydrothermal preparation of nanocrystalline magnetite Fe_3O_4. *Materials Research Bulletin*, *36*(3-4), 497-502.

Fang, M., Mishima, F., Akiyama, Y., and Nishijima, S. (2010). Fundamental study on magnetic separation of organic dyes in wastewater. *Physica C*, 470(20): 1827–1830.

Feng, D., Aldrich, C., & Tan, H. (2000). Treatment of acid mine water by use of heavy metal precipitation and ion exchange. *Minerals Engineering*, *13*(6), 623-642.

Force, B. A. T. (1989). Draft acid rock drainage technical guide. *Prepared by Steffen, Robertson and Kirsten (BC) Inc. in association with Norecol Environmental Consultants and Gormely Process Engineering*.

Freeze, R. A., & Cherry, J. A. (1979). Groundwater: Englewood Cliffs. *New Jersey*.

Freundlich, H. M. F. (1906). Over the adsorption in solution. *J. Phys. Chem*, *57*(385), e470.

Fu, F., & Wang, Q. (2011). Removal of heavy metal ions from wastewaters: a review. *Journal of Environmental Management*, *92*(3), 407-418.

Futalan, C. M., Kan, C. C., Dalida, M. L., Pascua, C., & Wan, M. W. (2011). Fixed-bed column studies on the removal of copper using chitosan immobilized on bentonite. *Carbohydrate polymers*, *83*(2), 697-704.

Gaikwad, R. W., Sapkal, R. S., & Sapkal, V. S. (2010). Removal of copper ions from acid mine drainage wastewater using ion exchange technique: factorial design analysis. *Journal of Water Resource and Protection*, *2*(11), 984.

Gao, Z., Cui, F., Zeng, S., Guo, L., & Shi, J. (2010). A high surface area superparamagnetic mesoporous spinel ferrite synthesized by a template-free approach and its adsorptive property. *Microporous and Mesoporous Materials*, *132*(1-2), 188-195.

Ge, Y., Cui, X., Kong, Y., Li, Z., He, Y., & Zhou, Q. (2015). Porous geopolymeric spheres for removal of Cu (II) from aqueous solution: synthesis and evaluation. *Journal of hazardous materials*, *283*, 244-251.

Ge, Y., Cui, X., Liao, C., & Li, Z. (2017). Facile fabrication of green geopolymer/alginate hybrid spheres for efficient removal of Cu (II) in water: batch and column studies. *Chemical Engineering Journal*, *311*, 126-134.

Geetha, S., & Ramamurthy, K. (2013). Properties of geopolymerised low-calcium bottom ash aggregate cured at ambient temperature. *Cement and Concrete Composites*, *43*, 20-30.

Ghosh, K., & Ghosh, P. (2018). Effect of Alkali Concentration on Mechanical Properties, Microstructure, Zeta Potential and Electrical Conductivity of Thermally Cured Fly-Ash-Blast Furnace Slag Based Blended Geopolymer Composites. *Oriental Journal of Chemistry*, *34*(2), 704.

Girginova, P.I., Daniel-da-Silva, A.L., Lopes, C.B., Figueira, P., Otero, M., Amaral, V.S., Pereira, E., and Trindade, T. (2010). Silica coated magnetite particles for magnetic removal of Hg^{2+} from water. *J. Coll. Interf. Sci.*, 345 (2): 234–240.

Gong, J., Chen, L., Zeng, G., Long, F., Deng, J., Niu, Q., & He, X. (2012). Shellac-coated iron oxide nanoparticles for removal of cadmium (II) ions from aqueous solution. *Journal of Environmental Sciences*, *24*(7), 1165-1173.

Goyal, M., Rattan, V. K., Aggarwal, D., & Bansal, R. C. (2001). Removal of copper from aqueous solutions by adsorption on activated carbons. *Colloids and Surfaces A: Physicochemical and Engineering Aspects*, *190*(3), 229-238.

Gray, N. F. (1998). Acid mine drainage composition and the implications for its impact on lotic systems. *Water Research*, *32*(7), 2122-2134.

Guo, L., Arafune, H., & Teramae, N. (2013). Synthesis of mesoporous metal oxide by the thermal decomposition of oxalate precursor. *Langmuir*, *29*(13), 4404-4412.

Gupta, A. K., & Gupta, M. (2005). Synthesis and surface engineering of iron oxide nanoparticles for biomedical applications. *Biomaterials*, *26*(18), 3995-4021.

Han, C., Cai, W., Tang, W., Wang, G., & Liang, C. (2011). Protein assisted hydrothermal synthesis of ultrafine magnetite nanoparticle built-porous oriented fibers and their structurally enhanced adsorption to toxic chemicals in solution. *Journal of Materials Chemistry*, *21*(30), 11188-11196.

Han, L., & Wei, Y. (2012). Low-temperature synthesis of Fe_3O_4 microroses and their application in water treatment. *Materials Letters*, *70*, 1-3.

Han, R., Zou, L., Zhao, X., Xu, Y., Xu, F., Li, Y., & Wang, Y. (2009). Characterization and properties of iron oxide-coated zeolite as adsorbent for removal of copper (II) from solution in fixed bed column. *Chemical Engineering Journal*, *149*(1-3), 123-131.

Hanjitsuwan, S., Hunpratub, S., Thongbai, P., Maensiri, S., Sata, V., & Chindaprasirt, P. (2014). Effects of NaOH concentrations on physical and electrical properties of high calcium fly ash geopolymer paste. *Cement and Concrete Composites*, *45*, 9-14.

Hansen, B. Ø., Kwan, P., Benjamin, M. M., Li, C. W., & Korshin, G. V. (2001). Use of iron oxide-coated sand to remove strontium from simulated Hanford tank wastes. *Environmental Science & Technology*, *35*(24), 4905-4909.

Hao, X.L., Zou, L.Y., Zhang, G.S., and Zhang, Y.B. (2009). Magnetic field assisted Fenton reactions for the enhanced degradation of methyl blue. Chin. *Chem. Lett.*, 20(1): 99–101.

Hao, Y. M., Man, C., & Hu, Z. B. (2010). Effective removal of Cu (II) ions from aqueous solution by amino-functionalized magnetic nanoparticles. *Journal of Hazardous Materials*, *184*(1-3), 392-399.

Hardjito, D. and Rangan, B. V. (2005), Development and Properties of Low-Calcium Fly Ash-based Geopolymer Concrete. *Research Report GC1, Faculty of Engineering*, Curtin University of Technology, Perth.

Hasan, S. H., & Srivastava, P. (2009). Batch and continuous biosorption of Cu2+ by immobilized biomass of Arthrobacter sp. *Journal of Environmental Management*, *90*(11), 3313-3321.

Hasfalina, C. M., Maryam, R. Z., Luqman, C. A., & Rashid, M. (2012). Adsorption of copper (II) from aqueous medium in fixed-bed column by kenaf fibres. *APCBEE Procedia*, *3*, 255-263.

Higashitani, K., & Oshitani, J. (1997). Measurements of magnetic effects on electrolyte solutions by atomic force microscope. *Process Safety and Environmental Protection*, *75*(2), 115-119.

Hsu, T. C. (2008). Adsorption of an acid dye onto coal fly ash. *Fuel*, *87*(13), 3040-3045.

Hua, M., Zhang, S., Pan, B., Zhang, W., Lv, L., & Zhang, Q. (2012). Heavy metal removal from water/wastewater by nanosized metal oxides: a review. *Journal of Hazardous Materials*, *211*, 317-331.

Ibrahim, O. A. A. (2011). *Evaluation of synthetic zeolite as engineering passive permeable reactive barrier*. Thesis, Cairo University, Egypt.

Iconaru, S. L., Guégan, R., Popa, C. L., Motelica-Heino, M., Ciobanu, C. S., & Predoi, D. (2016). Magnetite (Fe_3O_4) nanoparticles as adsorbents for As and Cu removal. *Applied Clay Science*, *134*, 128-135.

Jamal, H. Y. A. (2015). Removal of Heavy Metals from Acid Mine Drainage: A Review. *Int. J. New Technol. Sci. Eng.*, *2*, 77-84.

Jang, M., Chen, W., & Cannon, F. S. (2008). Preloading hydrous ferric oxide into granular activated carbon for arsenic removal. *Environmental Science & Technology*, *42*(9), 3369-3374.

Javadian, H., Ghorbani, F., Tayebi, H. A., & Asl, S. H. (2015). Study of the adsorption of Cd (II) from aqueous solution using zeolite-based geopolymer, synthesized from coal fly ash; kinetic, isotherm and thermodynamic studies. *Arabian Journal of Chemistry*, *8*(6), 837-849.

Johnson, D. B., & Hallberg, K. B. (2005). Acid mine drainage remediation options: a review. *Science of the Total Environment*, *338*(1-2), 3-14.

Kamariah, M.S. (2006). *Subsurface flow and free water surface flow constructed wetland with magnetic field for leachate treatment*; Thesis of Master of Engineering (Civil-Wastewater): Universiti Teknologi Malaysia.

Kanthimathi, G., Kotteeswaran, P., Muthuraman, M., Mahendran, M., & Kottaisamy, M. (2013). Atomic absorption and vibrational spectral magnetic studies on the removal of Cu (II) and Co (II) Ions using synthetic nano adsorbent Fe3O4. *Soft Nanoscience Letters*, *3*(04), 75.

Kara, I., Tunc, D., Sayin, F., & Akar, S. T. (2018). Study on the performance of metakaolin based geopolymer for Mn (II) and Co (II) removal. *Applied Clay Science*, *161*, 184-193.

Kara, İ., Yilmazer, D., & Akar, S. T. (2017). Metakaolin based geopolymer as an effective adsorbent for adsorption of zinc (II) and nickel (II) ions from aqueous solutions. *Applied Clay Science*, *139*, 54-63.

Kefeni, K. K., Msagati, T. A., & Mamba, B. B. (2017). Acid mine drainage: prevention, treatment options, and resource recovery: a review. *Journal of Cleaner Production*, *151*, 475-493.

Kleinmann, R. L. (1990). Acid mine drainage: an overview. In *Energy in the 90's* (pp. 281-286). ASCE.

Lan, S., Wu, X., Li, L., Li, M., Guo, F., & Gan, S. (2013). Synthesis and characterization of hyaluronic acid-supported magnetic microspheres for copper ions removal. *Colloids and Surfaces A: Physicochemical and Engineering Aspects*, *425*, 42-50.

Langmuir, D. (1997). Aqueous environmental. *Geochemistry Prentice Hall: Upper Saddle River, NJ*.

Langmuir, I. (1917). The constitution and fundamental properties of solids and liquids. 11. Liquids. *J. Am. Chem. Soc.*, *3*(9), 1848-1906.

Laurent, S., Forge, D., Port, M., Roch, A., Robic, C., Vander Elst, L., & Muller, R. N. (2008). Magnetic iron oxide nanoparticles: synthesis, stabilization, vectorization, physicochemical characterizations, and biological applications. *Chemical Reviews*, *108*(6), 2064-2110.

Lee, N. K., Khalid, H. R., & Lee, H. K. (2017). Adsorption characteristics of cesium onto mesoporous geopolymers containing nano-crystalline zeolites. *Microporous and Mesoporous Materials*, *242*, 238-244.

Leung, C. K., & Pheeraphan, T. (1995). Very high early strength of microwave cured concrete. *Cement and Concrete Research*, *25*(1), 136-146.

Li, L., Wang, S., & Zhu, Z. (2006). Geopolymeric adsorbents from fly ash for dye removal from aqueous solution. *Journal of Colloid and Interface Science*, *300*(1), 52-59.

Li, X. M., Xu, G., Liu, Y., & He, T. (2011). Magnetic Fe3O4 nanoparticles: Synthesis and application in water treatment. *Nanoscience & Nanotechnology-Asia*, *1*(1), 14-24.

Li, Y., Zhang, F. S., & Xiu, F. R. (2009). Arsenic (V) removal from aqueous system using adsorbent developed from a high iron-containing fly ash. *Science of the Total Environment*, *407*(21), 5780-5786.

Li, Z., Wang, H., He, S., Lu, Y., & Wang, M. (2006). Investigations on the preparation and mechanical properties of the nano-alumina reinforced cement composite. *Materials Letters*, *60*(3), 356-359.

Lin, Y., Chen, H., Lin, K., Chen, B., & Chiou, C. (2011). Application of magnetic particles modified with amino groups to adsorb copper ions in aqueous solution. *Journal of Environmental Sciences*, *23*(1), 44-50.

Liu, Y., Chen, M., & Yongmei, H. (2013). Study on the adsorption of Cu (II) by EDTA functionalized Fe_3O_4 magnetic nano-particles. *Chemical Engineering Journal*, *218*, 46-54.

Liu, Y., Yan, C., Zhang, Z., Wang, H., Zhou, S., & Zhou, W. (2016). A comparative study on fly ash, geopolymer and faujasite block for Pb removal from aqueous solution. *Fuel*, *185*, 181-189.

Lodeiro, P., Herrero, R., & de Vicente, M. S. (2006). The use of protonated Sargassum muticum as biosorbent for cadmium removal in a fixed-bed column. *Journal of Hazardous Materials*, *137*(1), 244-253.

López, D. L., Gierlowski-Kordesch, E., & Hollenkamp, C. (2010). Geochemical mobility and bioavailability of heavy metals in a lake affected by acid mine drainage: Lake Hope, Vinton County, Ohio. *Water, air, & soil pollution*, *213*(1-4), 27-45.

López, F. J., Sugita, S., Tagaya, M., & Kobayashi, T. (2014). Metakaolin-based geopolymers for targeted adsorbents to heavy metal ion separation. *Journal of Materials Science and Chemical Engineering*, 2(07), 16.

MacKenzie, K. J., & Bolton, M. J. (2009). Electrical and mechanical properties of aluminosilicate inorganic polymer composites with carbon nanotubes. *Journal of materials science*, *44*(11), 2851-2857.

Maingi, F.M., Mbuvi, H.M., Ng'ang'a, M.M., and Mwangi, H. (2017). Adsorption Kinetics and Isotherms of Methylene blue by Geopolymers Derived from Common Clay and Rice Husk Ash. *Physical Chemistry*. 7(4): 87-97.

Maleki, A., Hajizadeh, Z., Sharifi, V., & Emdadi, Z. (2019). A green, porous and eco-friendly magnetic geopolymer adsorbent for heavy metals removal from aqueous solutions. *Journal of cleaner production*, *215*, 1233-1245.

Massart, R. (1981). Preparation of aqueous magnetic liquids in alkaline and acidic media. *IEEE Transactions on Magnetics*, *17*(2), 1247-1248.

Matei, E., Predescu, A., & Vasile, E. (2011). Properties of magnetic iron oxides used as materials for wastewater treatment. In *Journal of Physics: Conference Series* (Vol. 304, No. 1, p. 012022). IOP Publishing.

McMillan, W. G., & Teller, E. (1951). The assumptions of the BET theory. *The Journal of Physical Chemistry*, *55*(1), 17-20.

Moreno-Piraján, J. C., Rangel, D., Amaya, B., Vargas, E. M., & Giraldo, L. (2006, December). Scale-up of pilot plant for adsorption of heavy metals. In *Anales de la Asociación Química Argentina* (Vol. 94, No. 4-6, pp. 71-82). Asociación Química Argentina.

Mužek, M. N., Svilović, S., & Zelić, J. (2014). Fly ash-based geopolymeric adsorbent for copper ion removal from wastewater. *Desalination and Water Treatment*, *52*(13-15), 2519-2526.

Mužek, M. N., Svilović, S., Ugrina, M., & Zelić, J. (2016). Removal of copper and cobalt ions by fly ash-based geopolymer from solutions-equilibrium study. *Desalination and Water Treatment*, *57*(23), 10689-10699.

Nidheesh, P. V., Gandhimathi, R., Ramesh, S. T., & Singh, T. S. A. (2012). Adsorption and desorption characteristics of crystal violet in bottom ash column. *Journal of Urban and Environmental Engineering*, *6*(1), 18-29.

Nieto, J. M., Sarmiento, A. M., Olías, M., Canovas, C. R., Riba, I., Kalman, J., & Delvalls, T. A. (2007). Acid mine drainage pollution in the Tinto and Odiel rivers (Iberian Pyrite Belt, SW Spain) and bioavailability of the transported metals to the Huelva Estuary. *Environment International*, *33*(4), 445-455.

Okada, I., Ozaki, M., & Matijević, E. (1991). Magnetic interactions between platelet-type colloidal particles. *Journal of colloid and interface science*, *142*(1), 251-256.

Oliveira, L. C., Petkowicz, D. I., Smaniotto, A., & Pergher, S. B. (2004). Magnetic zeolites: a new adsorbent for removal of metallic contaminants from water. *Water Research*, *38*(17), 3699-3704.

Oliveira, L. C., Rios, R. V., Fabris, J. D., Sapag, K., Garg, V. K., & Lago, R. M. (2003). Clay–iron oxide magnetic composites for the adsorption of contaminants in water. *Applied Clay Science*, *22*(4), 169-177.

Oltulu, M., & Şahin, R. (2013). Effect of nano-SiO_2, nano-Al_2O_3 and nano-Fe_2O_3 powders on compressive strengths and capillary water absorption of cement mortar containing fly ash: a comparative study. *Energy and Buildings*, *58*, 292-301.

Palomo, A., Grutzeck, M. W., & Blanco, M. T. (1999). Alkali-activated fly ashes: a cement for the future. *Cement and Concrete Research*, *29*(8), 1323-1329.

Pan, B., Qiu, H., Pan, B., Nie, G., Xiao, L., Lv, L., Zhang, W., Zhang, Q., & Zheng, S. (2010). Highly efficient removal of heavy metals by polymer-supported nanosized hydrated Fe (III) oxides: behavior and XPS study. *Water Research*, *44*(3), 815-824.

Panday, K. K., Prasad, G., & Singh, V. N. (1985). Copper (II) removal from aqueous solutions by fly ash. *Water Research*, *19*(7), 869-873.

Patel, H. (2019). Fixed-bed column adsorption study: a comprehensive review. *Applied Water Science*, *9*(3), 45.

Peng, Q., Liu, Y., Zeng, G., Xu, W., Yang, C., & Zhang, J. (2010). Biosorption of copper (II) by immobilizing Saccharomyces cerevisiae on the surface of chitosan-coated magnetic nanoparticles from aqueous solution. *Journal of Hazardous Materials*, *177*(1-3), 676-682.

Peng, X., Xu, F., Zhang, W., Wang, J., Zeng, C., Niu, M., & Chmielewská, E. (2014). Magnetic Fe_3O_4@ silica–xanthan gum composites for aqueous removal and recovery of Pb^{2+}. *Colloids and Surfaces A: Physicochemical and Engineering Aspects*, *443*, 27-36.

Poghossian, A. A. (1997). Determination of the pH_{pzc} of insulators surface from capacitance–voltage characteristics of MIS and EIS structures. *Sensor and Actuator B: Chemical*, 44, 551–553.

Ramakrishna, K. R., & Viraraghavan, T. (1997). Dye removal using low cost adsorbents. *Water Science and Technology*, *36*(2-3), 189-196.

Rangan, B. V. (2010). Fly ash-based geopolymer concrete. In *Proceedings of the International Workshop on Geopolymer Cement and Concrete* (pp. 68-106). Allied Publishers Private Limited.

Rao, V. B., & Rao, S. R. M. (2006). Adsorption studies on treatment of textile dyeing industrial effluent by flyash. *Chemical Engineering Journal*, *116*(1), 77-84.

Rattanasak, U., Pankhet, K., & Chindaprasirt, P. (2011). Effect of chemical admixtures on properties of high-calcium fly ash geopolymer. *International Journal of Minerals, Metallurgy, and Materials*, *18*(3), 364.

Revathi, T., Jeyalakshmi, R., Rajamane, N. P., & Sivasakthi, M. (2017). Evaluation of the Role of Cetyltrimethylammoniumbromide (CTAB) and Acetylenic Glycol (AG) Admixture on fly ash Based Geopolymer. *Oriental Journal of Chemistry*, *33*(2), 783-792.

Riahi, S., & Nazari, A. (2012). The effects of nanoparticles on early age compressive strength of ash-based geopolymers. *Ceramics International*, *38*(6), 4467-4476.

Schmücker, M., & MacKenzie, K. J. (2005). Microstructure of sodium polysialate siloxo-geopolymer. *Ceramics International*, *31*(3), 433-437.

Sen A.K and Arnab K.D. (1987). Adsorption of mercury (II) by coal fly ash. *Water Research*, *21*(8), 885-888.

Shahbazi, A., Younesi, H., & Badiei, A. (2011). Functionalized SBA-15 mesoporous silica by melamine-based dendrimer amines for adsorptive characteristics of Pb (II), Cu (II) and Cd (II) heavy metal ions in batch and fixed bed column. *Chemical Engineering Journal*, *168*(2), 505-518.

Shen, Y. F., Tang, J., Nie, Z. H., Wang, Y. D., Ren, Y., & Zuo, L. (2009). Preparation and application of magnetic Fe_3O_4 nanoparticles for wastewater purification. *Separation and Purification Technology*, *68*(3), 312-319.

Shipley, H. J., Yean, S., Kan, A. T., & Tomson, M. B. (2009). Adsorption of arsenic to magnetite nanoparticles: effect of particle concentration, pH, ionic strength, and temperature. *Environmental Toxicology and Chemistry: An International Journal*, *28*(3), 509-515.

Simate, G. S., & Ndlovu, S. (2014). Acid mine drainage: Challenges and opportunities. *Journal of Environmental Chemical Engineering*, *2*(3), 1785-1803.

Škvára, F., Jílek, T., & Kopecký, L. (2005). Geopolymer materials based on fly ash. *Ceram.-Silik*, *49*(3), 195-204.

Smith, R. T., Comer, J. B., Ennis, M. V., Branam, T. D., Butler, S. M., & Renton, P. M. (2001). *Toxic Metals Removal in Acid Mine Drainage Treatment Wetlands*. Indiana Geological Survey.

Somna, K., Jaturapitakkul, C., Kajitvichyanukul, P., & Chindaprasirt, P. (2011). NaOH-activated ground fly ash geopolymer cured at ambient temperature. *Fuel*, *90*(6), 2118-2124.

Tchobanoglous, G., Burton, F. L., & Stensel, H. D. (2003). Metcalf & Eddy wastewater engineering: treatment and reuse. *International Edition. McGrawHill*, *4*, 361-411.

Thomas, H. C. (1944). Heterogeneous ion exchange in a flowing system. *Journal of the American Chemical Society*, *66*(10), 1664-1666.

Trakal, L., Veselská, V., Šafařík, I., Vítková, M., Číhalová, S., & Komárek, M. (2016). Lead and cadmium sorption mechanisms on magnetically modified biochars. *Bioresource technology*, *203*, 318-324

Trgo, M., Medvidović, N. V., & Perić, J. (2011). Application of mathematical empirical models to dynamic removal of lead on natural zeolite clinoptilolite in a fixed bed column. *Indian Journal of Chemical Technology*, *18*(2), 123-131.

Tu, Y. J., You, C. F., & Chang, C. K. (2012). Kinetics and thermodynamics of adsorption for Cd on green manufactured nano-particles. *Journal of Hazardous Materials*, *235*, 116-122.

Van Jaarsveld, J. G. S., Van Deventer, J. S. J., & Lukey, G. C. (2002). The effect of composition and temperature on the properties of fly ash-and kaolinite-based geopolymers. *Chemical Engineering Journal*, *89*(1), 63-73.

Van Jaarsveld, J. G. S., Van Deventer, J. S. J., & Lukey, G. C. (2003). The characterisation of source materials in fly ash-based geopolymers. *Materials Letters*, *57*(7), 1272-1280.

Vasanth, K. K. (2003). Adsorption Isotherms for Basic Dye on to Low Cost Adsorbents. *Res. J. Chem. Environ*, *7*, 72-77.

Viraraghavan, T., & Ramakrishna, K. R. (1999). Fly ash for color removal from synthetic dye solutions. *Water Quality Research Journal of Canada*, *34*(3), 505-517.

Wang, J., Sun, J., Sun, Q., & Chen, Q. (2003). One-step hydrothermal process to prepare highly crystalline Fe3O4 nanoparticles with improved magnetic properties. *Materials Research Bulletin*, *38*(7), 1113-1118.

Wang, S., & Zhu, Z. H. (2005). Sonochemical treatment of fly ash for dye removal from wastewater. *Journal of Hazardous Materials*, *126*(1), 91-95.

Wang, S., Boyjoo, Y., Choueib, A., & Zhu, Z. H. (2005b). Removal of dyes from aqueous solution using fly ash and red mud. *Water Research*, 39(1), 129-138.

Wang, S., Li, L., & Zhu, Z. H. (2007). Solid-state conversion of fly ash to effective adsorbents for Cu removal from wastewater. *Journal of Hazardous Materials*, *139*(2), 254-259.

Wang, S., Li, L., Wu, H., & Zhu, Z. H. (2005a). Unburned carbon as a low-cost adsorbent for treatment of methylene blue-containing wastewater. *Journal of Colloid and Interface Science*, 292(2), 336-343.

Wang, Y., Pugh, R. J., & Forssberg, E. (1994). The influence of interparticle surface forces on the coagulation of weakly magnetic mineral ultrafines in a magnetic field. *Colloids and Surfaces A: Physicochemical and Engineering Aspects*, *90*(2-3), 117-133.

Weber, W. J., & Morris, G. C. (1962). Removal of biologically-resistant pollutants from waste waters by adsorption. *Advances in Water Pollution Research*, *2*, 231-266.

Weiner, E. R. (2012). *Applications of environmental aquatic chemistry: a practical guide*. CRC press.

Wieczorek-Ciurowa, K., & Kozak, A. (1999). The thermal decomposition of Fe $(NO_3)_3 \cdot 9H_2O$. *Journal of Thermal Analysis and Calorimetry*, *58*(3), 647-651.

Worch, E. (2012). *Adsorption technology in water treatment: fundamentals, processes, and modeling*. Walter de Gruyter.

Xu, H., & Van Deventer, J. S. J. (2000). The geopolymerisation of alumino-silicate minerals. *International Journal of Mineral Processing*, *59*(3), 247-266.

Xu, Y.B., Duan, X.J., Yan, J.N., and Sun, S.Y. (2009). Influence of magnetic field on Cr (VI) adsorption capability of given anaerobic sludge. *Biodegrad.*, 21(1): 1–10.

Yahaya, N. K. E. M., Abustan, I., Latiff, M. F. P. M., Bello, O. S., & Ahmad, M. A. (2011). Fixed-bed column study for Cu (II) removal from aqueous solutions using rice husk based activated carbon. *International Journal of Engineering and Technology*, *11*(1), 248-252.

Yan, A., Liu, X., Qiu, G., Wu, H., Yi, R., Zhang, N., & Xu, J. (2008). Solvothermal synthesis and characterization of size-controlled Fe3O4 nanoparticles. *Journal of Alloys and Compounds*, *458*(1-2), 487-491.

Yan, G., Viraraghavan, T., & Chen, M. (2001). A new model for heavy metal removal in a biosorption column. *Adsorption Science & Technology*, *19*(1), 25-43.

Yang, G., Tang, L., Lei, X., Zeng, G., Cai, Y., Wei, X., Zhou, Y., Li, S., Fang, Y., & Zhang, Y. (2014). Cd (II) removal from aqueous solution by adsorption on α-ketoglutaric acid-modified magnetic chitosan. *Applied Surface Science*, *292*, 710-716.

Yousef, Y. A., Wanielista, M. P., & Harper, H. H. (1985). Removal of highway contaminants by roadside swales. *Transportation Research Record*, (1017).

Yu, C., Dong, X., Guo, L., Li, J., Qin, F., Zhang, L., Shi, J., & Yan, D. (2008). Template-free preparation of mesoporous Fe_2O_3 and its application as absorbents. *The Journal of Physical Chemistry C*, *112*(35), 13378-13382.

Zhang, M., Zhang, H., Xu, D., Han, L., Niu, D., Tian, B., Zhang, J., Zhang, L., & Wu, W. (2011). Removal of ammonium from aqueous solutions using zeolite synthesized from fly ash by a fusion method. *Desalination*, *271*(1-3), 111-121.

Zhang, Y., & Liu, L. (2013). Fly ash-based geopolymer as a novel photocatalyst for degradation of dye from wastewater. *Particuology*, *11*(3), 353-358.

Zhao, L., Chang, X. L., Liao, R., Zhang, X., Xie, J., Yu, B., Wu, R., Wang, R., & Yang, S. T. (2014). Facile hydrothermal preparation of S-doped Fe_3O_4@ C nanoparticles for Cu^{2+} removal. *Materials Letters*, *135*, 154-157.

Zularisam, A.W., Fadil. O., and Johan, S. (2007). *Electromagnetic Technology on Sewage Treatment*; Thesis of Philosophy of Doctorate: Universiti Teknologi Malaysia.

CHAPTER 3. SYNTHESIS OF FLY ASH-BASED GEOPOLYMER AND ITS ENVIRONMENTAL IMPACT AND APPLICATIONS

3.1. Abstract

In this study, fly ash-based geopolymer were synthesized from Class-F fly ash and slag with an alkaline activating solution consisting of SiO_2/Na_2O. The geopolymer samples were characterized for their physical-chemical properties and their surface properties using XRD and SEM imaging. The geopolymer samples were also tested to investigate their environmental impacts when used for environmental applications. Results showed that the geopolymer samples can achieve compressive strength of about 50 MPa at the age of 7 days which is comparable to concrete materials. In an aqueous solution, the geopolymer samples increased the pH of the solution due to the alkaline nature of the activator solutions and fly ash. The geopolymer samples exhibited removal of copper from solution with specific removal capacity as high as 29 mg/g, which was comparable or larger than other materials and adsorbents such as zeolite or activated carbon. With its good physical-chemical properties, the geopolymer can be used in neutralizing acid waste streams and act as a reactive material for removal of heavy metals.

3.2. Introduction

Currently, there is a significant trend in recycling of waste materials (i.e., plastic, plant materials, fly ash and slag) and converting them to usable and valuable materials in support of a sustainable economy. These materials such as sewage sludge ash (Pan et al., 2003), fly ash (Panday et al., 1999), slag (Dimitrova, 1996), tree bark (Mulgund et al., 2011), and plant leaves (Al-Subu et al., 2011), are low cost or available at no cost and may be available in large quantities. One particular waste material which has drawn much attention recently is fly ash from coal-fired power plants.

Recently, fly ash has been widely used as the main material to produce geopolymer (Davidovits at 1989) as an alternative building or structure material. Geopolymer is produced by the reaction of alumina-silicate oxides in the fly ash and an alkali silicate solution under highly alkaline conditions. Geopolymer is generally used as a possible building material but recently it is also promoted for environmental applications, such as an adsorbent for heavy metals and environmental remediation. Some recent researches include batch adsorption of Cu^{2+} using fly ash-based geopolymer (Wang et al., 2007; Mužek et al., 2014; Al-Harahsheh et al., 2015) and metakaolin-based geopolymer (Ge et al., 2015; López et al., 2014; Kara et al., 2017). Cheng et al. (2012) reported adsorption capacities of 48.78 mg/g for Cu^{2+}, 147.06 mg/g for Pb^{2+}, and 67.57 mg/g for Cd^{2+} using metakaolin-based geopolymer. Using fly ash-based geopolymer, Al-Zboon et al. (2011) reported an adsorption capacity of 166.55 mg/g for Pb^{2+} for their batch adsorption experiments.

The aim of this study is to use different amounts of Class-F fly ash and slag to synthesize geopolymer with different concentrations of alkaline solution. The synthesized materials were characterized for their physical-chemical properties and the environmental impact of the geopolymer as an environmental material was investigated. The impact of geopolymer is an aqueous environment and as an adsorbent for a metal pollutant (Cu^{2+}) were studied. Environmental impact studies include pH change in aqueous system for different contact times, initial pHs, and initial copper concentrations.

3.3. Methods and Materials

3.3.1. Raw materials

Class F fly ash with a specific gravity of 2.61 g/cm^3 and a total specific area of 426 m^2/kg was used in the synthesis of geopolymer. Slag used was ground granulated blast-furnace slag

(GGBFS) with a specific gravity of 2.50 g/cm^3 and a total specific area of 455m^2/kg. Both raw materials were obtained from Ash Grove Cement Co., Overland Park, Kansas.

The chemical compositions of Class F fly ash and slag are shown in Table 3-1 (from Ash Grove Technical Center, 2016). Fly ash mainly consisted of SiO_2 (57.06%) and Al_2O_3 (18.82%). Its CaO content was less than 15% which was in compliance with ASTM C618 (2004). The main constituents in slag were SiO_2 (36.5%) and CaO (41.1%). As such, using slag to partially replace the fly ash in geopolymer mixture would affect the strength, due to the higher content of CaO and MgO in the geopolymer. The calcium in the system is known to shorten the setting time which could increase the rate of strength gain of geopolymer (Van Jaarsveld et al., 2002). Some studies have shown that the presence of calcium resulted in an increase in the compressive strength of the geopolymer (Dombrowski et al., 2007; García-Lodeiro et al., 2010; Oh et al., 2010).

Table 3-1. Chemical compositions of fly ash and slag from Ash Grove Technical Center, 2016

Major oxides compositions (wt %)	Fly ash (Class-F)	Slag
Si	57.06	36.5
Al	18.82	8.54
Fe	5.43	0.83
Ca	11.8	41.1
Mg	2.89	9.63
S	0.45	0.6
Na	0.64	0.29
K	1.12	0.44
Ti	1.22	1.32
P	0.22	0.32
Mn	0.06	0.16
Sr	0.24	0.27
LOI	0.03	2.46

Note: All values in mass %, expressed on an oven-dry basis; LOI: loss on ignition at 1000 ºC.

The activator used in making the geopolymer consisted of NaOH (solid) and Na_2SiO_3 (water glass, liquid). Their specifications are listed in Table 3-2.

Table 3-2. Specifications of sodium silicate solution and sodium hydroxide.

Product	Sodium silicate solution (Na_2SiO_3)	Sodium hydroxide (NaOH)
Company	Sigma-Aldrich	Fisher Scientific
Grade	Reagent	Certified ACS
Composition	Na_2O: 10.6%, SiO_2: 26.5%	NaOH Solids (≥97%)
Density	1.39 g/mL	2.13 g/mL
Formula	$(NaOH)_x$ $(Na_2SiO_3)_y \cdot zH_2O$	NaOH

3.3.2. Synthesis of the fly ash-based geopolymer

The process for synthesizing fly ash-based geopolymer is shown in Figure 3-1.

A specified quantity of fly ash sample was mixed with the alkaline activating solution (activator). The activator consisted of sodium silicate solution with solid NaOH giving a desired modulus (molar ratio SiO_2:Na_2O) of 1.0. Deionized water was used to dilute the concentration of the alkaline activating solution. The activator was allowed to equilibrate to room temperature prior to use. The ratio of alkaline liquid to fly ash used was 0.33. The obtained paste was mixed for 5 – 10 min, placed in 2"×2"×2" cubic molds according to ASTM (C 109, 2013) and then pre-cured for 24 hours at room temperature (22 – 25 ^oC). This process induced significant dissolution of silica and alumina from the fly ash resulting in a continuous matrix phase and an increase in the homogeneity of the geopolymer. The samples were demolded, placed in a closed cylindrical glass container and cured at a temperature of 50 ^oC in an oven for 7 days. The curing process was found to be beneficial in developing the strength of the geopolymer (Bakharev, 2006). The geopolymer samples were then washed at least 3 times with 200 mL of water to remove the excess sodium hydroxide. The samples were then crushed and grounded to obtain a particle size in the range of

0.42 – 2 mm by using a U.S. Standard Mesh Size No. 10 sieve (2 mm) (generally specified as 85% passing) and a U.S. Standard Mesh Size No. 40 sieve (0.42 mm) (generally specified as 95% retained). The sieved particles were washed several times with distilled water to remove any crushed fine. The sieved samples were then dried overnight at 105 ◦C in a vacuum oven and then stored in a desiccator.

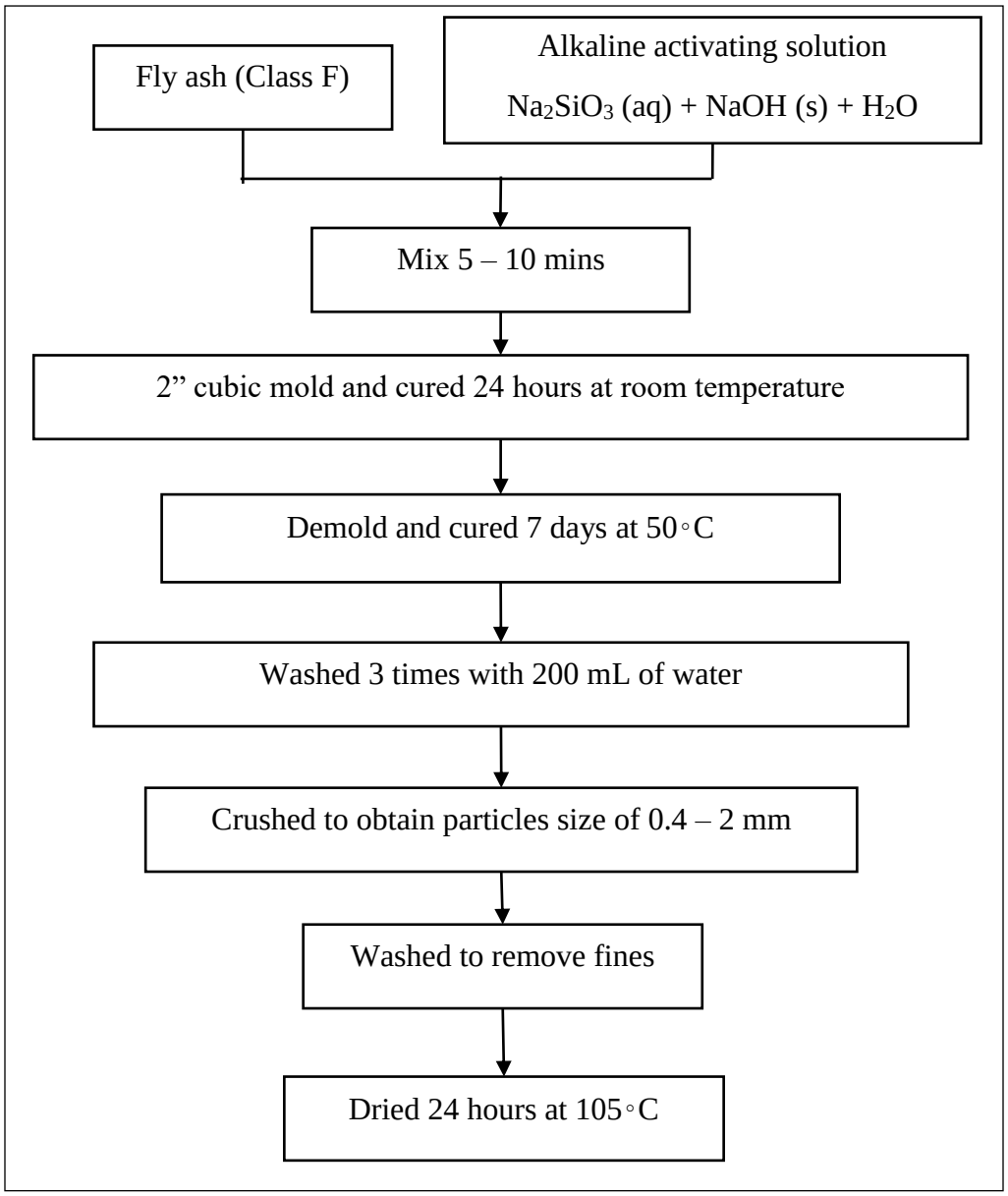

Figure 3-1. Procedure for synthesis of fly ash-based geopolymer

Table 3-3 presents the five different mixing ratios of geopolymer to investigate the influence of alkaline activator dosage (Na/Al) and Si/Al on compressive strength. The names of the samples in Table 3-3, for instance, G50, means geopolymer with alkaline concentration of 50% (by mass), and 10%S, means 10% of replacement of fly ash by slag in the mixture. In this study, the Si/Al molar ratio of the sample ranged from 2.74 to 2.90. Some studies performed on geopolymer with varying Si/Al ratios (Xu and Van Deventer, 2000; Fletcher et al., 2005; De et al., 2007), indicated that the optimum Si/Al molar ratios were around 2 – 3 and Si/Al ratio lower or higher than the optimum ratio would significantly impact the compressive strength. In addition, the high alkaline activator dosage would not only enhance the polymerization of the geopolymer structure but also create more pores (De Silva et al., 2007). Davidovits (2008) indicated that for fly ash-based geopolymer with a Si/Al ratio in the range of 2 to 3, the geopolymer may have the presence of both (poly) sialate-siloxo (-Si-O-Al-O-Si-O-) and (poly) sialate-disiloxo (-Si-O-Al-O-Si-O-Si-O-) polymer structures.

Table 3-3. Synthesis of fly ash-based geopolymer

Fly ash-based geopolymer Samples	Molar conc. of NaOH (mM)	Alkaline activator solution (Mass ratio of Na_2SiO_3 : NaOH : H_2O)	Mass ratio of alkaline solution : solids	Module of water glass (Molar ratio of SiO_2:Na_2O)	Molar ratio of Si/Al	Molar ratio of Na/Al	Molar ratio of H_2O/Na
G50	4.45	0.41 : 0.09 : 0.50	0.33	1	2.74	0.38	7.83
G60	6.68	0.49 : 0.11 : 0.40	0.33	1	2.77	0.45	4.46
G70	10.38	0.58 : 0.12 : 0.30	0.33	1	2.80	0.51	2.50
G60+10%S	6.68	0.49 : 0.11 : 0.40	0.33	1	2.83	0.47	4.49
G60+20%S	6.68	0.49 : 0.11 : 0.40	0.33	1	2.90	0.49	4.52

Note: G – geopolymer; 50, 60, and 70 – alkaline concentration in liquid activator; S – slag.

3.3.3. Characterization

The physical properties of the fly ash-based geopolymer samples measured were particle density and the compressive strength (ASTM C 109, 2013). Scanning electron microscopy (SEM) and X-ray diffraction (XRD) were conducted to characterize the surface and crystallization of the geopolymer. Other physical-chemical properties such as specific surface areas, cation exchange capacity, and pH at point of zero charge can be found in Appendix A which included method procedures and results. All samples used in the characterization were oven dried at 105 ^{o}C for 4 hour and cool to room temperature in a desiccator.

3.3.4. Environmental impact

Due to its alkaline nature, experiments were carried to investigate the environmental impact of geopolymer particles (0.42 – 2 mm) in an aqueous solution and their ability to adsorb metal ions. This study investigated the pH change of the aqueous solution and the amount of Cu^{2+} ion removed for different dosages of geopolymer, contact times, and initial pHs of the aqueous solutions. The geopolymer selected for this part of the study was based on the results of the physical-chemical characterization of the geopolymer samples.

All the experiments were performed using 100 mL Erlenmeyer flasks containing the desired mass of geopolymer and 50 mL of a solution with Cu^{2+} ion. The flask was shaken gently with speed of 200 rpm at room temperature (22 – 25 ^{o}C) for about 48 hours. The reacted suspension was filtered, and the pH of filtrate measured with a pH meter. The residual concentration of copper ion in the filtrate was analyzed using an inductively coupled plasma (ICP) atomic emission spectrometer (ICPE-9800 Series, Shimadzu Corporation, Kyoto, Japan).

Stock solutions of Cu^{2+} (1 – 300 mg/L) were prepared from analytical grade $CuSO_4.5H_2O$ (Fisher Scientific, Pittsburgh, PA, USA). In this study, the initial pH of solution used was adjusted

to pH values of 2.5, 3.0, and 4.0 by using 1 M concentration of H_2SO_4. All experiments were carried out in duplicates.

The amount of Cu^{2+} removed by the geopolymer at the end of the experiment (Q_t) was estimated using:

$$Q_t = (C_0 - C_t) \times V/m$$

where C_0 and C_t (mg/L) are the liquid-phase metal ion concentrations at initial and final conditions, V is the volume of the solution (L) and m is the mass of geopolymer used (g).

3.4. Results and Discussions

3.4.1. Physical-chemical characteristics of fly ash-based geopolymer

The physical properties of geopolymer including particle density and compressive strength are shown in Table 3-4. The particle density of the five prepared samples were similar at about 2.1 g/cm^3, even for the materials with 20 % substitution of slag.

Table 3-4. Properties of fly ash-based geopolymer (size: 0.42 - 2 mm)

Fly ash-based geopolymer Samples	Particle density, g/cm^3	Compressive strength for 2" cubic paste (7-days), MPa
G50	2.13 ± 0.56	36.57 ± 0.36
G60	2.09 ± 0.41	49.44 ± 2.45
G70	2.11 ± 0.47	35.68 ± 0.85
G60+10%S	2.10 ± 0.38	45.72 ± 3.45
G60+20%S	2.12 ± 0.35	51.09 ± 2.66

The compressive strength of the five samples were different. For the three sample without slag addition, the G60 has the highest strength (49.44 MPa) compared to other two samples. G60 has a Na/Al ration of 0.45 and Si/Al ration of 2.77. G60 results were similar to those reported by Zheng et al. (2010), where the high compressive strength (8 - 17 MPa) were reported for a

geopolymer with alkaline activator dosage of Na/Al: 0.98-2.07 and Si/Al ratio 1.8-2.7. A low alkali content in the activating solution in the mixture cannot promote the dissolution of Si and Al from fly ash particles. In contrast, a high alkaline content resulted in low compressive strength, as found in other studies by raising the alkali content of activating solution (Komljenović et al., 2010; Kupaei et al., 2014; and Rashidian et al., 2018). One reason is that soluble Si from the sodium silicate solution in the activator could negatively impact the solubility of fly ash particles resulting in a decrease in compressive strength.

For the sample with 10% slag, the compressive strength (45 MPa) was comparable to that of G60, However, with 20% of slag replacement the sample (G60+20%S) exhibited a compressive strength of 51 MPa. One possible reason is that the 41% wt of CaO in slag could have resulted in the formation of CaOH, aluminosilicate hydrate and C-S-H gels (Chi et al., 2012). Similar results were obtained by Ling et al. (2019). Due to the alkaline and reactive nature of geopolymer surfaces, the standard test methods for physical-chemical properties such as specific surface area, cation exchange capacity, and pH at point of zero charge may not be appropriate for geopolymer. As such, these physical-chemical properties are reported in Appendix A.

3.4.2. SEM-EDX analysis and XRD analysis

Figure 3-2 shows the SEM images (500x) and EDX spectra for the fly ash (Figure 3-2a) and geopolymer samples (G60) (Figure 3-2b), and G60+20%S (Figure 3-2c). The SEM image of the fly ash showed the presence of fine spherical particles while both G60 and G60+20% showed presence of layer spherical particles and continuous cementation paste which may be the main contributor to the compressive strength of the geopolymer. The EDX spectra showed a higher C content in the raw fly ash when compared to that of G60 and G60+20%S samples, while G60 and G60+20%S samples had higher Na and Si contents due to the addition of the activating solution.

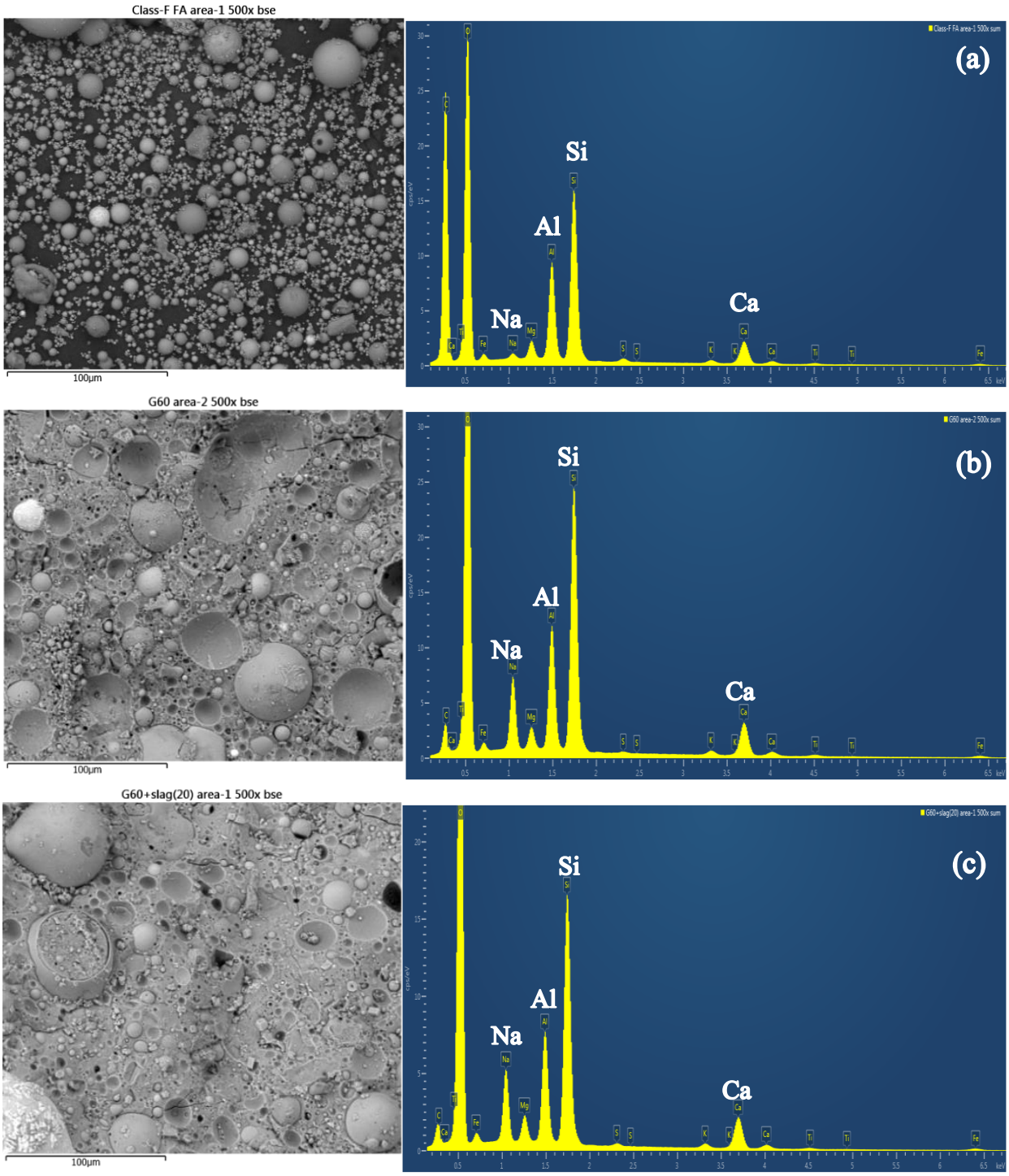

Figure 3-2. SEM images (500x) and EDX spectra of (a) Class-F fly ash, (b) geopolymer G60 and (c) G60+20%Slag

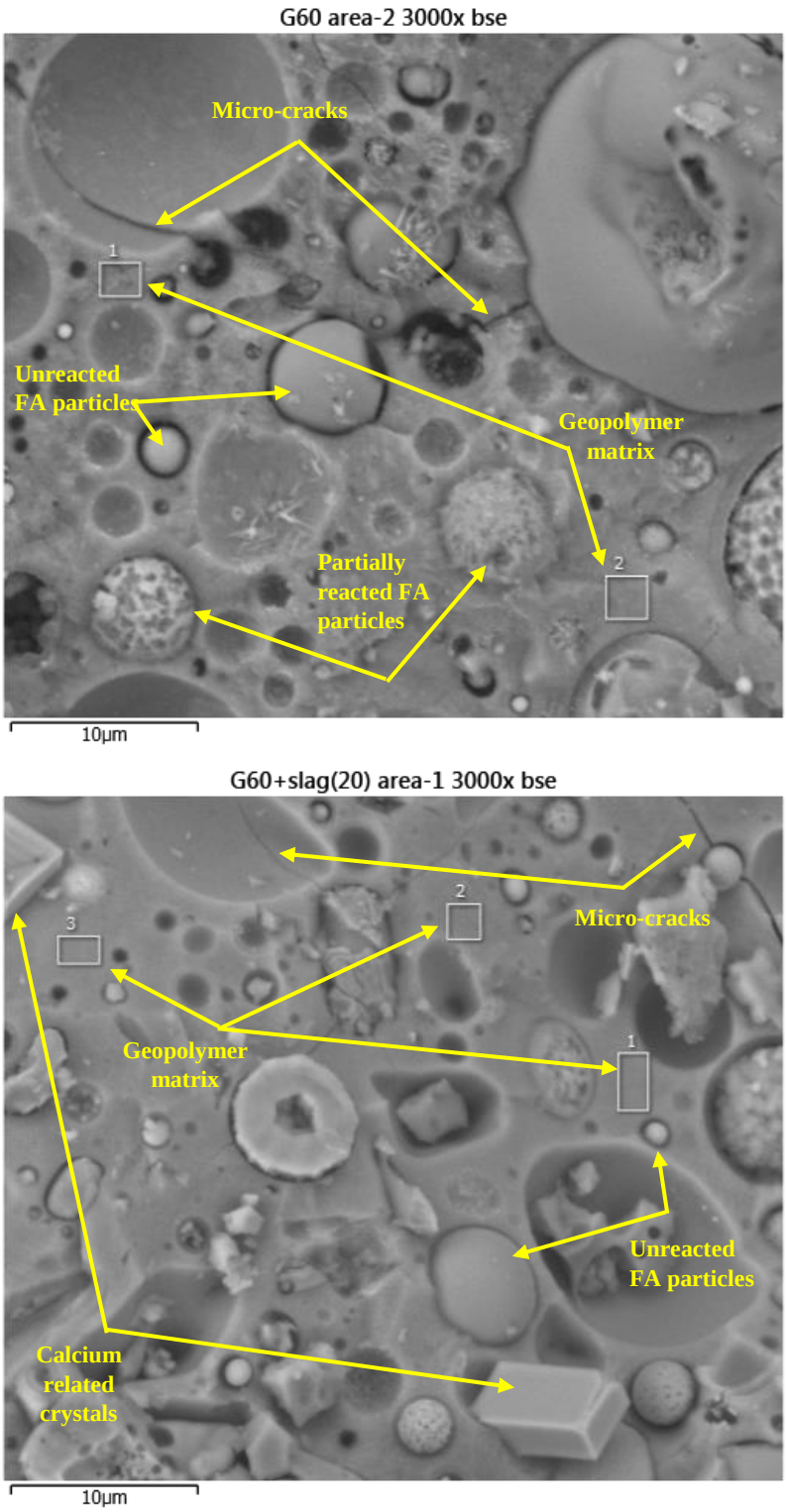

Figure 3-3. SEM image (3000x) of matrix of two geopolymer particle samples (G60 and G60+20%S).

Two SEM images (3000x) were taken for samples G60 and G60+20%S, as presented in Figure 3-3. The alkali aluminosilicate hydrate pastes were located at where the hydrates were bound to the un-hydrated fly ash particles. Hydrates seemed to form a dense structure with low porosity. The integrated structure of non-hydrated cores of fly ash particles shown had a relatively high density and hardness that were bounded by relatively dense binders which may explain the compressive strength of fly ash–based geopolymer (Liu et al., 2016).

For geopolymer G60+20%S, some calcite crystals with rhombohedral morphology were observed on sample surface, which probably due to carbonation of the sample. Micro-cracks were also observed in Figure 3-3, which were probably formed due to the drying of geopolymer particles during preparation and pretreatment.

Both samples G60 and G60+20%S had similar matrix spectra with relatively high Na content and low content of Al and Si. The G60+20%S samples had higher Ca content while G60 has higher content of Al, when compared to each other. From the morphology, there were some hydration reactions on the G60 sample surface as shown by the needle shape structures. For G60+20%S, there were some rhombohedral shapes which may be assumed as calcite crystals. The higher compressive strength of G60+20%S sample as compared to G60 sample may be due to the higher content of Ca in slag which can form calcite crystals.

Figure 3-4 presents the XRD patterns of raw Class-F fly ash and fly ash-based geopolymer (G60). Except for several small peak intensity variations, the overall XRD pattern of G60 sample was close to that of Class F fly ash, which were mainly quartz (SiO_2), mullite ($3Al_2O_3 \cdot 2SiO_2$), and calcite ($CaCO_3$) crystalline phase as shown in Figure 3-4. It can be implied that the main reasons for the variation in the compressive strength of the samples may be attributed to their different micro-structures including geopolymer reactions, effect of cracks, and unreacted fly ash particles.

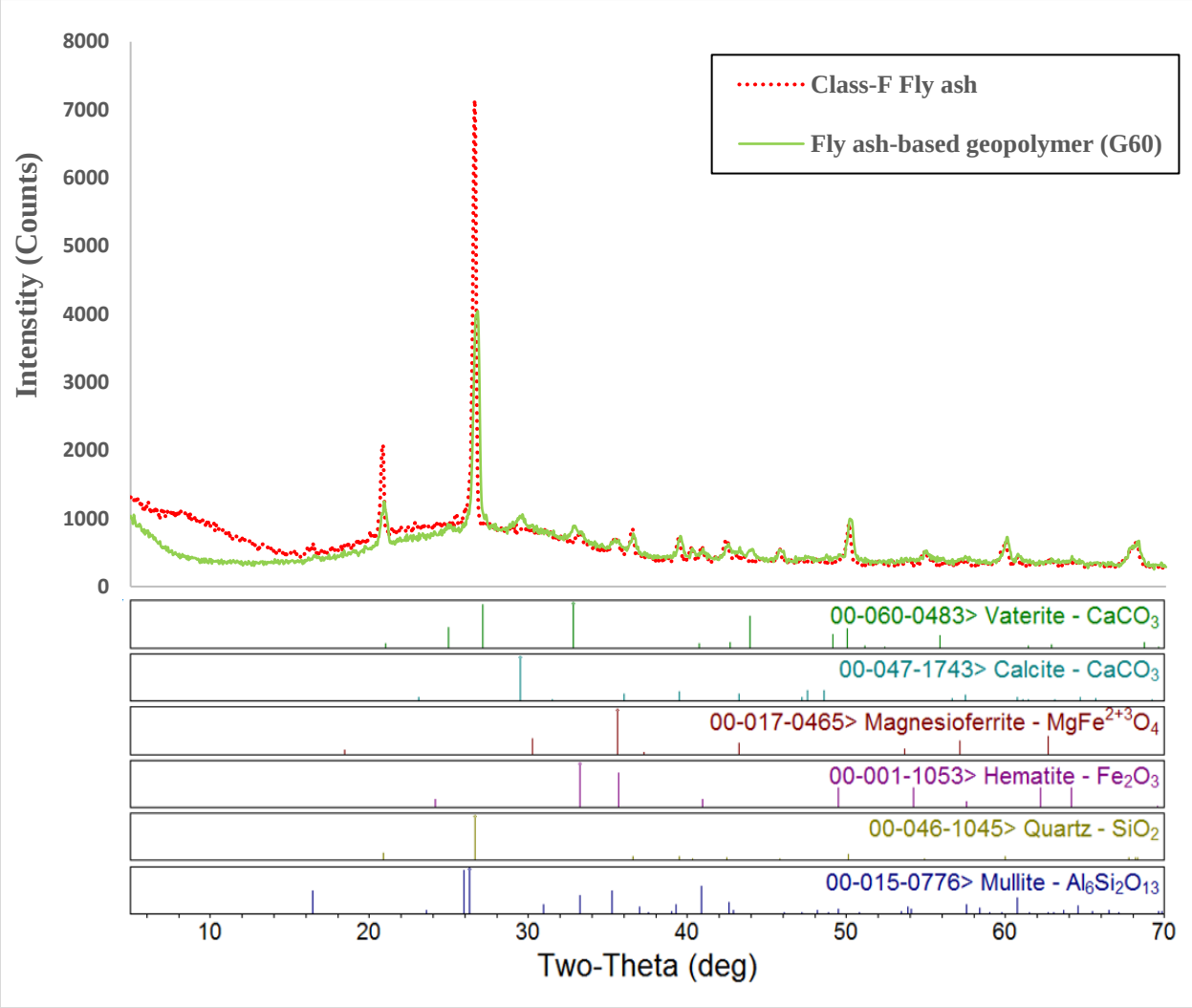

Figure 3-4. XRD patterns of Class-F fly ash and fly ash-based geopolymer G60 sample.

3.4.3. Environmental impact of geopolymer

Based on the physical-chemical characterization of the five geopolymer, geopolymer G60 was selected as a geopolymer sample to study its impact on aqueous solution and its ability to remove a pollutant such as Cu^{2+} ion.

- Effect on solution pH over time

Experiments with two masses of geopolymer (0.1 g and 0.5 g) in 50 mL of solution at an initial pH of 3.0 with 20 mg/L or 100 mg/L of Cu^{2+} were conducted. Figure 3-5 shows the changes

in pH and Cu^{2+} concentration with time. For experiments with 0.1 g of geopolymer, the pH of the solution increased to above pH 6 within 48 hours. For a higher dosage of 10 g/L, a pH of 6.0 was reached at slightly more than 4 hours. The increased in pH was due to the release of OH^- ions from the unreacted activator and from the interaction of H^+ ions in solution and calcite. The Cu^{2+} concentration in the experiments decreased with time while the pH increased with time. Plotted on Figure 3-5 is the theoretical solubility of copper ion (Stumm and Morgan, 1981). Solubility products for copper sulfate and copper hydroxides are $pK_{sp} = 2.64$ and $pK_{sp} = 19.34$, respectively. For Cu^{2+} concentration of 100 mg/L, there were a steep decline in the Cu^{2+} concentration for a pH approximately greater than 5.5. Based on the solubility curve for Cu^{2+}, it was likely that for the 100 mg/L Cu^{2+} solution, Cu^{2+} precipitated out from solution around that pH.

For an initial Cu^{2+} concentration of 200 mg/L, the color of geopolymer changed from gray (original material) to blue, which may indicate a certain level of Cu^{2+} precipitation as copper sulfate or hydroxide (data not provided).

For the 20 mg/L of Cu^{2+} solution with 0.1 g of geopolymer, it is also probable that the removal of Cu^{2+} may be due to adsorption onto the surfaces of the geopolymer.

The above results showed that use of geopolymer for environmental applications will have an impact on the pH of an aqueous solution if there are insufficient buffering capacity. However, the results also showed that geopolymer can be a useful environmental remedial material for solution with low pH and high metal contents such as acid mine drainage, industrial wastewaters from metal plating industries, and metal manufacturing industries. The geopolymer can be used to neutralize the pH of these wastewaters and at the same time remove the metal ions.

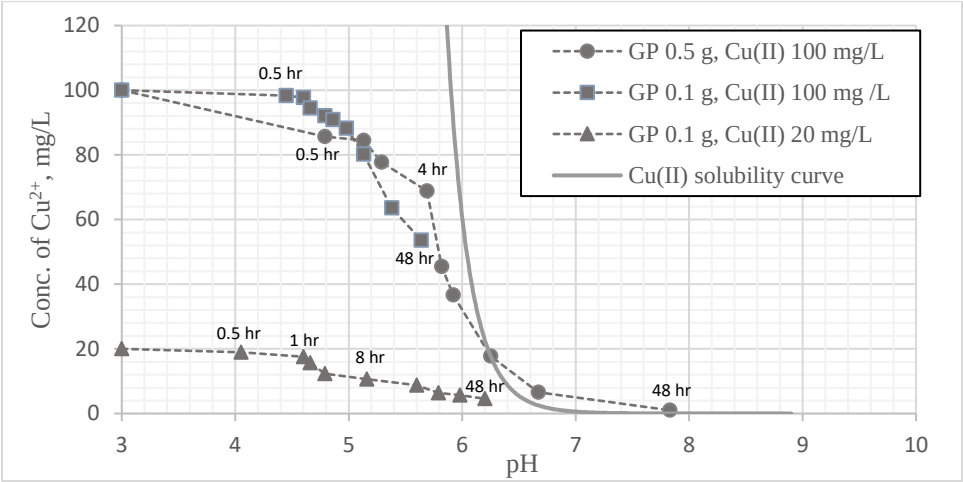

Figure 3-5. Change of pH and Cu^{2+} concentrations with time (50 mL Cu^{2+} solution; initial pH=3.0; Experimental time = 48 hours) (Bold line – theoretical solubility of Cu^{2+}).

- Effect of solution pH and different initial Cu^{2+} concentration

Experiments were conducted using 0.1 g of geopolymer in 50 mL solution with initial pHs of 2.5, 3.0, and 4.0 and with Cu^{2+} concentrations ranging from 5 to 300 mg/L. The final pH and Cu^{2+} concentration in the solution were measured after a contact time of 48 hours. As in the earlier experiments (section 3.3.1), the final pH of the solution increased with the addition of geopolymer. However, the final pH of the solution exhibits a decreasing trend for increasing initial Cu^{2+} concentration (Figure 3-6). This may be due to the concentration driving force which favors the surface affinity for Cu^{2+} ions in preference to H^+ ions, giving a descending trend of the final pH for higher initial Cu^{2+} concentrations.

Figure 3-6 also indicates a general increase in Cu^{2+} removal for a higher initial solution pH value. This may be attributed to hydrogen ions which act as competitors for available reactive sites on the geopolymer surface, and hence at low pH levels, H^+ ions are more concentrated, resulting in lower Cu^{2+} removal or increasing Cu^{2+} solubility. The higher Cu^{2+} removal for concentrations in the range of 300 mg/L could be due to possible precipitation of Cu^{2+}.

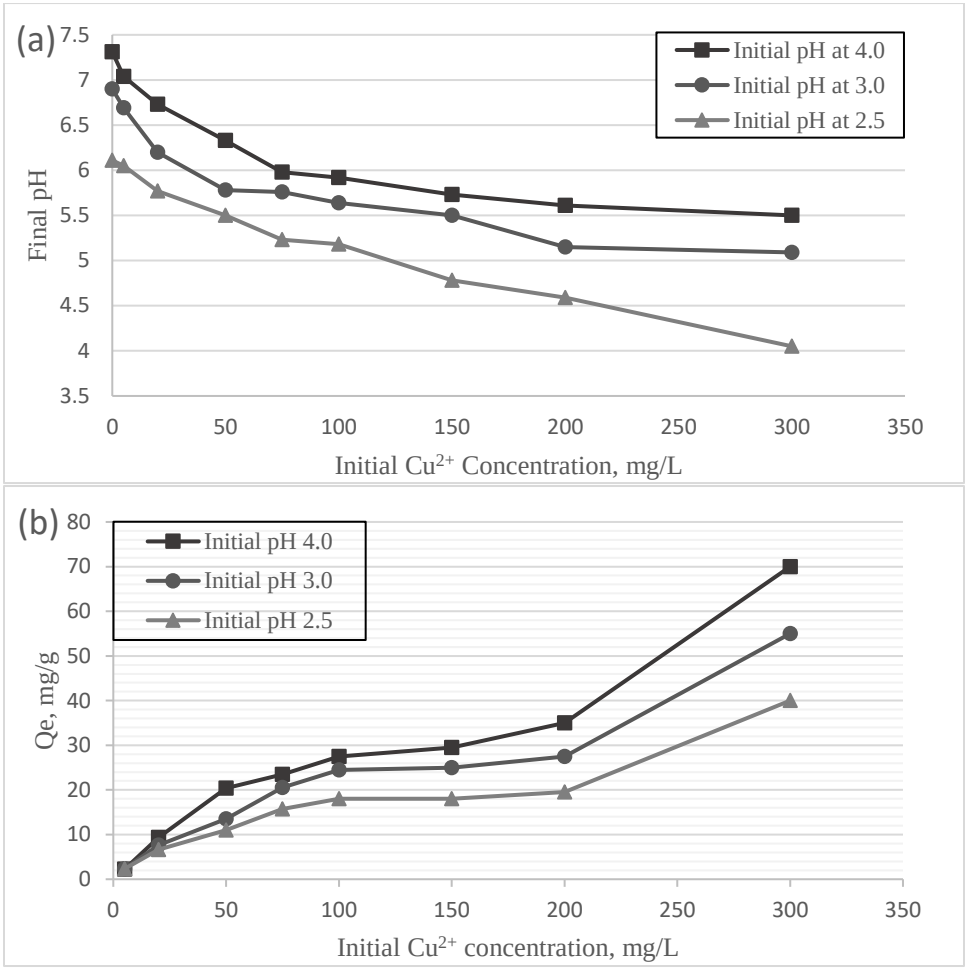

Figure 3-6. Effect of initial solution concentration on (a) removal of Cu^{2+} from solution and (b) final pH of solution (0.1 g of geopolymer in 50 mL Cu^{2+} solution with concentrations from 5 to 300 mg/L, and contact time 48 hours)

- Release of alkaline cations and other cations.

Experiments were conducted to investigate the extent of alkaline cations present in the final solution of a solution containing geopolymer with various Cu^{2+} concentrations. Experiments were conducted with a solution with an initial pH of 3.0, reaction time of 48 hours and Cu^{2+} concentrations of 0 to 300 mg/L. As shown in Figure 3-7, the concentration of total alkaline cations including Ca^{2+}, Mg^{2+}, K^{+} and Na^{+} ions increased with an increase in the initial Cu^{2+} concentration. Possible reasons for the increase are that Ca^{2+}, Mg^{2+}, K^{+} and Na^{+} ions were displaced from the

geopolymer through dissolution of their solids or an increase in Cu^{2+} concentration resulted in more Ca^{2+}, Mg^{2+}, K^{+} and Na^{+} ions being displaced from the surface of the geopolymer by the Cu^{2+} ions. However, from Figure 3-8 total mill-equivalents of Cu^{2+} removed by geopolymer (G60) was 1.73 meq/g at initial Cu^{2+}concentration of 300 mg/L. It is possible that some of the alkaline cations on the geopolymer surface were displaced by the copper but the majority may be due to dissolution of the solids.

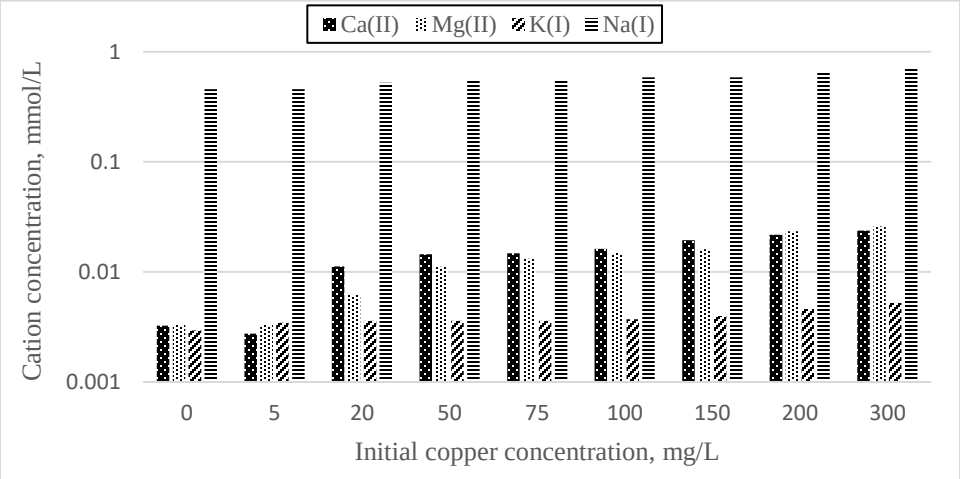

Figure 3-7. Amount of released cation in solution at different initial Cu^{2+} concentrations.

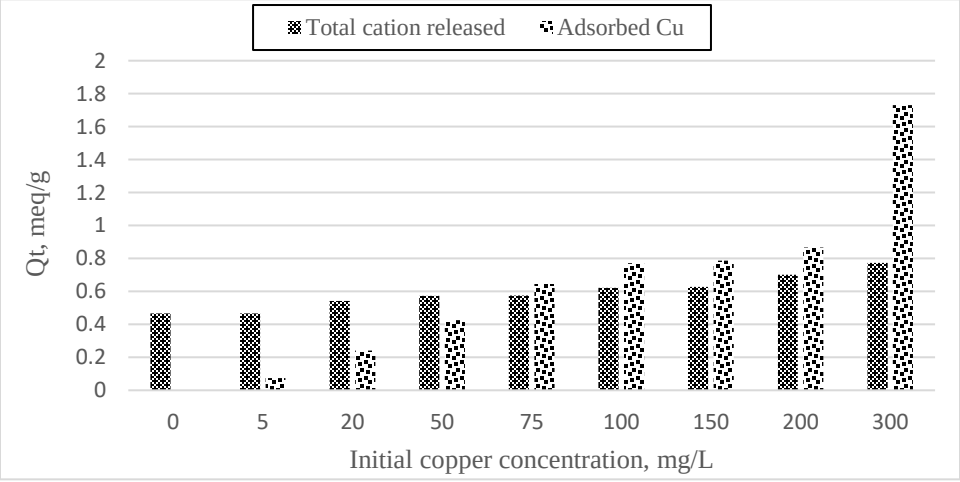

Figure 3-8. Total cation released in solution and removed Cu^{2+} at different initial Cu^{2+} concentrations.

- SEM-EDX after treated with Cu^{2+} solution

Figure 3-9 shows the SEM images (1500x) and EDX spectra for the geopolymer (G60) after removal of Cu^{2+}. The SEM image of the treated G60 showed the presence of a layer of solid (removed Cu^{2+}) and the presence of spherical particles (fly ash). The EDX spectra showed a higher Cu^{2+} content (~20%) on the surface of geopolymer (G60) after treated Cu^{2+} solution as compared to original G60 sample (Figure 3-2b). Also, the lower Na, Ca, Al and Si content were found on the surface of treated G60, which was due to the dissolution of the solids and the geopolymer surfaces were occupied by Cu^{2+} content. In addition, EDX spectra showed a high sulfur content (~4.6%) in the G60 after Cu^{2+} removal, which indicated copper sulfate may have precipitated on the surface of geopolymer.

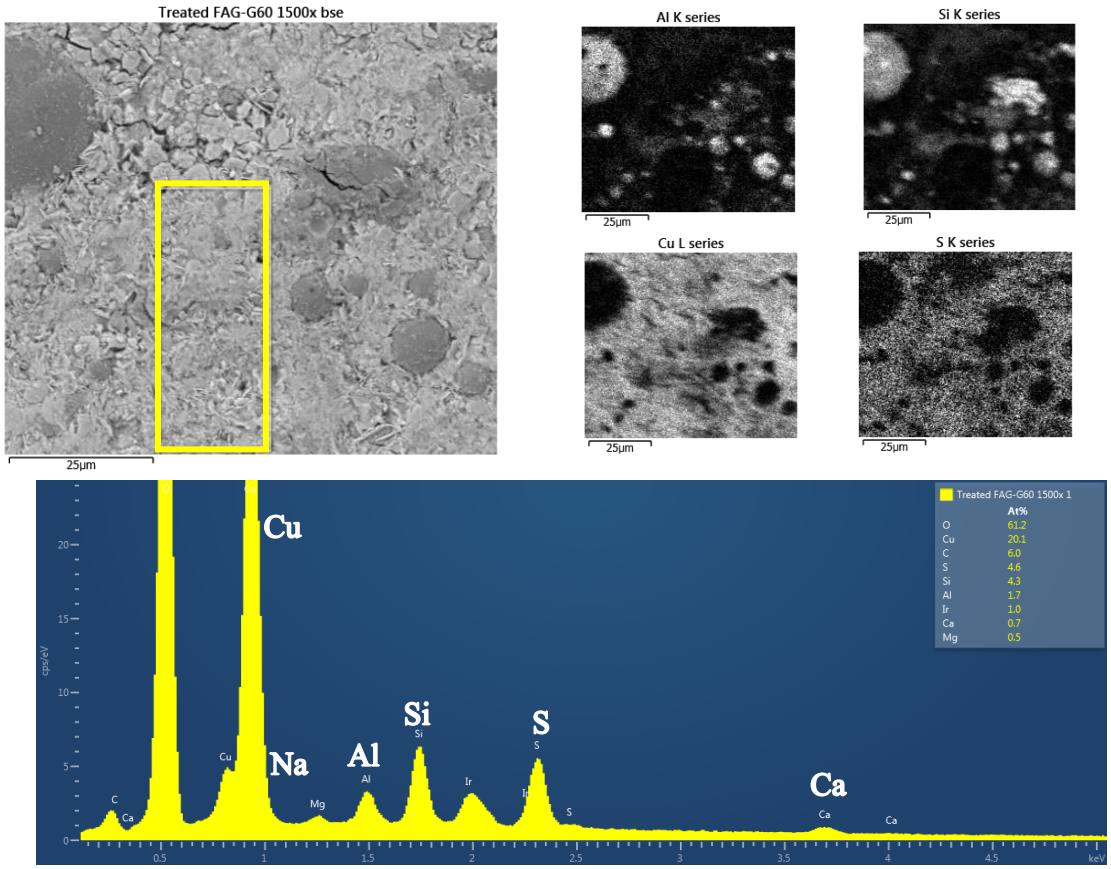

Figure 3-9. SEM images (1500x) and EDX spectra of geopolymer (G60) after Cu^{2+} removal.

3.4.4. Geopolymer in environmental application

Based on the above properties of the geopolymers, geopolymer can be made into particles with various sizes for removal of metals in acidic solution. Experiments of Cu^{2+} removal were conducted to assess the amount of Cu^{2+} removed by the geopolymer (G60) for two particles size 0.42 – 2 mm and 2 – 5 mm. The results of this study are presented in Figure 3-10.

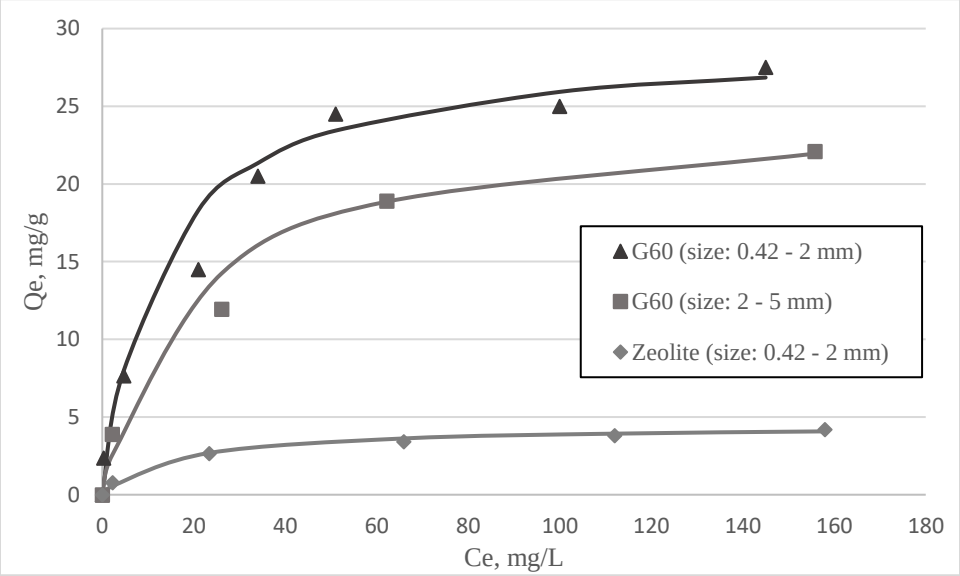

Figure 3-10. Effect of geopolymer (G60) particle size on removal of Cu^{2+} vs. zeolite (0.1 g of geopolymer mass, 0.5 g of zeolite mass, initial pH at 3.0; 50 mL of 0-200 mg/L Cu^{2+} solution; contact time = 48 hours).

Results from Figure 3-10 show that geopolymer (G60) particles of 0.42 – 2 mm size resulted in higher removal of Cu^{2+} than that of geopolymer particles size of 2 – 5 mm.

Also, geopolymer (G60) with particles size of 0.42 – 2 mm was compared with zeolite (0.42 – 2 mm) for removal of Cu^{2+}, which was presented in Figure 3-10. Results show that a geopolymer mass of 0.1 g removed more Cu^{2+} than that of 0.5 g zeolite under the same experimental conditions. The estimated removal capacity for the geopolymer was 29.41 mg/g while the zeolite value was 4.48 mg/g.

In comparison to other-adsorbents and geopolymer-based materials, the removal capacity of Cu^{2+} for this study were similar or better as shown in Table 3-5.

Table 3-5. Comparison of removal and adsorption capacities of various materials for Cu^{2+}.

Adsorbent	Particle dimeter, mm	Dosage, g/L	pH	Contact time, hours	q_{max}, mg/g	Reference
Class-F Fly ash-based geopolymer	0.42-2	0.1 g in 50 mL	3	48.00	29.41	This study
Activated carbon	0.045-0.15	4	5.00	0.75	54.00	Patnukao et al., 2008
Modified activated carbon	0.5-0.85	10	4.9	48.00	14.92	Chen et al., 2003
Natural zeolite	1-3	37	2.5-4.5	6.00	3.37	Motsi et al., 2009
Metakaolin-based geopolymer	1.19-1.41	20	4.00	24.00	48.78	Cheng et al., 2012
Metakaolin-based geopolymer	2-4	1.5	5.00	48.00	52.63	Ge et al., 2015
Fly ash	0.0048	20	8.00	2.00	1.39	Panday et al., 1985
Fly ash derived geopolymer	0.045	0.15	6.20	72.00	90.00	Wang et al., 2007

For example, the removal capacity for the geopolymer samples in this study was higher than the maximum adsorption capacity of activated carbon (14.92 mg/g with a particles size of 0.5 – 0.85 mm) (Chen et al., 2003). However, the removal capacity for this study was generally lower than metakaolin-based geopolymers with reported maximum adsorption capacities of 48.78 mg/g (Cheng et al., 2012) and 52.63 mg/g (Ge et al., 2015). Overall, by making the fly ash into a geopolymer, the removal capacity of copper was at least 20 times more than the fly ash itself.

Although the geopolymer sample has an impact on the pH of the solution, the geopolymer itself can be a useful material with environmental applications for treatment of acidic wastewaters with heavy metal contamination. Categories of wastewaters include acid mine drainage, metal processing industrial wastewaters, and electroplating wastewaters. Because of the high compressive strength of the geopolymer, the geopolymer can be made into particle sizes that are suitable as a filtration medium for wastewaters. In addition, the geopolymer can be made into pellet or gravel-sized material that can be placed in the path of acid mine drainage to neutralize the pH and to remove heavy metals in the drainage.

3.5. Conclusion

Several fly ash-based geopolymer mixes were made using an alkaline activator solution of SiO_2/Na_2O, Class-F fly ash, and slag. The fly ash-based geopolymer had good compressive strength properties and specific surface areas that are comparable to concrete. The geopolymer samples were tested for their environmental impact and was found to increase the pH of the solution they were exposed to.

The geopolymer samples were found to have good Cu^{2+} removal from acidic solution. Cu^{2+} removal efficiency of geopolymer was greater than 98% for an initial concentration of 20 mg/L. In addition, Cu^{2+} precipitations were found when the pH of the solution increased above 6.5.

The fly ash-based geopolymer could be a potential low-cost material to treat and neutralize acid mine drainage or acidic industrial wastewater and as for removal of heavy metals such as copper and lead.

3.6. References

Al-Subu, M. M., Salim, R., Braik, H., & Swaileh, K. M. (2001). Removal of dissolved copper from polluted water using plant leaves. II. Effects of copper concentration, plant leaves, competing ions and other factors. *Revista Internacional de Contaminación Ambiental*, *17*(3), 123-127.

Al-Harahsheh, M. S., Al Zboon, K., Al-Makhadmeh, L., Hararah, M., & Mahasneh, M. (2015). Fly ash based geopolymer for heavy metal removal: A case study on copper removal. *Journal of Environmental Chemical Engineering*, *3*(3), 1669-1677.

Alouani, M. E. L., Alehyen, S., Achouri, M. E. L., & Taibi, M. (2018). Removal of cationic dye-methylene blue-from aqueous solution by adsorption on fly ash-based geopolymer. *J Mater Environ Sci*, *9*(1), 32-46.

Al-Zboon, K., Al-Harahsheh, M. S., & Hani, F. B. (2011). Fly ash-based geopolymer for Pb removal from aqueous solution. *Journal of hazardous materials*, *188*(1-3), 414-421.

ASTM, C. (2013). Standard test method for compressive strength of hydraulic cement mortars (using 2-in. or [50-mm] cube specimens). *Annual Book of ASTM StandardsAnnual Book of ASTM Standards*, *4*(1), 1-9.

Bakharev, T. (2006). Thermal behaviour of geopolymers prepared using class F fly ash and elevated temperature curing. *Cement and Concrete Research*, *36*(6), 1134-1147.

Balistrieri, L. S., & Murray, J. W. (1981). The surface chemistry of goethite (alpha FeOOH) in major ion seawater. *American Journal of Science*, *281*(6), 788-806.

Blake, G. R., & Hartge, K. H. (1965). Methods of soil analysis. Part 1 physical and mineralogical properties. *Am. Soc. of Agron. J*, *57*, 373-390.

Cheng, T. W., Lee, M. L., Ko, M. S., Ueng, T. H., & Yang, S. F. (2012). The heavy metal adsorption characteristics on metakaolin-based geopolymer. *Applied Clay Science*, *56*, 90-96.

Chi, M. (2012). Effects of dosage of alkali-activated solution and curing conditions on the properties and durability of alkali-activated slag concrete. *Construction and Building Materials*, *35*, 240-245.

Davidovits, J. (1989). Geopolymers and geopolymeric materials. *Journal of Thermal Analysis and Calorimetry*, *35*(2), 429-441.

Davidovits, J. (2008). *Geopolymer chemistry and applications*. Geopolymer Institute, Saint Quentin, France.

De Silva, P., Sagoe-Crenstil, K., & Sirivivatnanon, V. (2007). Kinetics of geopolymerization: role of Al_2O_3 and SiO_2. *Cement and Concrete Research*, *37*(4), 512-518.

Dimitrova, S. V. (1996). Metal sorption on blast-furnace slag. *Water Research, 30*(1), 228-232.

Dombrowski, K., Buchwald, A., & Weil, M. (2007). The influence of calcium content on the structure and thermal performance of fly ash based geopolymers. *Journal of Materials Science*, *42*(9), 3033-3043.

Fletcher, R. A., MacKenzie, K. J., Nicholson, C. L., & Shimada, S. (2005). The composition range of aluminosilicate geopolymers. *Journal of the European Ceramic Society*, *25*(9), 1471-1477.

García-Lodeiro, I., Fernández-Jiménez, A., Palomo, A., & Macphee, D. E. (2010). Effect of calcium additions on N–A–S–H cementitious gels. *Journal of the American Ceramic Society*, *93*(7), 1934-1940.

Ge, Y., Cui, X., Kong, Y., Li, Z., He, Y., & Zhou, Q. (2015). Porous geopolymeric spheres for removal of Cu (II) from aqueous solution: synthesis and evaluation. *Journal of hazardous materials*, *283*, 244-251.

Kara, İ., Yilmazer, D., & Akar, S. T. (2017). Metakaolin based geopolymer as an effective adsorbent for adsorption of zinc (II) and nickel (II) ions from aqueous solutions. *Applied Clay Science*, *139*, 54-63.

Komljenović, M., Baščarević, Z., & Bradić, V. (2010). Mechanical and microstructural properties of alkali-activated fly ash geopolymers. *Journal of Hazardous Materials*, *181*(1-3), 35-42.

Kupaei, R. H., Alengaram, U. J., & Jumaat, M. Z. (2014). The effect of different parameters on the development of compressive strength of oil palm shell geopolymer concrete. *The Scientific World Journal*, *2014*, 898536.

Ling, Y., Wang, K., Li, W., Shi, G., & Lu, P. (2019). Effect of slag on the mechanical properties and bond strength of fly ash-based engineered geopolymer composites. *Composites Part B: Engineering*, *164*, 747-757.

Liu, M. Y. J., Alengaram, U. J., Santhanam, M., Jumaat, M. Z., & Mo, K. H. (2016). Microstructural investigations of palm oil fuel ash and fly ash based binders in lightweight aggregate foamed geopolymer concrete. *Construction and Building Materials*, *120*, 112-122.

López, F. J., Sugita, S., Tagaya, M., & Kobayashi, T. (2014). Metakaolin-based geopolymers for targeted adsorbents to heavy metal ion separation. *Journal of Materials Science and Chemical Engineering*, 2(07), 16.

Maingi, F. M., Mbuvi, H. M., & Mwangi, H. (2017). Adsorption kinetics and isotherms of methylene blue by geopolymers derived from common clay and rice husk ash. *Physical Chemistry*, *7*(4), 87-97.

Mall, I. D., Srivastava, V. C., Kumar, G. V. A., & Mishra, I. M. (2006). Characterization and utilization of mesoporous fertilizer plant waste carbon for adsorptive removal of dyes from aqueous solution. *Colloids and Surfaces A: Physicochemical and Engineering Aspects*, *278*(1-3), 175-187.

Motsi, T., Rowson, N. A., & Simmons, M. J. H. (2009). Adsorption of heavy metals from acid mine drainage by natural zeolite. *International Journal of Mineral Processing*, *92*(1-2), 42-48.

Mulgund, M. G., Kininge, P. T., Pillai, M. M., & Sanandam, M. R. (2011). Biosorptive removal of heavy (Cd^{2+}, Pb^{2+} and Cu^{2+}) from aqueous solutions by Cassia angustifolia bark. *International Journal of Engineering, Science and Technology*, *3*, 1642-1647.

Mužek, M. N., Svilović, S., & Zelić, J. (2014). Fly ash-based geopolymeric adsorbent for copper ion removal from wastewater. *Desalination and Water Treatment*, *52*(13-15), 2519-2526.

Oh, J. E., Monteiro, P. J., Jun, S. S., Choi, S., & Clark, S. M. (2010). The evolution of strength and crystalline phases for alkali-activated ground blast furnace slag and fly ash-based geopolymers. *Cement and Concrete Research*, *40*(2), 189-196.

Pan, S. C., Lin, C. C., & Tseng, D. H. (2003). Reusing sewage sludge ash as adsorbent for copper removal from wastewater. *Resources, Conservation and Recycling*, *39*(1), 79-90.

Panday, K. K., Prasad, G., & Singh, V. N. (1985). Copper (II) removal from aqueous solutions by fly ash. *Water Research*, *19*(7), 869-873.

Patnukao, P., Kongsuwan, A., & Pavasant, P. (2008). Batch studies of adsorption of copper and lead on activated carbon from Eucalyptus camaldulensis Dehn. bark. *Journal of Environmental Sciences*, *9*(20), 1028-1034.

Sumner, M. E., & Miller, W. P. (1996). Cation exchange capacity and exchange coefficients. *Methods of soil analysis part 3—chemical methods*, (methodsofsoilan3), 1201-1229.

Van Jaarsveld, J. G. S., Van Deventer, J. S. J., & Lukey, G. C. (2002). The effect of composition and temperature on the properties of fly ash-and kaolinite-based geopolymers. *Chemical Engineering Journal*, *89*(1-3), 63-73.

Stumm, W., & Morgan, J. J. (2012). *Aquatic chemistry: chemical equilibria and rates in natural waters* (Vol. 126). John Wiley & Sons, New York, USA

Wang, S., Li, L., & Zhu, Z. H. (2007). Solid-state conversion of fly ash to effective adsorbents for Cu removal from wastewater. *Journal of hazardous materials*, *139*(2), 254-259.

Xu, H., & Van Deventer, J. S. J. (2000). The geopolymerisation of alumino-silicate minerals. *International Journal of Mineral Processing*, *59*(3), 247-266.

Zhang, M. L., Zhang, H. Y., Xu, D., Han, L., Niu, D. X., Tian, B. H., Zhang, J., Zhang, L. Y., & Wu, W. S. (2011). Removal of ammonium from aqueous solutions using zeolite synthesized from fly ash by a fusion method. *Desalination*, *271*(1-3), 111-121.

Zhao, X. S., Lu, G. Q., & Zhu, H. Y. (1997). Effects of ageing and seeding on the formation of zeolite Y from coal fly ash. *Journal of Porous Materials*, *4*(4), 245-251.

Zheng, L., Wang, W., & Shi, Y. (2010). The effects of alkaline dosage and Si/ Al ratio on the immobilization of heavy metals in municipal solid waste incineration fly ash-based geopolymer. *Chemosphere*, *6*(79), 665-671.

CHAPTER 4. FLY ASH-BASED GEOPOLYMER FOR HEAVY METALS REMOVAL IN ACIDIC SOLUTION APPLICATIONS

4.1. Abstract

Five different geopolymer samples made with different mix proportions were used for removal of heavy metals (Cu^{2+}, Cd^{2+} and Pb^{2+}). In a single metal solution, batch study results showed that Pb^{2+} was favorably removed than Cu^{2+} and Cd^{2+}, while Cu^{2+} was the least removed of the three metals. In a multi-metal solution, Cd^{2+} removal was significantly affected due to competition while Cu^{2+} removal was marginally affected. For a single metal solution with an initial metal concentration between 5 to 500 mg/L, the asymptotic removal (maximum) capacities found for Cu^{2+}, Cd^{2+} and Pb^{2+} ranged from 20.66 – 35.21, 28.74 – 42.02, and 116.28 – 121.95 mg/g for initial pHs of 2.5, 3.0, and 4.0, respectively, at room temperature of 21 – 23 ^{o}C. The geopolymer can be used to neutralize the pH of acidic waste streams, such as acid mine drainage and acidic industrial waste waters, and at the same time, precipitate and adsorb metal pollutants.

4.2. Introduction

Acid mine drainage (AMD) is a global environmental problem and is commonly found in old and new mines in the mining industry (Johnson & Hallberg, 2005). Acid mine drainage is formed by the oxidation of sulfide such as pyrites to sulfate resulting in an acidic solution which in turn causes the release of heavy metals from the overburden. Common heavy metals found in AMD are arsenic, cadmium, zinc, copper and lead, which can ultimately contaminate surface waters and groundwaters, and accumulate in soil (Kalin et al., 2006).

To minimize environmental impact of AMD, the drainage is treated by removing metals and neutralizing the acidity. The most common method to treat AMD is by chemical precipitation using alkaline materials (Kaur et al., 2018), such as limestone (Iakovleva et al., 2015), caustic

soda, and hydrated lime (Skousen et al., 1996). Even through these materials are low cost and have high removal efficiencies, some of major disadvantages include needing a large amount of the material during treatment, difficulty in separation of the precipitates from liquid, and disposal of excess sludge (Feng et al., 2000). Other methods to treat AMD include use of low cost adsorbents made from natural materials or waste products. Adsorbents include activated carbon (Baskaran et al., 2010), clay (Yavuz et al., 2003), mud (Nadaroglu et al., 2010), and zeolite (Motsi et al., 2009). In addition, certain waste products from manufacturing industries or agriculture may have the potential to be made into inexpensive adsorbents, such as sewage sludge ash (Pan et al.,2003), fly ash (Panday et al., 1999; Gupta & Torres, 1998), slag (Dimitrova, 1996; Dimitrova & Mehandgiev, 1998), bark (Mulgund et al., 2011), and plant leaves (Al-Subu et al., 2011). However these materials tend to have low adsorption capacities and unable to neutralize the acidic pH of AMD.

Currently, there is a trend in recycling of fly ash and slag from coal-fired power plants and cement plants to usable and valuable materials by reacting solid aluminosilicate in the fly ash with an alkaline solution. The material formed is identified as geopolymer (Davidovits, 2005). This material is easy to make at room temperature and at a low cost. In addition, it can be used as an adsorbent for heavy metals. Several researchers have investigated geopolymer as a potential material for removal of Cd^{2+} (Javadian et al., 2015), Ni^{2+} (Kara et al., 2017), Pb^{2+} (Al-Zboon et al., 2011; López et al., 2014), Cu^{2+} (Wang et al., 2007; Al-Harahsheh et al., 2015; Ge et al., 2015), ammonium (Zhang et al., 2010), and dyes (Atun et al., 2011; Li et al., 2006; and Alouani et al., 2017). Table 4-1 summarizes the results of above researchers using geopolymer as an adsorbent. The adsorption capacities for various geopolymers presented in Table 4-1 show that geopolymer has the potential material to remove heavy metals in aqueous solutions.

Table 4-1. Geopolymer as adsorbent on removal of pollutants

Precursors	Alkali activator	Particle size, mm	Pollutants	Adsorption capacity, mg/g	Reference
Class-F fly ash	14 M NaOH	0.2	Cu^{2+}	152.31	Al-Harahsheh et al., 2015
Class-F fly ash	NaOH	0.045	Cu^{2+}	98.4	Wang et al., 2007
Class-F fly ash	NaOH and Na_2SiO_3	0.071-0.09	Cu^{2+}	79.11	Mužek et al., 2014
Coal fly ash	14M NaOH	0.2	Pb^{2+}	174.34	Al-Zboon et al., 2011
Class-F fly ash	Solid NaOH	0.075	Cd^{2+}	26.246	Javadian et al., 2015
Metakaolin	Na_2SiO_3, H_2O_2 and K12	2-4	Cu^{2+}	52.63	Ge et al., 2015
Metakaolin	NaOH and Na_2SiO_3	0.15	Zn^{2+}	74.53	Kara et al., 2017
			Ni^{2+}	42.61	
Metakaolin	8 M NaOH	0.125	Cs^{+}	43	López et al., 2014
			Pb^{2+}	35	
			Cu^{2+}	15	
			Cd^{2+}	3	
			Ni^{2+}	1	
			Zn^{2+}	2	
Class-C fly ash	3 M NaOH	0.09	thionine	0.008	Atun et al., 2011
			safranine	0.006	
Class-F fly ash	NaOH	--	methylene blue	38.38	Li et al., 2006
			crystal violet	97.92	
Class-F fly ash	12 M NaOH	0.12-0.45	methylene blue	0.669	Alouani et al., 2018
Class-F fly ash	NaOH powder (600°C)	< 0.15	ammonium	37.45	Zhang et al., 2011

The objective of this study is to investigate fly ash-based geopolymer (FAG) as a reactive material or adsorbent for removal of heavy metals (Cu^{2+}, Cd^{2+}, and Pb^{2+}) in an acidic solution such as acid mine drainage. Several fly ash-based geopolymers were synthesized using different ratios of alkaline solution to fly ash and slag. The effect of initial pH solution on individual heavy metals removal was investigated. Experiments were also conducted with all metals in the solution to assess the competitive removal of the metals by the geopolymer.

4.3. Methods and Materials

4.3.1. Fly ash-based geopolymers

Five fly ash-based geopolymers were synthesized as presented in Table 4-2. They were labeled as G50, G60, G70, G60+10%S, and G60+20%S. A specified quantity of fly ash (Class F) with or without slag were reacted with certain mass of alkaline solution. The alkaline activating solution was formulated by blending sodium silicate solution and different concentrations of NaOH solution. The physical properties of the five geopolymers are presented in Table 4-2. Because of the alkaline and reactive nature of geopolymer surfaces and the standard test methods used may not be appropriate for the geopolymers, the cation exchange capacity, specific surface area and pH at point of zero charge of the five samples are reported in Appendix A.

Table 4-2. Synthesized fly ash-based geopolymer and its characterization**

Fly ash-based geopolymer samples	Molar conc. of NaOH (mM)	Alkaline activating solution (Mass ratio of Na_2SiO_3 : NaOH : H_2O)	Particle density, g/cm^3	Compressive strength for 2" cubic paste (7-days), MPa
G50	4.45	0.41 : 0.09 : 0.50	2.13 ± 0.56	36.57 ± 0.36
G60	6.68	0.49 : 0.11 : 0.40	2.09 ± 0.41	49.44 ± 2.45
G70	10.38	0.58 : 0.12 : 0.30	2.11 ± 0.47	35.68 ± 0.85
G60+10%S	6.68	0.49 : 0.11 : 0.40	2.10 ± 0.38	45.72 ± 3.45
G60+20%S	6.68	0.49 : 0.11 : 0.40	2.12 ± 0.35	51.09 ± 2.66

* Mass ratio of alkaline solution to fly ash/slag = 0.33:1
** Other properties (cation exchange capacity, specific surface area and pH at point of zero charge) are presented in Appendix A.

4.3.2. Preparation of synthetic acid mine drainage

Solutions of Cu^{2+} (0.5 – 300 mg/L), Cd^{2+} (0.5 – 500 mg/L), and Pb^{2+} (0.5 – 200 mg/L) were prepared from analytical grade $CuSO_4.5H_2O$, $CdSO_4.5H_2O$, and $PbSO_4.5H_2O$, respectively (Sigma-Aldrich, St. Louis, MO, USA). For single metal removal studies, the initial metal

concentrations were 20 mg/L of Cu^{2+}, 10 mg/L of Cd^{2+}, and 10 mg/L of Pb^{2+} simulating acid mine drainage (Motsi et al., 2009). Generally, acid mine drainage lacks a bicarbonate buffer system and has an acidic pH ranged from 2.5 to 4.0 (Thorsten, 2013). In this study, the initial pH of solution was adjusted to three different pH values (2.5, 3.0, and 4.0) by using 1 M concentration of H_2SO_4.

4.3.3. Batch study

Batch experiments were performed using 100 mL Erlenmeyer flasks with 0.1 g and 0.05 g of geopolymer and 50 mL of metal solution, shaken gently at a speed of 180 rpm at room temperature (21 – 23 ^oC). The solution was then filtered, and the final pH of filtrate measured by a pH meter and the finial equilibrium concentration of the metal analyzed using an inductively coupled plasma (ICP) atomic emission spectrometer (ICPE-9800 Series, Shimadzu Corporation, Kyoto, Japan). All experiments were carried out in duplicate and the average concentrations were reported. The first set of batch experiments were conducted using 20 mg/L of Cu^{2+}, 10 mg/L of Cd^{2+} and 10 mg/L of Pb^{2+} individually in a simulated acid mine drainage solution (single metal solution). The initial pH of the simulated acid mine solution was adjusted to three different values (2.5, 3.0, and 4.0) by using 1 M concentration of H_2SO_4. The metal concentrations and pHs selected were in the range where precipitation of the metals were minimized as determined in Chapter 3. The experimental matrix for the five geopolymers are presented in Table 4-3. The second set of experiments were conducted with all three metals in one solution. The multi-metal solution had an initial pH of 3.0 and with 0.05 g of geopolymer sample G60. The metal concentrations were the same as the first set of single metal experiments. The third set of experiments were conducted at higher initial concentrations of Cu^{2+}, Cd^{2+} and Pb^{2+} in the range of 5 to 500 mg/L. Geopolymer G60 was used as the material/adsorbent for the third set of experiments and the initial pH of the solutions were 2.5, 3.0, and 4.0.

Table 4-3. Matrix of batch experiments

Geopolymer samples	Metals	Mass, g	pH	Initial Conc., mg/L	Contact Time, hours
G50	Cu^{2+}	0.1	2.5, 3, 4	0 – 20	48
G60					
G70					
G60+10%S					
G60+20%S					
Zeolite					
G50	Cd^{2+}	0.05	2.5, 3, 4	0 – 10	48
G60					
G70					
G60+10%S					
G60+20%S					
Zeolite					
G50	Pb^{2+}	0.05	2.5, 3, 4	0 – 10	48
G60					
G70					
G60+10%S					
G60+20%S					
Zeolite					

4.3.4. Analysis of data from batch studies

The experimental data for the removal of the heavy metals were analyzed using adsorption isotherms by assuming that removal was by adsorption (for low concentration) even though the mechanism of removal may be due to reaction of the metals such as precipitation on the geopolymer surface (for high metal concentrations). The isotherms used were Langmuir, Freundlich, and BET as present in Table 4-4.

Table 4-4. Adsorption isotherm models

Isotherm	Equation	Reference
Langmuir model	$q_e = \frac{q_m K_L C_e}{1 + K_L C_e}$	Langmuir, 1917
Freundlich model	$q_e = K_F C_e^{1/n}$	Freundlich, 1906
BET model	$q_e = \frac{K_B C_e Q_M}{(C_s - C_e)[1 + \frac{(K_B - 1)C_e}{C_s}]}$	Brunauer et al., 1938

C_e = equilibrium concentration (mg/L), Q_e = amount of ion adsorbed (mg/g), Q_m = equilibrium capacity obtained from the isotherm model or monolayer equilibrium adsorption capacity (mg/g), K_L = Langmuir adsorption equilibrium constant (L/mg), K_F = Freundlich adsorption capacity (mg/g)(L/mg) $^{1/n}$, n = adsorption intensity, C_s = saturation (solubility limit) concentration of the solute. (mg/L), K_B = a parameter related to the binding intensity for all layers.

4.4. Results and Discussions

4.4.1. Batch experiments for initial metal concentration < 20 mg/L

Figure 4-1 shows the removal of Cu^{2+}, Cd^{2+} and Pb^{2+} for all five geopolymer samples and zeolite. Results showed that the G60 geopolymer, with 60% alkaline solution (6.68 mM of NaOH), showed slightly better removal of Cu^{2+}, Cd^{2+} and Pb^{2+}, in comparison with G50 (50% alkaline solution with 4.45 mM of NaOH) and G70 (70% alkaline solution with 10.38 mM of NaOH). The metal removal for G50 was found to be higher than that of G70, which indicates that higher alkaline concentration in geopolymer mix did not improve the metal removal due to the lower surface area produced as shown in Appendix A. For the G60 with 20% slag, removal of metals was slightly higher than G60 with 10% slag, but both samples had lower metal removal than G60. As before, this may be due to the low surface areas of G60+20%S and G60+10%S as compared to G60 (Appendix A).

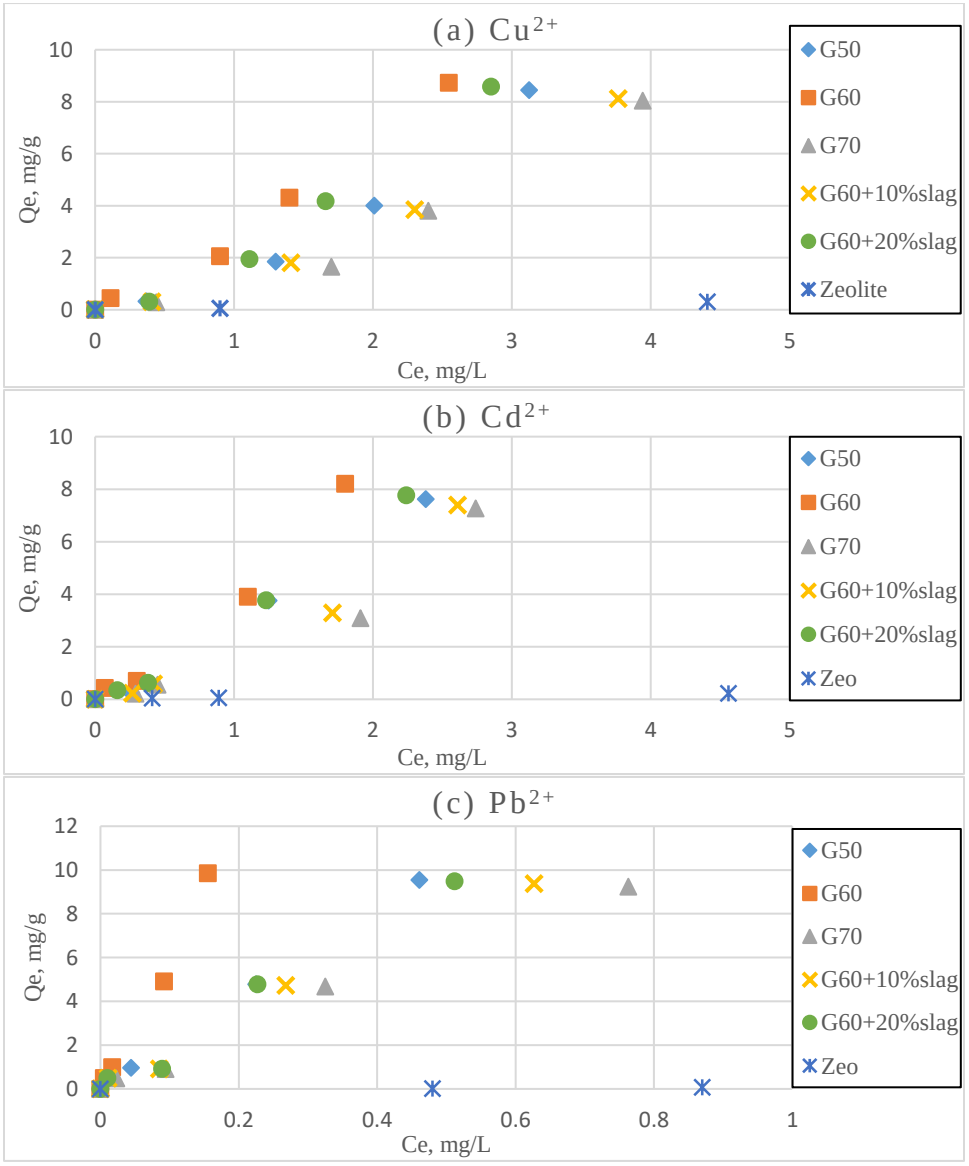

Figure 4-1. Removal of Cu2+ (a), Cd2+ (b) and Pb2+ (c) by geopolymer samples at initial pH 3.0, geopolymer mass 0.1 g for Cu2+ and 0.05 g for Cd2+ and Pb2+, contact time 48 hours.

From Figure 4-1, all geopolymer samples showed higher metal removal than that of zeolite for the same conditions. This can be explained by the low surface area of zeolite (14 – 15 m^2/g) as compared to the geopolymer samples and the reactive nature of the geopolymer surfaces.

Using the geopolymer sample G60 (with highest metal removal of all five geopolymers, the effect of solution pH on metal removal was investigated for three different initial solution pH

(2.5, 3.0, and 4.0). Results are presented in Figure 4-2. The removal of the three metals seemed to increase for an increase in the initial pHs. One possible reason is that the higher H^+ ions concentration in the lower initial pH solution would compete with the metal ions. However, it may be possible that some precipitation may occur at higher pH due to excess hydroxide ion from the activation solution (Albrecht et al., 2011).

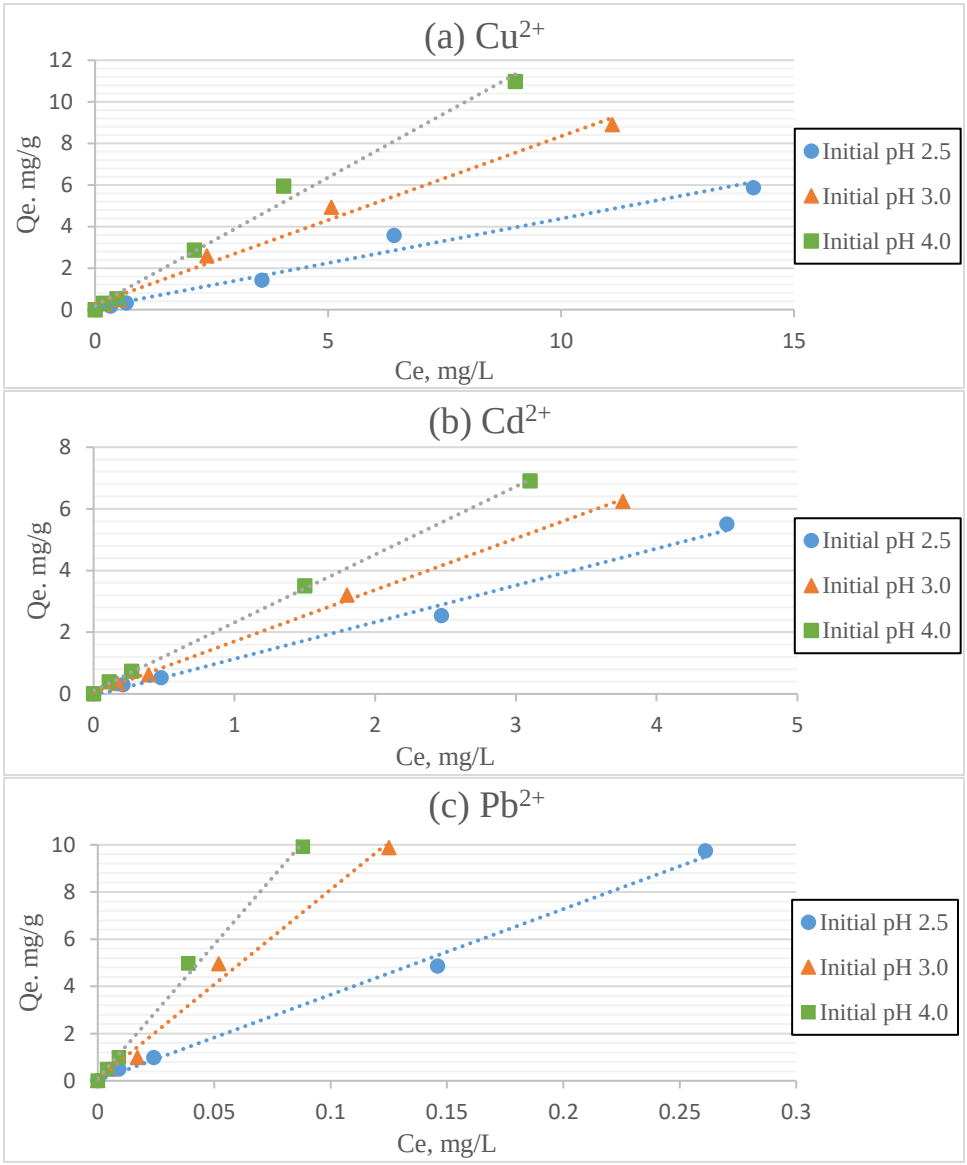

Figure 4-2. Removal/adsorption isotherms of G60 sample (0.05 g) with initial concentration of (a) Cu^{2+} (0 – 20 mg/L), (b) Cd^{2+} (0 – 10 mg/L), and (c) Pb^{2+} (0 – 10 mg/L) at three different initial pH 2.5, 3.0, and 4.0.

The data from batch tests were modeled using both Freundlich isotherm model and linear model as presented in Table 4-5. Both model gave R^2 value greater than 0.9. The *1/n* value for all three metals and three initial pH were slightly less than 1. A 1/n value of less than 1 indicates that removal/adsorption was favorable for all three metals. Also a *1/n* value close to 1 would indicate that removal/adsorption was on fairly homogeneous over the surface of the geopolymer. With 1/n close to a value of 1, the Freundlich model is similar to that of a linear model. Comparing the removal/adsorption capacities (K_F) for all three metal, the removal of Pb^{2+} was more favorable than Cd^{2+}, followed by Cu^{2+}.

Table 4-5. Isotherm parameters for three metals on geopolymer (G60) at three initial pHs.

Freundlich model									
Initial pH	Copper (Cu^{2+})			Cadmium (Cd^{2+})			Lead (Pb^{2+})		
	K_F, $mg^{(1-n)}g^{-1}L^n$	1/n	R^2	K_F, $mg^{(1-n)}g^{-1}L^n$	1/n	R^2	K_F, $mg^{(1-n)}g^{-1}L^n$	1/n	R^2
2.5	0.487	0.963	0.989	1.171	0.958	0.993	28.879	0.883	0.994
3.0	1.078	0.902	0.991	1.721	0.975	0.996	75.432	0.980	0.969
4.0	1.395	0.953	0.982	2.491	0.871	0.998	114.910	0.993	0.997
Linear model									
Initial pH	Copper (Cu^{2+})			Cadmium (Cd^{2+})			Lead (Pb^{2+})		
	K_{Linear}, L/g	R^2		K_{Linear}, L/g	R^2		K_{Linear}, L/g	R^2	
2.5	0.438	0.970		1.176	0.989		36.389	0.994	
3.0	0.841	0.981		1.681	0.998		81.042	0.987	
4.0	1.263	0.989		2.250	0.998		114.930	0.995	

4.4.2. Competitive metals removal

Using geopolymer G60 and an initial pH of 3.0, batch studies were conducted with all three metals present in acidic solution. Figure 4-3 shows the adsorption isotherm for each of the metal in the multi-metal solution and the removal/adsorption isotherm of the metal in a single metal solution. Figure 4-3 shows that the removal of Cu^{2+} was slightly affected by the presence of other competing ions. The K_F ($mg^{(1-n)}g^{-1}L^n$) of the Freundlich model decreased from a value of 1.075 to a

value of 0.763 in the multi-metal solution. Removal of Cd^{2+} were significantly affected as shown in Figure 4-3. The K_F ($mg^{(1-n)}g^{-1}L^n$) of the Freundlich model for single metal solution for Cd^{2+} was about 6 times (1.721) larger than the K_F value (0.304) for the multi-metal solution. Removal of Pb^{2+} in the multi-metal solution decreased as compared to a single metal solution but the decrease was not as severe as that of Cd^{2+}. The results showed that the metals affected most in the multi-metal solution were in the order of $Cd^{2+} > Pb^{2+} > Cu^{2+}$.

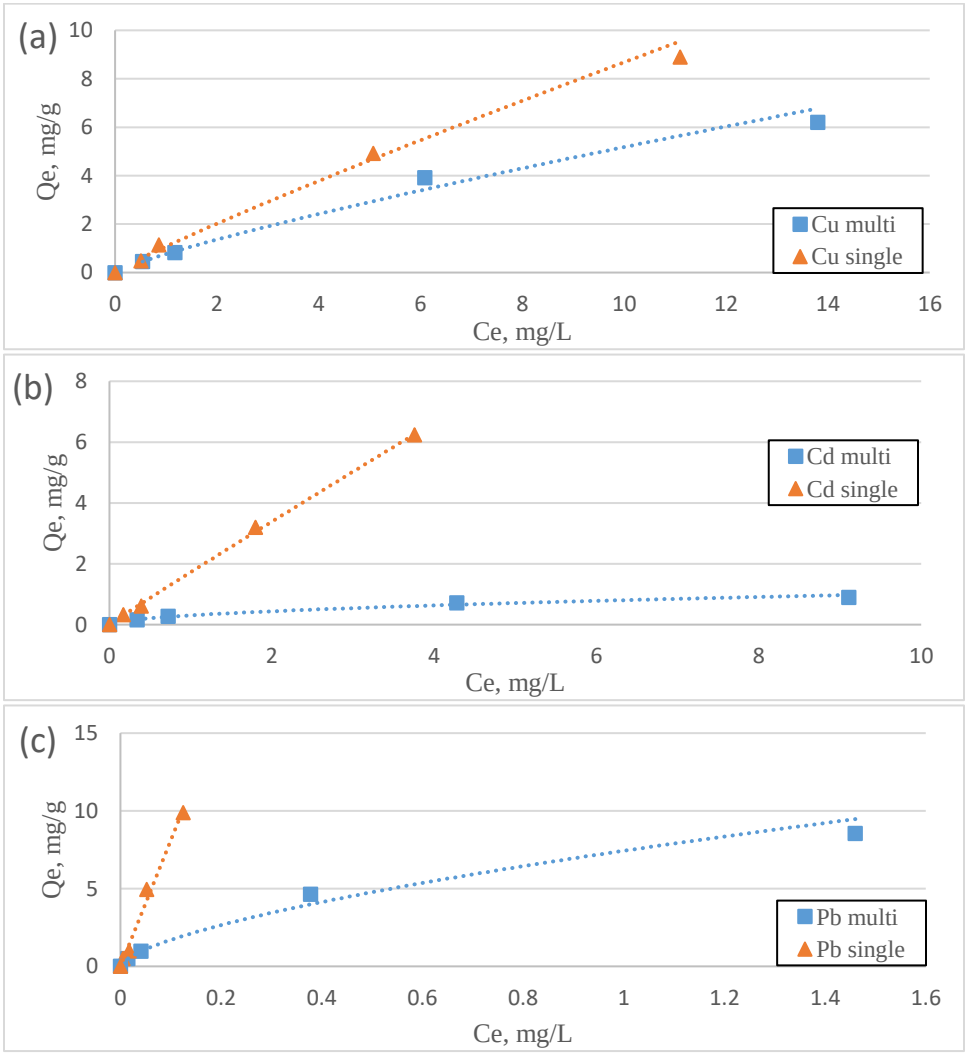

Figure 4-3. Comparison of removal of metals from multi-metal and single metal solutions containing (a) Cu^{2+} (0 – 20 mg/L), (b) Cd^{2+} (0 – 10 mg/L), and (c) Pb^{2+} (0 – 10 mg/L) respectively, at initial pH 3.0.

4.4.3. Removal of heavy metals at higher metals concentration

Experiments conducted in Section 3.1 and 3.2 were for metal concentration ranges from 0 – 20 mg/L, which are typically found in acid mine drainage. To determine the maximum removal/adsorption capacity of the geopolymer, a higher metal concentration range was used (Cu^{2+}: 0 – 300 mg/L; Cd^{2+}: 0 – 500 mg/L; Pb^{2+}: 0 – 200 mg/L). Batch experimental data are presented in Figure 4-4 for Cu^{2+}, Cd^{2+}, and Pb^{2+}. Isotherms for Cu^{2+} and Cd^{2+} follow that of a Type II isotherm, which is common for physical adsorption if adsorption is occurring but may also correspond to multilayer adsorption or precipitation of the metal. As in the earlier experiments on the effect of initial pH, similar results were obtained here as shown in Figure 4-4, where a higher initial pH resulted in higher removal of the metals.

The full experimental data were modeled using Langmuir, Freundlich, and BET model. For Langmuir and Freundlich models, the data modeled were for initial metal concentrations of 0 – 200 mg/L of Cu^{2+}, 0 – 300 mg/L of Cd^{2+}, 0 – 200 mg/L of Pb^{2+}, respectively and where the mass removed have reached an asymptotic value. The values of the asymptotic removal capacity (maximum) (Q_{max}), (which is similar to monolayer equilibrium adsorption capacity, if adsorption is occurring) and the Langmuir adsorption equilibrium constant, K_L, are presented in Table 4-4 for the removal of Cu^{2+}, Cd^{2+} and Pb^{2+} by geopolymer at pH 2.5, 3.0, and 4.0. The coefficient of determination (R^2), obtained with the Langmuir model was the highest among the three isotherm models (note range of data modeled as explained above). Unlike the results of low metal concentration in Section 3.1 where the isotherms were generally linear, the *1/n* values of Cu^{2+}, Cd^{2+} and Pb^{2+}, for example at an initial of pH 3.0, were 0.41, 0.222, and 0.695, respectively which was an indication of favorable removal/adsorption of these metal ions by the geopolymer samples. In addition, the BET model was used since it is probable that precipitation and/or multilayer

adsorption may occur at initial metal (Cu^{2+} and Cd^{2+}) concentrations over 200 mg/L and 300 mg/L, respectively.

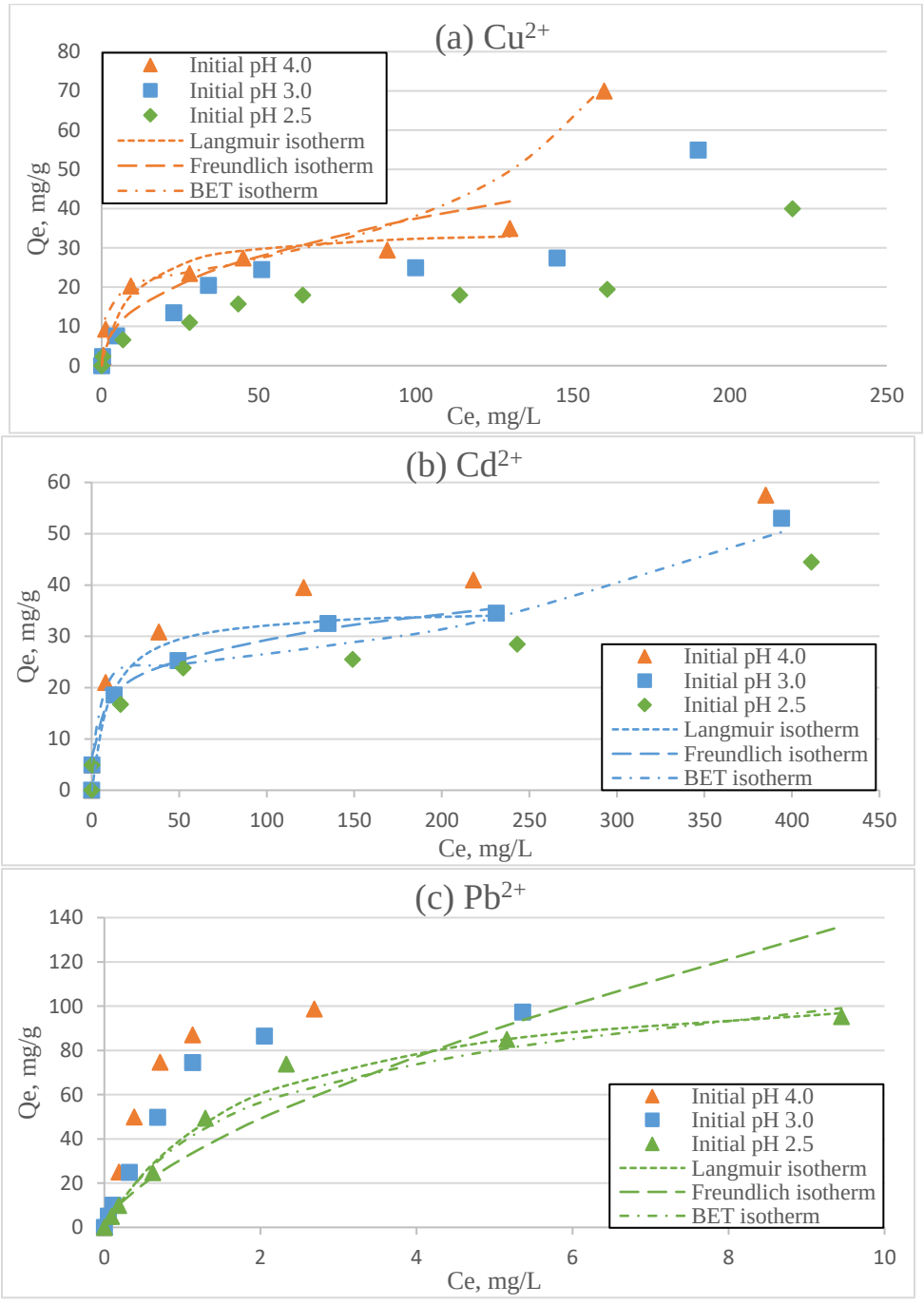

Figure 4-4. Removal of (a) Cu^{2+} (0 – 300 mg/L), (b) Cd^{2+} (0 – 500 mg/L) and (c) Pb^{2+} (0 – 200 mg/L) on 0.1 g of geopolymer (G60) at pH 2.5, 3.0, and 4.0 (50 mL of Cu^{2+} solution and contact time 48 hours) (Models fit are shown for one initial pH for each metal)

Table 4-6. Isotherm parameters for removal of Cu^{2+}, Cd^{2+} and Pb^{2+} on geopolymer (G60).

Metals	Isotherm	Parameter	Initial pH 2.5	Initial pH 3.0	Initial pH 4.0
Cu^{2+}	Langmuir*	Q_m, mg/g	20.66	29.41	35.21
		K_L, L/mg	0.08	0.07	0.11
		R^2	0.987	0.981	0.986
	Freundlich*	K_F, $mg^{(1-n)}g^{-1}L^n$	3.47	4.1	5.28
		1/n	0.36	0.41	0.43
		R^2	0.982	0.981	0.959
	BET	Q_m, mg/g	10.4	18.25	21.65
		K_{BET}	481	68.5	231
		C_S, mg/L	320	270	230
		R^2	0.978	0.967	0.953
Cd^{2+}	Langmuir*	Q_m, mg/g	28.74	35.59	42.02
		K_L, L/mg	0.112	0.095	0.138
		R^2	0.995	0.995	0.997
	Freundlich*	K_F, $mg^{(1-n)}g^{-1}L^n$	10.46	10.60	13.89
		1/n	0.185	0.222	0.210
		R^2	0.923	0.992	0.981
	BET	Q_m, mg/g	19.04	22.98	30.11
		K_{BET}	5251	2176	3321
		C_S, mg/L	750	725	830
		R^2	0.999	0.998	0.999
Pb^{2+}	Langmuir	Q_m, mg/g	116.28	119.05	121.95
		K_L, L/mg	0.528	0.966	1.745
		R^2	0.993	0.985	0.971
	Freundlich	K_F, $mg^{(1-n)}g^{-1}L^n$	30.981	47.643	74.114
		1/n	0.659	0.695	0.736
		R^2	0.952	0.938	0.944
	BET	Q_m, mg/g	91.74	104.17	109.89
		K_{BET}	36	48	91
		C_S, mg/L	53	47	45
		R^2	0.988	0.982	0.970

* Data modeled for concentration range of Cu^{2+}: 0 – 200 mg/L, Cd^{2+}: 0 – 300 mg/L.

From Table 4-6, the asymptotic removal (maximum) capacity of Cu^{2+} ions based on Langmuir model for geopolymer (G60) were 20.66, 29.41, and 35.21 mg/g for an initial pH of 2.5, 3.0, and 4.0 respectively. Based on the asymptotic removal capacity, Pb^{2+} was more favorably removed than Cu^{2+} and Cd^{2+} for all three initial pHs. Cu^{2+} had the lowest asymptotic removal

capacity of three metals tested. Possible mechanisms of metal removal include surface adsorption, surface complexation and precipitation at high metal concentrations.

4.5. Conclusion

Experiments on removal of heavy metals from acidic solution onto geopolymer were conducted. In a single metal solution, for metal concentrations less than 20 mg/L, removal of metals from the most favorable to the least favorable followed the sequence of $Pb^{2+} > Cu^{2+} > Cd^{2+}$. The extent of metal removal was found to be directly proportional to the pH value of the solution, where removal of metal decreased in more acidic solution, which may be due to the presence and effect of hydrogen ion competition. In a multi-metal solution, Cd^{2+} was the most affected by the presence of the other two metals, Cu^{2+} and Pb^{2+}. Cu^{2+} was minimally affected by the other two metals in a multi-metal solution. For the single metal solution experiments, the asymptotic removal (maximum) capacity of Cu^{2+}, Cd^{2+} and Pb^{2+} were found to range from 20.66 – 35.21, 28.74 – 42.02, and 116.28 – 121.95 mg/g for initial pH 2.5 to 4.0 respectively. Removal of heavy metals was not only due to adsorption to the geopolymer surfaces but also due to precipitation of metal from the solution.

These results confirm that geopolymer can be used as a material for pH neutralizing acidic waste streams such as acid mine drainage and acidic industrial wastewaters in addition to removal of heavy metals. It can be a substitute for more expensive adsorbents such as zeolite or activated carbon.

4.6. References

Al-Subu, M. M., Salim, R., Braik, H., & Swaileh, K. M. (2001). Removal of dissolved copper from polluted water using plant leaves. II. Effects of copper concentration, plant leaves, competing ions and other factors. *Revista Internacional de Contaminación Ambiental*, *17*(3), 123-127.

Albrecht, T. W. J., Addai-Mensah, J., & Fornasiero, D. (2011). Effect of pH, concentration and temperature on copper and zinc hydroxide formation/precipitation in solution CHEMECA 2011: Engineering a better world. *Engineers Australia, Sydney, NSW*.

Al-Harahsheh, M. S., Al Zboon, K., Al-Makhadmeh, L., Hararah, M., & Mahasneh, M. (2015). Fly ash based geopolymer for heavy metal removal: A case study on copper removal. *Journal of Environmental Chemical Engineering*, *3*(3), 1669-1677.

Alouani, M. E. L., Alehyen, S., Achouri, M. E. L., & Taibi, M. (2018). Removal of cationic dye-methylene blue-from aqueous solution by adsorption on fly ash-based geopolymer. *J Mater Environ Sci*, *9*(1), 32-46.

Al-Zboon, K., Al-Harahsheh, M. S., & Hani, F. B. (2011). Fly ash-based geopolymer for Pb removal from aqueous solution. *Journal of Hazardous Materials*, *188*(1-3), 414-421.

Atun, G., Hisarlı, G., Kurtoğlu, A. E., & Ayar, N. (2011). A comparison of basic dye adsorption onto zeolitic materials synthesized from fly ash. *Journal of Hazardous materials*, *187*(1-3), 562-573.

Baskaran, P. K., Venkatraman, B. R., Hema, M., & Arivoli, S. (2010). Adsorption studies of copper ion by low cost activated carbon. *J. Chem. Pharm. Res*, *2*(5), 642-655.

Brunauer, S., Emmett, P. H., & Teller, E. (1938). Adsorption of gases in multimolecular layers. *J. Am. Chem. Soc*, *60*(2), 309-319.

Davidovits, J. (2005). Geopolymer chemistry and sustainable development. The poly (sialate) terminology: a very useful and simple model for the promotion and understanding of green-chemistry. In *Proceedings of the world congress Geopolymer* (pp. 9-15). Saint Quentin, France.

Dimitrova, S. V. (1996). Metal sorption on blast-furnace slag. *Water Research*, *30*(1), 228-232.

Dimitrova, S. V., & Mehandgiev, D. R. (1998). Lead removal from aqueous solutions by granulated blast-furnace slag. *Water Research*, *32*(11), 3289-3292.

Feng, D., Aldrich, C., & Tan, H. (2000). Treatment of acid mine water by use of heavy metal precipitation and ion exchange. *Minerals Engineering*, *13*(6), 623-642.

Freundlich, H. M. F. (1906). Over the adsorption in solution. *J. Phys. Chem*, *57*(385), e470.

Ge, Y., Cui, X., Kong, Y., Li, Z., He, Y., & Zhou, Q. (2015). Porous geopolymeric spheres for removal of Cu (II) from aqueous solution: Synthesis and evaluation. *Journal of Hazardous Materials*, *283*, 244-251.

Gupta, G., & Torres, N. (1998). Use of fly ash in reducing toxicity of and heavy metals in wastewater effluent. *Journal of Hazardous Materials*, *57*(1-3), 243-248.

Iakovleva, E., Mäkilä, E., Salonen, J., Sitarz, M., Wang, S., & Sillanpää, M. (2015). Acid mine drainage (AMD) treatment: Neutralization and toxic elements removal with unmodified and modified limestone. *Ecological Engineering*, *81*, 30-40.

Javadian, H., Ghorbani, F., Tayebi, H. A., & Asl, S. H. (2015). Study of the adsorption of Cd (II) from aqueous solution using zeolite-based geopolymer, synthesized from coal fly ash; kinetic, isotherm and thermodynamic studies. *Arabian Journal of Chemistry*, *8*(6), 837-849.

Johnson, D. B., & Hallberg, K. B. (2005). Acid mine drainage remediation options: a review. *Science of the total environment*, *338*(1-2), 3-14.

Kalin, M., Fyson, A., & Wheeler, W. N. (2006). The chemistry of conventional and alternative treatment systems for the neutralization of acid mine drainage. *Science of the Total Environment*, *366*(2-3), 395-408.

Kara, İ., Yilmazer, D., & Akar, S. T. (2017). Metakaolin based geopolymer as an effective adsorbent for adsorption of zinc (II) and nickel (II) ions from aqueous solutions. *Applied Clay Science*, *100*(139), 54-63.

Kaur, G., Couperthwaite, S. J., Hatton-Jones, B. W., & Millar, G. J. (2018). Alternative neutralisation materials for acid mine drainage treatment. *Journal of Water Process Engineering*, *22*, 46-58.

Langmuir, I. (1917). The constitution and fundamental properties of solids and liquids. 11. Liquids. *J Am Chem Soc*, *3*(9), 1848-1906.

Li, L., Wang, S., & Zhu, Z. (2006). Geopolymeric adsorbents from fly ash for dye removal from aqueous solution. *Journal of colloid and interface science*, *300*(1), 52-59.

López, F. J., Sugita, S., Tagaya, M., & Kobayashi, T. (2014). Metakaolin-based geopolymers for targeted adsorbents to heavy metal ion separation. *Journal of Materials Science and Chemical Engineering*, *2*(07), 16.

Motsi, T., Rowson, N. A., & Simmons, M. J. H. (2009). Adsorption of heavy metals from acid mine drainage by natural zeolite. *International Journal of Mineral Processing*, *92*(1-2), 42-48.

Mulgund, M. G., Kininge, P. T., Pillai, M. M., & Sanandam, M. R. (2011). Biosorptive removal of heavy (Cd^{2+}, Pb^{2+} and Cu^{2+}) from aqueous solutions by Cassia angustifolia bark. *International Journal of Engineering, Science and Technology*, *3*, 1642-1647.

Nadaroglu, H., Kalkan, E., & Demir, N. (2010). Removal of copper from aqueous solution using red mud. *Desalination*, *251*(1-3), 90-95.

Pan, S. C., Lin, C. C., & Tseng, D. H. (2003). Reusing sewage sludge ash as adsorbent for copper removal from wastewater. *Resources, Conservation and Recycling*, *39*(1), 79-90.

Panday, K. K., Prasad, G., & Singh, V. N. (1985). Copper (II) removal from aqueous solutions by fly ash. *Water Research*, *19*(7), 869-873.

Skousen, J., Hilton, T., & Faulkner, B. (1996). Overview of acid mine drainage treatment with chemicals. *Green Lands*, *26*(3), 40-49.

Thorsten, C. "Some Chemistry of Acid Mine Drainage". CR Scientific LLC. Web. April 2013. http://www.crscientific.com/article-amd.html

Wang, S., Li, L., & Zhu, Z. H. (2007). Solid-state conversion of fly ash to effective adsorbents for Cu removal from wastewater. *Journal of hazardous materials*, *139*(2), 254-259.

Yavuz, Ö., Altunkaynak, Y., & Güzel, F. (2003). Removal of copper, nickel, cobalt and manganese from aqueous solution by kaolinite. *Water Research*, *4*(37), 948-952.

Zhang, M., Zhang, H., Xu, D., Han, L., Niu, D., Tian, B., Zhang, J., Zhang, L., & Wu, W. (2011). Removal of ammonium from aqueous solutions using zeolite synthesized from fly ash by a fusion method. *Desalination*, *271*(1-3), 111-121.

CHAPTER 5. USE OF THE GEOPOLYMER AS MEDIA IN FIXED-BED COLUMN FOR REMOVAL OF HEAVY METALS

5.1. Abstract

Fixed bed column studies were carried out using fly ash-based geopolymer as the filtration medium for removal of metal (Cu^{2+}, Cd^{2+}, and Pb^{2+}) in low pH solutions. Breakthrough curves showed that the uptake affinity of the geopolymer for metals were in the order of $Pb^{2+} > Cd^{2+} > Cu^{2+}$ for a single metal solution. In a multi-metal solution (with all three metal ions Cu^{2+}, Cd^{2+}, and Pb^{2+}), the uptake affinity of the geopolymer was in the order of $Pb^{2+} > Cu^{2+} > Cd^{2+}$ showing that there were competition for alkaline sites on the geopolymer. Of the three models (Bohart-Admas, Thomas, and Yan models) used, Thomas model gave the best fit of the experimental data. The experimental results showed that geopolymer can be used as a filtration medium in a fixed bed column for the uptake of metals from acidic waste stream such as acid mine drainage and industrial wastewaters.

5.2. Introduction

Several strategies have been reported for the removal and recovery of metal ions from acid mine drainage and acidic industrial wastewaters. These strategies include ion-exchange (Gaikwad et al., 2010), membranes filtration (Ricci et al., 2015), chemical precipitation (Olds et al., 2013; Tolonen et al., 2014), and adsorption (Motsi et al., 2009). Among these, chemical precipitation is the most common and the lowest cost. Adsorption is considered as a promising treatment method due to its high removal efficiency, simplicity, availability of low-cost adsorbents, elimination of low level concentration of target pollutant, and its environmental-friendly characteristics (Bhatnagar & Sillanpää, 2010). To treat the waste stream, a continuous flow system is the most efficient where the media can be easily replaced and regenerated, if needed. Fixed-bed columns or

placement of media in the path of the flow are some of the more common continuous flow treatment methods used. For continuous flow system, the contact time of the media with the contaminated waste stream is an important factor which determines the efficiency of removal.

The potential of geopolymer made by alkaline-activated fly ash has been demonstrated for removal of heavy metals in batch studies. However, limited studies have been reported in the literature on fixed-bed column packed with geopolymer. Some of the studies include removal of dyes using fly ash-based geopolymer (EI Alouani et al., 2018) and metakaolin-based geopolymer (Barbosa, et al., 2018), heavy metals in removal of Cu^{2+} using fly ash-based geopolymer (Ge et al., 2015 and 2017) and Zn^{2+}, Ni^{2+}, Co^{2+} and Mn^{2+} using makaolin-based geopolymer (Kara et al., 2017; 2018). Makaolin-based geopolymer was used in fixed-bed column for the removal of Zn^{2+} and Ni^{2+} (Kara et al., 2017) and removal Co^{2+} and Mn^{2+} (Kara et al., 2018) with flow rates ranging from 0.5 – 6 mL/min and adsorbent amount ranging from 0.4 – 0.6 g/L. However, the researchers did not conduct breakthrough analysis and modeling of the data. Ge et al. (2015) investigated column packed with geopolymeric spheres (2 – 4 mm) on Cu^{2+} removal for three different bed heights (0.5, 2.2, and 3 cm). The breakthrough curves data were analyzed using three different models (Thomas, Bohart-Adams, and Yoon-Nelson models) (Ge et al., 2017). They found the uptake rate constants decreased with increasing bed heights (1, 2, and 3 cm), while the uptake capacities were in the range of 10 – 26 mg/g.

The objective of this study is to assess the use of geopolymer particles as a filtration media in a fixed bed column for the treatment of acidic waste streams with metal ions. Single metal experiments were conducted along with a multi-metal (three metals) experiment. The flow rate and the bed depth were varied and the metal uptake capacities estimated based on the breakthrough curves.

5.3. Materials and Methods

5.3.1. Materials and geopolymer preparation

The material used as the media for the fixed bed column was a fly ash-based geopolymer. The geopolymer was made of Class F (as defined in ASTM C618) fly ash and an alkaline activator solution. The alkaline activator consisted of sodium silicate solution (water glass, $3Na_2O{\cdot}3SiO_2$), solid NaOH, and water in a mass ratio of 0.49:0.11:0.40. The mass ratio of the alkaline activator to the fly ash and the activator was 0.33:1. The geopolymer was prepared by mixing the fly ash and the activator for 5 – 10 mins and placing the paste in a mold to cure for 24 hours at room temperature (21 – 23 ^{o}C). It was then demold and cured in an oven for 7 days at 50 ^{o}C. The geopolymer was then washed 3 times with water and crushed to the appropriate particles size. Particles size used for the column experiments ranged from 0.42 – 2 mm.

5.3.2. Fixed bed column setup

Fixed bed column experiments were conducted using polypropylene columns with an inner diameter 1 cm and a length of 15 cm. Wire meshes were placed at both ends (inlet and outlet) to hold the fly ash-based geopolymer in the column. The fixed bed column set up is shown in Figure 5-1, which was considered as the rapid small-small column test.

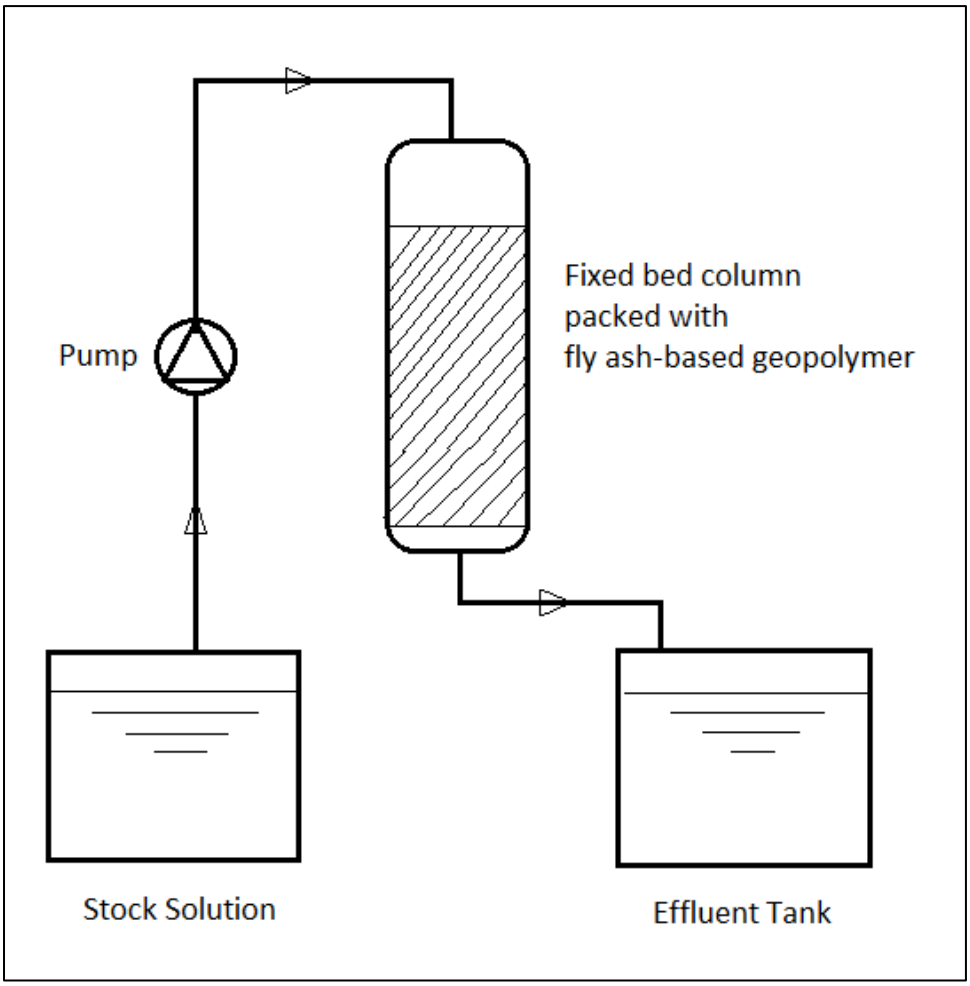

Figure 5-1. Schematic diagram of fixed bed column setup.

Acidic solution simulating acid mine drainage was fed into the column in a down flow direction by using a variable flow rate peristaltic pump. Solution leaving the bottom of the column was collected at regular intervals and analyzed for the target metal using an inductively coupled plasma (ICP) atomic emission spectrometer (ICPE-9800 Series, Shimadzu Corporation, Kyoto, Japan). Experiments were conducted until there were a breakthrough of the metal in the effluent and the effluent concentration was approximately equal to the influent concentration. To study the metal uptake capacity of the geopolymer, the depth of the media in the column and solution flow rate were varied.

5.3.3. Feed solution

Low pH solution (pH 4.0) were prepared with analytical grade $CuSO_4$, $CdSO_4$, and $PbSO_4$ to obtain individual solution with 10 mg/L of Cu^{2+}, Cd^{2+} and Pb^{2+}, respectively. To simulate acid mine drainage, a mixture of Cu^{2+}, Cd^{2+} and Pb^{2+} at 10 mg/L was prepared (multi-metal solution). Solutions were adjusted to pH 4.0 with 1 M of sulfuric acid. Typical pH of acid mine drainage ranged from 2.5 to 6 (Kleinmann, 1990) with concentration of Cu^{2+}, Cd^{2+} and Pb^{2+} in the range of 1.8 – 35.9 mg/L, 0.01 – 11 mg/L, and 0.6 – 45 mg/L, respectively (Feng et al., 2000; Archer et al., 2004; López, et al., 2010; Nieto et al., 2007). Higher pH solution (greater than 5.0) was not investigated due to the possible precipitation of the metals on the media which may clog the filtration process and impact the flow.

5.3.4. Column operation

The first set of experiments were conducted with feed water containing individual metal at 10 mg/L in the solution. Hydraulic loading of the columns was investigated by using flow rates of 5 and 10 mL/min with bed depth of 2, 5, and 10 cm, giving empty bed contact time of between 0.31 to 1.57 minutes. The second set of column experiment was conducted with the simulated acid mine drainage with all three metals in the solution (multi-metal solution) at concentrations of 10 mg/L for each metal. Column bed depth was 5 cm and the flow rate was 5 mL/min giving an EBCT of 0.79 minutes. The experimental matrix for the column experiments are presented Table 5-1.

Table 5-1. Experimental conditions for column studies

Column No.	Sample	Bed depth, cm	Flow rate, mL/min	EBCT, min	pH	Metals	Initial Conc., mg/L
C_1	G60	2	10	0.16	4	Cu^{2+}	10
C_2		2	5	0.31		Cu^{2+}	
C_3		10	5	1.57		Cu^{2+}	
C_4		5	5	0.79		Cu^{2+}	
C_5		5	5	0.79		Cd^{2+}	
C_6		5	5	0.79		Pb^{2+}	
C_7		5	5	0.79		Cu^{2+}, Cd^{2+}, Pb^{2+}	

5.3.5. Analysis of data

The breakthrough curves obtained from the experiments were used to assess the performance of the column as an uptake bed for metals. For our analysis, the time when the metal concentration in the effluent reaches 5% of the influent value ($C_t = 0.05\ C_0$), was defined as the breakthrough time (t_b). When the metal ions concentration in the effluent exceeds 95% of that in the influent ($C_t = 0.95\ C_0$), it was assumed exhaustion time (t_e) has been established (Patel, 2019).

The total mass of metal removed (m_{ads}, mg) in the column for a given influent metal concentration and flow rate was estimated based on the area (A) above the breakthrough curve or under the mass transfer curve which is obtained by integrating the removed metal concentration (C_{ads}, mg/L) over time in the following equation (Hasan et al., 2009).:

$$m_{ads} = \frac{QA}{1000} = \frac{Q}{1000} \int_{t=0}^{t=t_e} C_{ads}\, dt$$

The uptake capacity (q_0, mg/g) was calculated by dividing the total mass removed with the known amount of the geopolymer particles (m_s, g) packed in the column:

$$q_0 = \frac{m_{ads}}{m_s}$$

Three models, Bohart-Admas's model (Bohart & Adams, 1920), Thomas model (Thomas, 1944), and Yan model (Yan et al., 2001) were used to analyze and model the breakthrough curves. From the models, the maximum uptake capacities were estimated and compared with the uptake capacity, q_0.

- Bohart-Adamas model

The basic assumptions of Bohart–Adams model is that intra-particle diffusion and external mass resistance were negligible, and that-adsorption kinetics was controlled by the surface

chemical reaction between the solute and the adsorbent. Although these assumptions are usually not validated in real systems (Bohart & Adams, 1920), the equation can be simplified to a form which is easy to use. The equation is

$$\ln\left(\frac{C_0}{C_t}\right) = k_{BA}C_0 t - k_{BA}C_{BA}\frac{H}{v}$$

where C_0 is initial solute concentration (mg/L), C_t is effluent solute concentration (mg/L), k_{BA} is rate constant (mL/mg min), C_{BA} is removal capacity (mg/L), H is bed depth (cm), v is the linear flow velocity (cm/min) and t is the service time (min). It can be used to predict the service time of the column for the scale up of the experiments. (Lodeiro, et al., 2006)

The removal capacity q_{BA} in mg/g is estimated using:

$$q_{BA} = \frac{C_{BA}BV_s}{m} = \frac{C_{BA}}{\rho}$$

where q_{BA} is the removal capacity (mg/g), BVs is the fixed bed volume (L), m is the mass of the bed (g) and p is the apparent density of the adsorbent in the fixed bed (g/L).

The values describing the characteristic operational parameters of the column (k_{BA} and q_{BA}) can be determined from the plot of $In\ (C_0/C_t)$ versus t for a given bed depth, initial concentration and flow rate through the column.

- Thomas model

The Thomas model assumes that adsorption and kinetics obey the Langmuir model and second-order kinetics, respectively (Thomas, 1944). In addition, the model assumes sorption is not limited by the chemical reaction, and it also controlled by the mass transfer at the interface (Ghasemi et al., 2011). The linearized form of the Thomas model is as (Biswas & Mishra, 2015):

$$\ln\left(\frac{C_0}{C_t} - 1\right) = \frac{k_{Th}q_{Th}m}{Q} - k_{Th}C_0 t$$

where k_{Th} is the Thomas kinetic coefficient (mL/min mg), t is the total flow time (min), and Q is the volumetric flow rate (mL/min). Uptake capacity and mass of the adsorbent are denoted as q_{Th} (mg/g) and m (g). A plot of ln $[(C_0/C_t) - 1]$ versus t gives the value of k_{Th} and q_{Th}.

- Yan's model

Yan model is an empirical model used for describing the adsorption process in a fixed-bed system (Yan et al., 2001). The mathematical description of this model is given as:

$$\log\left(\frac{C_e}{C_0 - C_e}\right) = a\log(V) - a\log\left(\frac{q_Y m_s}{C_0}\right)$$

The model parameters a, and adsorption capacity, q_Y can be estimated by fitting the experimental data to the adjusted model:

$$\frac{C_e}{C_0} = 1 - \frac{1}{1 + \left(\frac{V_{eff} C_0}{m_s q_Y}\right)^a}$$

Yan's model can generally describe the complete breakthrough curves but has an empirical parameter a, which is dependent on experimental conditions (Lodeiro, et al., 2006). As such, Yan's model may not be used to scale up the system.

5.4. Results and Discussions

5.4.1. Effect of flow rate on the breakthrough curves

Results showing the effect of flow rate (5 and 10 mL/min) with a fixed-bed of 2 cm bed depth on the uptake of copper are presented in Figure 5-2. These are equivalent to an empty bed contact time (EBCT) of 0.31 and 0.16 minutes for the rapid small-small column test.

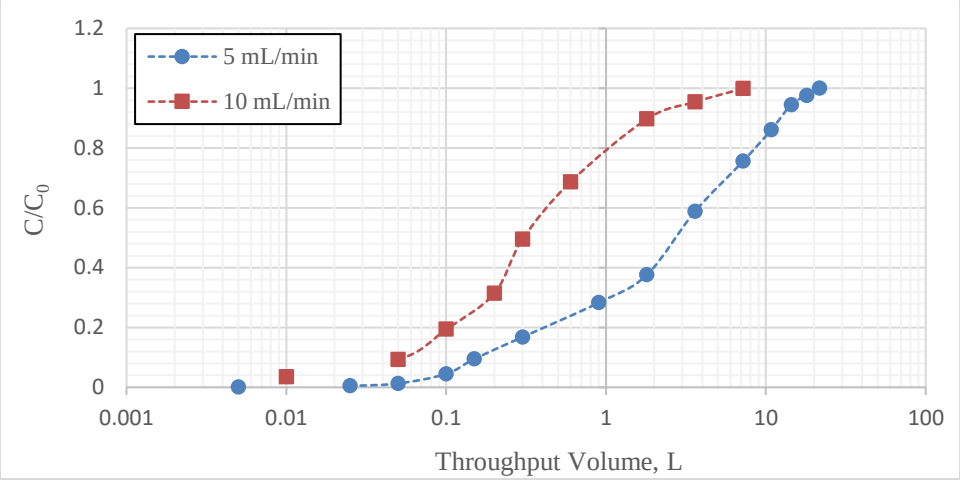

Figure 5-2. Breakthrough curves for uptake of Cu^{2+} onto geopolymer (G60) for flow rate 5 and 10 mL/min (influent concentration 10 mg/L, pH 4.0, bed height 2 cm).

As expected, the breakthrough curve for the columns with the higher flow rate (10 mL/min) appeared earlier than the breakthrough curve for a flow rate of 5 mL/min. The breakthrough time (t_b) for a flow rate of 10 mL/min was 5 min and for a flow rate of 5 mL/min it was 30 min. The estimated uptake capacities (total mass removed per gram of sample) were 17.20 mg/g and 2.15 mg/g for a flow rate of 5 mL/min and 10 mL/min, respectively (Table 5-2). Even though the flow rate was doubled, i.e., the contact time was halved, the mass removed was not reduced proportionately, but by eight times. As in many column experiments, diffusion of the metal ions to the surface may be the limiting step (Vijayaraghavan et al., 2005). Since the reduction in mass removed was more than 50% for a doubling of the flow rate, it is probable that diffusion was involved in the metal uptake.

5.4.2. Effect of bed height on breakthrough curves

Results of bed depth on the uptake of heavy metals are presented in Figure 5-3. The bed depths were for 2, 5 and 10 cm and the influent concentration was Cu^{2+} of 10 mg/L and the flow rate was 5 mL/min. As expected, the column with the shallowest bed depth (2 cm) experienced

breakthrough first followed by the 5 cm bed depth and then the 10 cm bed depth. Breakthrough times were 30 min, 270min, and 1080 min for 2, 5, and 10 cm bed depth, respectively. The uptake capacities (q_0) were 17.20 mg/g, 19.26 mg/g, and 24.04 mg/g for 2 cm, 5 cm and 10 cm, respectively (Table 5-2). The masses removed per gram of sample were of similar magnitude indicating that at the flow rates tested the mechanism of metal uptakes were similar and was probably diffusion limited.

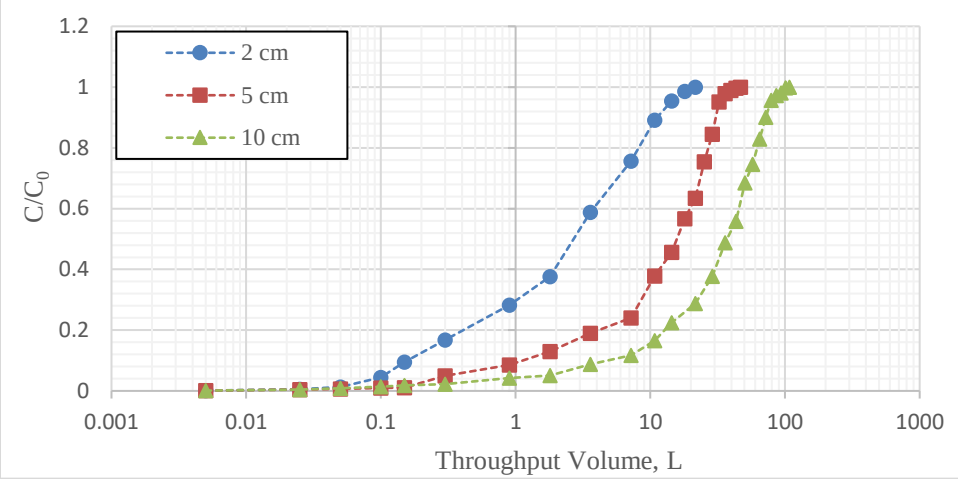

Figure 5-3. Effect of bed depth on uptake of Cu^{2+} onto geopolymer (G60) (influent concentration 10 mg/L, flow rate 5 mL/min, pH 4.0).

5.4.3. Comparison of heavy metals uptake in single-metal solution

The breakthrough curves for Cu^{2+}, Cd^{2+} and Pb^{2+} ions for single-metal solutions at a flow rate of 5 mL/min through a 5 cm bed depth column and an influent concentration of 10 mg/L for each metal are shown in Figure 5-4. The breakthrough curve for Cu^{2+} was the earliest of the three metals followed by Cd^{2+} and Pb^{2+}. The uptake capacities (total mass removed per gram of sample) were in the following order: Pb^{2+} (59.41 mg/g) > Cd^{2+} (28.74 mg/g) > Cu^{2+} (19.26 mg/g), which suggests that Pb^{2+} was removed more than Cu^{2+} and Cd^{2+}. The higher uptake of Pb^{2+} may be due to the physico-chemical properties of Pb^{2+} with a higher atomic weight, ionic radius of Pb^{2+} and

smaller *Z/R* (charge/radius) ratio than those of Cu^{2+} and Cd^{2+} (Jing et al., 2009) and the low solubility of Pb^{2+} as compared to the other metals based on lead solubility products. The column results are in the agreement with the findings of the batch experiments in Chapter 4.

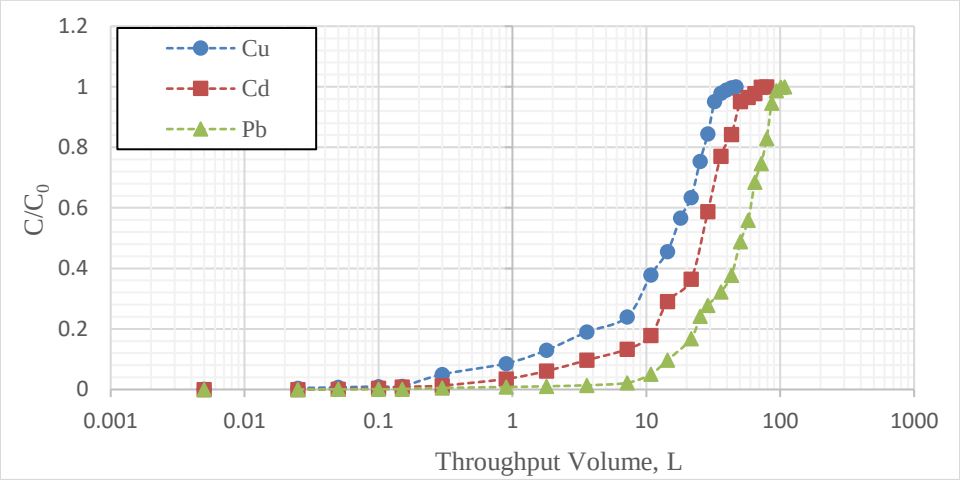

Figure 5-4. Breakthrough curves of geopolymer (G60) in fixed-bed column (5 cm height) for single metal (Cu^{2+}, Cd^{2+} and Pb^{2+}) solution with influent concentration 10 mg/L at flow rate 5 mL/min and pH 4.0.

5.4.4. Comparison of heavy metal uptake in multi-metal solution

Breakthrough curves for Cu^{2+}, Cd^{2+} and Pb^{2+} for a multi-metal solution are presented in Figure 5-5. The influent concentration was 10 mg/L for each metal ion, the influent pH was 4.0 with a flow rate of 5 mL/min and a bed depth of 5 cm. In comparison to the single metal results, the breakthrough curves showed that there were competition for metal uptake sites on the geopolymer. Unlike the single metal results, Cd^{2+} was found to breakthrough first instead of Cu^{2+}. Pb^{2+} was shown to breakthrough last which indicates that the geopolymer has a stronger metal uptake affinity for Pb^{2+} than the other two metals, Cu^{2+} and Cd^{2+}. The breakthrough curves for all three metals showed a gradual increase instead of a steep increase as for a single metal solution. This shows that there were competition among the three metals for uptake sites.

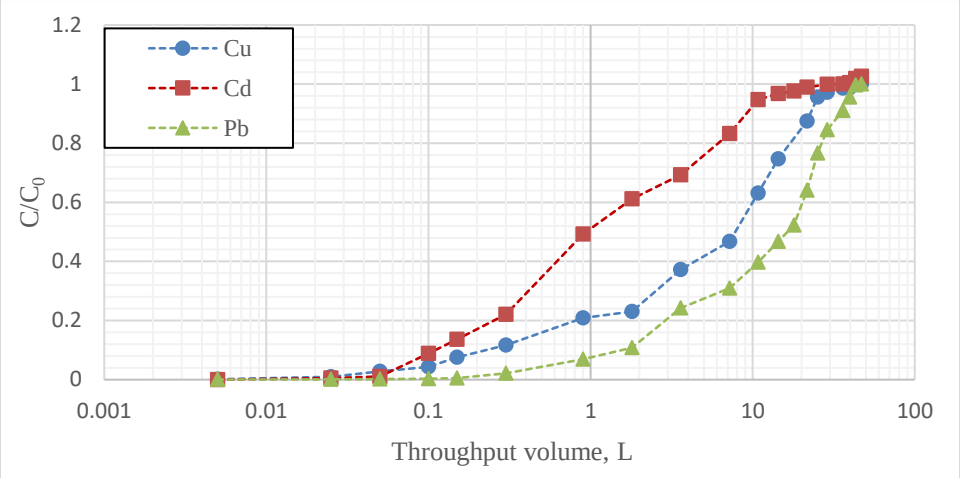

Figure 5-5. Breakthrough curves of geopolymer (G60) fixed-bed column (5 cm height) for multi-metal (Cu^{2+}, Cd^{2+} and Pb^{2+}) solution with influent concentration 10 mg/L at flow rate 5 mL/min and pH 4.0.

The uptake capacity (mass removed per gram of sample) were 10.85, 3.39 and 19.99 mg/g for Cu^{2+}, Cd^{2+}, and Pb^{2+}, respectively, which were less than those for the single metal solutions. In a competitive condition, the metal uptake affinity for the metals was in the order of $Pb^{2+} > Cu^{2+} > Cd^{2+}$, which was different for non-competitive condition, which was in the order of $Pb^{2+} > Cd^{2+} > Cu^{2+}$.

5.4.5. Application of models

Modeling results of the three models for all the column studies are presented in Table 5-2. Included in Table 5-2 are the observed breakthrough times, exhaustion times, and the uptake capacities from the experimental breakthrough curve data. For the single metal experiments, the masses removed per gram of sample estimated by Thomas model were the closest to uptake capacities estimated from the breakthrough curves. Estimated values by the Bohart-Adams model were at least 2 times higher than the estimated uptake capacity. On the other hand, Yan model reported masses removed per gram of sample that were 2 or 3 times lower than the uptake capacities. The R^2 values for Bohart-Adams model ranged from 0.35 to 0.68. Both Thomas and

Yan models had R^2 values which were greater than 0.8. The k_{BA} values for the Bohart-Adams model and the k_{Th} values for the Thomas model for experiments column C_2, C_3 and C_4 were very different even though the flow rates were similar at 5 mL/min. Since k_{Th} and k_{Th} are rate constants, these values for experiments C_2, C_3 and C_4 should be similar as the flow rate was the same.

For the multi-metal experiments, the mass removed per gram of sample (q_{Th}) for the Thomas model was similar to that of the uptake capacity estimated from the area of the breakthrough curve data. As in the single metal experiment, Bohart-Adams model overestimated while Yan model underestimated the mass removed per gram of sample. Of the three models considered, the Thomas model appeared to be a more suitable and appropriate model to describe metal uptake in the fixed-bed column with geopolymer as the media. As an example, the three models were plotted against the experimental results for column C_3 (Figure 5-6). It can be seen that Thomas model gave a better fit to the experimental data than Bohart-Adams and Yan models.

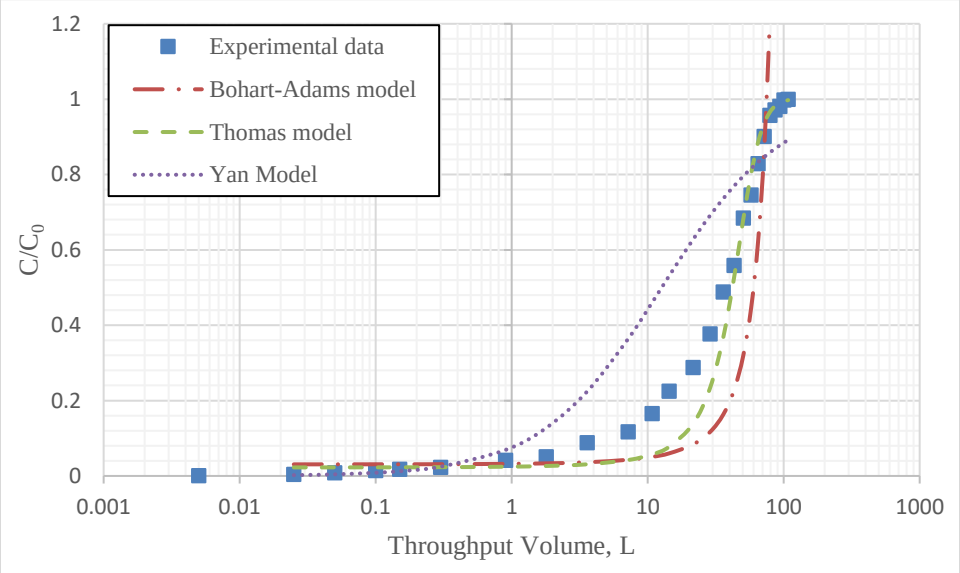

Figure 5-6. Breakthrough curve data and fit of three models (Bohart-Adams, Thomas, and Yan model) for a single metal (Cu^{2+}) solutions. (Influent concentration of 10 mg/L, initial pH of 4.0, flow rate of 5 mL/min, and of 10 cm bed depth)

Table 5-2. Column data and parameters obtained from breakthrough analysis, Bohart-Admas, Thomas, and Yan models for different column

Column No.	Metal ions	Final pH	Breakthrough analysis			Bohart-Admas model			Thomas model			Yan model		
			T_b, min	T_e, min	Uptake capacity (q_0), mg/g	k_{BA}, mL/min-mg	q_{BA}, mg/g	R^2	k_{Th}, mL/min-mg	q_{Th}, mg/g	R^2	*a*	q_Y, mg/g	R^2
C_1	Cu^{2+}	4.62	5	360	2.15	0.29	16.10	0.36	1.20	3.27	0.87	4.28	0.72	0.90
C_2	Cu^{2+}	5.81	30	2880	17.20	0.12	40.55	0.43	0.23	20.60	0.74	1.85	4.73	0.97
C_3	Cu^{2+}	7.44	1080	15840	24.04	0.02	45.82	0.66	0.04	25.64	0.91	0.30	7.74	0.83
C_4	Cu^{2+}	6.69	270	6480	19.26	0.06	39.36	0.62	0.11	21.86	0.89	0.70	6.22	0.86
C_5	Cd^{2+}	6.92	720	10080	28.74	0.03	65.89	0.64	0.07	36.08	0.90	0.81	13.06	0.83
C_6	Pb^{2+}	6.77	2880	17280	59.41	0.03	91.99	0.68	0.05	62.31	0.87	0.83	35.58	0.84
C_7	Cu^{2+}	6.28	60	5040	11.58	0.05	35.22	0.47	0.12	15.03	0.86	0.64	3.00	0.84
	Cd^{2+}	6.28	10	2160	1.98	0.05	23.57	0.35	0.16	7.00	0.80	0.84	1.26	0.94
	Pb^{2+}	6.28	360	7920	19.98	0.06	41.90	0.56	0.11	24.65	0.83	0.80	7.60	0.89

5.5. Conclusion

For single metal experiments with the same flow rate and bed depth condition, Cu^{2+} was found to be the least removed as compared to Cd^{2+} and Pb^{2+} and had the earliest breakthrough time. The geopolymer had a stronger affinity for Pb^{2+} which resulted in a longer breakthrough time and a higher uptake capacity than Cd^{2+} and Cu^{2+}. In a multi-metal solution, competition for metals uptake was observed whereby Cd^{2+} was the least removed instead of Cu^{2+}. Pb^{2+} continued to be strongly removed in the multi-metal solution experiment. The metal uptake affinity in a single metal solution was in the order of $Pb^{2+} > Cd^{2+} > Cu^{2+}$, but the metal uptake affinity was in the order of $Pb^{2+} > Cu^{2+} > Cd^{2+}$ for a multi-metal solution. Of the three metals tested, Bohart–Adams, Thomas, and Yan models, Thomas model fitted the experimental data better and gave values of mass uptake per gram of sample that was similar to the uptake capacity estimated using the experimental results. The results of the column experiments showed that fixed-bed column with geopolymer as the filtration media can be used for the treatment of acidic waste streams such as acid mine drainage, industrial wastewaters and landfill leachates.

5.6. References

Archer, M. J. G., & Caldwell, R. A. (2004). Response of six Australian plant species to heavy metal contamination at an abandoned mine site. *Water, Air, and Soil Pollution*, *157*(1-4), 257-267.

Barbosa, T. R., Foletto, E. L., Dotto, G. L., & Jahn, S. L. (2018). Preparation of mesoporous geopolymer using metakaolin and rice husk ash as synthesis precursors and its use as potential adsorbent to remove organic dye from aqueous solutions. *Ceramics International*, *44*(1), 416-423.

Bhatnagar, A., & Sillanpää, M. (2010). Utilization of agro-industrial and municipal waste materials as potential adsorbents for water treatment-A Review. *Chemical Engineering Journal*, *157*(2-3), 277-296.

Bohart, G. S., & Adams, E. Q. (1920). Some aspects of the behavior of charcoal with respect to chlorine. *Journal of the American Chemical Society*, *42*(3), 523-544.

El Alouani, M., Alehyen, S., El Achouri, M., & Taibi, M. H. (2018). Adsorption of cationic dye onto fly ash-based geopolymer: Batch and fixed bed column studies. In *MATEC Web of Conferences* (Vol. 149, p. 02088). EDP Sciences.

Feng, D., Aldrich, C., & Tan, H. (2000). Treatment of acid mine water by use of heavy metal precipitation and ion exchange. *Minerals Engineering*, *13*(6), 623-642.

Gaikwad, R. W., Sapkal, R. S., & Sapkal, V. S. (2010). Removal of copper ions from acid mine drainage wastewater using ion exchange technique: factorial design analysis. *Journal of Water Resource and Protection*, *2*(11), 984.

Ge, Y., Cui, X., Kong, Y., Li, Z., He, Y., & Zhou, Q. (2015). Porous geopolymeric spheres for removal of Cu (II) from aqueous solution: Synthesis and evaluation. *Journal of Hazardous Materials*, *283*, 244-251.

Ge, Y., Cui, X., Liao, C., & Li, Z. (2017). Facile fabrication of green geopolymer/alginate hybrid spheres for efficient removal of Cu (II) in water: batch and column studies. *Chemical Engineering Journal*, *311*, 126-134.

Ghasemi, M., Keshtkar, A. R., Dabbagh, R., & Safdari, S. J. (2011). Biosorption of uranium (VI) from aqueous solutions by Ca-pretreated Cystoseira indica alga: breakthrough curves studies and modeling. *Journal of Hazardous Materials*, *189*(1-2), 141-149.

Hasan, S. H., & Srivastava, P. (2009). Batch and continuous biosorption of Cu^{2+} by immobilized biomass of Arthrobacter sp. *Journal of Environmental Management*, *11*(90), 3313-3321.

Jing, X., Liu, F., Yang, X., Ling, P., Li, L., Long, C., & Li, A. (2009). Adsorption performances and mechanisms of the newly synthesized N, N′-di (carboxymethyl) dithiocarbamate chelating resin toward divalent heavy metal ions from aqueous media. *Journal of Hazardous Materials*, *167*(1-3), 589-596.

Kara, I., Tunc, D., Sayin, F., & Akar, S. T. (2018). Study on the performance of metakaolin based geopolymer for Mn (II) and Co (II) removal. *Applied Clay Science*, *161*, 184-193.

Kara, İ., Yilmazer, D., & Akar, S. T. (2017). Metakaolin based geopolymer as an effective adsorbent for adsorption of zinc (II) and nickel (II) ions from aqueous solutions. *Applied Clay Science*, *139*, 54-63.

Kleinmann, R. L. (1990). Acid mine drainage: an overview. In *Energy in the 90's* (pp. 281-286). ASCE.

Lodeiro, P., Herrero, R., & de Vicente, M. E. (2006). The use of protonated Sargassum muticum as biosorbent for cadmium removal in a fixed-bed column. *Journal of Hazardous Materials*, *137*(1), 244.

López, D. L., Gierlowski-Kordesch, E., & Hollenkamp, C. (2010). Geochemical mobility and bioavailability of heavy metals in a lake affected by acid mine drainage: Lake Hope, Vinton County, Ohio. *Water, Air, & Soil Pollution*, *213*(1-4), 27-45.

Motsi, T., Rowson, N. A., & Simmons, M. J. H. (2009). Adsorption of heavy metals from acid mine drainage by natural zeolite. *International Journal of Mineral Processing*, *92*(1-2), 42-48.

Nieto, J. M., Sarmiento, A. M., Olías, M., Canovas, C. R., Riba, I., Kalman, J., & Delvalls, T. A. (2007). Acid mine drainage pollution in the Tinto and Odiel rivers (Iberian Pyrite Belt, SW Spain) and bioavailability of the transported metals to the Huelva Estuary. *Environment International*, *33*(4), 445-455.

Olds, W. E., Tsang, D. C., Weber, P. A., & Weisener, C. G. (2013). Nickel and zinc removal from acid mine drainage: roles of sludge surface area and neutralising agents. *Journal of Mining*, *2013*.

Patel, H. (2019). Fixed-bed column adsorption study: a comprehensive review. *Applied Water Science*, *9*(3), 45.

Ricci, B. C., Ferreira, C. D., Aguiar, A. O., & Amaral, M. C. S. (2015). Integration of nanofiltration and reverse osmosis for metal separation and sulfuric acid recovery from gold mining effluent. *Separation and Purification Technology*, *154*, 11-21.

Thomas, H. C. (1944). Heterogeneous ion exchange in a flowing system. *Journal of the American Chemical Society*, *66*(10), 1664-1666.

Tolonen, E. T., Sarpola, A., Hu, T., Rämö, J., & Lassi, U. (2014). Acid mine drainage treatment using by-products from quicklime manufacturing as neutralization chemicals. *Chemosphere*, *117*, 419-424.

Vijayaraghavan, K., Jegan, J., Palanivelu, K., & Velan, M. (2005). Biosorption of copper, cobalt and nickel by marine green alga Ulva reticulata in a packed column. *Chemosphere*, *60*(3), 419-426.

Yan, G., Viraraghavan, T., & Chen, M. (2001). A new model for heavy metal removal in a biosorption column. *Adsorption Science & Technology*, *19*(1), 25-43.

CHAPTER 6. MAGNETIC FLY ASH-BASED GEOPOLYMER AND ITS ENVIRONMENTAL APPLICATION

6.1. Abstract

Magnetic geopolymers were synthesized by incorporating magnetic Fe_3O_4 particles to modify fly ash-based geopolymer. Two different synthesis methods were investigated. For the method where prepared magnetic Fe_3O_4 was incorporated into the geopolymer, the magnetic properties of the final material was only slightly reduced in the synthesis process as compared to the added magnetic Fe_3O_4. Magnetic fly ash geopolymer of less than 0.177 mm was made and characterized for its physical properties and environmental applications. Magnetic fly ash geopolymer showed similar metal removal properties as fly ash geopolymer with a maximum uptake capacity of 111.1 mg/g. The magnetic fly ash geopolymer has a saturation magnetization of 18 emu/g and was found to separate out from an aqueous solution within 2 minutes by using a magnetic field of 0.48 Tesla. Applications of the magnetic fly ash geopolymer include using it as a fine powder material to maximize heavy metals removal and recovery in wastewater treatment.

6.2. Introduction

Heavy metals in industrial waste waters are of special concern, since they can accumulate in different components of environment (Nordberg et al., 2014). Removal of heavy metals from wastewaters before they are discharged are desired for both human health and aquatic ecosystems. Conventional technologies for heavy metals removal from aqueous solutions involve physical-chemical treatments such as precipitation, adsorption, membrane filtration and ion exchange (Aziz et al., 2008; Shipley et al., 2013). Some challenges with these technologies include, for instance, generating of a large amount of sludge from precipitation which may increase treatment cost. Membrane system has high treatment cost owing to the high energy cost and frequent change of

membranes. Adsorption is the most popular method among the above-mentioned technologies (Bereket et al., 1997). Depending on the type of waste waters, it may be an economic and effective treatment technology for industrial wastewaters. Suitable selection of the adsorbent is one of the key points in developing a proper adsorption system as specific type of adsorbent may play a dominant role in the adsorption process.

Geopolymer has been categorized as an environmentally friendly material due to its low temperature manufacturing process and low CO_2 emission as compared to producing standard cementitious materials (Duxson et al., 2007). Most studies related to geopolymer are focused on the field of concrete building materials applications. However, recently it was reported as an effective material for removal of pollutants in water/wastewater treatment. Geopolymer can be used to remove heavy metals from aqueous solutions with some advantages such as low cost, high efficiency, and simple production (Wang et al., 2007; Mužek et al., 2014; and Al-Harahsheh et al., 2015).

Researchers have studied the use of the granular geopolymer particles (size: 0.6 – 2 mm) for environmental applications such as adsorption or precipitation. The granular particles can be used in a column treatment system or as a media placed in the path of the waste streams. Use of fine geopolymer particles have some advantages in that they have large surface areas and can be easily dispersed to maximize contact with the pollutants in an aqueous solution, such as in a slurry form. However, this treatment suffers from some drawbacks such as the need to separate out the geopolymer, if it needs to be regenerated and, as in precipitation, can produce large quantities of residual sludge (Peng et al., 2010). To overcome these drawbacks, a magnetic signature can be applied to the geopolymer to generate a novel magnetic reactive/adsorbent material which can be separated from the aqueous phase. Rapid separation of the materials from solution by using an

external magnetic field without filtration or centrifugation, allows the magnetic materials to be recovered and reused (Foroughi et al., 2015) or for the metals removed to be recovered.

The objective of this study is to synthesize magnetic geopolymer by using two methods to incorporate different amounts of magnetic Fe_3O_4 in fly ash-based geopolymer. The synthesized materials were characterized for its magnetization properties and other physical-chemical and environmental properties. Based on the initial characterization, a magnetic geopolymer was selected and investigated further for its environmental impact and uptake capacity for a heavy metal in contaminated wastewater. This investigation is expected to shed light on the mix of magnetic Fe_3O_4 as a magnetic material to create magnetic composite materials for various application including environmental application.

6.3. Materials and Methods

6.3.1. Magnetic iron oxide synthesis

Magnetic iron oxide particles (Fe_3O_4) were synthesized by using iron (III) nitrate non-ahydrate ($Fe(NO_3)_3 \cdot 9H_2O$) as the starting material. A solution of 1 g/mL of iron nitrate was prepared by dissolving iron nitrate. Batches of magnetic iron oxide were prepared by placing 4 mL of iron nitrate solution in quartz crucibles and the solution calcined at a temperature of 500 °C for 20 min in a gas stream with Argon and 5% H_2 gas. The samples were then cooled in the same gas stream inside the furnace to room temperature. About 0.6 g of pure magnetic Fe_3O_4 particles (size of 10 – 100 nm) were collected from each crucible. Preliminary calcining temperature at 450 °C, 500 °C and 550 °C were tested and 500 °C was found to be the preferred calcine temperature.

6.3.2. Geopolymer preparation

The geopolymer was made of Class F (as defined in ASTM C618) fly ash and an alkaline activator solution. The alkaline activator consisted of sodium silicate solution (water glass,

$3Na_2O{\cdot}3SiO_2$), solid NaOH, and water in a mass ratio of 0.49:0.11:0.40. The mass ratio of the alkaline activator to the fly ash and the activator was 0.33:1. The geopolymer was prepared by mixing the fly ash and the activator for 5 – 10 mins and placing the paste in a mold to cure for 24 hours at room temperature. It was then demold and cured for 7 days at 50^{o}C. The geopolymer was then washed 3 times with water and crushed to the appropriate particles size. Particles sizes used for preparation of magnetic fly ash-based geopolymer ranged from 0.6 – 2 mm.

6.3.3. Preparation of magnetic fly ash-based geopolymer

To prepare a geopolymer with magnetic properties, two methods were used in this study. The purpose is to add magnetic properties to the geopolymer which can allow the geopolymer to be separated easily in an aqueous environment.

- Method 1

In the first method, about 3, 6 and 9 gram of fly ash-based geopolymer (FAG) particles (0.6 – 2 mm) were added to 4 mL of ferric nitrate solution (1 g/L) for 24 hours to ensure optimal coating of the geopolymer with iron nitrate. The saturated solid materials were loaded in quartz crucibles and calcined at 500 °C for 20 min in Argon with 5% H_2 gas. The solids were then cooled in the same gas inside the furnace to room temperature. The fly ash-based geopolymer coated with iron oxide (MC-FAG) were collected and sieved through a 30 mesh (0.6 mm) sieve 3 times to remove extra and weakly-bonded Fe_3O_4 particles on the surface of the geopolymer. The MC-FAG granular particles retained in the sieve were grounded to fine particles to a size of less than 0.177 mm by passing through an 80 mesh sieve. The synthesis of MC-FAG is illustrated in Figure 6-1. The particles were identified as MC-FAG1, MC-FAG2, and MC-FAG3. In addition to the above, MC-FAG were prepared using 0.25 g/mL and 0.5 g/mL of iron nitrate and 3 gram of geopolymer. These samples were identified as MC-FAG1-1 and MC-FAG1-2. For comparison purpose, zeolite

coated with magnetic Fe_3O_4 was also prepared. These samples were identified as MC-Z1 and MC-Z2. Table 6-1 presents the conditions for the prepared MC-FAG and MC-Z.

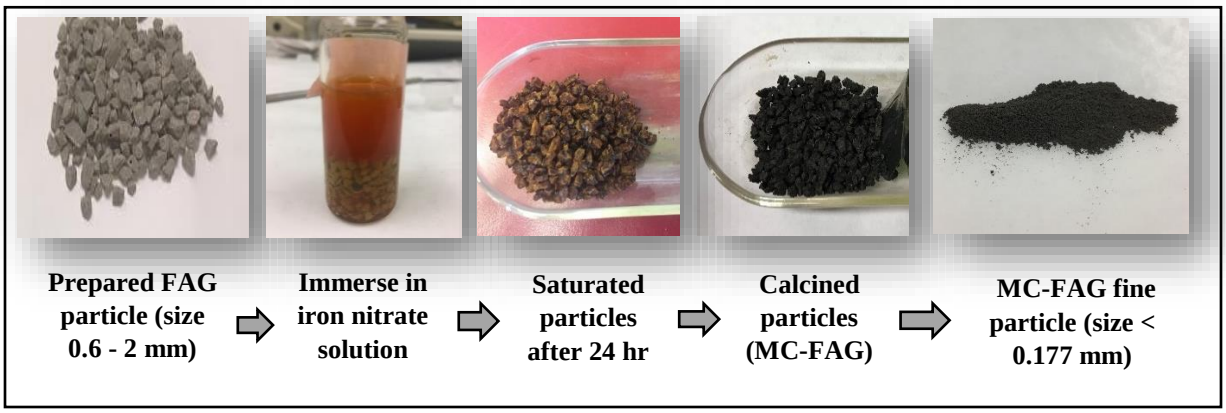

Figure 6-1. Synthesis process (Method 1) for magnetic coated fly ash-based geopolymer (MC-FAG).

Table 6-1. Mixture proportions to synthesize magnetic coated fly ash-based geopolymer and zeolite (MC-FAG and MC-Z).

Sample No.	Calcine temperature, °C	Conc. of $Fe(NO_3)_3$ solution, g/mL	Volume of $Fe(NO_3)_3$ solution, mL	Mass of FAG or zeolite, g	Mass ratio of FAG or zeolite to $Fe(NO_3)_3$ solution	Fe_3O_4 wt%
Magnetic Fe_3O_4	450	1	4	0	--	100
	500	1	4	0	--	100
	550	1	4	0	--	100
MC-FAG1	500	1	4	3	0.75	16.67
MC-FAG2	500	1	4	6	1.5	9.09
MC-FAG3	500	1	4	9	2.25	6.25
MC-Z1	500	1	4	3	0.75	16.67
MC-Z2	500	1	4	6	1.5	9.09
MC-FAG1-1	500	0.25	4	3	3	9.09
MC-FAG1-2	500	0.5	4	3	1.5	4.76

- Method 2

The second method of synthesizing magnetic fly ash geopolymer (MFAG) is shown in Figure 6-2. In this method, various amounts (3, 6 and 10 g) of prepared magnetic Fe_3O_4 were evenly mixed with the fly ash (30 g). The mixed materials were then reacted with 12 mL of alkaline

solution (6 mL of sodium silicate solution + 6 mL of 6.68 M of NaOH solution). The ratio of liquid to solid was fixed at about 0.4. The obtained paste was mixed for 5 min and was subjected to ultrasound for 5 min to enhance dispersion. The obtained paste mixture was poured into a 1"×1"×1" cubic mold and pre-cured for 24 h at room temperature (21 – 23 ^{o}C). The samples were then demolded, placed in a cylindrical glass container which was closed, and cured at a temperature of 50 ^{o}C in an oven for 7 days. The MFAG cubes were crushed and grounded to obtain a MFAG sample with particle size of less than 0.177 mm. The MFAG sample were washed several times with distilled water to remove surface alkalinity, and oven dried overnight. A magnet was used to separate the MFAG and any nonmagnetic fines. Table 6-2 presents the different samples prepared and the mix proportions of the raw material.

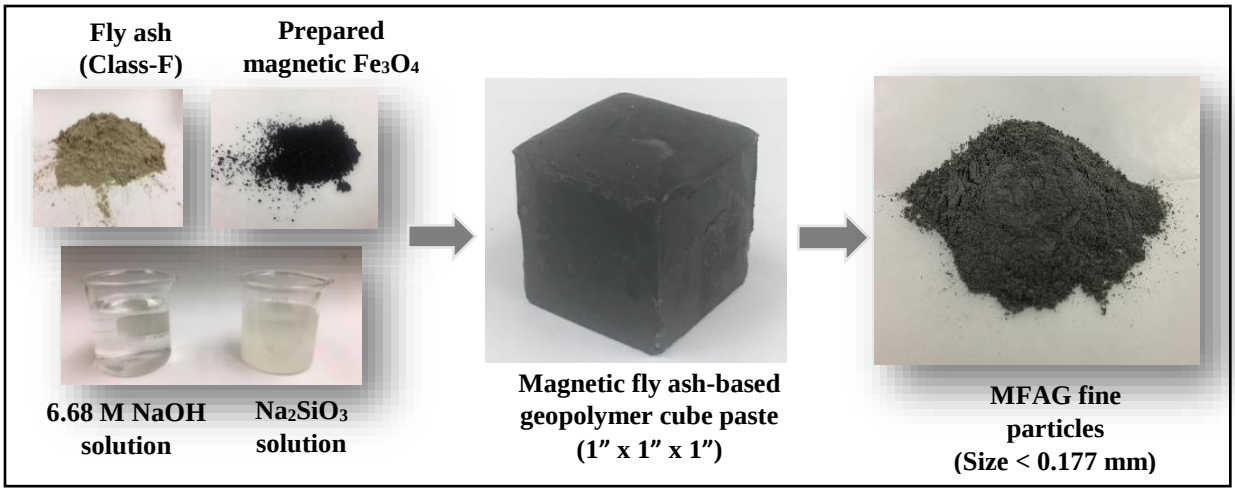

Figure 6-2. Synthesis process (Method 2) for magnetic fly ash-based geopolymer (MFAG).

Table 6-2. Mixture proportion of magnetic fly ash-based geopolymer (MFAG).

Sample No.	Mass of FA, g	Volume of alkaline solution, mL	Mass of Fe_3O_4, g	Mass ratio of FA to Fe_3O_4 solids	Fe_3O_4 wt%
FAG	30	12	0	--	0
MFAG1	30	12	10	3	18.40
MFAG2	30	12	6	5	11.92
MFAG3	30	12	3	10	6.34

6.3.4. Characterization

Initial screening of all the samples were conducted by measuring the magnetic properties, the pH change in aqueous solution and the single point batch experiments of the samples for metal removal.

The magnetic behavior of the samples was measured at 298 ± 1K by a Superconducting Quantum Interference Device (SQUID, MPMS-XL7, Quantum Design, USA). The results were reported in terms of 8.06 emu/g.

Solution pH changes and single point batch experiments were conducted using 50 mL of metal (Cu^{2+}) solution and a fixed amount of powder (0.1 g) in 50 mL centrifuge tubes and capped. The tubes were then agitated on a rotary shaker for 24 hours, a speed of 30 rpm. The initial Cu^{2+} concentration was 100 mg/L. The final pH of the solution was measured and the metal uptake q_t (mg/g) was determined by the following equation:

$$q_t = \frac{C_0 - C_t}{m} V$$

where C_0 and C_t (mg/L) are the metal concentration in liquid phase at the initial and at time t, respectively; m is the sample mass (g); V is volume of the metal solution (L).

The initial pH of the solution was adjusted 3.0 ± 0.1 by adding 1M H_2SO_4 solutions. The solid and liquid phases were magnetically separated using a magnet with a magnetic field strength of 0.48 Tesla. The metal concentrations in the filtrate were determined by ICP atomic emission spectrometry (ICPE-9800 Series, Shimadzu Corporation, Kyoto, Japan).

Based on the initial screening, a magnetic fly ash-based geopolymer was selected for further testing. This geopolymer was characterized for its physical-chemical properties. The specific surface area of the magnetic fly ash-based geopolymer was determined using nitrogen

BET method. Compressive strength was determined by using the method from ASTM C 109 (2013). SEM images were taken using a scanning electron microscopes (Quanta FEG 250, Hillsboro, Oregon, USA).

6.3.5. Batch experiments

Batch experiments were conducted using 50 mL of metal (Cu^{2+}) solution and various masses of magnetic geopolymer powder in 60 mL centrifuge tubes and capped. The initial pHs of the solutions for all the tests were adjusted to 3.0 ± 0.1 by adding 1M H_2SO_4 solutions. The tubes were agitated on a rotary shaker at a speed of 30 rpm at room temperature (21 – 23 ^oC). The solution was then filtered and the final pH of filtrate measured by a pH meter and the final equilibrium concentration of the metal analyzed using an inductively coupled plasma (ICP) atomic emission spectrometer (ICPE-9800 Series, Shimadzu Corporation, Kyoto, Japan). All experiments were carried out in duplicate and the average concentration reported.

The first set of experiments were conducted to assess the effect of MFAG dosage and initial Cu^{2+} concentration on the pH of the solution by using masses of MFAG ranging from 0.01 to 0.1 g and initial Cu^{2+} concentrations ranging from 0 to 200 mg/L. The second set of experiments were conducted to assess the kinetics of removal by MFAG using contact time ranging from 0 – 2 hours and a MFAG mass of 0.1 g and Cu^{2+} concentration of 100 mg/L. Two kinetic models, pseudo-first-order and pseudo-second-order, were used for the analysis. In addition, the experimental data were fitted using two isotherm models, Langmuir and Freundlich models, to obtain the maximum uptake capacity.

6.3.6. Magnetic separation and settling tests

Preliminary magnetic separation tests were conducted using 0.1 g of fine sample mixed with 50 mL copper solution for 5 min. The turbidity (NTU) and suspended solids of the mixture were measured with and without a magnetic field of 0.48 Tesla.

Further tests were conducted using a standard settling test (White, 1975). A 1 liter measuring cylinder was used with different concentrations of the magnetic particles (100, 500, and 1000 mg/L) uniformly distributed. Figure 6-3 shows that a magnetic field of 0.11 Tesla was fixed at the bottom of cylinder, and another magnetic field of 0.48 Tesla was placed on side of cylinder for 10 seconds at each descending position. The turbidity and the suspended solids of the suspensions were measured with and without a magnetic field.

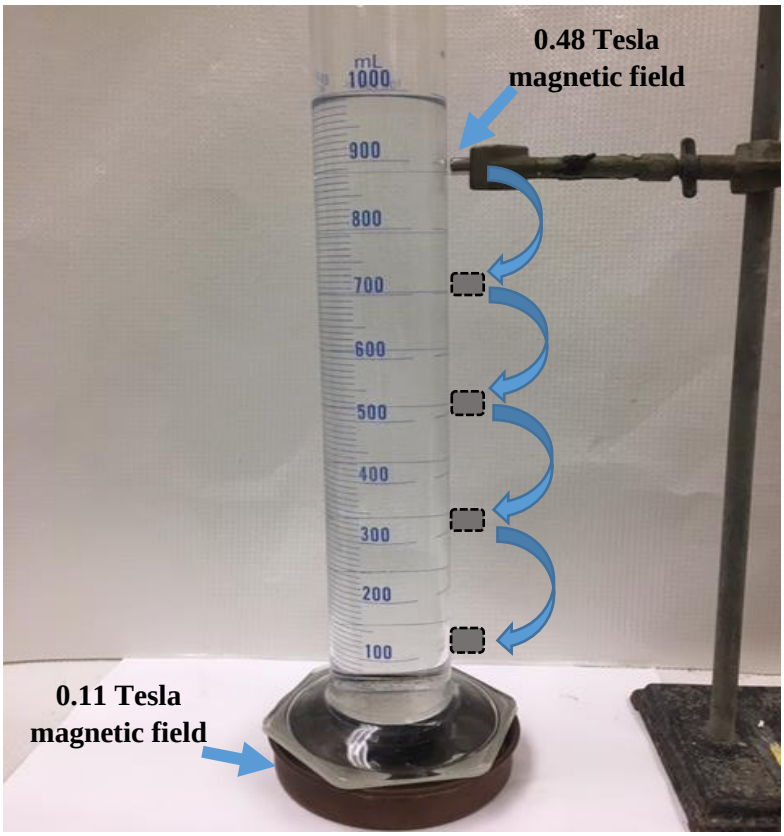

Figure 6-3. Settling test with magnetic field placement.

6.4. Results and Discussions

6.4.1. Initial characterization and screening

- Magnetization of samples

The saturation magnetization of all prepared samples are presented in Table 6-3. The saturation magnetization of Fe_3O_4 at high field yield (90 kOe) was found to be between 89 and 92 emu/g for the three different calcine temperatures. The calcine temperature of 500 ^oC seemed to give a slightly better saturated magnetization.

For the coated samples from Method 1, the saturation magnetization was found to be between 0.93 and 1.52 emu/g at a high field yield of 30 kOe. The relative level of magnetization for samples prepared using Method 1 (geopolymer coated with Fe_3O_4 were in the range of 1 – 2%). As a comparison, the zeolite materials were found to have a relative level of magnetization of (4 – 6 %). Although the amount of Fe_3O_4 were not measured, it can be assumed that the relative level of magnetization reflects the level of Fe_3O_4 coating on the surface of the geopolymer assuming that the Fe_3O_4 did not lose its magnetization during the preparation process.

For Method 2, the magnetic fly ash-based geopolymer showed high saturation magnetizations ranging from 6.8 to 15.81 emu/g (Table 6-3). Assuming no reduction in the magnetization of the Fe_3O_4 (92.47 emu/g), the estimated masses of Fe_3O_4 based on magnetization fraction was 7 – 17% (Table 6-3). These were close to the 6.34 to 18.4% by weight of Fe_3O_4 added to prepare the MFAG samples.

The fly ash-based geopolymer itself had a saturation magnetization of 0.94 emu/g while raw material Class-F fly ash had a saturation magnetization of 1.07 emu/g. This indicates that the fly ash contained small amounts of magnetic iron oxide which may come from the 5.43% by

weight of Fe as per the chemical composition provided by the manufacturer (Ash Grove Technical Center, 2016).

Table 6-3. Saturation magnetization with magnetic field.

Method type	Sample	H, kOe	M, emu/g	Level of Magnetization
Prepared Fe_3O_4	450°C Fe_3O_4	90.01	89.42	97%
	500°C Fe_3O_4	90.01	92.47	100%
	550°C Fe_3O_4	90.00	92.12	100%
Method 1	MCFAG1	30.00	1.52	2%
	MCFAG2	30.00	1.10	1%
	MCFAG3	30.00	0.85	1%
	MCZ1	30.00	5.31	6%
	MCZ2	29.99	4.14	4%
	MCFAG1-1	30.00	0.93	1%
	MCFAG1-2	30.00	1.13	1%
Method 2	MFAG1	30.00	15.81	17%
	MFAG2	30.00	8.06	9%
	MFAG3	30.00	6.80	7%
Fly ash-based geopolymer	FAG	29.97	0.94	1%
Class-F fly ash	Fly ash	30.00	1.07	1%

- Single point removal of Cu^{2+} by different samples

All the prepared particles, magnetic samples and non-magnetic samples, were used for copper removal. The results of the single point test are shown in Figure 6-4(a).

The results indicated that the synthesized MFAG2 from Method 2 had the highest uptake of Cu^{2+} (49.81 mg/g) which was slightly higher than that of non-magnetic geopolymer (49.79 mg/g). From Method 2, MFAG1 had the uptake of Cu^{2+} (45.08 mg/g) which was less than that of MFAG2 and non-magnetic geopolymer. A possible reason is that addition (18.4% *wt*) of Fe_3O_4 into the geopolymer can impact the removal of the metal. The uptake of Cu^{2+} (49.68 mg/g) for sample MFAG3 was close to that of MFAG2 and non-magnetic geopolymer.

The raw fly ash removed about 21.40 mg/g of Cu^{2+}. Thus, the results indicated that the metal removal properties by the geopolymer were not affected by the presence of the magnetic Fe_3O_4 ($\leq$ 11.9% *wt*).

Except for MC-FAG3, the magnetic-coated geopolymer particles from Method 1 gave a lower uptake of Cu^{2+} than that of Method 2. The Cu^{2+} removed by the MCFAG-3 was 48 mg/g, which was comparable to MFAG2. A possible reason is that reactive sites were reduced by the high concentration of iron during the synthesis process, or iron precipitation may have occurred and accumulated on the surface reducing the surface area.

All the synthesized magnetic geopolymer showed improved metal uptake behavior compared to the magnetic Fe_3O_4 which had limited uptake of Cu^{2+} ion (1.40 mg/g). As a comparison, zeolite showed a Cu^{2+} uptake of 2.55 mg/g which was higher than the magnetic-coated zeolite (MCZ-1: 0.85 mg/g and MCZ-2: 1.35 mg/g). The decreased metal uptake was due to the low metal uptake affinity of the magnetic iron oxide which reduced the metal uptake affinity of the zeolite.

Figure 6-4(b) shows the pH change when the samples were added to acidic solution. The magnetic fly ash-based geopolymer all gave pH changes that were less than the fly ash-based geopolymer.

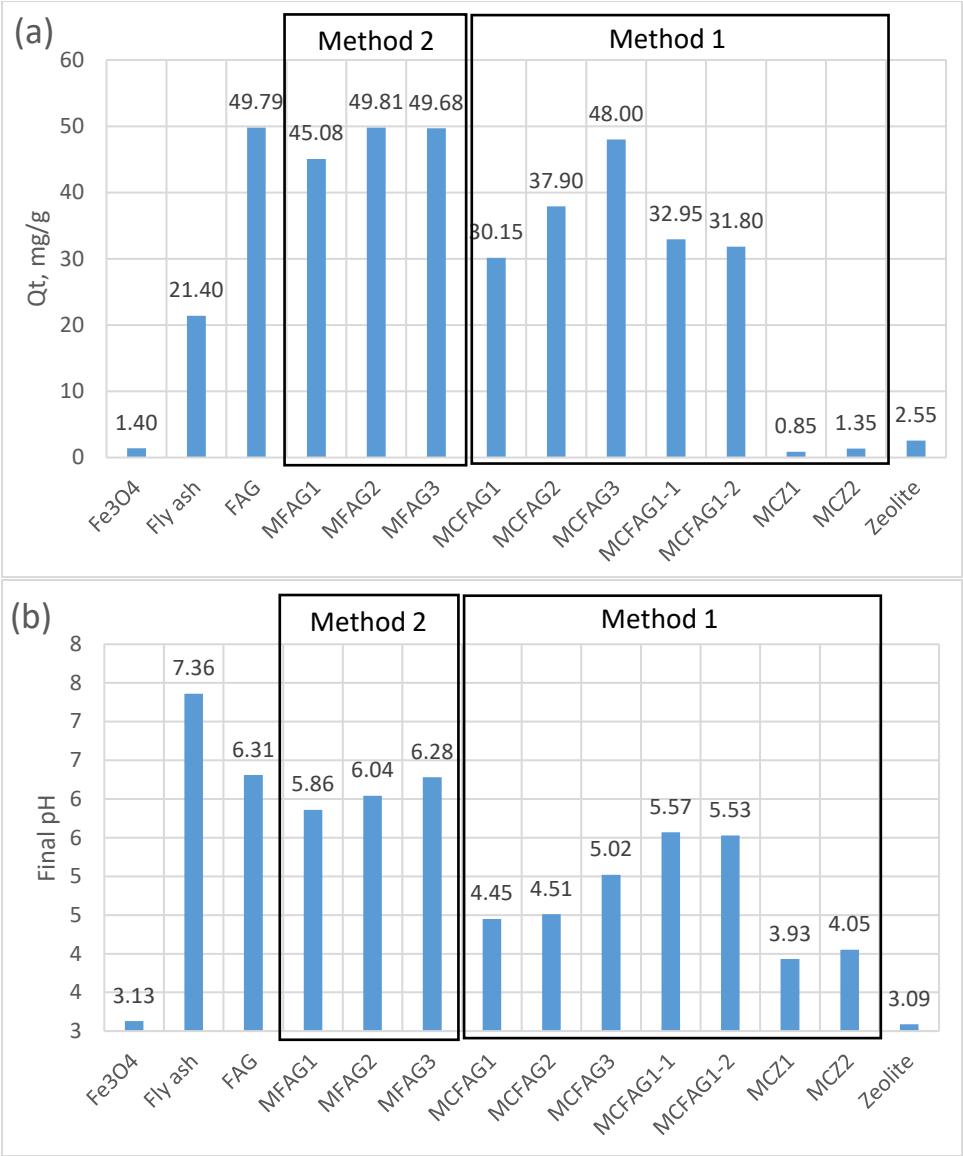

Figure 6-4. Comparison of different magnetic geopolymer and zeolite on single point of copper removal (a) and pH of solution (b). Condition: 100 mg/L of initial concentration, initial pH 3.0, and 24 hour of contact time.

6.4.2. Magnetization of MFAG2 samples

Magnetization curves of Fe_3O_4 and MFAG2 sample are shown in Figure 6-5.

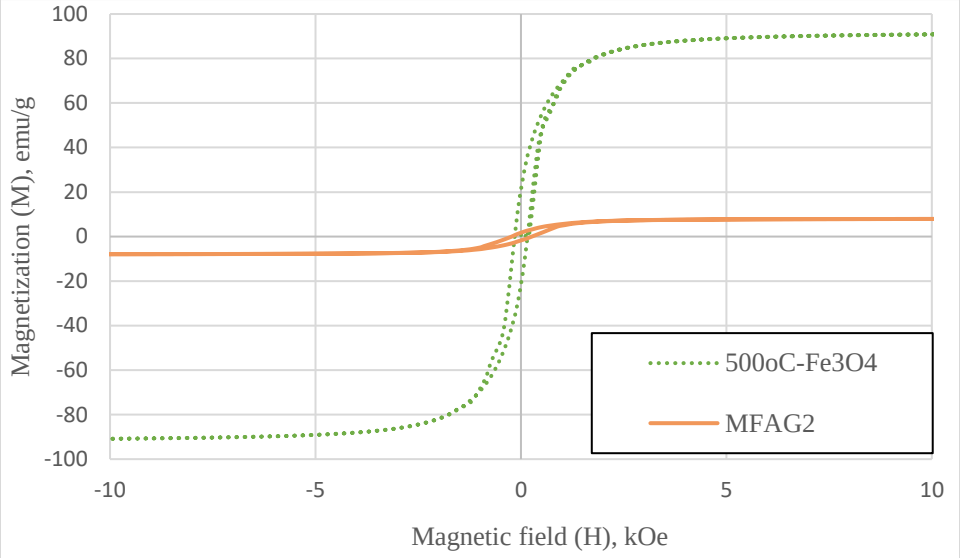

Figure 6-5. Magnetization curve of a single (a) 500°C Fe_3O_4 particles (mass = 15.57 mg) and (b) MFAG2 sample (mass = 6.2 mg).

The magnetization curve showed a hysteresis loop meaning that the magnetic behavior of magnetic Fe_3O_4 particles in the geopolymer was preserved when they were fixed in the geopolymer matrix. The magnetization saturates at a value of 8.06 emu/g for a high field yield of 30 kOe (Table 6-3).

6.4.3. Physical-chemical properties of MFAG2

For MFAG2 sample, the nitrogen BET surface area was 36.46 m^2/g and compressive strength was 34.5 MPa, which were comparable to the fly ash-based geopolymer with surface area of 32.39 m^2/g and compressive strength of 33.8 MPa. Figure 6-6(a) shows the SEM image (5000x) and EDX spectra data of prepared MFAG2 from Method 2. The MFAG2 sample contained Fe content based on Fe X-ray map and spectra data. Figure 6-6(b) shows the SEM image (5000x) and spectra data of MFAG2 after treatment in the Cu^{2+} solution. Based on Cu X-ray map and spectra data, Cu was found on the surface of MFAG2.

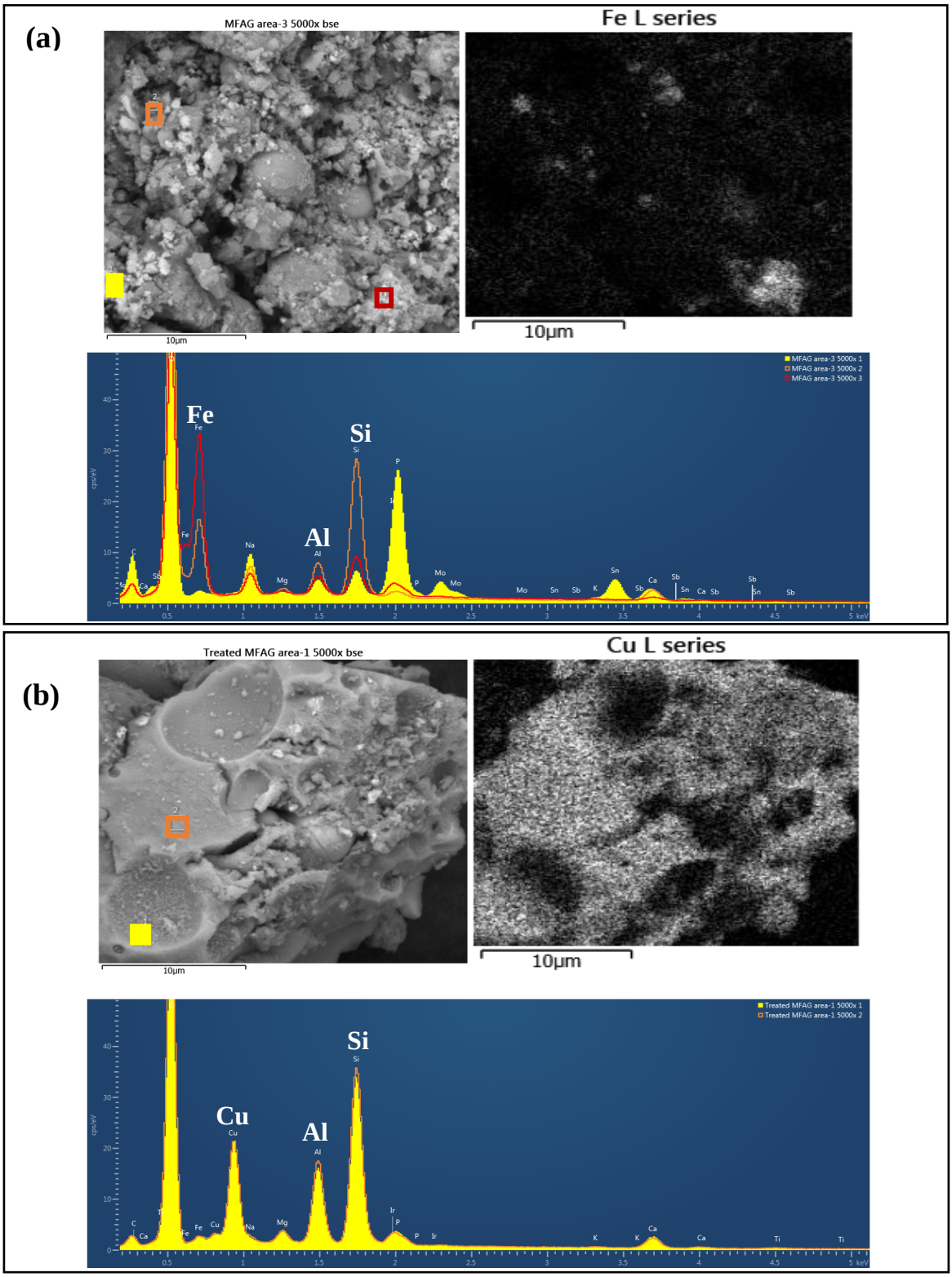

Figure 6-6. SEM images (5000x) and EDX spectra of MFAG2 (a) before and (b) after treated with Cu^{2+} solution.

6.4.4. Effect of MFAG2 mass and initial concentration of Cu^{2+} on pH of solution

Figure 6-7 shows the impact of mass (0.01 – 0.1 g) of MFAG2 on the pH of the solution when different masses were added to the copper solution. The final pH of solution increased with increased addition of MFAG2 which was expected. For the low Cu^{2+} concentration of 10 mg/L, 0.1 g of MFAG2 gave a final pH of 7.68 which was higher than the pH of 6.04 from single point test with 100 mg/L of Cu^{2+} concentration. Fine FAG (< 0.177 mm) particles showed similar trend of final pH of solution and its final pH was slightly higher than that of MFAG2. The alkaline sites of geopolymer can contribute towards the pH of the solution and to metal uptake.

As a comparison, the mass (0.01 – 0.1 g) of FAG (0.6 – 2 mm) added into 20 mg/L of Cu^{2+} solution also increase the pH of solution as shown in Figure 6-7. For FAG with size 0.6 – 2 mm, the final pH change was less than that of MFAG2 and FAG (< 0.177 mm). A possible reason is that larger particle size (less surface area) of FAG (0.6 – 2 mm) was used as compared to MFAG2 and FAG (< 0.177 mm) along with the higher Cu^{2+} concentration (20 mg/L) used.

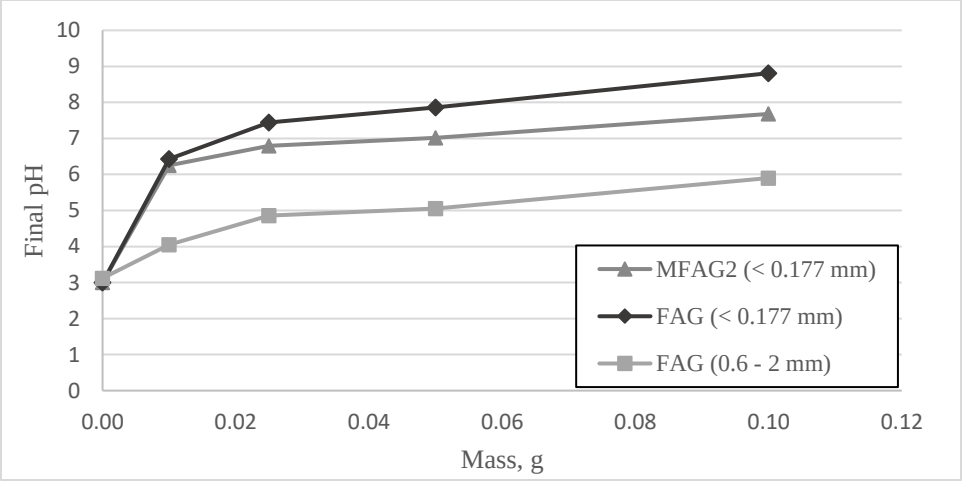

Figure 6-7. Effect of mass of MFAG2 on final pH of solution. Condition: 50 mL of Cu^{2+} solution, and initial pH 3, and 24 hour contact time. MFAG2 (< 0.177 mm) and FAG (< 0.177 mm): 10 mg/L of initial Cu^{2+} concentration. FAG (0.6 – 2 mm): 20 mg/L of initial Cu^{2+} concentration.

Figure 6-8 shows the effect of initial Cu^{2+} concentration (0 – 200 mg/L) on final pH of solution. The final pH decreased with increased Cu^{2+} concentration. This may be due to the initial metals concentration providing an important driving force to overcome the mass transfer resistance of metal ions between the aqueous and solid phases (Ibrahim et al., 2010). As such, the more mass of Cu^{2+} in solution can compete with H^{+} ion (acidity) for available reactive sites on the solids.

Also, as a comparison, FAG (< 0.177 mm) resulted in higher final pH of the solution than that of MFAG2, and FAG (0.6 – 2 mm) resulted in lower final pH of the solution than that of MFAG2, even though the mass of FAG (0.6 – 2 mm) used was twice larger than MFAG2. The possible reason may be due to the larger particle size (less surface area) of FAG (0.6 – 2 mm) as compared to that of MFAG2 (< 0.177 mm) and FAG (< 0.177 mm).

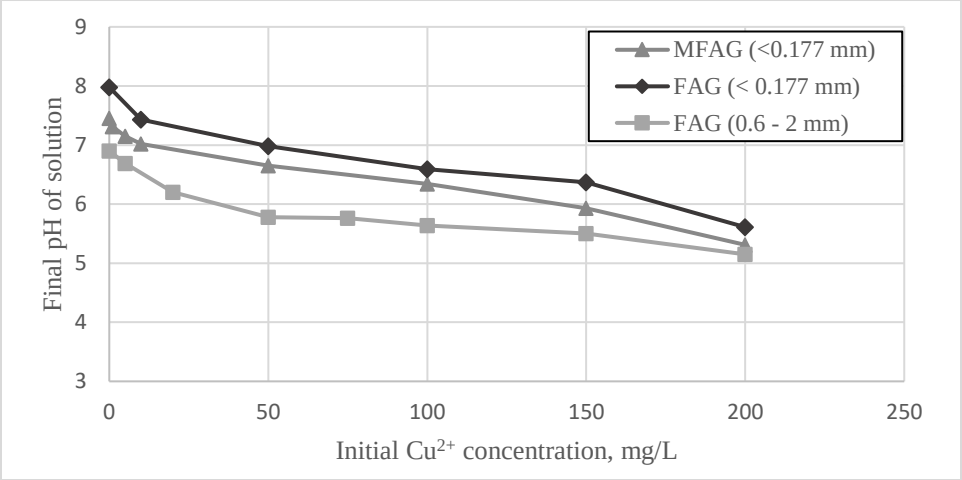

Figure 6-8. Effect of initial Cu^{2+} concentration on final pH of solution. Condition: 50 mL of Cu^{2+} solution, initial pH 3, and 24 hour contact time. 0.05 g of MFAG2 (< 0.177 mm) and FAG (< 0.177 mm) and 0.1 g of FAG (0.6 – 2 mm).

6.4.5. Kinetics of metal uptake on MFAG2

The kinetics of metal uptake for MFAG2 are presented in Figure 6-9 for initial pHs of 2.5, 3.0, and 4.0. The copper solution used was 50 mL with an initial concentration of 100 mg/L and the mass of MFAG2 used was 0.1 g. Figure 6-9 shows a rapid uptake within the first two hours,

and then the uptake gradually slowed down. Steady state conditions were reached at about 24 hours. The time taken to reach steady state conditions decreased with increasing the initial pH of solution. This behavior may be connected to the competitive uptake process of Cu^{2+} ion and H^{+} ion in acidic solution.

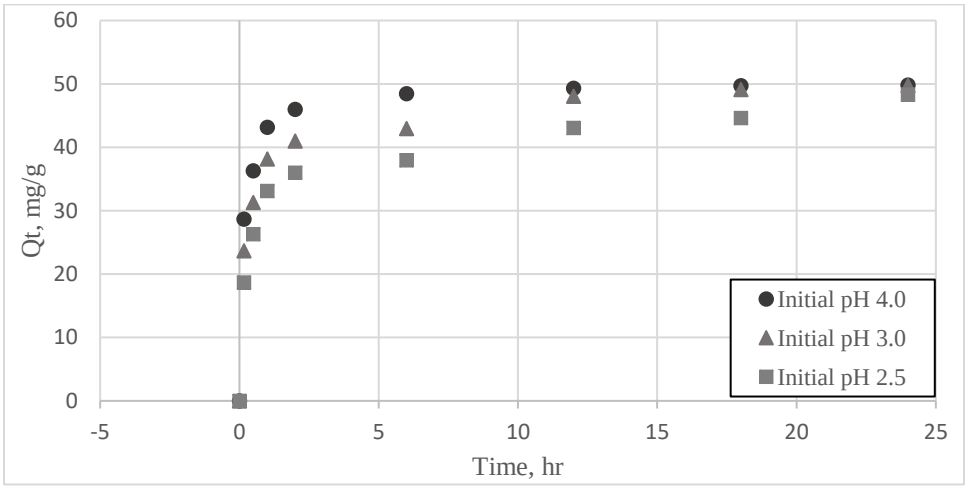

Figure 6-9. Effect of contact time on copper uptake rate. Condition: 100 mg/L of initial copper concentration, 50 mL of solution volume, and 0.1 g of sample mass.

Two kinetic models, pseudo-first-order and pseudo-second-order, were used to fit the data as shown in Figure 6-10. Eq. (1) and (2) present the linear forms of the pseudo-first-order (Lagergren, 1898) and the pseudo-second-order kinetics (Ho & McKay, 1999), respectively:

$$\log(q_e - q_t) = \log q_e - \frac{k_1 t}{2.303} \qquad (1)$$

$$\frac{t}{q_t} = \frac{1}{k_2} q_e^2 + \frac{t}{q_e} \qquad (2)$$

where t is the contact time (min), q_e (mg/g), and q_t (mg/g) are the amounts of Cu^{2+} uptake at steady state conditions and at any time t, k_1 (min^{-1}) and k_2 (g/mg min) is the rate constant of the pseudo first-order and the pseudo-second-order kinetics, respectively. Figure 6-10(a) represents the plot of $\ln(q_e - q_t)$ versus t. It shows good linearity with an $R^2 = 0.9506$. The plot of t/q_t versus t is given in Figure 6-10(b) where the pseudo-second-order model fits the data well ($R^2 = 0.999$). Table 6-4

summarized the results of the modelling. These results indicate that the pseudo-second-order kinetic model yielded a better fit and suggests that Cu^{2+} uptake kinetic using MFAG can be described by the pseudo-second-order equation. Other researchers (Mobasherpour et al., 2014; Venkatesan & Rajagopalan, 2016; Rabelo et al., 2012) reported similar results where a pseudo-second-order model was a better fit for Cu^{2+} uptake onto different adsorbents a first-order-model.

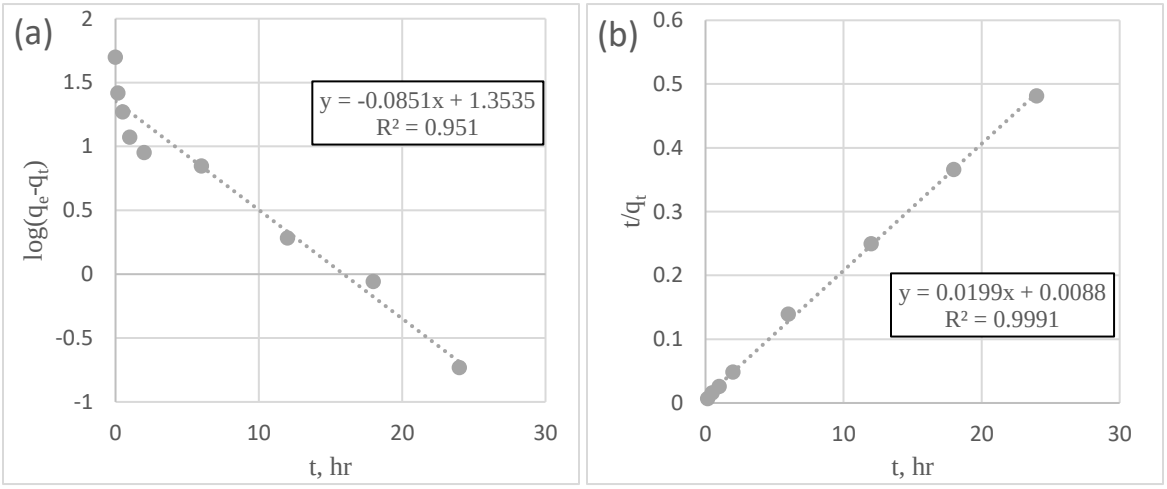

Figure 6-10. Kinetic models of Cu^{2+} uptake on magnetic geopolymer: (a) Pseudo-first-order, and (b) pseudo-second-order. Conditions: 50 mL of Cu^{2+} solution, initial pH of 3.0, and MFAG2 mass of 0.1 g.

Table 6-4. Kinetic parameters for uptake of Cu^{2+} on MFAG2.

Kinetic model	Parameters	Initial pH of solution		
		2.5	3.0	4.0
Pseudo-first order	q_e, mg/g	26.51	22.57	13.13
	k_1, hr^{-1}	0.11	0.20	0.21
	R^2	0.892	0.951	0.874
Pseudo-second order	q_e, mg/g	47.85	50.25	50.25
	k_2, g/mg·hr	6.60E-06	3.48E-06	1.39E-06
	R^2	0.995	0.999	0.999

6.4.6. Release of cations in solution

Figure 6-11 illustrated the release of cations (Ca, Mg, K, and Na) in solution. Na^+ concentration ranged from 30 – 40 mg/L since a high concentration of NaOH and Na_2SiO_3 was

used in the synthesis process. Calcium ion released from MFAG may come from calcium compounds dissolving into the solution due to its acidity. Concentrations of aluminum and iron ions in solution were found to be below the detection limit of the ICP. This results may suggest that the synthesized MFAG was stable in fixing the aluminum and iron ions in its structure and was not impacted by the acidic solution.

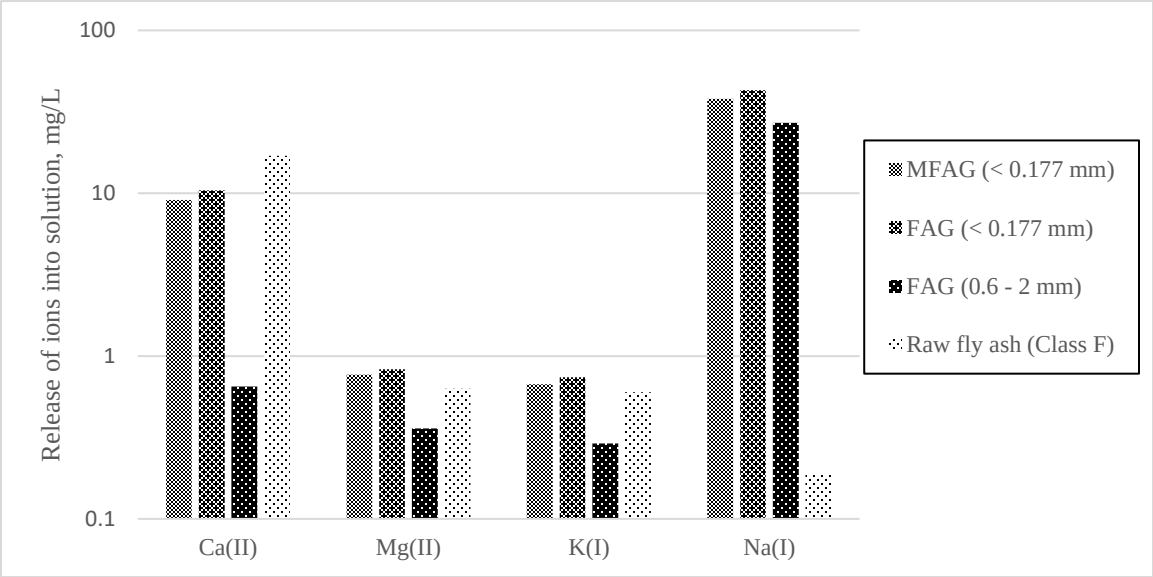

Figure 6-11. Release of cation in solution. Condition: 50 mL of 100 mg/L Cu^{2+} solution, initial pH of 3.0, and 24 hour contact time. 0.05 g of MFAG2 (< 0.177 mm) and FAG (< 0.177 mm), 0.1 g of FAG (0.6 – 2 mm) and 0.05 g of raw fly ash (Class-F).

As a comparison, FAG (< 0.177 mm) resulted in higher release of cations in solution than that of MFAG2. A possible reason may be due to the addition of Fe_3O_4 into geopolymer which may reduce cation release. FAG (0.6 – 2 mm) resulted in lower final pH of solution than that of MFAG2, even though the mass of FAG (0.6 – 2 mm) used was twice larger than MFAG2. A possible reason may be due to the larger particle size (less surface area) of FAG (0.6 – 2 mm) as compared to that of MFAG2 (< 0.177 mm) and FAG (< 0.177 mm).

In addition, as a comparison, raw fly ash (Class-F) resulted in higher release of Ca^{2+} and less Na^{+} in solution than that of the other three geopolymers. Other cations were not detected in solution as they may be below the detection limits of the ICP.

6.4.7. Isotherm studies

Two isotherms, Langmuir and Freundlich models, were used to fit the data of the batch experiments. The isotherms are mathematically expressed as follows. The Langmuir isotherm model is shown below:

$$\frac{C_e}{q_e} = \frac{1}{K_L q_m} + \frac{C_e}{q_m} \qquad (3)$$

where q_m is the maximum adsorption capacity (mg/g); q_e is the amount of Cu^{2+} uptake at equilibrium (mg/g); and K_L is the Langmuir constant (L/g).

The Freundlich isotherm model displays the relationship between the amount of Cu^{2+} uptake by MFAG (q_e, mg/g) and the equilibrium concentration of Cu^{2+} (*Ce*, mg/L) in solution:

$$q_e = K_F C_e^{1/n} \qquad (4)$$

where K_F and n are Freundlich constants that were related to the adsorption capacity and the adsorption intensity respectively.

Figure 6-12 shows uptake of Cu^{2+} for 0.05 g of MFAG2 (< 0.177 mm) in solution. As a comparison, Cu^{2+} uptake onto 0.05 g of FAG (< 0.177 mm) and 0.1 g of FAG (0.6 – 2 mm) were plotted as shown in Figure 6-12. The K_L, Q_m, n, K_F values and the regression correlation coefficients (R^2) for Langmuir and Freundlich isotherms are given in Table 6-5. The R^2 correlation indicate that experimental data was better fitted using the Langmuir model (R^2 = 0.981 – 0.999) as compared to the Freundlich model (R^2 = 0.901 – 0.981). The maximum uptake capacity (Q_m) for Cu^{2+} was 111.11 mg/g for MFAG2 (< 0.177 mm) which was slightly higher than uptake capacity

(102.04 mg/g) for FAG (< 0.177 mm). A possible reason may be due to the higher BET surface area (36.46 m^2/g) of MFAG2 as compared to that (32.39m^2/g) of FAG. In addition, both fine geopolymer particles showed much higher uptake capacity as compared to 29.41 mg/g for gravel-sized FAG (0.6 – 2 mm) at initial pH 3.0.

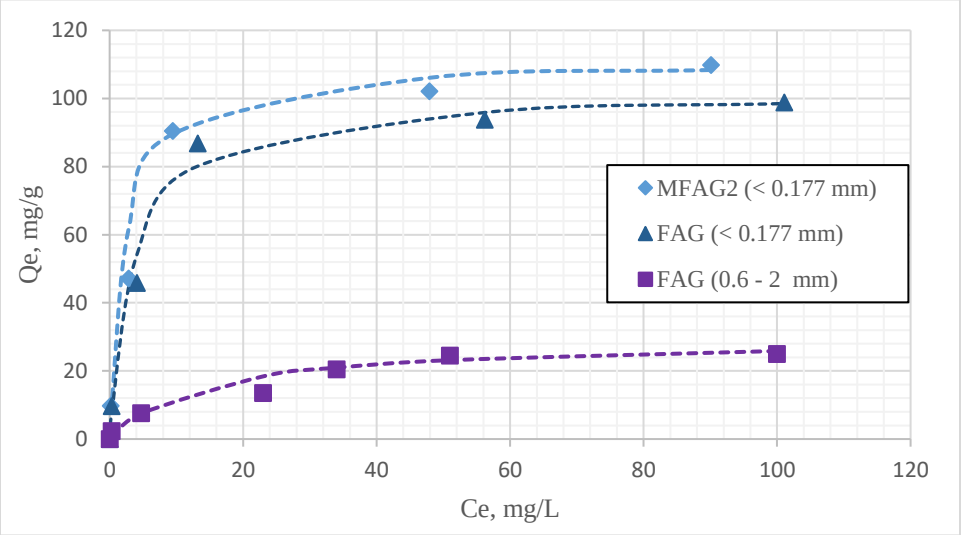

Figure 6-12. Isotherms for uptake of Cu^{2+}. Condition: 50 mL of Cu^{2+} solution, initial pH 3, and 24 hour contact time. 0.05 g of MFAG2 and FAG (<0.177 mm), and 0.1 g of FAG (0.6 – 2 mm).

Table 6-5. Isotherm parameters for Cu^{2+} ion uptake on MFAG2 and FAG (particle size < 0.177mm), and FAG (particle size: 0.6 – 2mm).

Model	Parameters	Samples		
		MFAG2 (< 0.177 mm)	FAG (< 0.177 mm)	FAG (0.6 – 2 mm)
Langmuir	Q_m, mg/g	111.11	102.04	29.41
	K_L, L/mg	0.44	0.28	0.07
	R^2	0.999	0.999	0.981
Freundlich	K_F, $mg^{(1-n)}g^{-1}L^n$	17.85	20.49	4.10
	1/n	0.51	0.40	0.41
	R^2	0.945	0.901	0.981

6.4.8. Settling of MFAG2 particles with and without a magnetic field

Compared to traditional solid-liquid separation method, such as gravity and centrifugal technique, magnetic separation can be more effective and can separate the solids rapidly. A preliminary magnetic separation test (Figure 6-13) was performed with fine MFAG2 particles and separated using a magnet (magnetic field of 0.48 Tesla). The particles was separated within 10 s. More than 95% of the fine particles were recovered from solution by the magnet (Figure 6-13). When the external magnetic field was removed, the fine particles could be dispersed again in solution by physical shaking. Without the magnet, the fine particles settled to the bottom of the tube in 20 min.

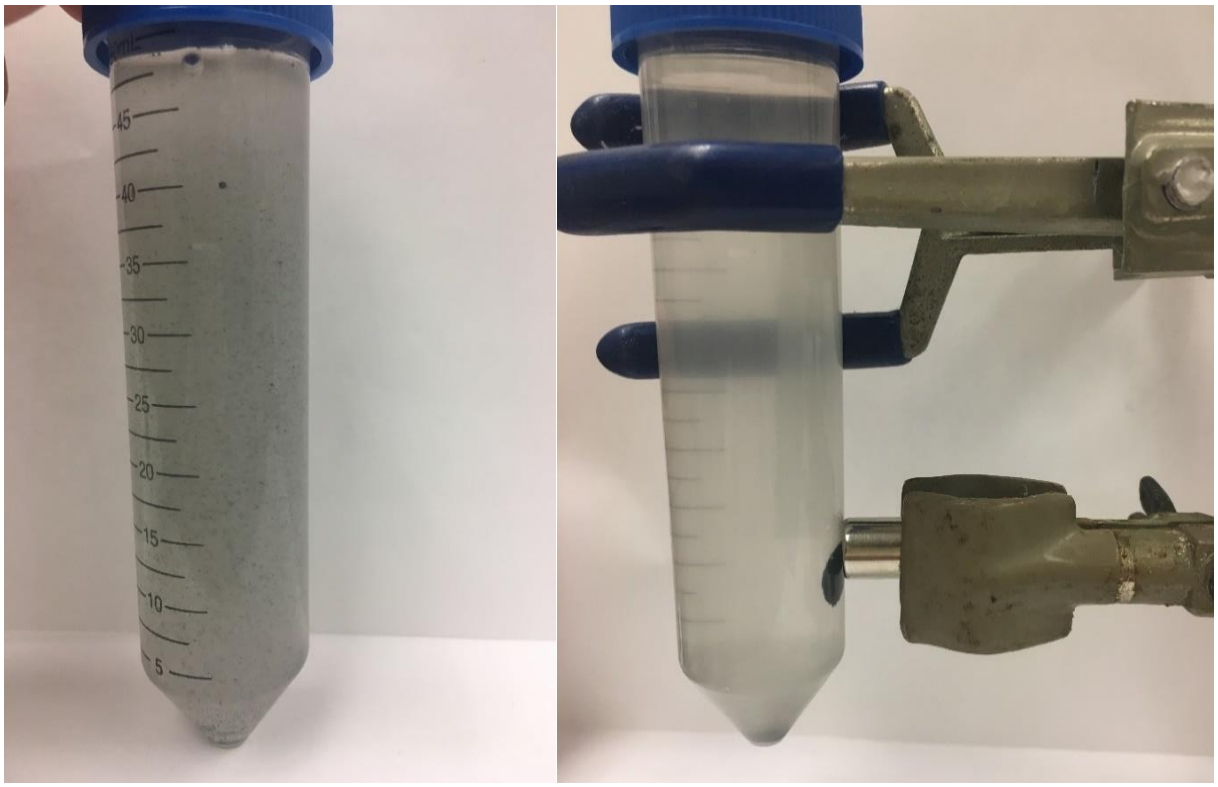

Figure 6-13. Magnetic separation of synthesized MFAG2. Left: before and right: after. Conditions: 50 mL of Cu^{2+} solution, initial pH of 3.0, and MFAG2 mass of 0.1 g.

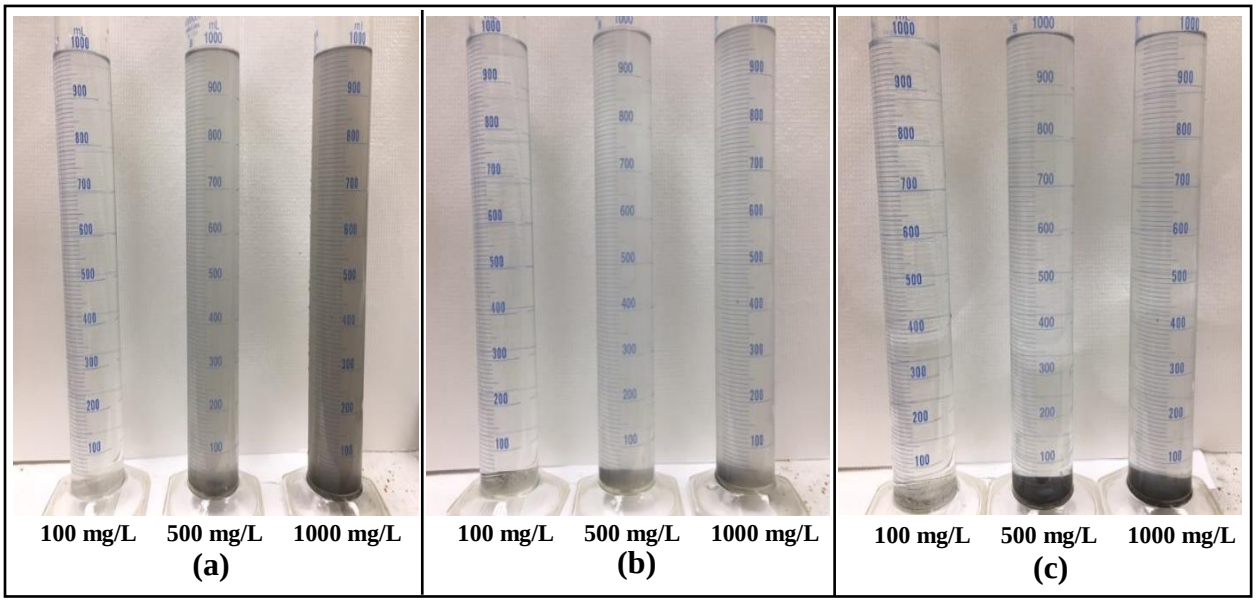

Figure 6-14. Settling MFAG2 particles in solution (a) mixture, (b) without magnetic field (2 hours), (c) with magnetic field (5 min).

Figure 6-14 shows the standard settling test of MFAG2 particles in 1 liter measuring cylinder with and without a magnetic field. The concentration of MFAG2 solids were 100, 500, and 1000 mg/L (left to right). The settling with the magnetic field showed denser accumulation of particles at the bottom of cylinder as compared to that of gravitional settling without a magnetic field.

Table 6-6 shows the turbidities and suspended solids concentrations in solution with and without magnetic settling. The magnetic settling showed significantly lower turbidities from 68.3 to 0.655 NTU within 5 min of settling for 100 mg/L of fine MFAG2 solids. For gravitational settling, the turbidity reached in 2 hours was 6.15 NTU from a starting turbidity of 68.3 NTU. The suspended solids for the magnetic settling was 35.1 mg/L after 5 mins for a starting suspended solids of 1000 mg/L. In contrast, the suspended solids was 158.3 mg/L after 2 hours of gravitational settling. The results from Table 6-6 showed the magnetic geopolymer particles can be rapidly separated from water solution by a magnetic field.

Table 6-6. The turbidity and suspended solids with and without magnetic settling.

Settling	Parameters	Total solids concentration		
		100 mg/L	500 mg/L	1000 mg/L
Mixture	Turbidity, NTU	68.3	376	745
Without magnetic field	10 mins - Turbidity, NTU	10.9	56.4	114
	2 hours - Turbidity, NTU	6.15	29.5	49.5
	Suspended solids, mg/L	29.2	104.6	158.3
With magnetic field	1 min Turbidity, NTU	8.2	27.1	50.6
	5 mins - Turbidity, NTU	0.655	4.53	8.16
	Suspended solids, mg/L	2.8	16.3	35.1

6.5. Conclusion

Two methods for preparing magnetic geopolymer were presented. Method 2 incorporated pre-prepared magnetic Fe_3O_4 particles in the synthesis of the geopolymer while Method 1 synthesized the magnetic Fe_3O_4 particles on the surface of the geopolymer by soaking the geopolymer with iron nitrate and calcining the prepared material. Method 2 was found to be a more effective method than Method 1. With Method 2, the magnetic properties of the Fe_3O_4 particles was found to be preserved in the synthesis process. The prepared magnetic fly ash-based geopolymer (MFAG2) in this study can be applied to neutralize the pH and at the same time remove heavy metals from industrial acidic wastewater or drinking water system. Experimental results showed that fine MFAG2 particles (< 0.177 mm) had an uptake capacity of Cu^{2+} (111.11 mg/g) and the initial acidic pH (3.0) was increased to pH of 7.68. The magnetic geopolymer was effectively separated with a magnetic field within minutes as compared to gravitational settling which requires about two hours for comparable results.

The magnetic geopolymer fine particles may be used in applications where removal of heavy metals is required followed by separation of the geopolymer with the possibility of recovery of metals and reuse of the geopolymer.

Since the magnetic geopolymer were made from an industrial waste (fly ash) and iron nitrate, the cost to manufacture is low and at the same time helps to reduce fly ash waste.

6.6. References

Al-Harahsheh, M. S., Al Zboon, K., Al-Makhadmeh, L., Hararah, M., & Mahasneh, M. (2015). Fly ash based geopolymer for heavy metal removal: a case study on copper removal. *Journal of Environmental Chemical Engineering*, *3*(3), 1669-1677.

Aziz, H. A., Adlan, M. N., & Ariffin, K. S. (2008). Heavy metals (Cd, Pb, Zn, Ni, Cu and Cr (III)) removal from water in Malaysia: post treatment by high quality limestone. *Bioresource Technology*, *99*(6), 1578-1583.

Bereket, G., Arog, A. Z., & Özel, M. Z. (1997). Removal of Pb (II), Cd (II), Cu (II), and Zn (II) from aqueous solutions by adsorption on bentonite. *Journal of Colloïd and Interface Science*, *187*(2), 338-343.

Foroughi, F., Hassanzadeh-Tabrizi, S. A., Amighian, J., & Saffar-Teluri, A. (2015). A designed magnetic CoFe2O4–hydroxyapatite core–shell nanocomposite for Zn (II) removal with high efficiency. *Ceramics International*, *41*(5), 6844-6850.

Ho, Y. S., & McKay, G. (1999). Pseudo-second order model for sorption processes. *Process Biochemistry*, *34*(5), 451-465.

Ibrahim, M. M., Ngah, W. W., Norliyana, M. S., Daud, W. W., Rafatullah, M., Sulaiman, O., & Hashim, R. (2010). A novel agricultural waste adsorbent for the removal of lead (II) ions from aqueous solutions. *Journal of Hazardous Materials*, *182*(1-3), 377-385.

Lagergren, S. (1898). About the theory of so-called adsorption of soluble substances. 1-39.

Mobasherpour, I., Salahi, E., & Ebrahimi, M. (2014). Thermodynamics and kinetics of adsorption of Cu (II) from aqueous solutions onto multi-walled carbon nanotubes. *Journal of Saudi Chemical Society*, *18*(6), 792-801.

Mužek, M. N., Svilović, S., & Zelić, J. (2014). Fly ash-based geopolymeric adsorbent for copper ion removal from wastewater. *Desalination and Water Treatment*, *52*(13-15), 2519-2526.

Nordberg, G. F., Fowler, B. A., & Nordberg, M. (Eds.). (2014). *Handbook on the Toxicology of Metals*. Academic press.

Peng, Q., Liu, Y., Zeng, G., Xu, W., Yang, C., & Zhang, J. (2010). Biosorption of copper (II) by immobilizing Saccharomyces cerevisiae on the surface of chitosan-coated magnetic nanoparticles from aqueous solution. *Journal of Hazardous materials*, *177*(1-3), 676-682.

Rabelo, R. B., Vieira, R. S., Luna, F. M. T., Guibal, E., & Beppu, M. M. (2012). Adsorption of copper (II) and mercury (II) ions onto chemically-modified chitosan membranes: Equilibrium and kinetic properties. *Adsorption Science & Technology*, *30*(1), 1-21.

Shipley, H. J., Engates, K. E., & Grover, V. A. (2013). Removal of Pb (II), Cd (II), Cu (II), and Zn (II) by hematite nanoparticles: effect of sorbent concentration, pH, temperature, and exhaustion. *Environmental Science and Pollution Research*, *20*(3), 1727-1736.

Venkatesan, G., & Rajagopalan, V. (2016). Adsorption kinetic models for the removal of Cu (II) from aqueous solution by clay liners in landfills. *International Journal of Environmental Science and Technology*, *13*(4), 1123-1130.

Wang, S., Li, L., & Zhu, Z. H. (2007). Solid-state conversion of fly ash to effective adsorbents for Cu removal from wastewater. *Journal of Hazardous materials*, *139*(2), 254-259.

White, M. J. D. (1975). Settling of activated sludge; theory and practice. In *Apresentado em: Conference on the Application of Chemical Engineering to the Treatment of Sewage and Industrial Liquid Efficient, New York, 16-17 Abr. 1975.*

CHAPTER 7. GENERAL CONCLUSIONS

Fly ash-based geopolymers were made using an alkaline activator solution and fly ash. Some of the advantages of making geopolymers include use of fly ash waste products to reduce the amount of fly ash that are need to be disposed of, the process of making geopolymer does not require specialized equipment, and fly ash is low cost materials. The synthesized fly ash-based geopolymer has good compressive strength properties and comparable specific surface areas. It could be used as a potential low-cost substitute for more expensive adsorbents such as zeolite or activated carbon.

Some of the applications of fly ash-based geopolymer include making pellet or gravel-sized material as filtration media and as materials that can be placed in the path of acidic waste stream, such as acid mine drainage and acidic industrial wastewaters, to neutralize the pH and remove heavy metals. Of the three metals tested, the uptake behavior of fly ash-based geopolymer followed the following sequence of Pb^{2+} > Cu^{2+} > Cd^{2+} in single metal solution for metal concentrations less than 20 mg/L. In a multi-metal solution, Cd^{2+} was the most affected by the presence of the other two metals Cu^{2+} and Pb^{2+}. Cu^{2+} was minimally affected by the other two metals in a multi-metal solution. For the single metal solution experiments, the maximum uptake capacity of Cu^{2+}, Cd^{2+} and Pb^{2+} were found to range from 20.66 – 35.21, 28.74 – 42.02, and 116.28 – 121.95 mg/g for initial pH 2.5 to 4.0 respectively. Removal of heavy metals was probably due to precipitation and adsorption on the geopolymer surface.

Fly ash-based geopolymer can be used as a filtration media in fixed-bed columns for the treatment of acidic waste streams contaminated with heavy metals such as acid mine drainage, industrial wastewaters and landfill leachates. Fly ash-based geopolymer shows a stronger affinity for Pb^{2+} which resulted in a longer breakthrough time and a higher uptake capacity than Cd^{2+} and

Cu^{2+} for single metal solution with the same flow rate and bed depth condition. In a multi-metal solution, competition for uptake was observed whereby Cd^{2+} was the least uptake instead of Cu^{2+}. Pb^{2+} continued to be strongly uptake in the multi-metal solution experiment. The uptake affinity in a single metal solution was in the order of $Pb^{2+} > Cd^{2+} > Cu^{2+}$, but the uptake affinity in a multi-metal solution was in the order of $Pb^{2+} > Cu^{2+} > Cd^{2+}$.

In addition, the fine fly ash-based geopolymer particles were magnetized by incorporating magnetic Fe_3O_4 into the geopolymer. The magnetic fly ash-based geopolymer can neutralize the pH and remove heavy metals from industrial acidic wastewater or drinking water system. The magnetic geopolymer can be used in applications where removal of heavy metals is required followed by separation of the adsorbent with the possibility of recovery of metals and reuse of the adsorbent.

APPENDIX A. CHARACTERIZATION: METHOD AND PROCEDURE

- Cation exchange capacity

The total cation exchange capacity (CEC) of prepared samples was determined by the standard method of ion exchange with ammonium chloride (Sumner et al., 1996). The mass of 1 g sample was left to stand for 24 h in 100 ml of ammonia chloride solution, at pH 7, with occasional shaking. After completion of ion exchange, the suspension was filtered and the concentration of exchangeable Ca^{2+}, Mg^{2+}, K^{+} and Na^{+} was determined in the filtrate, whose sum calculated per kg of sample is the total CEC. The concentrations of Ca^{2+}, Mg^{2+}, Na^{+} and K^{+} were determined by an inductively coupled plasma (ICP) atomic emission spectrometer (ICPE-9800 Series, Shimadzu Corporation, Kyoto, Japan).

Table A-1. Experimental data and calculations of cation exchange capacity

Laboratory Record for CEC Data						Calculations				
Sample	Mass of sample, g	Ca, mg/L	Mg, mg/L	K, mg/L	Na, mg/L	Ca, cmol/kg	Mg, cmol/kg	K, cmol/kg	Na, cmol/kg	CEC, cmol/kg
G50	1	104	7.9	3.8	194	52.00	6.58	0.97	84.35	143.91
G60	1	117	5.6	3.1	198	58.50	4.67	0.79	86.09	150.05
G70	1	97.4	8.8	4.2	218	48.70	7.33	1.08	94.78	151.89
G60+10%S	1	129	9.5	4.7	186	64.50	7.92	1.21	80.87	154.49
G60+20%S	1	156	10.2	5.48	157.7	78.00	8.50	1.41	68.57	156.47

- Specific surface area

The specific surface area (SSA) were determined by measuring the amount of a liquid required to cover the surface of the prepared samples (Blake and Hartge, 1965). The method in this study was based on the weight of ethylene glycol adsorbed as monomolecular layer on the sample surface.

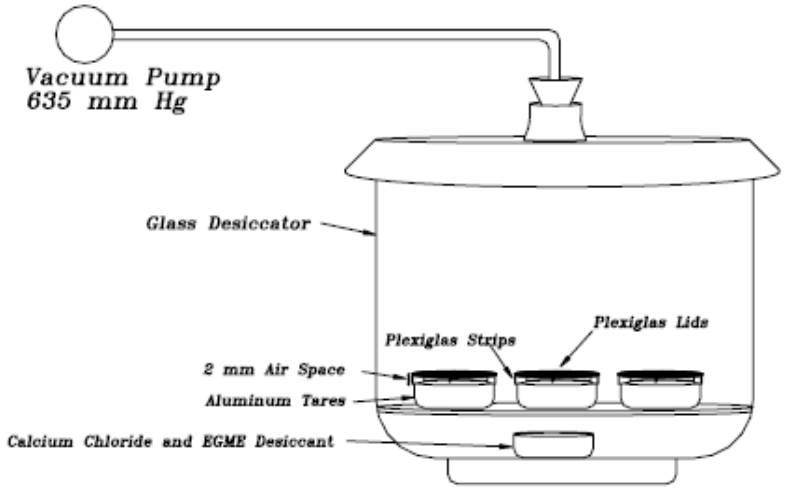

Figure A-1. Experimental apparatus of specific surface area by using ethylene glycol

Weigh approximately 120 g of calcium chloride ($CaCl_2$) into a 1-L beaker and place the beaker in oven (105 ^oC) for 2 hour to remove all traces of H_2O. Then, weigh 20 g of glycol into a 400 mL beaker. Remove the $CaCl_2$ from the oven and weigh out 100 grams without cooling, and add it to the beaker containing the glycol. Mix the contents immediately and thoroughly with a spatula. After mixture has cooled, place it in a culture chamber and spread it uniformly over bottom. Store the culture chamber in sealed desiccator.

Place approximately 1 gram of oven dried sample in the bottom of a clean dry aluminum tare. Determine the mass of the sample to the nearest 0.001 g. Use a small pipette, gently place approximately 1 mL of laboratory grade ethylene glycol over the surface of sample by distributing the liquid dropwise from a pipette. Gently mix the sample and ethylene glycol together using a slow swirling motion of the hand until the mixture forms a slurry and the appearance of the slurry is uniform. Swirling the mixture in the aluminum tare with a circular hand motion allows for no sample loss and a uniform coverage of all sample particles by the ethylene glycol. Place the tare into a vacuum desiccator and place a small lid over the tare, leaving a gap of 2 to 3 mm between

the lid and the tare. Cover the chamber and place it in a desiccator. Attach the desiccator to a vacuum pump and begin evacuating using a vacuum of at about 550 mm Hg, close the stopcock and allow the desiccator to stand at a temperature of 22 ± 1°C. After 12 to 16 hours, apply the vacuum pump again for 30 minutes to remove any foreign vapors which may have reduced the vacuum.

When the sample has been in the desiccator for about 48 hours, and determine the mass of the sample/glycol mixture. Repeat this step again at approximately 24 hours. The weight of the mixture should not vary more than 0.001 g. If the weight varies by more than 0.001 g, place the tare back in the desiccator and weigh it again in approximately 4 hours. Then the surface area of the sample, SSA in m^2/g, was calculated as:

$$SSA = \frac{W_a}{0.00031\ W_s}$$

where *SSA* is specific surface area in m^2/g, *Wa* is weight of ethylene glycol retained by the sample in grams (final slurry weight – *Ws*), 0.00031 is the Dyal-Hendricks value for the weight of glycol required to form a monomolecular layer on a square meter of surface (g/m^2), *Ws* is oven dry weight of sample (g)

It is recommended that periodically a "control" sample be tested to monitor the accuracy of the tests.

- Point of zero charge

The point of zero charge (pH_{pzc}) of the prepared samples were determined by solid addition method (Balistrieri and Murray, 1981) using KNO_3 (0.01 M) solution. Initial pH of (0.01M) KNO_3 solutions (pH_i) was adjusted from pH 2 to 12 by adding either (0.01 M) HCl or 0.01 M (NaOH).

Weigh 0.1g of prepared sample and add into 100 mL of 0.01 M KNO_3 solution in 200 mL conical flasks and stirred for 24 h of contact time and final pH (pH_f) of solution was measured. The difference between the initial and final pH (pH_i–pH_f) was plotted against the initial pH (pH_i) and the point where $pH_i - pH_f = 0$ was taken as the pH_{pzc}. The result of sample G60 is shown in below.

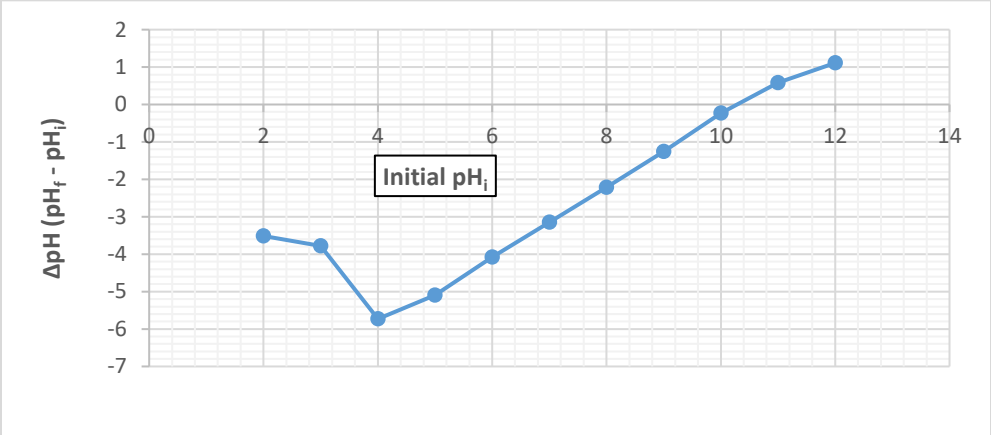

Figure A-2. Results of pH at point of zero charge (ΔpH vs. pH_i)

Results of CEC, SSA, pH_{pzc} for prepared fly ash-based samples are shown in Table A-2.

Table A-2. Results of characteristics of geopolymers

Fly ash-based geopolymer Samples	CEC, cmol/kg	SSA, m^2/g	pH_{pzc}
G50	144	123	10.16 ± 0.21
G60	150	135	10.28 ± 0.16
G70	152	129	10.29 ± 0.43
G60+10%S	154	120	10.22 ± 0.32
G60+20%S	156	114	10.25 ± 0.33

These three properties (CEC, SSA, and pH_{pzc}) are important factor for removal of heavy metals on geopolymer. The methods of these characterization are commonly used for soil analysis, the results from these analysis can provide an indicator for these properties. But their effectiveness need be developed in further. Because geopolymer solids show the reactivity in aqueous phase due to the alkaline nature.

- Scanning Electron Microscope/ Energy Dispersive X-Ray

Scanning electron microscope (SEM) micrographs of the geopolymer samples were taken using FEI Quanta 250 FE-SEM. SEM was performed to show the ash particles morphology and topography before and after the geopolymerization process. For this analysis, the images are observed at 50 – 5000X magnification. The SEM is equipped with an EDX which was used to characterize the microstructure and the chemical compositions of geopolymer samples.

The raw fly ash (Class-F) particles and geopolymer particles (< 0.177 mm and 0.42 – 2 mm) prepared in this study are cast in epoxy so as to get a smooth surface finish.

The microstructure, EDX chemical distribution and elemental mapping of fly ash-based geopolymer samples are shown in below figures (A-3 to A-9). The corresponding EDX analysis confirms the presence of silicon, calcium, aluminum, sodium, potassium, magnesium, iron, titanium, sulfur, oxygen and carbon.

From these figures (A-3 to A-9), it is obvious that the main chemical species present is silicon, aluminum, sodium and calcium. From the elemental mapping, it is clear that there are some zones that are present which include a silicon rich zone, a calcium enriched zone and a complex zone which contains all species including calcium, silicon, aluminum, iron, sodium, oxygen, magnesium and carbon. Some crystalline layers contain phosphorus, tin, antimony, molybdenum, which may due to the raw fly ash. Some iridium were found because samples were coated with iridium for conductivity. It should lead to a featureless map unless there is severe topography.

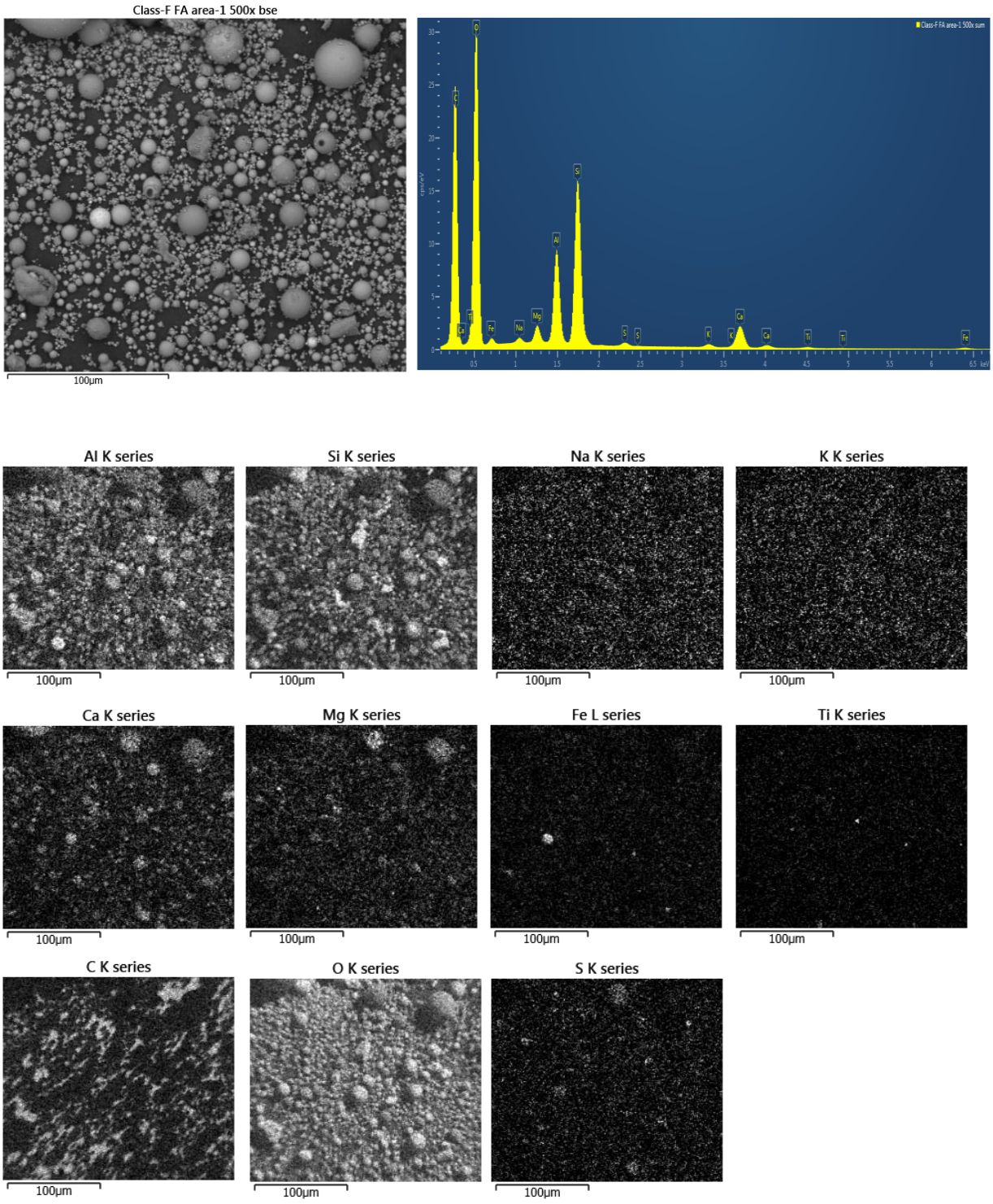

Figure A-3. SEM (500x) of Raw fly ash particles (Class-F)

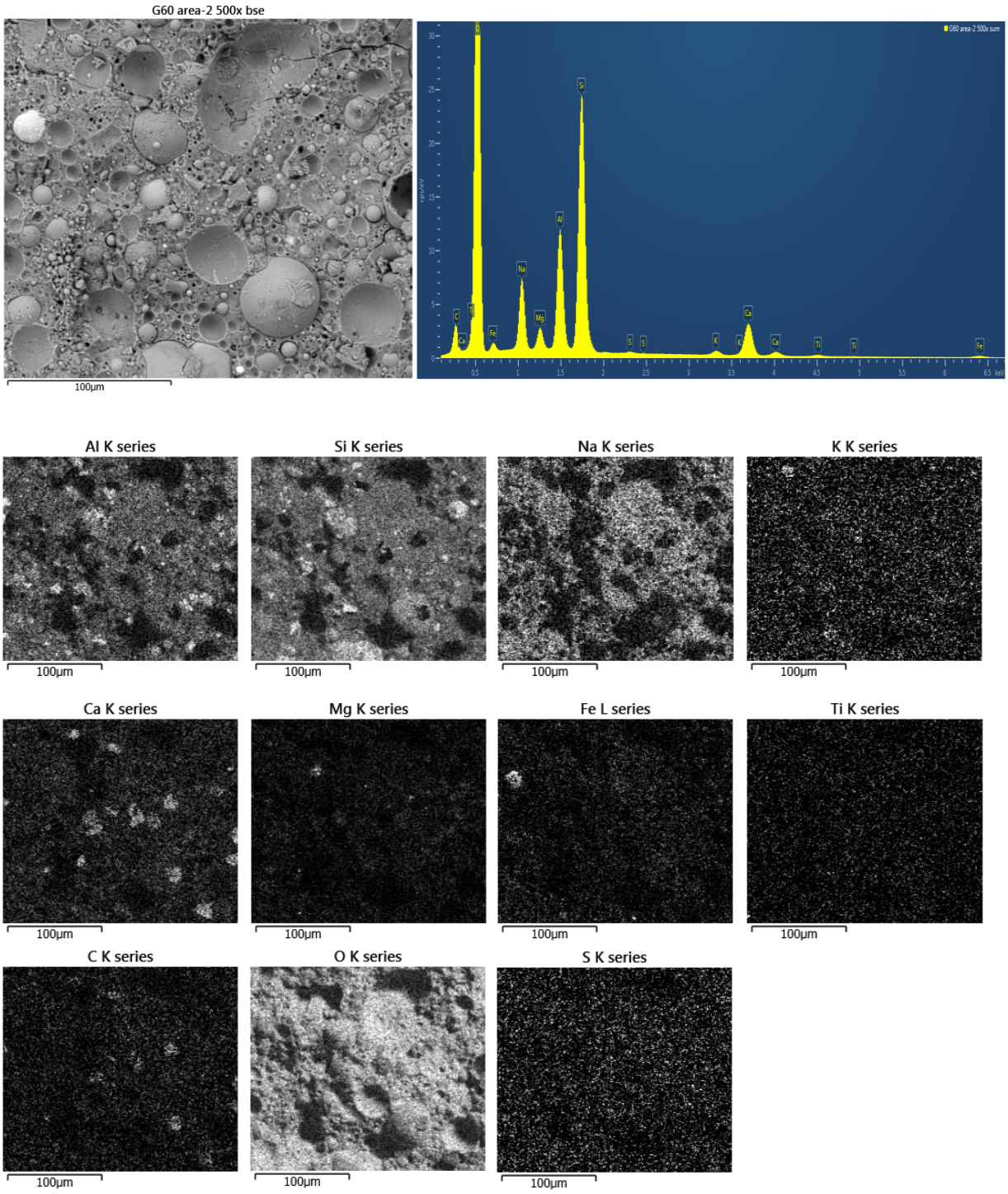

Figure A-4. SEM (500x) of Fly ash-based geopolymer particles (G60) (size: 0.42 – 2 mm)

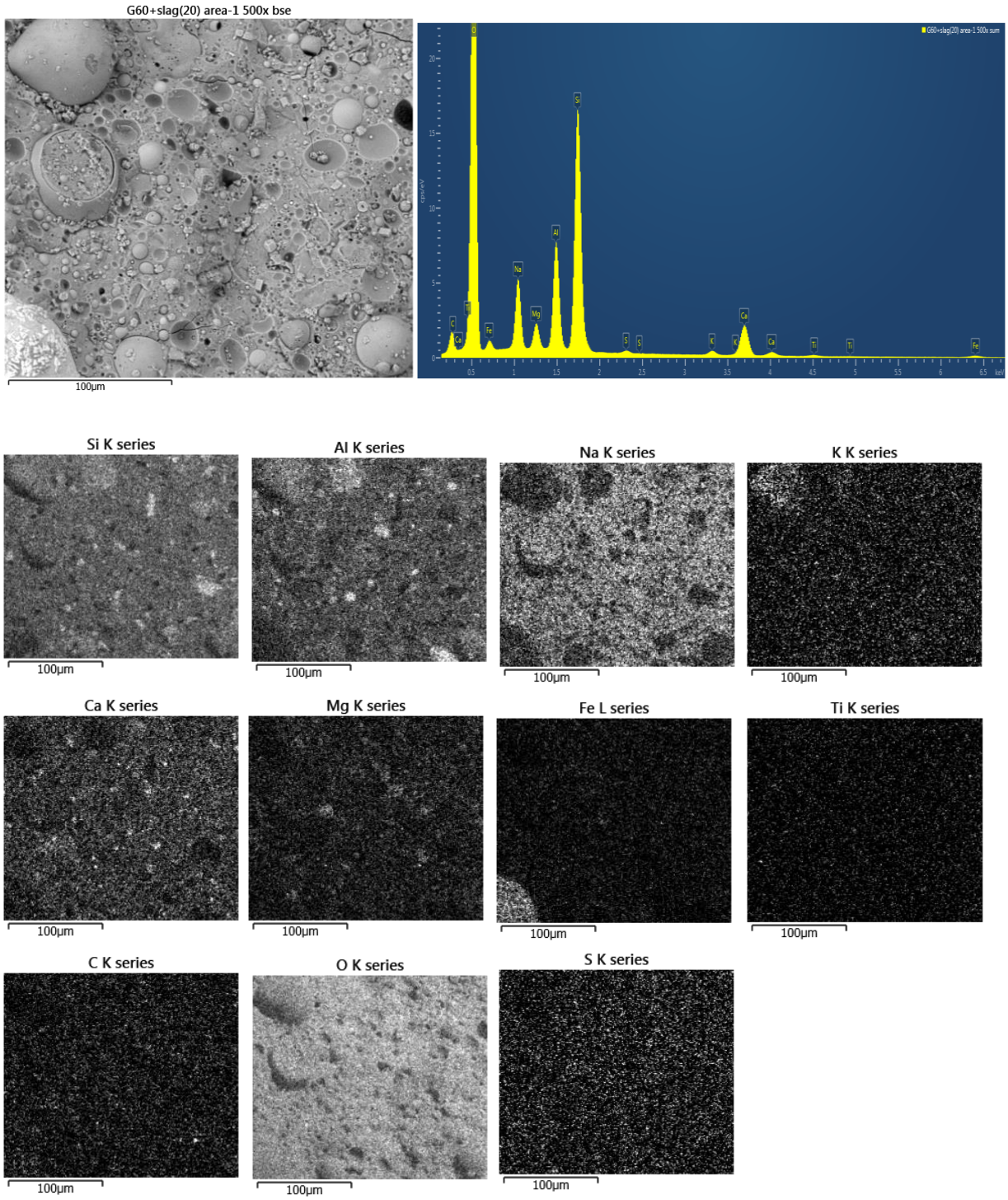

Figure A-5. SEM (500x) of Fly ash-based geopolymer particles (G60+20%Slag) (size: 0.42 – 2 mm)

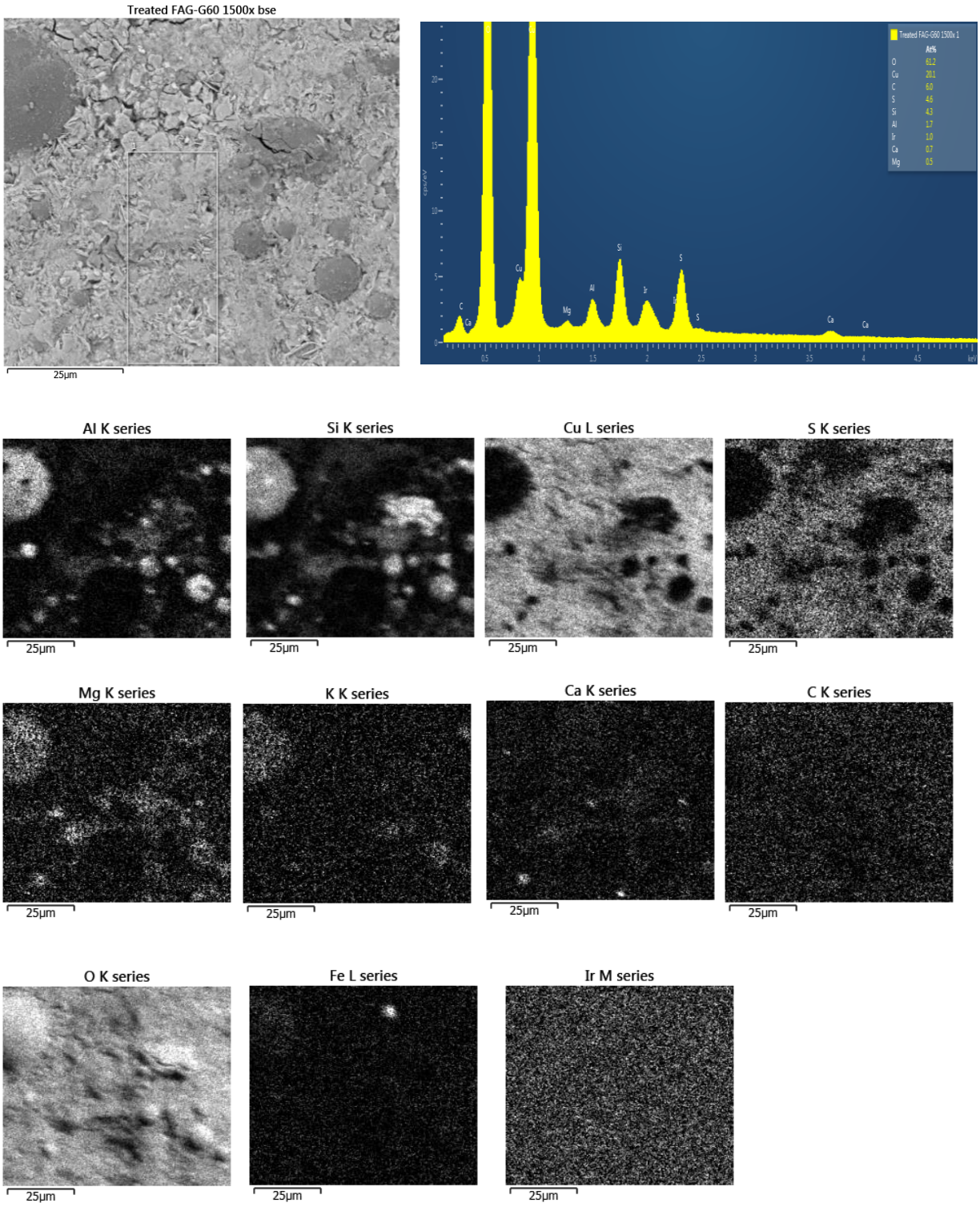

Figure A-6. SEM (1500x) of Fly ash-based geopolymer particles (G60) (size: 0.42 – 2 mm) after treated with Cu2+ solution

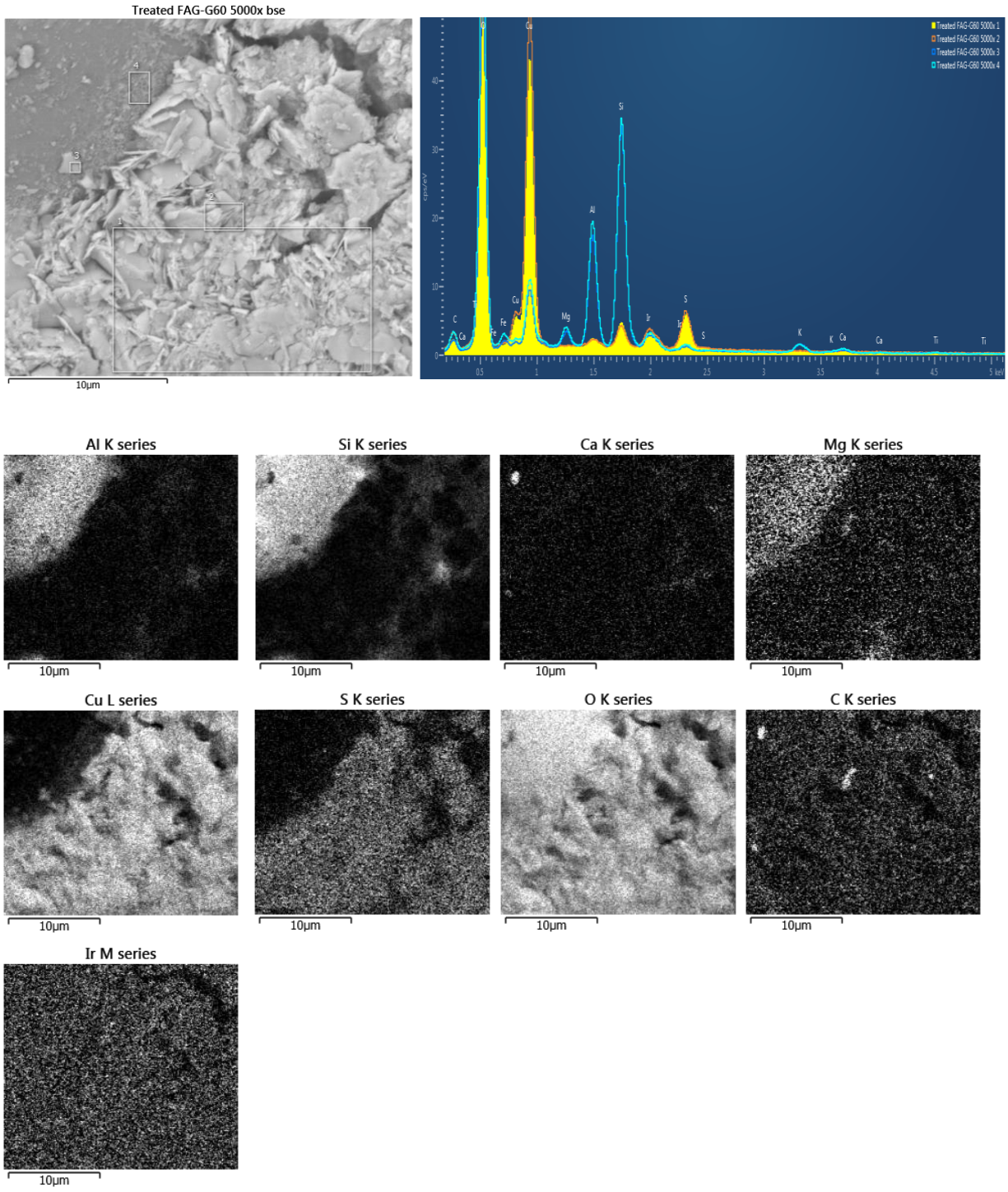

Figure A-7. SEM (5000x) of Fly ash-based geopolymer particles (G60) (size: 0.42 – 2 mm) after treated with Cu2+ solution

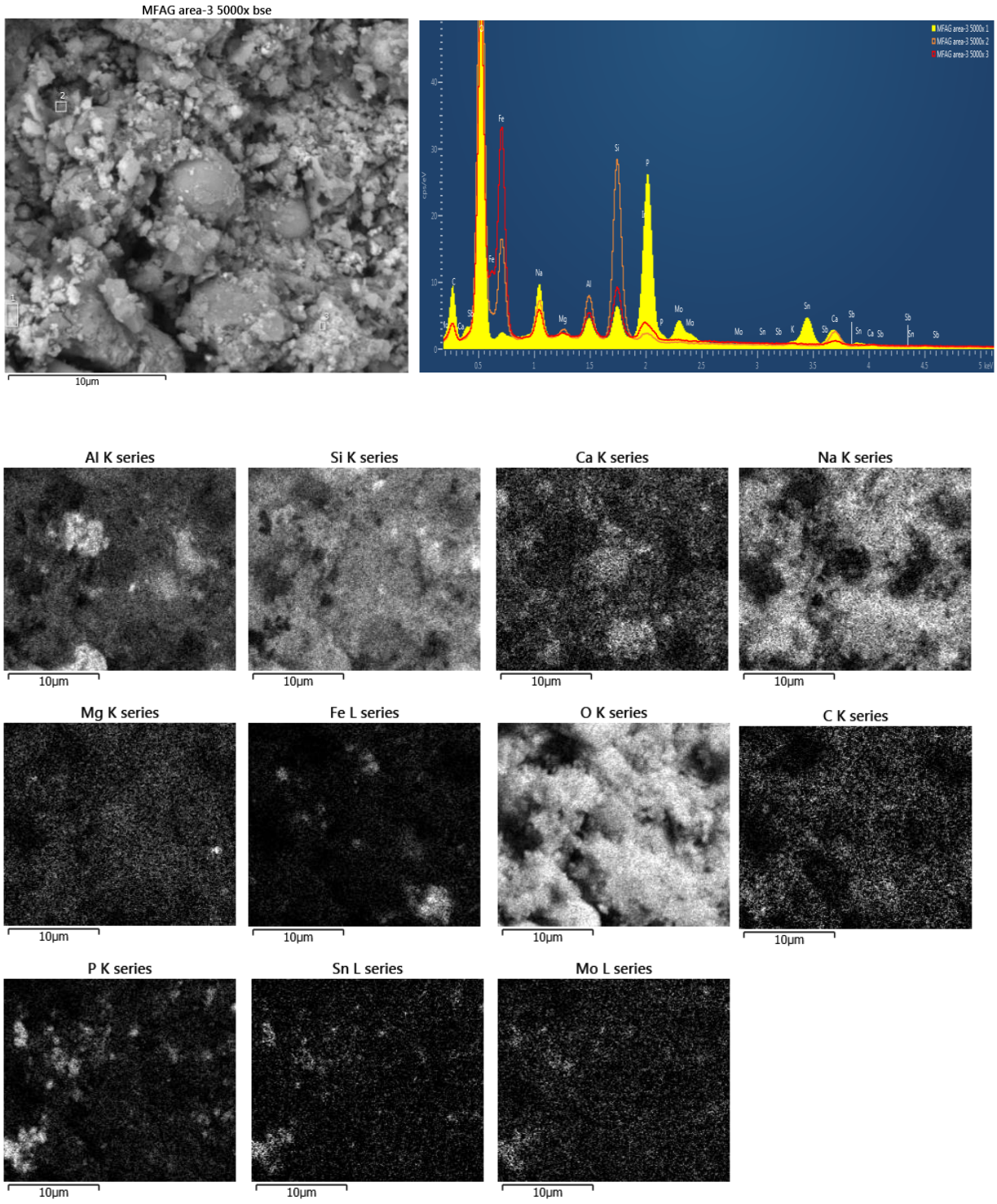

Figure A-8. SEM (5000x) of Magnetic fly ash-based geopolymer particles (MFAG2 from Method 2) (size: < 0.177 mm)

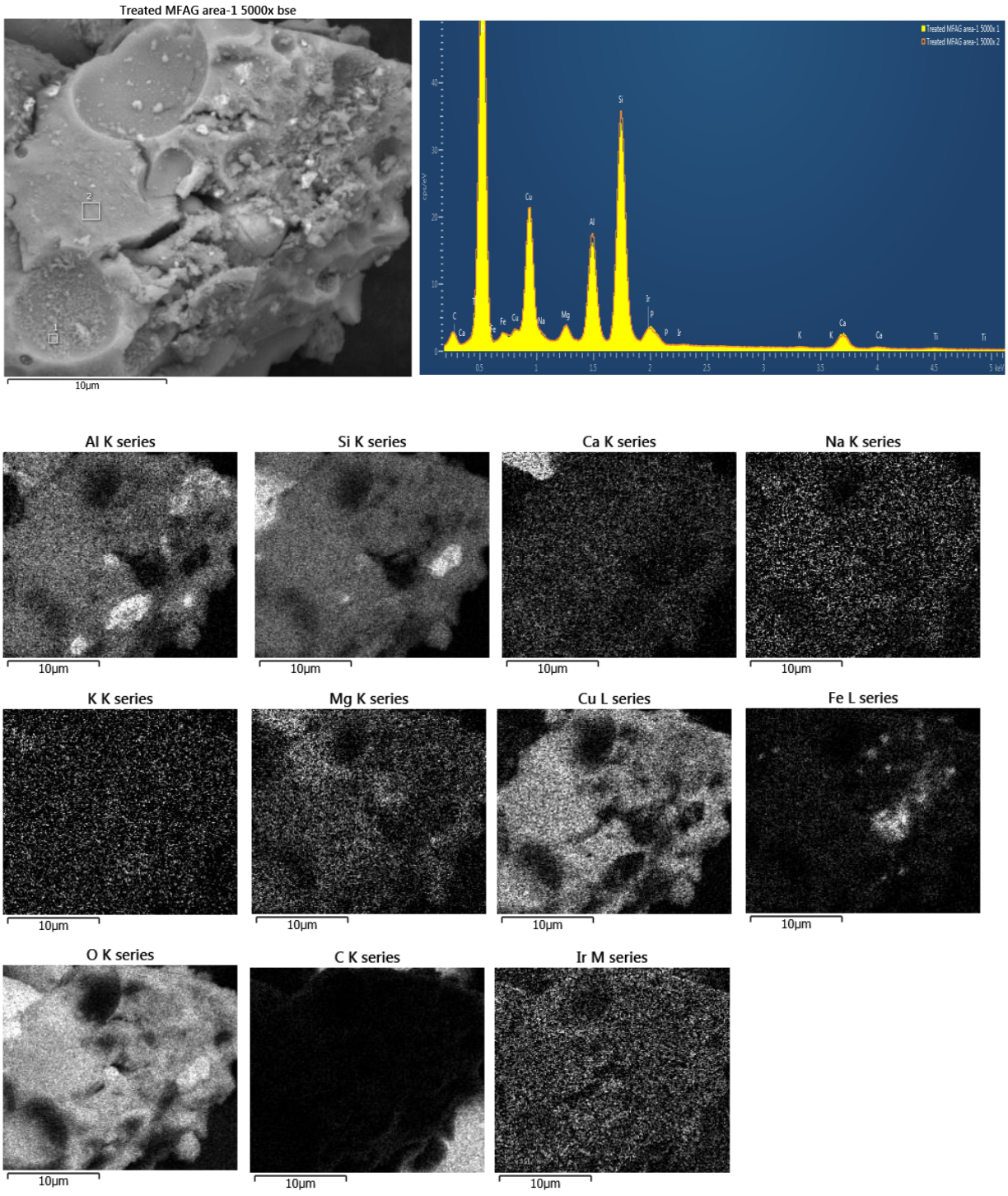

Figure A-9. SEM (5000x) of Magnetic fly ash-based geopolymer particles (MFAG2 from Method 2) (size: < 0.177 mm) after treated Cu2+ solution

- X-Ray Diffraction

XRD data was obtained using a Siemens D500 x-ray diffractometer that is equipped with a diffracted beam monochromator (carbon) and a sample spinner. The medium resolution slits were 0.15 DS. The XRD patterns were obtained by a scanning rate of 1 degree per minute from 10 to 80 degrees (2θ) and steps of 0.05 degrees (2θ). The wavelength selected was 6.065 X 10-7 in (15.40562 nm) (Cu).

Approximately 5g of the geopolymer is collected after carrying out the compressive test for the cast cylinder. The collected pieces of geopolymer are grounded to a fine powder by using a hammer to it. The powder consists of particles with sizes of 100µm or less by passing the ground powder through a sieve shaker with a 100µm sieve. The fine powder is then collected and fit into a sample holder of 0.5 in radius and 0.1 in height. The Class-F fly ash, is presented as a fine powder, and is used as it is for the X-ray analysis.

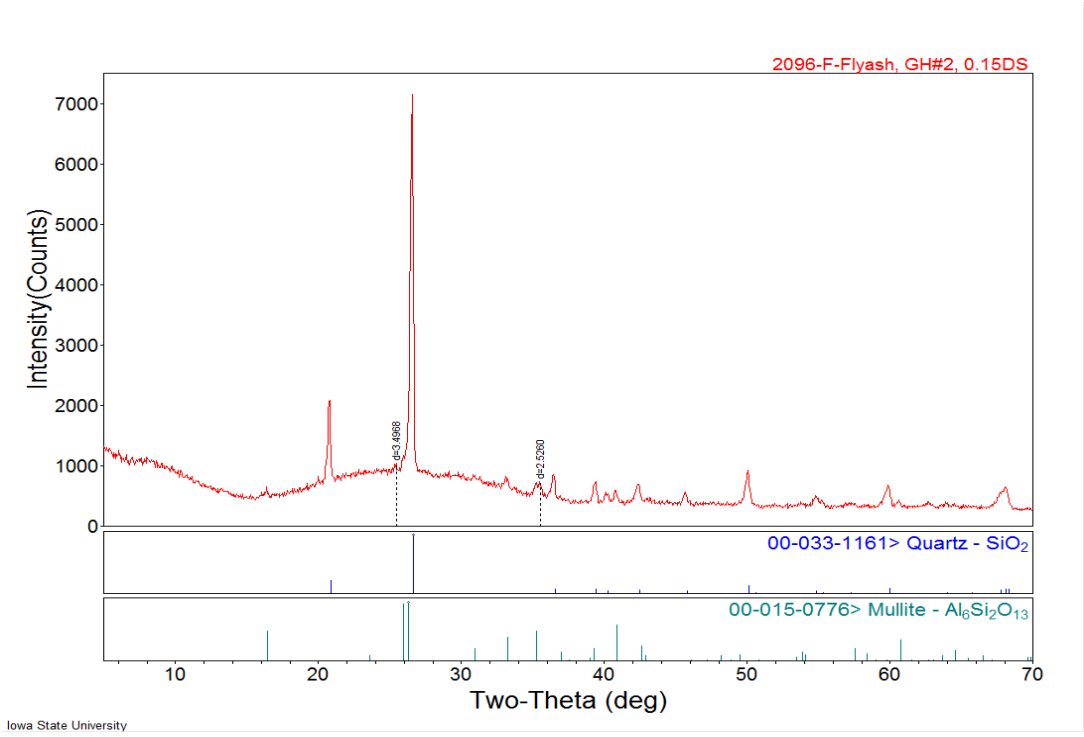

Figure A-10. XRD results of Class-F fly ash

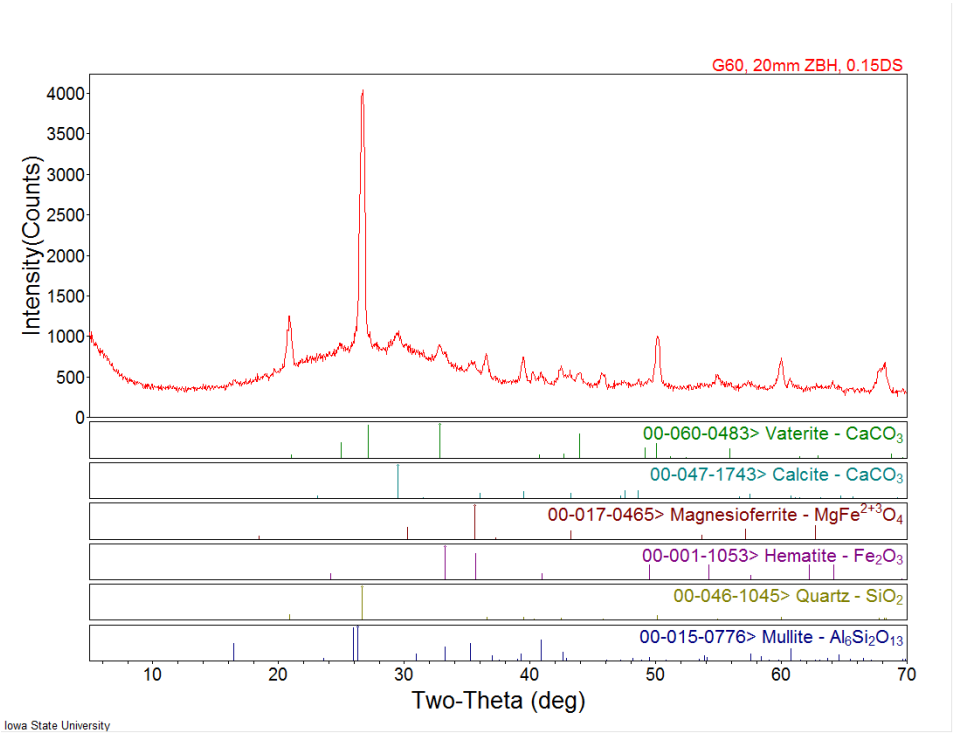

Figure A-11. XRD results of geopolymer (G60)

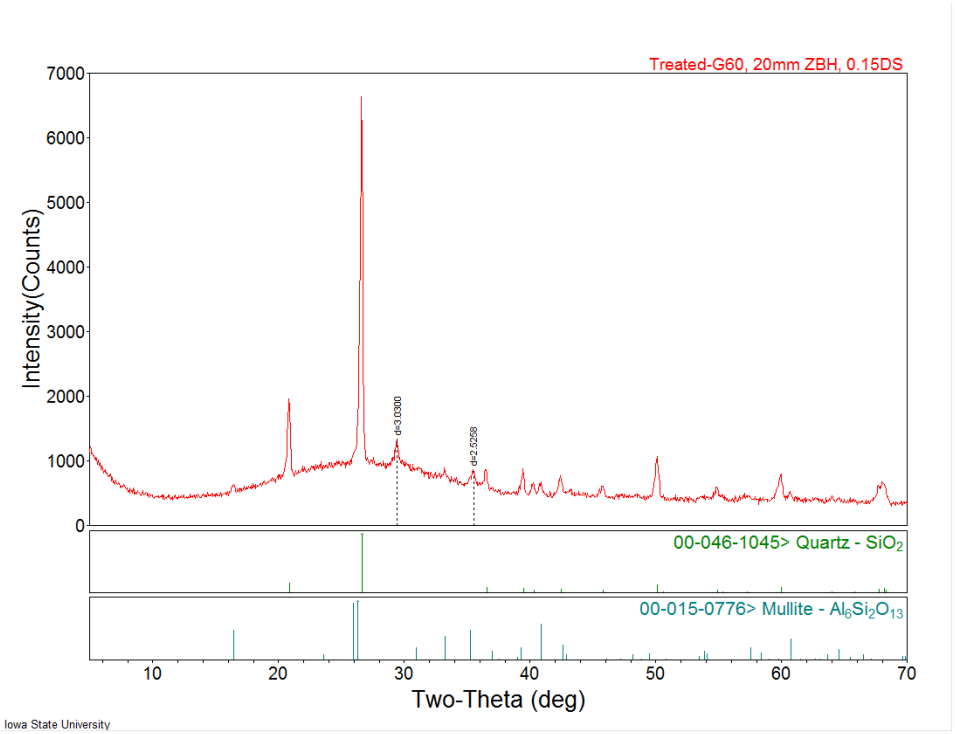

Figure A-12. XRD results of geopolymer (G60) after treated copper solution

All the crystalline phases were identified by the X-Ray diffraction method. Above figures illustrate the XRD pattern for raw fly ash (Class-F), fly ash-based geopolymer (G60), and G60 treated with Cu^{2+} solution. The major components of this raw Class-F fly ash are Quartz (SiO_2) and sodium-aluminum-silica complex like Mullite. The main peaks correspond to Calcite ($CaCO_3$) were found in G60 which is formed due to the interaction between the CaO present in fly ash and the alkaline solution. A deduction can be made regarding this complex amorphous phase. It seems to have formed a reaction zone around the unreacted silica particles. The calcium enriched zone from SEM could be from the calcite identified by the X-Ray diffraction. There are some crystalline phases originally existent in the fly ash (quartz and mullite) which have not been transformed by the activation reaction. This relatively large amount of fly ash still present in the hardened samples is an indicator of incomplete geopolymerization reaction.

APPENDIX B. EXPERIMENTAL DATA OF CHAPTER 3

Table B-1. Batch adsorption data (20 mg/L of Cu^{2+}, initial pH at 3.0, 0.1 g of geopolymer)

Time, hr	Final pH	Conc., mg/L	Q, mg/g
0	3.00	20	0
0.5	4.05	18.9	0.55
1	4.60	17.53	1.235
2	4.66	15.66	2.17
4	4.79	12.3	3.85
8	5.16	10.67	4.665
16	5.60	8.71	5.645
24	5.79	6.41	6.795
36	5.98	5.71	7.145
48	6.20	4.56	7.72

Table B-2. Batch adsorption data (100 mg/L of Cu^{2+}, initial pH at 3.0, 0.1 g of geopolymer)

Time, hr	Final pH	Conc., mg/L	Q, mg/g
0	3.00	100	0
0.5	4.45	98.35	0.825
1	4.60	97.71	1.145
2	4.66	94.43	2.785
4	4.79	92.12	3.94
8	4.86	90.93	4.535
16	4.98	88.22	5.89
24	5.13	80.21	9.895
36	5.38	63.62	18.19
48	5.64	53.57	23.215

Table B-3. Batch adsorption data (100 mg/L of Cu^{2+}, initial pH at 3.0, 0.5 g of geopolymer)

Time, hr	Final pH	Conc., mg/L	Q, mg/g
0	3.00	100	0
0.5	4.79	85.6	1.44
1	5.13	84.5	1.55
2	5.29	77.7	2.23
4	5.69	68.8	3.12
8	5.82	45.5	5.45
16	5.92	36.7	6.33
24	6.25	17.8	8.22
36	6.67	6.53	9.347
48	7.83	1.01	9.899

Table B-4. Batch adsorption data for cation release (contact time 48 hours, initial pH at 3.0, and 0.1g of geopolymer)

Initial Cu^{2+} Conc., mg/L	Q, mg/g	Final pH	Ca, mg/L	Mg, mg/L	K, mg/L	Na, mg/L
0	0	6.9	0.13	0.08	0.23	21
5	2.36	6.69	0.11	0.08	0.27	21
20	7.65	6.2	0.45	0.15	0.28	24
50	13.5	5.78	0.58	0.27	0.28	25
75	20.5	5.76	0.59	0.32	0.28	25
100	24.5	5.64	0.65	0.36	0.29	27
150	25	5.5	0.78	0.39	0.31	27
200	27.5	5.15	0.87	0.57	0.36	30
300	55	5.09	0.95	0.63	0.41	33

Table B-5. Batch adsorption data for different particle size of geopolymer and comparison with zeolite (contact time 48 hours and initial pH at 3.0)

	Initial Cu conc., mg/L	C_e, mg/L	Solution volume, L	Mass of FAG, g	Q_e, mg/g	Final pH
FAG (G60) (size: 0.42-2 mm)	0	0	0.05	0.1	0	6.9
	5	0.28	0.05	0.1	2.36	6.69
	20	4.7	0.05	0.1	7.65	6.2
	50	21	0.05	0.1	14.5	5.78
	75	34	0.05	0.1	20.5	5.76
	100	51	0.05	0.1	24.5	5.64
	150	100	0.05	0.1	25	5.5
	200	145	0.05	0.1	27.5	5.15
	Initial Cu conc., mg/L	C_e, mg/L	Solution volume, L	Mass of FAG, g	Q_e, mg/g	Final pH
FAG (G60) (size: 2-5 mm)	0	0	0.05	0.1	0	5.86
	10	2.22	0.05	0.1	3.89	5.88
	50	26.1	0.05	0.1	11.95	5.96
	100	62.2	0.05	0.1	18.9	5.61
	200	155.8	0.05	0.1	22.1	5.51
	Initial Cu conc., mg/L	C_e, mg/L	Solution volume, L	Mass of zeolite, g	Q_e, mg/g	Final pH
Zeolite (size: 0.42-2 mm)	0	0	0.05	0.5	0	3.1
	10	2.28	0.05	0.5	0.772	3.05
	50	23.4	0.05	0.5	2.66	3.11
	100	65.9	0.05	0.5	3.41	3.21
	150	112	0.05	0.5	3.8	3.18
	200	158	0.05	0.5	4.2	3.19

APPENDIX C. EXPERIMENTAL DATA OF CHAPTER 4

Table C-1. Batch adsorption data of three metals for different geopolymers (contact time 48 hours and initial pH at 3.0)

		Single Cu^{2+} solution				Single Cd^{2+} solution				Single Pb^{2+} solution			
Sample	V, L	Initial conc., mg/L	Ce, mg/L	Mass of sample, g	Qe, mg/L	Initial conc., mg/L	Ce, mg/L	Mass of sample, g	Qe, mg/L	Initial conc., mg/L	Ce, mg/L	Mass of sample, g	Qe, mg/L
G50	0.05	0.00	0.00	0.10	0.00	0.00	0.00	0.05	0.00	0.00	0.00	0.05	0.00
	0.05	1.00	0.37	0.10	0.32	0.50	0.26	0.05	0.24	0.50	0.01	0.05	0.49
	0.05	5.00	1.30	0.10	1.85	1.00	0.40	0.05	0.60	1.00	0.04	0.05	0.96
	0.05	10.00	2.01	0.10	4.00	5.00	1.25	0.05	3.75	5.00	0.23	0.05	4.78
	0.05	20.00	3.13	0.10	8.44	10.00	2.38	0.05	7.62	10.00	0.46	0.05	9.54
G60	0.05	0.00	0.00	0.10	0.00	0.00	0.00	0.05	0.00	0.00	0.00	0.05	0.00
	0.05	1.00	0.11	0.10	0.45	0.50	0.07	0.05	0.43	0.50	0.01	0.05	0.50
	0.05	5.00	0.90	0.10	2.05	1.00	0.30	0.05	0.70	1.00	0.02	0.05	0.98
	0.05	10.00	1.40	0.10	4.30	5.00	1.10	0.05	3.90	5.00	0.09	0.05	4.91
	0.05	20.00	2.55	0.10	8.73	10.00	1.80	0.05	8.20	10.00	0.16	0.05	9.85
G70	0.05	0.00	0.00	0.10	0.00	0.00	0.00	0.05	0.00	0.00	0.00	0.05	0.00
	0.05	1.00	0.44	0.10	0.28	0.50	0.29	0.05	0.21	0.50	0.02	0.05	0.48
	0.05	5.00	1.70	0.10	1.65	1.00	0.45	0.05	0.55	1.00	0.09	0.05	0.91
	0.05	10.00	2.40	0.10	3.80	5.00	1.91	0.05	3.09	5.00	0.33	0.05	4.68
	0.05	20.00	3.94	0.10	8.03	10.00	2.74	0.05	7.26	10.00	0.76	0.05	9.24
G60+10 %S	0.05	0.00	0.00	0.10	0.00	0.00	0.00	0.05	0.00	0.00	0.00	0.05	0.00
	0.05	1.00	0.41	0.10	0.30	0.50	0.27	0.05	0.23	0.50	0.01	0.05	0.49
	0.05	5.00	1.41	0.10	1.80	1.00	0.42	0.05	0.58	1.00	0.09	0.05	0.92
	0.05	10.00	2.30	0.10	3.85	5.00	1.71	0.05	3.29	5.00	0.27	0.05	4.73
	0.05	20.00	3.77	0.10	8.12	10.00	2.61	0.05	7.39	10.00	0.63	0.05	9.37
G60+20 %S	0.05	0.00	0.00	0.10	0.00	0.00	0.00	0.05	0.00	0.00	0.00	0.05	0.00
	0.05	1.00	0.39	0.10	0.31	0.50	0.16	0.05	0.34	0.50	0.01	0.05	0.49
	0.05	5.00	1.11	0.10	1.95	1.00	0.38	0.05	0.62	1.00	0.09	0.05	0.91
	0.05	10.00	1.66	0.10	4.17	5.00	1.23	0.05	3.77	5.00	0.23	0.05	4.77
	0.05	20.00	2.85	0.10	8.58	10.00	2.24	0.05	7.76	10.00	0.51	0.05	9.49
Zeolite	0.05	0.00	0.00	0.10	0.00	0.00	0.00	0.10	0.00	0.00	0.00	0.10	0.00
	0.05	1.00	0.90	0.10	0.05	0.50	0.41	0.10	0.05	0.50	0.48	0.10	0.01
	0.05	5.00	4.41	0.10	0.30	1.00	0.89	0.10	0.06	1.00	0.87	0.10	0.07
	0.05	10.00	8.77	0.10	0.62	5.00	4.56	0.10	0.22	5.00	4.44	0.10	0.28
	0.05	20.00	17.53	0.10	1.23	10.00	8.98	0.10	0.51	10.00	8.32	0.10	0.84

Table C-2. Batch adsorption data of three metals with low concentration in single-component solution (contact time 48 hours)

	Experimental condition			Initial pH at 2.5		Initial pH at 3.0		Initial pH at 4.0	
	Initial Cu conc., mg/L	Solution volume, L	Mass of sample, g	Ce, mg/L	Qe, mg/g	Ce, mg/L	Qe, mg/g	Ce, mg/L	Qe, mg/g
Single Cu^{2+} solution	0	0.05	0.05	0.00	0.00	0.00	0.00	0.00	0.00
	0.5	0.05	0.05	0.33	0.17	0.21	0.29	0.18	0.32
	1	0.05	0.05	0.67	0.33	0.51	0.49	0.47	0.53
	5	0.05	0.05	3.58	1.42	2.40	2.60	2.13	2.87
	10	0.05	0.05	6.42	3.58	5.07	4.93	4.05	5.95
	20	0.05	0.05	14.13	5.87	11.10	8.90	9.02	10.98
Single Cd^{2+} solution	0	0.05	0.05	0.00	0.00	0.00	0.00	0.00	0.00
	0.5	0.05	0.05	0.21	0.29	0.17	0.33	0.11	0.39
	1	0.05	0.05	0.48	0.52	0.39	0.61	0.27	0.73
	5	0.05	0.05	2.47	2.53	1.80	3.20	1.50	3.50
	10	0.05	0.05	4.50	5.50	3.76	6.24	3.10	6.90
Single Pb^{2+} solution	0	0.05	0.05	0.00	0.00	0.00	0.00	0.00	0.00
	0.5	0.05	0.05	0.01	0.49	0.01	0.50	0.00	0.50
	1	0.05	0.05	0.02	0.98	0.02	0.98	0.01	0.99
	5	0.05	0.05	0.15	4.85	0.05	4.95	0.04	4.96
	10	0.05	0.05	0.26	9.74	0.13	9.88	0.09	9.91

Table C-3. Batch adsorption data of three metals in multi-component solution (contact time 48 hours)

	Solution volume, L	Mass of sample, g	Initial Conc., mg/L			Ce, mg/L			Qe, mg/g		
			Cd^{2+}	Cu^{2+}	Pb^{2+}	Cd^{2+}	Cu^{2+}	Pb^{2+}	Cd^{2+}	Cu^{2+}	Pb^{2+}
Multi-metal solution	0.05	0.05	0	0	0	0	0	0	0	0	0
	0.05	0.05	0.5	1	0.5	0.34	0.54	0.02	0.16	0.46	0.49
	0.05	0.05	1	2	1	0.73	1.17	0.04	0.28	0.83	0.96
	0.05	0.05	5	10	5	4.28	6.08	0.38	0.72	3.92	4.62
	0.05	0.05	10	20	10	9.11	13.8	1.46	0.89	6.2	8.54

Table C-4. Batch adsorption data of three metals with high concentration in single-component solution (contact time 48 hours)

	Experimental Conditions			Initial pH 2.5			Initial pH 3.0			Initial pH 4.0		
	Initial conc., mg/L	Solution volume, L	Mass of sample, g	Ce, mg/L	Qe, mg/g	Final pH	Ce, mg/L	Qe, mg/g	Final pH	Ce, mg/L	Qe, mg/g	Final pH
Single Cu^{2+} solution	0	0.05	0.1	0.00	0.00	6.11	0.00	0.00	6.90	0.00	0.00	7.31
	5	0.05	0.1	0.34	2.33	6.05	0.28	2.36	6.69	0.53	2.24	7.04
	20	0.05	0.1	6.80	6.60	5.77	4.70	7.65	6.20	1.30	9.35	6.73
	50	0.05	0.1	28.00	11.00	5.50	23.00	13.50	5.78	9.30	20.35	6.33
	75	0.05	0.1	43.50	15.75	5.23	34.00	20.50	5.76	28.00	23.50	5.98
	100	0.05	0.1	64.00	18.00	5.18	51.00	24.50	5.64	45.00	27.50	5.92
	150	0.05	0.1	114.00	18.00	4.78	100.00	25.00	5.50	91.00	29.50	5.73
	200	0.05	0.1	161.00	19.50	4.59	145.00	27.50	5.15	130.00	35.00	5.61
	300	0.05	0.1	220.00	40.00	4.05	190.00	55.00	5.09	160.00	70.00	5.50
Single Cd^{2+} solution	0	0.05	0.1	0.00	0.00	6.47	0.00	0.00	6.77	0.00	0.00	7.27
	10	0.05	0.1	0.17	4.92	6.24	0.13	4.94	6.44	0.10	4.95	6.91
	50	0.05	0.1	16.50	16.75	6.13	12.90	18.55	6.27	8.03	20.99	6.54
	100	0.05	0.1	52.30	23.85	5.66	49.40	25.30	5.70	38.30	30.85	6.13
	200	0.05	0.1	149.00	25.50	5.27	135.00	32.50	5.36	121.00	39.50	5.74
	300	0.05	0.1	243.00	28.50	5.17	231.00	34.50	5.13	218.00	41.00	5.56
	500	0.05	0.1	411.00	44.50	5.04	394.00	53.00	5.11	385.00	57.50	5.23
Single Pb^{2+} solution	0	0.05	0.1	0.00	0.00	8.31	0.00	0.00	8.70	0.00	0.00	8.89
	10	0.05	0.1	0.09	4.96	8.11	0.05	4.97	8.30	0.04	4.98	8.56
	20	0.05	0.1	0.18	9.91	7.89	0.11	9.95	8.14	0.07	9.96	8.31
	50	0.05	0.1	0.62	24.69	7.52	0.32	24.84	7.62	0.19	24.91	8.02
	100	0.05	0.1	1.29	49.35	7.12	0.68	49.66	7.33	0.38	49.81	7.74
	150	0.05	0.1	2.33	73.83	6.67	1.13	74.43	6.91	0.71	74.64	7.22
	175	0.05	0.1	5.16	84.92	6.42	2.05	86.48	6.68	1.13	86.94	6.79
	200	0.05	0.1	9.45	95.28	6.31	5.36	97.32	6.42	2.69	98.66	6.55

APPENDIX D. EXPERIMENTAL DATA OF CHAPTER 5

Table D-1. Column data for first set of experiment (flow rate and bed depth)

	Time, min	Volume, L	Conc., mg/L	C/Co
Single Cu^{2+} solution, bed depth 2 cm, flow rate 10mL/min	0	0	0	0
	1.00	0.01	0.35	0.035
	5.00	0.05	0.93	0.093
	10.00	0.1	1.94	0.194
	20.00	0.2	3.14	0.314
	30	0.3	4.95	0.495
	60	0.6	6.87	0.687
	180	1.8	8.97	0.897
	360	3.6	9.54	0.954
	720	7.2	9.99	0.999
	1440	14.4	10	1
Single Cu^{2+} solution, bed depth 2 cm, flow rate 5 mL/min	Time, min	Volume, L	Conc., mg/L	C/Co
	0	0	0	0
	1.00	0.005	0.011	0.0011
	5.00	0.025	0.052	0.0052
	10.00	0.05	0.13	0.013
	20.00	0.1	0.45	0.045
	30	0.15	0.95	0.095
	60	0.3	1.68	0.168
	180	0.9	2.83	0.283
	360	1.8	3.76	0.376
	720	3.6	5.88	0.588
	1440	7.2	7.56	0.756
	2160	10.8	8.91	0.891
	2880	14.4	9.55	0.955
	3600	18	9.86	0.986
	4320	21.6	10	1
Single Cu^{2+} solution, bed depth 5 cm, flow rate 5 mL/min	Time, min	Volume, L	Conc., mg/L	C/Co
	0	0	0	0
	1.00	0.005	0.01	0.001
	5.00	0.025	0.046	0.0046
	10.00	0.05	0.071	0.0071
	20.00	0.1	0.098	0.0098
	30	0.15	0.11	0.011
	60	0.3	0.5	0.05
	180	0.9	0.86	0.086
	360	1.8	1.3	0.13
	720	3.6	1.9	0.19
	1440	7.2	2.4	0.24
	2160	10.8	3.78	0.378
	2880	14.4	4.56	0.456
	3600	18	5.67	0.567
	4320	21.6	6.34	0.634
	5040	25.2	7.54	0.754
	5760	28.8	8.45	0.845
	6480	32.4	9.51	0.951
	7200	36	9.79	0.979
	7920	39.6	9.89	0.989
	8640	43.2	9.97	0.997
	9360	46.8	10	1

Continuing on next page

Table D-1. (Continued)

	Time, min	Volume, L	Conc., mg/L	C/Co
Single Cu^{2+} solution, bed depth 10 cm, flow rate 5 mL/min	0	0	0	0
	1.00	0.005	0.011	0.0011
	5.00	0.025	0.042	0.0042
	10.00	0.05	0.087	0.0087
	20.00	0.1	0.143	0.0143
	30	0.15	0.181	0.0181
	60	0.3	0.227	0.0227
	180	0.9	0.42	0.042
	360	1.8	0.51	0.051
	720	3.6	0.88	0.088
	1440	7.2	1.17	0.117
	2160	10.8	1.66	0.166
	2880	14.4	2.25	0.225
	4320	21.6	2.88	0.288
	5760	28.8	3.77	0.377
	7200	36	4.88	0.488
	8640	43.2	5.59	0.559
	10080	50.4	6.85	0.685
	11520	57.6	7.46	0.746
	12960	64.8	8.29	0.829
	14400	72	9.01	0.901
	15840	79.2	9.57	0.957
	17280	86.4	9.72	0.972
	18720	93.6	9.81	0.981
	20160	100.8	9.98	0.998
	21600	108	10	1

Table D-2. Column data for second set of experiment (single metal solution)

	Time, min	Volume, L	Conc., mg/L	C/Co
Single Cd^{2+} solution, bed depth 5 cm, flow rate 5 mL/min	0	0	0	0
	1.00	0.005	0	0
	5.00	0.025	0	0
	10.00	0.05	0.012	0.0012
	20.00	0.1	0.039	0.0039
	30	0.15	0.086	0.0086
	60	0.3	0.13	0.013
	180	0.9	0.35	0.035
	360	1.8	0.61	0.061
	720	3.6	0.97	0.097
	1440	7.2	1.33	0.133
	2160	10.8	1.79	0.179
	2880	14.4	2.91	0.291
	4320	21.6	3.65	0.365
	5760	28.8	5.88	0.588
	7200	36	7.71	0.771
	8640	43.2	8.42	0.842
	10080	50.4	9.51	0.951
	11520	57.6	9.65	0.965
	12960	64.8	9.78	0.978
	14400	72	9.99	0.999
	15840	79.2	10	1

Continuing on next page

Table D-2. (Continued)

	Time, min	Volume, L	Conc., mg/L	C/Co
Single Pb^{2+} solution, bed depth 5 cm, flow rate 5 mL/min	0	0	0	0
	1.00	0.005	0	0
	5.00	0.025	0.001	0.0001
	10.00	0.05	0.005	0.0005
	20.00	0.1	0.008	0.0008
	30	0.15	0.013	0.0013
	60	0.3	0.052	0.0052
	180	0.9	0.081	0.0081
	360	1.8	0.106	0.0106
	720	3.6	0.139	0.0139
	1440	7.2	0.22	0.022
	2160	10.8	0.51	0.051
	2880	14.4	0.97	0.097
	4320	21.6	1.68	0.168
	5040	25.2	2.42	0.242
	5760	28.8	2.78	0.278
	7200	36	3.22	0.322
	8640	43.2	3.77	0.377
	10080	50.4	4.88	0.488
	11520	57.6	5.59	0.559
	12960	64.8	6.85	0.685
	14400	72	7.46	0.746
	15840	79.2	8.29	0.829
	17280	86.4	9.46	0.946
	18720	93.6	9.87	0.987
	20160	100.8	9.99	0.999
	21600	108	10	1

Table D-3. Column data for second set of experiment (multi-metal solution)

Second set of experiment (multi-metal solution)				
	Time, min	Volume, L	Conc., mg/L	C/Co
Multi solution of Cd^{2+}, bed depth 5 cm, flow rate 5 mL/min	0	0	0	0
	1.00	0.005	0	0
	5.00	0.025	0.047	0.0047
	10.00	0.05	0.11	0.011
	20.00	0.1	0.89	0.089
	30	0.15	1.36	0.136
	60	0.3	2.21	0.221
	180	0.9	4.93	0.493
	360	1.8	6.12	0.612
	720	3.6	6.93	0.693
	1440	7.2	8.32	0.832
	2160	10.8	9.47	0.947
	2880	14.4	9.68	0.968
	3600	18	9.77	0.977
	4320	21.6	9.89	0.989
	5760	28.8	9.99	0.999
	7200	36	10	1
	7920	39.6	10.043	1.0043
	8640	43.2	10.192	1.0192
	9360	46.8	10.258	1.0258

Continuing on next page

Table D-3. (Continued)

	Time, min	Volume, L	Conc., mg/L	C/Co
Multi solution of Pb^{2+}, bed depth 5 cm, flow rate 5 mL/min	0	0	0	0
	1.00	0.005	0.004	0.0004
	5.00	0.025	0.009	0.0009
	10.00	0.05	0.016	0.0016
	20.00	0.1	0.028	0.0028
	30	0.15	0.051	0.0051
	60	0.3	0.213	0.0213
	180	0.9	0.69	0.069
	360	1.8	1.08	0.108
	720	3.6	2.42	0.242
	1440	7.2	3.09	0.309
	2160	10.8	3.97	0.397
	2880	14.4	4.68	0.468
	3600	18	5.23	0.523
	4320	21.6	6.41	0.641
	5040	25.2	7.66	0.766
	5760	28.8	8.45	0.845
	7200	36	9.11	0.911
	7920	39.6	9.56	0.956
	8640	43.2	9.87	0.987
	9360	46.8	9.99	0.999
Multi solution of Cu^{2+}, bed depth 5 cm, flow rate 5 mL/min	Time, min	Volume, L	Conc., mg/L	C/Co
	0	0	0	0
	1.00	0.005	0.013	0.0013
	5.00	0.025	0.097	0.0097
	10.00	0.05	0.28	0.028
	20.00	0.1	0.43	0.043
	30	0.15	0.76	0.076
	60	0.3	1.17	0.117
	180	0.9	2.09	0.209
	360	1.8	2.3	0.23
	720	3.6	3.72	0.372
	1440	7.2	4.68	0.468
	2160	10.8	6.31	0.631
	2880	14.4	7.47	0.747
	4320	21.6	8.75	0.875
	5040	25.2	9.56	0.956
	5760	28.8	9.72	0.972
	7200	36	9.95	0.995
	7920	39.6	9.97	0.997
	8640	43.2	10	1
	9360	46.8	10	1

APPENDIX E. EXPERIMENTAL DATA OF CHAPTER 6

Table E-1. Batch Cu^{2+} adsorption data of different magnetic samples for initial screening test (initial pH 3.0 and contact time 24 hours)

	Sample		Co, mg/L	Ce, mg/L	Volume, L	Mass, g	Qe, mg/g	Final pH
Initial screening, particle size < 0.177 mm	Fe3O4		100	86.00	0.01	0.10	1.40	3.13
	Fly ash		100	57.2	0.05	0.10	21.40	7.36
	FAG		100	0.413	0.05	0.10	49.79	6.31
	Method 2	MFAG1	100	9.85	0.05	0.10	45.08	5.86
		MFAG2	100	0.386	0.05	0.10	49.81	6.04
		MFAG3	100	0.632	0.05	0.10	49.68	6.28
	Method 1	MCFAG1	100	39.7	0.05	0.10	30.15	4.45
		MCFAG2	100	24.2	0.05	0.10	37.90	4.51
		MCFAG3	100	4	0.05	0.10	48.00	5.02
		MCFAG1-1	100	34.1	0.05	0.10	32.95	5.57
		MCFAG1-2	100	36.4	0.05	0.10	31.80	5.53
		MCZ1	100	98.3	0.05	0.10	0.85	3.93
		MCZ2	100	97.3	0.05	0.10	1.35	4.05
	Zeolite		100	94.9	0.05	0.10	2.55	3.09

Table E-2. Batch Cu^{2+} adsorption data of magnetic geopolymer compared to non-magnetic geopolymer with different mass (initial pH 3.0 and contact time 24 hours)

Sample	Co, mg/L	Ce, mg/L	Volume, L	Mass, g	Qe, mg/g	Final pH
MFAG2 (< 0.177 mm)	10	0.015	0.05	0.10	4.99	7.68
	10	0.168	0.05	0.05	9.83	7.02
	10	4.6	0.05	0.025	10.80	6.79
	10	7.8	0.05	0.01	11.00	6.25
FAG (< 0.177 mm)	10	0.1	0.05	0.10	4.95	8.81
	10	0.5	0.05	0.05	9.50	7.86
	10	5.98	0.05	0.025	8.04	7.44
	10	9.53	0.05	0.01	2.35	6.43
FAG (0.6 -2 mm)	20	18.9	0.05	0.01	5.50	4.05
	20	17.15	0.05	0.025	5.70	4.86
	20	13.85	0.05	0.05	6.15	5.05
	20	6.49	0.05	0.1	6.76	5.9

Table E-3. Batch Cu^{2+} adsorption data of magnetic geopolymer at different initial pHs

Experimental Conditions				Initial pH 2.5		Initial pH 3.0		Initial pH 4.0	
Time, hr	Co, mg/L	Volume, L	Mass, g	Ct, mg/L	Qt, mg/g	Ct, mg/L	Qt, mg/g	Ct, mg/L	Qt, mg/g
0.00	100.00	0.05	0.10	100.00	0.00	100.00	0.00	100.00	0.00
0.17	100.00	0.05	0.10	62.60	18.70	52.60	23.70	42.60	28.70
0.50	100.00	0.05	0.10	47.40	26.30	37.40	31.30	27.40	36.30
1.00	100.00	0.05	0.10	33.70	33.15	23.70	38.15	13.70	43.15
2.00	100.00	0.05	0.10	28.00	36.00	18.00	41.00	8.00	46.00
6.00	100.00	0.05	0.10	24.10	37.95	14.10	42.95	3.10	48.45
12.00	100.00	0.05	0.10	13.87	43.07	3.87	48.07	1.37	49.32
18.00	100.00	0.05	0.10	10.77	44.62	1.77	49.12	0.57	49.72
24.00	100.00	0.05	0.10	3.39	48.31	0.39	49.81	0.29	49.86
36.00	100.00	0.05	0.10	1.06	49.47	0.06	49.97	0.16	49.92
48.00	100.00	0.05	0.10	0.13	49.94	0.01	49.99	0.00	50.00

Table E-4. Batch Cu^{2+} adsorption data of magnetic geopolymer for cation release

Release Cation Conc., mg/L	Ca(II)	Mg(II)	K(I)	Na(I)
MFAG2 (< 0.177 mm)	9.1	0.77	0.67	38
FAG (< 0.177 mm)	10.4	0.83	0.74	43
FAG (0.6 - 2 mm)	0.65	0.36	0.29	27
Raw fly ash (Class F)	17	0.63	0.6	0.19

Table E-5. Batch Cu^{2+} adsorption data of magnetic geopolymer compared to non-magnetic geopolymer (initial pH 3.0)

	Co, mg/L	Ce, mg/L	Volume, L	Mass, g	Qe, mg/g	Final pH
MFAG2 (< 0.177 mm)	0	0	0.05	0.05	0.00	7.45
	1	0.01	0.05	0.05	0.99	7.31
	5	0.075	0.05	0.05	4.93	7.15
	10	0.168	0.05	0.05	9.83	7.02
	50	2.843	0.05	0.05	47.16	6.65
	100	9.47	0.05	0.05	90.53	6.34
	150	47.89	0.05	0.05	102.11	5.93
	200	90.12	0.05	0.05	109.88	5.31
FAG (< 0.177 mm)	Co, mg/L	Ce, mg/L	Volume, L	Mass, g	Qe, mg/g	Final pH
	0	0	0.05	0.05	0.00	7.98
	10	0.3	0.05	0.05	9.70	7.43
	50	4.1	0.05	0.05	45.90	6.98
	100	13.21	0.05	0.05	86.79	6.59
	150	56.2	0.05	0.05	93.80	6.37
	200	101.1	0.05	0.05	98.90	5.61
FAG (0.6 - 2 mm)	Co, mg/L	Ce, mg/L	Volume, L	Mass, g	Qe, mg/g	Final pH
	0	0	0.05	0.1	0.00	6.9
	5	0.28	0.05	0.1	2.36	6.69
	20	4.7	0.05	0.1	7.65	6.2
	50	23	0.05	0.1	13.50	5.78
	75	34	0.05	0.1	20.50	5.76
	100	51	0.05	0.1	24.50	5.64
	150	100	0.05	0.1	25.00	5.5
	200	145	0.05	0.1	27.50	5.15
	300	190	0.05	0.1	55.00	5.09